Grid Monitoring and Advanced Control of Distributed Power Generation Systems

Timbus, Adrian Vasile

Publication date:
2007

Document Version
Publisher's PDF, also known as Version of record

Grid Monitoring and Advanced Control of Distributed Power Generation Systems

by

Adrian Timbus

Dissertation submitted to the Faculty of Engineering, Science & Medicine at Aalborg University
in partial fulfilment of the requirements for the degree of
Doctor of Philosophy in Electrical Engineering

Aalborg University
Institute of Energy Technology
Denmark, May, 2007

Aalborg University
Institute of Energy Technology
Pontoppidanstræde 101
DK-9220 Aalborg East

Printed in Denmark by Aalborg University

This thesis has been typeset in LaTeX 2_ε.

Preface

This thesis is written under the research project 2058-03-0003 entitled *Reliable grid conditions detection and control in distributed power generation systems* financially supported by the Danish Research Council, Risø National Laboratory, Energinet.dk and Aalborg University. This project is divided in two sub-projects, one entitled *Reliable grid condition detection and control of single phase distributed power generation systems* dealing with single phase systems and the work in this thesis which treats three phase power generation systems.

The research work was carried out under the guidance of Prof. Remus Teodorescu (main supervisor), Prof. Frede Blaabjerg from Institute of Energy Technology, Aalborg University, Senior Scientist Poul Sørensen from Risø National Laboratory and Kent Søbrink from Energinet.dk. I would like to express my gratitude for their kindness and support provided during the thesis period. In addition, a steering committee, comprising representatives from all parties involved in the project and relevant industrial partners, have been very active in the project. Many thanks to all of them for their guidance and helpful comments.

I would also like to express my appreciation and to thank for their interference to two of my closest collaborators, Marco Liserre from Politecnico di Bari, Italy, and Pedro Rodriquez from Universidad Politècnica de Catalunya, Spain. Both of them showed a high interest in my work and their ideas prove to be valuable information for my research.

I also appreciate the financial support offered by the above mentioned institutions and I owe again special thanks to my supervisors for giving me the possibility of doing this research.

Finally, I would like to thank to my family for their patience and support they showed during the time I was working on this thesis.

Aalborg, May, 2007

Adrian Timbus

Abstract

The need for more energy production and the constraints in reducing the CO_2 emissions are some factors facilitating the growth of distributed power generation systems based on renewable energy resources. Consequently, large penetration of distributed generators has been reported in some countries creating concerns about power system stability. This leads to a continuous evolution of grid interconnection requirements towards a better controllability of generated power and an enhanced contribution of distributed power generation systems to power system stability. As an example, the latest published grid codes stress the ability of distributed generators, especially wind turbines, to stay connected during short grid disturbances and in addition to provide active/reactive power control at the point of common coupling.

Based on the above facts, the need for improving and adding more features to the control of distributed power generation systems (DPGS) arises. As a consequence, this thesis focuses on grid monitoring methods and possible approaches in control in order to obtain a more reliable and flexible power generation system during normal and faulty grid conditions.

First part of the thesis investigates possible algorithms for fast and accurate identification of utility network variables such as voltage amplitude, frequency, phase angle and line impedance. Special attention has been paid to grid synchronization algorithm in terms of accurate estimation of grid voltage phase angle. It has been found that the identification of positive and negative sequence components and in addition, the capability of the algorithm to follow only the positive sequence component, plays a crucial role in providing a clean synchronization angle even during severe voltage unbalance caused by grid faults. Several algorithms for phase angle detection have been investigated and two novel algorithms that prove to be very robust against grid voltage disturbances have been developed.

The proposed synchronization algorithms have been further developed in order to estimate also the amplitude of grid voltage and the frequency of utility network. As a result, fast and accurate identification of both variables has been achieved. In addition, positive and negative sequence components of grid voltage can also be calculated. Simple, yet powerful filtering techniques, based on second order generalized integrator (SOGI) and delay signal cancellation (DSC) have been used to separate the sequence components. Simulation and experimental results attest the accuracy and effectiveness of the developed algorithms in identifying the frequency, phase angle and magnitude of grid voltages during severe distortions of utility network.

Methods for identification of grid impedance have also been investigated in this thesis. The state of the art methodologies for assessing the value of line impedance have been studied, leading to the development of two new methods for identification of line impedance. First method uses variations in both active and reactive power at the point of common coupling (PCC) to obtain current and voltage fluctuation in two operating points, based on which the algorithm is extracting the values for both resistive and inductive part of line impedance. Because this methodology can create voltage fluctuation at the connection point, it can be subject for flicker emission. As a consequence, a second method, which uses a grid voltage control loop to set the

reference for reactive power has been developed. If in the first method the variations in power are made consecutively (first variation in active power is made then variation in reactive power follows), in the second method the variation of reactive power occurs at the same time when variation in active power happens, in order to cancel out the voltage fluctuation at the point of common coupling. The results presented confirm the accuracy and effectiveness of both methods developed.

A considerable part of this thesis is dealing with control of grid side converter of a distribution system during normal and faulty grid conditions. The state of the art control structures for grid tied power converters have been initially identified and different types of controllers have been studied and compared. The possibility of using the information about grid variables into the control structure in order to improve the control of DPGS has also been investigated. As a consequence, improved behavior of resonant controller has been noticed if grid frequency information is forwarded to its internal model. Additionally, controllers such as dead beat and hysteresis controller improve their robustness to parameter mismatch if the identified value of grid impedance is passed to the controller. Moreover, several control strategies to provide flexible active and reactive power control during grid faults have been developed using the information of positive and negative sequence components. Simulation and experimental results are presented in order to validate the above studies.

The research done in this thesis makes it possible to assess the behavior and control abilities of a grid connected power converter when running on faulty grid conditions. Furthermore, this study can serve as a good basis for deeper investigation in some particular areas and also for further research on control of DPGS during grid disturbances.

Contents

Part I

Report

Chapter 1

Introduction

The work documented in this thesis concentrates on three issues particular to distribution power generation units connected to utility network. The first issue is the synchronization with the utility grid and focus is set on influence of voltage distortions on the synchronization algorithm. The second issue is related to grid monitoring and algorithms able to identify the voltage amplitude, grid frequency and line impedance are investigated. Accurate and fast response is the main design criteria for these algorithms. The third and last issue discussed in this thesis is the control of grid side converter during voltage fault conditions. Possibilities to provide flexible active and reactive power control during grid disturbances are investigated.

The beginning of this chapter discusses the background and motivation of the research work deposed in this thesis. This is followed by a short history of distributed generation and a brief description of the main concepts of today's market is given. Next, the problem statement and necessary limitations are highlighted and, at the end, the outline of the thesis is presented.

1.1 Background and motivation

Distributed power generation based on renewable energy resources experiences a constant increasing growth. In the last years, wind power market continued to grow at an average cumulative rate of nearly 30%, being declared one of the fastest growing markets in the world. Nowadays, there is almost 75 GW wind power installed around the world and Europe itself has set a target of 75 GW to be installed by 2010 [1], which will generate 5.5% of the European electricity. Although, majority of installation of wind power is located in Europe[1], lately markets in Asia and North America register also an exponential increase.

Another renewable energy technology which gains acceptance as a way of maintaining and improving living standards without harming the environment is the photovoltaic technology. Its exponentially growth is owed to the governments and utility companies that support programs focusing on PV systems. A total worldwide installation of nearly 4 GW photovoltaic power has been reported in 2006 [2].

The majority of renewable energy systems are connected to the utility network and spread along the power system. As a consequence, the conventional unidirectional way of energy production, from the power plants down to the load consumers has been changed. Some countries, as is the case of Denmark, already reached a large penetration of distributed generation into its power system, and therefore the concern about stability of utility network and reliability of power delivery appears. Consequently, grid interconnection requirements are evolving towards demanding distributed generators to accommodate control algorithms that would enable

[1]Europe accounts for 80% of the total installation worldwide.

a better control of generated power and the ability to contribute to power system stability if necessary. One of such requirement, which is the major driver of this research work, is the necessity of distributed systems, wind turbines in special, to ride through short grid disturbances. According to grid codes in Germany, Denmark, Spain and many other countries, wind turbines are requested to withstand balanced and unbalanced grid faults for a certain amount of time, providing either active or reactive power, depending on the severity of the fault.

Therefore, the control of distributed power generation systems (DPGS) and, especially their interaction with utility network during grid faults, is becoming a timely subject.

1.2 Distributed power generation

The worldwide economy is mainly running on fossil fuels which are largely recognized as a major cause of environmental destruction [3]. Consequently, an overall growth in alternative energy generation technologies and markets has been register in the last decade. The demand for renewable energy generation systems has been growing of about 30% per year, mainly due to a general increasing demand for electricity, a rising interest in clean technologies, energy security and saturation of oil resources [4].

Among the alternative energy sources, after hydro power, the wind energy knows the largest utilization. The power of the wind and methods to use it have been of mankind interest since the 7^{th} century BC. In that earlier period, the wind mills were recorded as vertical-axis mills and used for grinding grains in the highlands of Afghan. The first horizontal-axis wind mills were reported in Persia, Tibet and China around 1000 AD. It is assumed that the Crusaders have contributed to bring the knowledge of wind mills to Europe, sometime in the twelve century [5].

In 1891, the first wind turbine (WT) generating electricity was reported in Denmark and was built by Poul la Cour. Since then, the wind turbine industry known a rising and falling development, mostly influenced by the world economic condition, wars or price crises for conventional energy resources, mainly oil. Today, a large variety of wind turbine technologies are available on the market, and detailed classification of them can be found in literature [6–9]. Wind power generation is the most mature alternative energy solution, a total capacity of nearly 75 GW wind power is installed around the world, with more than 15 GW installed in 2006 only [10].

Another alternative resource, which register a large growth in the last decade is the photovoltaic (PV) technology. Historically, photovoltaic systems have been used as power supply for special loads, such as communication satellites. The continuous advances in the area of semiconductor material led to the development of commercial PV cells, making the photovoltaic systems a prominent alternative energy source [11]. Although a number of large demonstration projects (MW scale) were constructed in the past, high interest is now focusing on incorporating the power modules into the buildings, in order to reduce the overall cost and space requirements [12]. However, "PV farms" are still under consideration in some countries like Germany, Spain, USA, etc.

Fuel cells is also an interesting technology for many companies and governments mainly due to its higher efficiency (around 70%) related to the wind energy conversion (around 40%) and photovoltaic (around 20% using the new technologies of polycrystalline silicon wafers) [4]. The fuel cell technology produces electric power by electrochemical reactions between hydrogen and oxygen without the combustion processes. Unlike turbines and engine generator sets, fuel cells have no moving parts and thus no mechanical inefficiencies. The only byproducts of fuel cell operation are water and heat. However, hydrogen fuel is produced by subjecting hydrocarbon resources (natural gas or fuels) to steam under pressure (called reforming or gasification). This process often requires combustion and chemical reactions that produce carbon dioxide and other

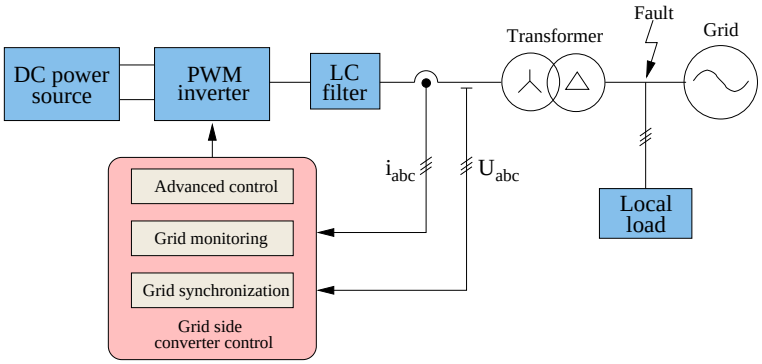

Figure 1.1: *Diagram of grid side converter and its control, highlighting the main goals of this project.*

environmental emissions. There is a new trend of using the wind power or photovoltaics to produce hydrogen by means of electrolysis, the process of producing hydrogen becoming pollution free.

The last technology to produce electrical power discussed here is the micro-turbine. Micro-turbine is a new type of combustion turbine used for stationary energy generation applications with outputs of 25 up to 500 kW, which can be located on sites with space limitations for power production. Waste heat recovery can be used in combined heat and power systems to achieve energy efficiency levels greater than 80 percent.

As energy generation will mature, it is likely that power systems will become complex, conglomerate systems, employing various forms of energy generation, storage and transmission. Therefore, hybrid systems will have a word to say in the near future of distributed energy. Different combinations like wind – fuel cell or solar – fuel cell may become interesting in the future.

Majority of these renewable energy systems are installed along the power system constituting so called *distributed generation*. This way, the traditional approach of energy production and its distribution is changing, and consequently, reliable power delivery faces new challenges. Therefore, grid interconnection demands imposed by transmission system operators (TSO) are becoming stricter, challenging the control of DPGS. Power electronics play an important role in converting the input power to a power suitable to be delivered to utility network. Easier and more flexible grid interconnection is achieved using power electronics converters as power system interface. Therefore, the control of these converters is evolving towards flexibility and reliability of generated power in order to meet the utility network requirements during both normal and faulty grid conditions.

1.3 Problem statement

Based on the investigation of grid faults influence onto the control of grid side converter, the goal of this project is to develop advanced control algorithms which would enable the distribution systems to withstand grid faults and, at the same time, to provide a variety of flexible control options of the delivered power. Additionally, the project should contribute with solutions for fast and accurate monitoring of grid variables such as voltage magnitude, grid frequency and line impedance. Besides that, a synchronization algorithm robust to grid disturbances should also be developed.

Fig. 1.1 illustrates a diagram of grid connected power converter highlighting the three major subjects investigated in this thesis. The aims of this research work can be covered by the following statements:

- *identification of grid disturbances influence on the control of grid side converter, and based on this, the development of synchronization and control algorithms which would provide more flexibility of power delivery and improve the behavior of power generation systems when running on grid fault conditions.*
- *development of algorithms capable to monitor fast and accurately the grid variables such as voltage amplitude, grid frequency and line impedance.*

In order to accomplish these goals, the research work has been carried out on three main areas:

Grid synchronization This is an important and necessary feature of grid tied converters control due to the requirement of synchronizing the delivered power with the power system. Under certain circumstances, phase angle jumps may appear in utility network voltage, therefore a fast and accurate phase angle detection is a critical information for reliable power delivery. Grid monitoring is also useful for enabling distributed generation to participate in primary control, in this case a very accurate frequency estimation being necessary. Moreover, during grid faults, especially unbalanced faults, the negative sequence component of grid voltage influences the phase angle detection, leading to oscillations at double fundamental frequency in control variables. Consequently, the development of a phase angle detection algorithm robust to grid disturbances is a necessity.

Grid monitoring Due to the demands regarding operation boundaries in respect to voltage and frequency values published in grid codes, grid monitoring plays an important role in deciding when the generation system should cease energizing the utility network. Alike synchronization algorithm, grid monitoring can be also influenced by grid disturbances, providing erroneous values to the control and, hence, leading to undesired disconnection. Therefore, elaboration of algorithms capable to track accurately the voltage magnitude, grid frequency and line impedance values and yet being robust to grid disturbances is compulsory.

Advanced control Using the information from the algorithms developed for both grid synchronization and grid monitoring, control of grid tied converters should become more robust to disturbances occurring in the power system. The information about utility network parameters can be used to adjust the control variables[2] in order to ensure system stability. Moreover, other methodologies to provide flexible control of generated power, depending on grid voltage conditions, need to be investigated.

1.3.1 Project limitations

As previously described in § 1.2, there is a large variety of distributed generation systems on the market. In most cases, the power conversion is realized by power electronics devices and the existent topologies are numerous. Even though wind turbine applications are getting most attention in this thesis, the outcome of this research should be applicable to a broad

[2]Normally, in the situation of plant variations (utility grid in this case), the gains of controllers should be adjusted in order to keep the system stable.

variety of DPGS. As a consequence, only the grid side converter, represented here by a voltage source inverter (VSI), and supplied by a dc power source is considered in this work, as Fig. 1.1 illustrates. This way, the algorithms investigated would be appropriate for any distribution system interfacing the utility network using a PWM driven dc-ac power converter.

Furthermore, when discussing about influence of grid faults on the control of grid side converter, the focus is set on unbalanced faults rather than balanced ones. Nevertheless, whenever is considered important, influence of balanced faults is also discussed. Additionally, the fault is considered unbalanced in respect to voltage amplitude[3], while the impedance is considered the same on all three phases during the fault. A final interface of the power converter with the power system is considered to be made through a Δy transformer which would not allow the flow of zero sequence component of grid voltage through the power converter.

1.3.2 Tools used

MATLAB®/Simulink® [13] is used as simulation platform on which the algorithms are developed and, in addition, *PLECS* [14] toolbox for Simulink® is used to implement the model of the plant. This is a toolbox for simulating electrical circuits within Simulink® environment and is specially designed for power electronics systems. For experimental implementation of algorithms, dSpace 1103 platform [15] is used due to its high power processing capabilities and well interconnection with Simulink®. The power converter, LC filter and the isolation transformer used in laboratory for evaluating the proposed algorithms are commercial products provided by Danfoss A/S and Axel Aakerman A/S respectively.

1.4 Thesis outline

The thesis is divided in two major parts, i.e. **Part I – Report** and **Part II – Publications**. The first part constitutes a summary report of the work deposed in this thesis and it is structured on several chapters, as follows:

Chapter 1 states the aim of this project, its limitations and the tools and approaches used to reach the goals established at the beginning of the work. Additionally, this chapter gives also a guideline on how this thesis should be used.

Chapter 2 describes the basic aspects of control of grid connected power converters. The state of the art control structures and affiliated controllers are presented in this chapter. Their advantages and disadvantages when used for controlling grid connected power generation systems are highlighted throughout the content of this chapter.

Chapter 3 introduces the first major subject treated in this thesis, i.e. grid synchronization. Influence of grid disturbances on the accuracy of phase angle detection is first analyzed and based on the knowledge gained by this study, two synchronization algorithms robust to any kind of grid disturbances have been developed and discussed in this chapter.

Chapter 4 addresses another main subject of this thesis which is grid monitoring. Based on the experience with synchronization algorithms developed in the previous chapter, these algorithms are further developed to comply with monitoring requirements of both voltage amplitude and grid frequency. Additionally, a large part of this chapter discusses methods for identifying the grid impedance.

[3]The amplitude of three phases is not the same in situation of unbalanced faults and phase jump is also occurring during such conditions.

Chapter 5 describes the possibility of controlling grid connected power converters during grid fault conditions. Using information from grid monitoring and with the help of robust synchronization, several control possibilities during unbalanced fault condition have been developed and described in this chapter. In addition to this, the adaptiveness and robustness of proportional resonant and dead beat current controllers are also addressed in this chapter.

Chapter 6 concludes the thesis and gives some guidelines for further work which would be possible due to the knowledge acquired during this study. Additionally, this chapter highlights the achievements of this thesis. Although it is not the author's privilege to judge the novelty and significance of his own work, it might be worth pointing out the directions on which efforts have been deposed in order to bring novelty and improvements regarding grid interconnection of DPGS.

The second part of the thesis, i.e. **Part II – Publications**, constitutes the backbone of the work deposed in this project. While the report presented in the first part is aiming for giving a brief overview of the work in this project, the research articles composing the second part describe in detail every study developed during the thesis period. Additionally, these articles provide access to relevant simulation and experimental results, validating the implementation of the algorithms discussed.

1.5 How to use this thesis

Fig. 1.2 shows the relation between the introductory report and the publications presented in the second part of the thesis. For keeping consistency of reading and for a better understanding of a particular subject, it is suggested that after approaching a chapter, its affiliated publications suggested by Fig. 1.2 should be read. All technical explanations and results are presented in the

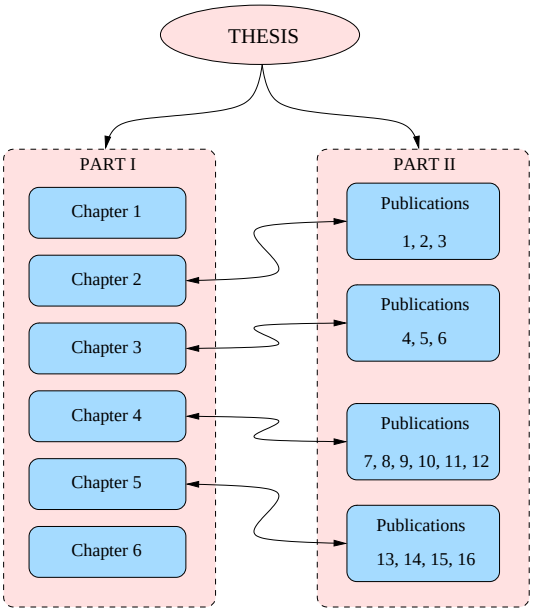

Figure 1.2: *The content of the thesis structured in two parts – introductory chapters and their related publications.*

publications, therefore the chapters composing the first part are limited to the introduction of a particular subject, discussion of problems and comment on the solution and achievements.

Chapter 2

Control of grid connected power converters

This chapter gives a description of state of the art control structures and strategies for grid tied power converters. Implementation of control structure on different reference frames such as stationary *abc*, stationary $\alpha\beta$ and synchronous rotating *dq* frames is first discussed. This is followed by a discussion of control strategies for grid connected power converters. Possible current controllers and their contribution to total harmonic distortion is then presented, followed by an evaluation of controllers during transient operation conditions such as input power variations and grid voltage faults.

2.1 Role of power electronics for DPGS

It has been explained previously that, due to large variety of renewable power sources, power electronics play an important role in energy conversion. As [6–8, 16] show, different power converter topologies are used to interface distributed power generation systems (DPGS) with the utility network. Introduction of power electronics for DPGS provide several advantages such as energy optimal operation by employing a control algorithm to extract the maximum available power. In addition, load control, reduced noise, controllable active and reactive power and improved power quality are just some of the benefits power electronics offer. Because grid interconnection requirements are evolving towards the demand of reliable and controllable power delivery from DPGS, the control structures developed for grid connected power converters should accommodate algorithms that would help DPGS to comply with grid interconnection requirements imposed by the transmission or distribution network operators. As a consequence, power converters and their control play an important role in guarantying reliable power delivery in the future.

In this work, the investigation is limited to control of three phase pulse width modulated (PWM) voltage source inverter (VSI), illustrated in Fig. 2.1. In order to apply to a broad range of DPGS, the input power nature is disregarded, the inverter being powered by a dc power source. As previously explained, this sets some limitations in the project but accounts for a larger number of power generation resources.

2.2 Control structures for grid converters

PWM driven voltage source inverters are largely utilized in drives applications especially where adjustable speed is necessary [17]. Consequently, their control has been detailed studied in the past and three main possibilities to structure it arise: i) *stationary abc reference frame*, ii) *stationary $\alpha\beta$ reference frame* and iii) *synchronous rotating dq reference frame.*

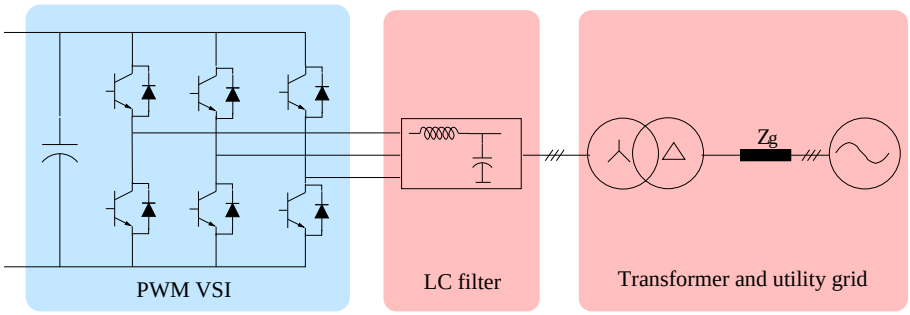

Figure 2.1: *The system considered in this project comprising a PWM driven voltage source inverter, an LC filter, distribution transformer and utility network.*

Due to similarity between drives and grid connected applications, these control structures have been also ported to grid tied inverters constituting the basis for grid converter control. The following paragraphs give a brief description of each of the above control structures, pointing out their main advantages and disadvantages.

2.2.1 Stationary *abc* control structure

For stationary *abc* frame control, the control structure is implemented in *abc* frame, hence giving the possibility to control independent each phase current. Three controllers are necessary in this case, however, the filter and transformer connection should be considered in case each phase current is to be controlled individually. Since in case of star connected load, the sum of the three currents has to be zero, additional caution has to be payed to this fact when individual current control is desired. The cross coupling between phases has to be accounted in the design of the controller, usually leading to a more complex controller. Controllers such as hysteresis and dead beat are normally employed for current regulation [18–23] in *abc* frame. A detailed analysis of hysteresis controller design regarding the connection of the load is presented in [18]. In addition to this, an adaptive hysteresis band needs to be implemented in order to obtain a quasi-constant switching frequency. These issues, together with the necessity of high sampling frequency constitute the disadvantages when designing and implementing hysteresis controller. However, its fast dynamics is a strong argument for implementing it into a grid connected power generation system.

Belonging to the family of predictive controllers, dead-beat controller is widely employed for sinusoidal current regulation of different applications due to its high dynamic response [24–31]. In order to achieve best reference tracking, the working principle of dead-beat controller is to calculate the derivative of the controlled variable (grid current in this case) in order to predict the effect of the control action. The controller is developed on the basis of filter and grid model, hence being sensitive to model and parameter mismatch. However, robustness to parameters discordance in a relative large range can be achieved using different approaches as presented in [28, 32–34].

Portability of other linear controllers such as proportional-integral (PI) controller to *abc* reference frame has also been investigated in [35, 36]. As a result, complex controller matrix due to the off diagonal terms owed to the cross coupling between phases has been obtained, constituting a serious drawback when implementing PI controllers in *abc* frame. Other type of controllers employed for current regulation in *abc* frame are discussed in [37, 38]. Apart from hysteresis and PI controllers, predictive, neural network and fuzzy logic based controller are

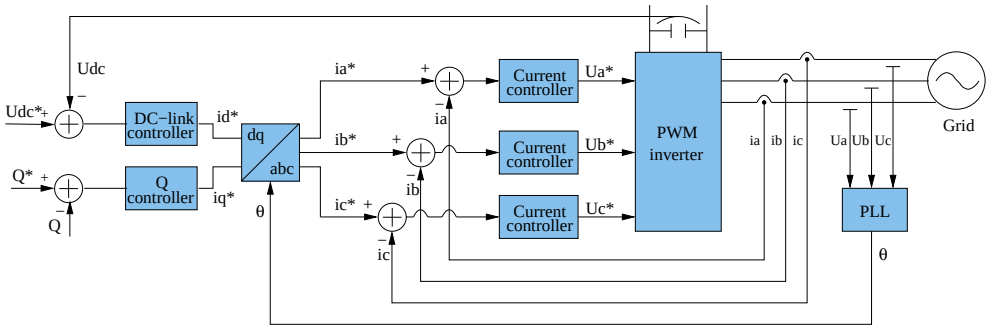

Figure 2.2: *Control structure implemented in stationary* abc *reference frame using three current controllers.*

described there.

In case of *abc* frame control, a three phase synchronization system as depicted in Fig. 2.2 is normally used for generating the phase angle necessary in control, however three individual single phase synchronization systems could also be implemented, as Publication 3 discusses. In this case, each current can be controlled in relation to its corresponding voltage and if the neutral point is connected to the middle point in dc-link, the three phase system would behave as three independent single phase systems.

2.2.2 Stationary $\alpha\beta$ control structure

In situation when the control structure is implemented in *stationary* $\alpha\beta$ *frame*, a transformation module (2.1b) is necessary to transfer the feedback variables into a stationary quadrature system $\alpha\beta$. Compared to above control structure, the advantage of implementing the control in $\alpha\beta$ stationary frame is that the number of controlled variables is reduced from three to two, hence necessitates less computational power when implemented in digital signal processors or micro-controllers. In addition, information about filter/transformer connection is not necessary to be accounted when designing the controllers, like is the case for *abc* reference frame control. Consequently, independent control of each phase current is not possible using this control structure.

$$U_{\alpha\beta} = \begin{bmatrix} U_\alpha & U_\beta \end{bmatrix}^T = [T_{\alpha\beta}]\, U_{abc} \tag{2.1a}$$

$$[T_{\alpha\beta}] = \sqrt{\frac{2}{3}} \begin{bmatrix} 1 & -\frac{1}{2} & -\frac{1}{2} \\ 0 & \frac{\sqrt{3}}{2} & -\frac{\sqrt{3}}{2} \end{bmatrix} \tag{2.1b}$$

Inspecting (2.1b) may be noticed that the transformation in $\alpha\beta$ reference frame is possible without the information of phase angle, therefore, depending on the control strategy adopted, the phase angle signal illustrated in Fig. 2.3 may not be necessary.

Due to limitations of PI controllers when controlling sinusoidal quantities, a new controller type denoted *proportional-resonant* (PR) has gained large popularity lately, especially for grid connected converters [39–43]. Another advantageous feature of PR controller is the possibility of implementing harmonic compensator based on generalized integrators [42], without interfering with controller dynamics, achieving a high quality delivered current.

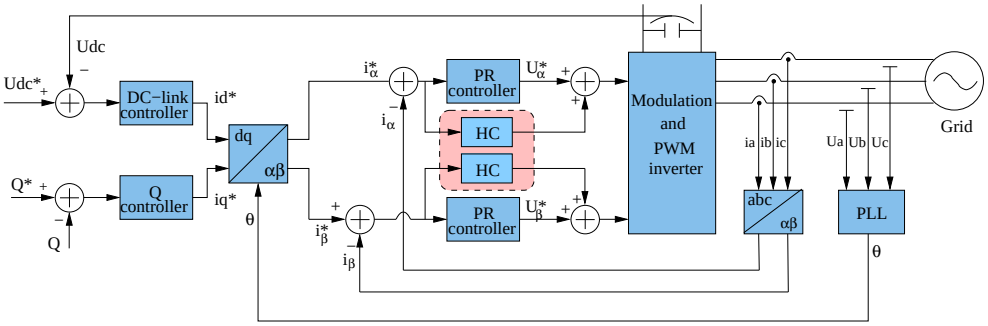

Figure 2.3: *Structure of control implemented in $\alpha\beta$ stationary reference frame using PR controllers for current regulation.*

2.2.3 Synchronous rotating reference frame

In case of *synchronous rotating reference frame*, also denoted as *dq* frame, the control is implemented in a reference frame which rotates with the same frequency as the grid angular frequency. In order to transform the feedback variables in this reference frame, the phase angle of grid voltage is necessary (2.2b), constituting a disadvantage of this structure. However, the control variables transformed in *dq* frame appear as dc quantities, hence facilitating easier control and signal processing, e.g. filtering. In this situation, employment of PI controllers for current regulation is appropriate, however, as Fig. 2.4 illustrates, cross-coupling terms and grid voltage feed-forward may be necessary in order to obtain best results.

$$U_{dq} = \begin{bmatrix} U_d & U_q \end{bmatrix}^T = [T_{dq}]\, U_{\alpha\beta} \tag{2.2a}$$

$$U_{dq} = \begin{bmatrix} cos\theta & sin\theta \\ -sin\theta & cos\theta \end{bmatrix} U_{\alpha\beta} \tag{2.2b}$$

Publication 1 on page 73 extends the implementation of current controllers in different reference frames. The transfer functions of proportional-integral (PI), proportional-resonant (PR), dead-beat (DB) and hysteresis controllers are presented. Possibility of implementing the same controller in more than one reference frame is also addressed by showing the implementation of PI controller in both *dq* rotating reference frame and *abc* stationary frame. In addition to the implementation of controllers, different schemes for harmonic compensation, depending on the reference frame, is also discussed in that publication. It has been shown that it is less complicated to implement harmonic compensator (HC) in stationary reference frame such as $\alpha\beta$ or *abc* using generalized integrators (GI) than implementation in synchronous rotating reference frame where several low-pass and high-pass filters need to be used. Noticeable is the fact that the HC can be totally decoupled from the current controller, hence the HC can be implemented in a reference frame and the current controller in a different one.

2.3 Control strategies for grid connected power converters

Normally, multiple cascaded loops are used to control PWM driven VSI converters. As illustrated in Figs. 2.2, 2.3 and 2.4, the most common strategy is the dc-link voltage control cascaded with an inner current loop control [44–50]. When implemented in a reference frame other than *abc*, control can be oriented to the grid voltage vector or the virtual flux vector [51, 52]. In the situation when reactive power control is demanded at the point of common coupling, a reactive

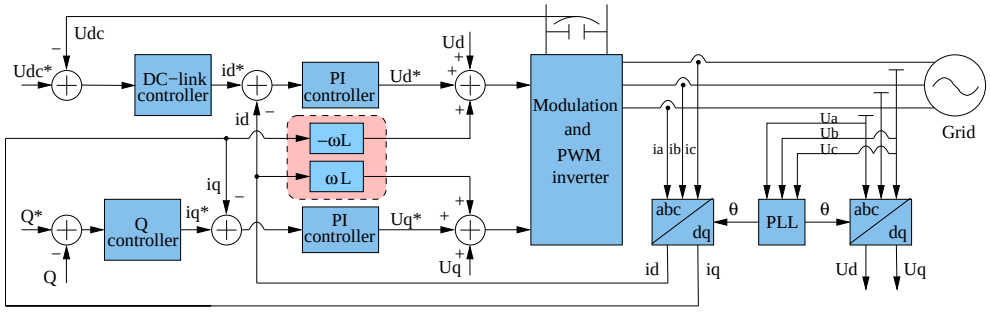

Figure 2.4: *Structure of control implemented in synchronous rotating reference frame using PI controllers for current regulation.*

power controller can be used whereas, in case unity power factor is a must, the reactive current reference i_q^* can be set to zero, hence no reactive power controller is necessary. A third level loop controlling the grid frequency and the grid voltage amplitude can also be implemented in case of DPGS, providing frequency and voltage control at the point of common coupling.

Moreover, in the above strategies, the dc-link voltage control can be replaced by an active power control [53–55] supposing that an active and reactive power reference is supplied to the grid side converter. In addition, direct power control [51, 56, 57] is another possible control technique which can be applied to PWM driven power converters.

2.4 Current controllers for grid converters

This section gives an overview of controllers to be used for current regulation for grid connected power converters. The discussion is limited to the contribution of linear controllers (proportional-integral PI, proportional-resonant PR and dead-beat DB) to grid current harmonic pollution. Additionally, the behavior of these controllers during transient operation conditions such as input power variations and grid voltage faults is also addressed.

Publication 2 on page 87 addresses the behavior of current controllers on three important issues for grid connected power converters: i) *total harmonic distortion of grid current* ii) *input power variation* and iii) *grid voltage fault.*

The PI controller is tested using two sets of implementation. First, it is implemented in dq reference frame using the transfer function in eq. (2.3) below:

$$G_{PI}^{(dq)}(s) = \begin{bmatrix} K_p + \frac{K_i}{s} & 0 \\ 0 & K_p + \frac{K_i}{s} \end{bmatrix} \tag{2.3}$$

where K_p is the proportional and K_i is the integral gain of the controller. A structure of dq control involving cross coupling and feed forward of the grid voltages as depicted in Fig. 2.4 is used. Since grid voltage feed-forward is employed in this control structure, the dynamics of the control is expected to be high during grid voltage fluctuations. Every deviation of the grid voltage amplitude will be reflected into the d- and q-axis component of the voltage, leading to a fast response of the control system.

The second implementation of PI controller is done in abc stationary reference frame using

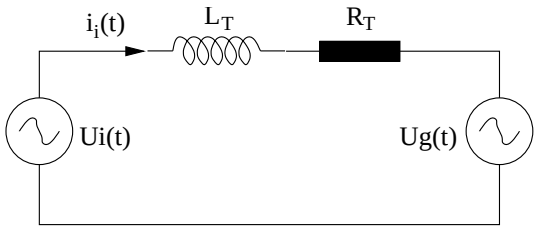

Figure 2.5: *Representation of single phase circuit used to derived the dead beat controller equation where* $L_T = L_i + L_g$ *and* $R_T = R_i + R_g$.

the matrix of the controller derived in [36] and shown in (2.4):

$$G_{PI}^{(abc)}(s) = \frac{2}{3} \cdot \begin{bmatrix} K_p + \frac{K_i s}{s^2+\omega_0^2} & -\frac{K_p}{2} - \frac{K_i s+\sqrt{3}K_i\omega_0}{2\cdot(s^2+\omega_0^2)} & -\frac{K_p}{2} - \frac{K_i s-\sqrt{3}K_i\omega_0}{2\cdot(s^2+\omega_0^2)} \\ -\frac{K_p}{2} - \frac{K_i s-\sqrt{3}K_i\omega_0}{2\cdot(s^2+\omega_0^2)} & K_p + \frac{K_i s}{s^2+\omega_0^2} & -\frac{K_p}{2} - \frac{K_i s+\sqrt{3}K_i\omega_0}{2\cdot(s^2+\omega_0^2)} \\ -\frac{K_p}{2} - \frac{K_i s+\sqrt{3}K_i\omega_0}{2\cdot(s^2+\omega_0^2)} & -\frac{K_p}{2} - \frac{K_i s-\sqrt{3}K_i\omega_0}{2\cdot(s^2+\omega_0^2)} & K_p + \frac{K_i s}{s^2+\omega_0^2} \end{bmatrix} \tag{2.4}$$

The controller matrix in this case gets complex due to the off-diagonal terms owed to the cross-coupling between the phases.

Furthermore, the proportional-resonant controller is implemented in $\alpha\beta$ stationary reference frame using the following transfer function of the controller:

$$G_{PR}^{(\alpha\beta)}(s) = \begin{bmatrix} K_p + \frac{K_i s}{s^2+\omega^2} & 0 \\ 0 & K_p + \frac{K_i s}{s^2+\omega^2} \end{bmatrix} \tag{2.5}$$

where: ω is the resonance frequency of the controller, K_p is the proportional gain and K_i is the integral gain of the controller.

The equation of predictive dead beat (DB) controller can be derived using Kirchhoff's law on the single phase circuit illustrated in Fig. 2.4. In this case, the equation for the current through the inverter i_i (controlled current) can be expressed as:

$$\frac{di_i(t)}{dt} = -\frac{R_T}{L_T} i_i(t) + \frac{1}{L_T}(U_i(t) - U_g(t)) \tag{2.6}$$

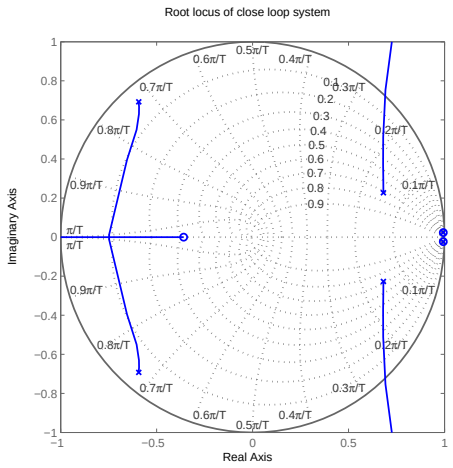

Figure 2.6: *Root locus method for tuning the gains of linear controllers.*

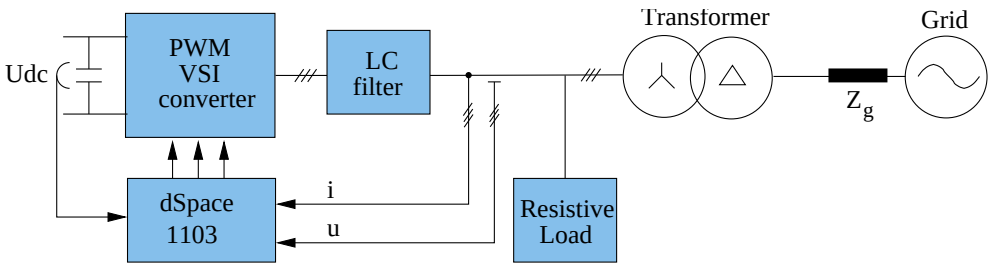

Figure 2.7: *Schematic of the laboratory setup connected to a grid simulator through a Δy transformer and having a resistive load.*

where L_T is the total inductance and R_T is the total resistance upstream of the grid converter, $U_i(t)$ and $U_g(t)$ is the inverter and grid voltage respectively. Solving this, the controller equation can be derived as in a discrete manner:

$$G_{DB}^{(abc)} = \frac{1}{b} \cdot \frac{1 - az^{-1}}{1 - z^{-1}} \tag{2.7}$$

where a and b are denoted as:

$$a = e^{-\frac{R_T}{L_T}Ts}; \qquad b = -\frac{1}{R_T}\left(e^{-\frac{R_T}{L_T}Ts} - 1\right) \tag{2.8}$$

Mentionable here is the fact that no harmonic compensator has been implemented in neither of the cases. Tuning of PI and PR controllers is made using root locus method shown in Fig. and detailed described in § V in Publication 2, while the parameters of dead-beat controller are calculated using eq. (2.8).

For evaluation of controllers, an experimental setup as illustrated in Fig. 2.7 has been used. The setup comprises the power converter, controlled by a dSpace 1103 digital controller board and powered by a controllable dc power supply, which is connected through an LC filter and a transformer to a programmable ac source. A resistive local load has been introduced due to the limitation of ac source to sink power. The behavior of controllers during normal and transient operation conditions is explained in the following sections.

2.4.1 Grid current harmonic distortion

Although Publication 1 describes the modalities for implementing harmonic compensators for both PI and PR controllers, Publication 2 treats the contribution of the controller itself (without the harmonic compensator) to the total harmonic distortion. In addition, the programmable ac source which emulates the grid has been programmed to provide ideal sinusoidal voltage, hence the harmonics present it the grid current waveform are generated by the current controller and system non-linearity.

The results in case of harmonic distortion test are presented in Fig. 2.8 and Fig. 2.9 respectively. As it can be observed, the spectra is similar for PI and PR controllers, while more harmonics but with lower magnitude are present in case of dead-beat control as illustrated in Fig. 2.9(b). The total harmonic distortion (THD) of grid current has been measured using a Voltech 3000 power analyzer and the final values are summarized in Table 2.1. Based on these results, it can be concluded that all controllers generate a fairly low current distortion, PI controller implemented in *abc* frame having the best performance. Although the results presented in Table 2.1 have low values, when grid voltage has a considerably high content of low order

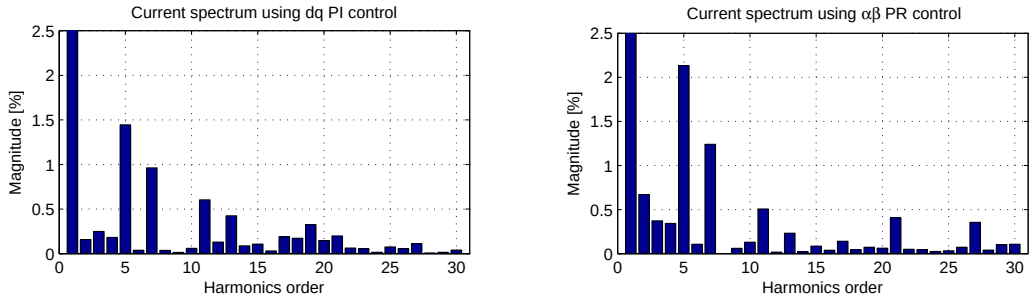

(a) (b)

Figure 2.8: *Harmonic spectrum of the grid current in the case of: (a) dq PI control and (b) $\alpha\beta$ stationary control using PR controller.*

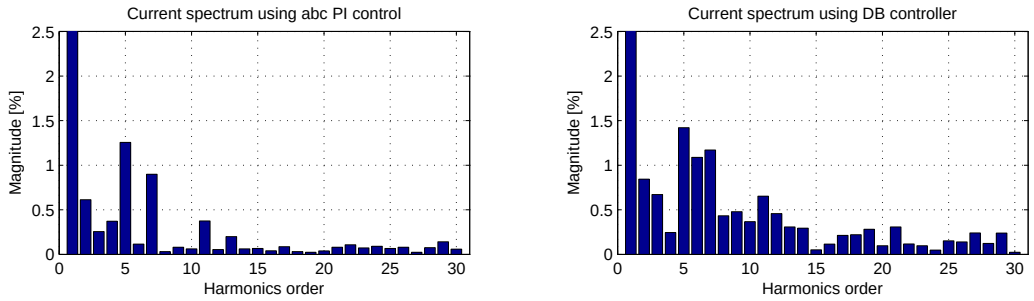

(a) (b)

Figure 2.9: *Harmonic spectrum of the grid current in the case of: (a) equivalent of PI used in abc frame and (b) dead beat control.*

harmonics (5^{th}, 7^{th}, etc.), these harmonics will propagate in the output current, therefore a harmonic compensator might be necessary in order to keep the THD below the requested 5%, according to [60].

2.4.2 Transient operation conditions

In addition to total harmonic distortion of grid current, the investigated controllers have been also tested in transient operation conditions. First test simulates the situation of increase in input power by instantly increasing the current reference from 4 to 6 A. As Fig. 2.10 and Fig. 2.11 illustrate, all controllers have good dynamics, being able to track closely the current

Current controller	THD generated
PI controller (*dq* frame)	1.77 %
PR controller	2.60 %
Dead-beat controller	2.40 %
PI controller (*abc* frame)	1.72 %

Table 2.1: *Summary of total harmonic distortion generated by each considered controller when running on ideal voltage conditions.*

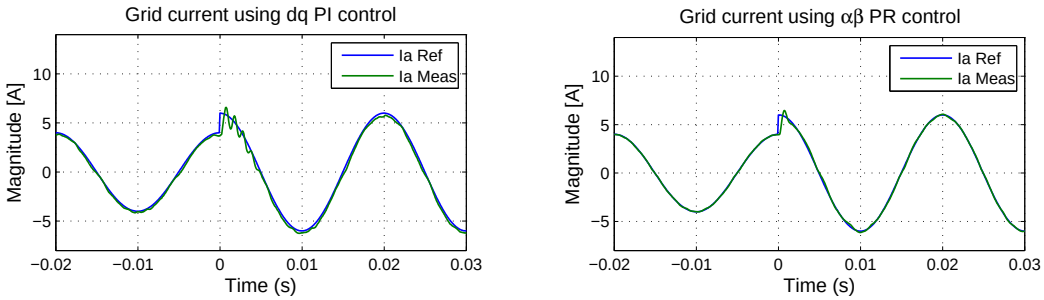

(a) (b)

Figure 2.10: *Dynamics of the controllers in the case of 2A current reference step: (a) PI controller implemented in dq frame and (b) PR controller in $\alpha\beta$ stationary frame.*

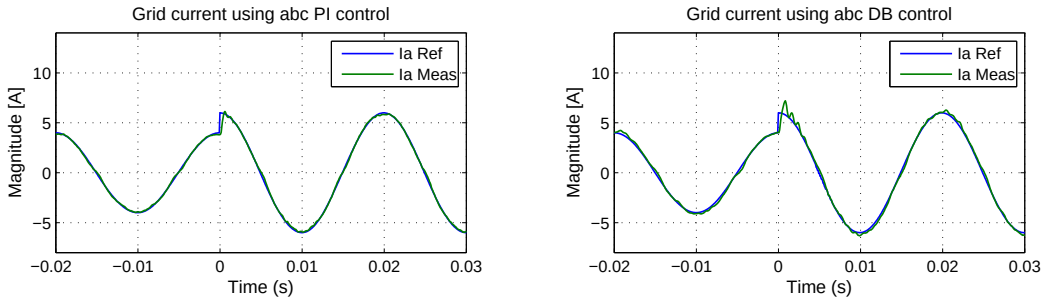

(a) (b)

Figure 2.11: *Dynamics of the controllers in the case of 2A current reference step: (a) equivalent of PI in abc frame and (b) DB controller in abc frame.*

reference, without high overshoot and oscillations, during such transient condition, with PR and PI implemented in *abc* having the best performance.

The second test for transient conditions simulates the situation of a grid fault. In this case, the ac voltage source emulating the grid has been programmed to produce 0 V on one phase while keeping the other two phases at nominal value. The Δy transformer connected in between the grid converter and the power source plays an important role as [58] reports, preventing the voltage to go to 0 V on the secondary side. Consequently, this situation is more convenient from the grid converter point of view, however, attention should be paid to the fact that large unbalance occurs during such a voltage fault. In order to keep a clean synchronization angle during the fault, a synchronization algorithm as described in Publication 5 has been used during this test. The synchronization algorithm is based on a Phase-Locked Loop (PLL) and a pre-filter which separates the positive and negative sequences of grid voltage. Only the positive sequence component is used as input in the PLL, hence the synchronization angle is not distorted due to unbalance conditions of the utility grid.

The response of controllers in such situation is depicted in Fig. 2.12 and Fig. 2.13. A large overshoot appears in case of using PR controller mainly due to the lack of grid voltage feed-forward loop. Similar behavior is noticed in case PI controllers implemented in *abc* frame are used, highlighting the importance of voltage feed-forward loop in such situation. The best behavior in case of grid voltage fault is noted when dead-beat controller is used. A detailed description of the behavior of current controllers used for grid connected converters can be

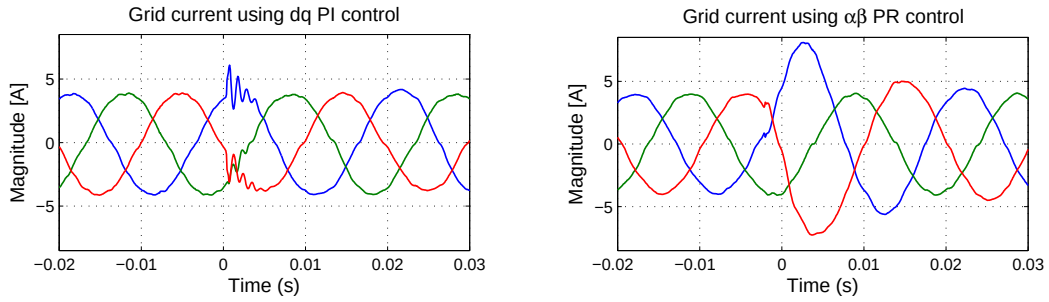

(a) (b)

Figure 2.12: *Response of the controller in the case of single phase fault: (a) PI controller implemented in dq frame and (b) PR controller in stationary frame.*

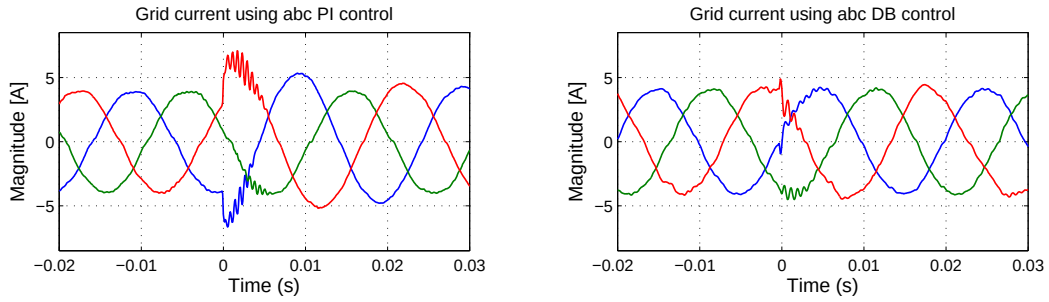

(a) (b)

Figure 2.13: *Response of the controller in the case of single phase fault: (a) equivalent of PI in abc frame and (b) DB controller in abc frame.*

found in Publication 2.

2.5 Summary

This chapter gives a brief insight in control of grid connected power converters. Control structures implemented in stationary *abc*, stationary $\alpha\beta$ and synchronous rotating *dq* reference frame have been described and the utilization of different controllers suitable for these frames have been addressed. Due to reduced number of necessary current controllers and because it can also be implemented without the grid voltage phase angle information, the most convenient control structure for implementation appears to be stationary $\alpha\beta$ reference frame.

In addition, the chapter discusses the performance of different current controllers during steady state and transient operation conditions. In steady state conditions, the contribution of the controller to the total harmonic distortion of grid current is investigated. Although harmonic compensator can be implemented in each case, solely the controllers contribution to the current THD has been addressed. In such situation, the lowest distortion has been achieved using PI controller implemented in *abc* reference frame.

For testing the controllers in transient operation conditions, two situations are considered. First, the performance of controllers during input power variations is pursued and the obtained results show a good tracking capability of all investigated controllers. Second, the response of

the controllers to a grid voltage fault has been investigated and the importance of grid voltage feed-forward in case of linear controllers for achieving satisfactory results has been highlighted.

Chapter 3

Grid synchronization

This chapter highlights the influence of grid disturbances onto the synchronization algorithm and the necessity of developing a robust synchronization system for grid connected power converters. The state of the art synchronization algorithms are first introduced, followed by the influence of voltage disturbances on the accuracy of phase angle detection. The necessity of extracting the positive sequence component and its usage as input for the synchronization algorithm in order to provide a clean synchronization angle is highlighted. Consequently, two robust synchronization systems have been developed and tested against severe grid distortions and the results presented validate their suitability for grid connected power generation systems.

3.1 Background and state of the art

Initially, synchronization of delivered power with the utility network was a basic requirement for interconnecting distributed power generators with the power system. This requirement is still valid for photovoltaic systems [59–61] but lately, in case of wind turbines, reactive power control at the point of common coupling is requested [62,63]. Consequently, DPGS should accommodate an algorithm capable of detecting the phase angle of grid voltage in order to synchronize the delivered power. Moreover, the phase angle plays an important role in control, being used to transform the feedback variables to a suitable reference frame in which the control structure is implemented. Hence, phase angle detection have a significant role in control of grid connected power generation systems.

Numerous research works are reporting several algorithms capable of detecting the grid voltage phase angle, i.e. zero crossing detection, the use of `arctan` function or phase-locked loop (PLL) technique.

Zero crossing detection [64] is a simple method for estimating the phase angle of utility grid by means of detecting the zero crossings of voltage waveform. Owing to the fact that grid voltage is sinusoidal, the maximum number of zero crossings in a period is three, being no information about the evolution of phase angle for a half of fundamental period. As a consequence, this method has low dynamics, proving itself unsuitable for applications where continuously accurate phase angle detection is necessary.

Arctan – another solution for detecting the phase angle of grid voltage is the use of `arctan` function applied to voltages transformed into a Cartesian coordinate system such as stationary $\alpha\beta$. This method has been used in drives applications [44], for transforming feedback variables to a reference frame suitable for control purposes. However, when used in conjunction with grid connected power converters, additional filtering is necessary in order

to obtain a clean synchronization signal in situation when distortions are present in the voltage waveform.

Phase-locked loop (PLL) is a phase tracking algorithm widely applied in communication technology [65, 66], being able to provide an output signal synchronized with its reference input in both frequency and phase. Although its main application is in communication systems, PLL is also recognized as an algorithm suitable for systems connected to utility network, due to the fact that it can facilitate information about grid voltage amplitude, grid frequency and the phase angle at the point of common coupling (PCC).

All the above methods are able to provide an accurate synchronization angle under ideal voltage conditions. However, grid voltage may experience deviations from its normal waveform, due to the presence of harmonics, unbalance and even notches. Such anomalies have a serious affect on the phase angle detection algorithms, therefore further considerations have to be done in order to obtain a robust synchronization algorithm. Next section discusses the influence of some grid disturbances on the above listed synchronization algorithms.

3.2 Influence of voltage disturbances

3.2.1 Voltage faults and unbalance

Large number of research works reported a negative influence of voltage faults, especially unbalanced faults, on the synchronization algorithm, leading to estimation of an oscillatory phase angle signal. With regard to voltage magnitude, grid faults can be divided in two major categories [58]:

- balanced faults – when all three grid voltages register same amplitude drop/swell, hence the system is still balanced during the fault
- unbalanced faults – in case one or two phases experience amplitude drop/swell and consequently the system is becoming unbalanced. In this case, the negative sequence component of grid voltage appears, having a large influence on synchronization and control of grid connected power generation systems.

Regarding the above described synchronization algorithms, the influence of voltage amplitude on the accuracy of phase angle detection can be minimized by normalization to the nominal value of grid voltage amplitude. However, the appearance of negative sequence component during unbalanced grid faults has a significant effect on the synchronization method [67–77]. In a situation when grid voltages are severely unbalanced like is the case illustrated in Fig. 3.1(a), positive and negative sequence components appear as illustrated in Fig. 3.1(b). In this case, the grid voltage locus is defined by an ellipse rather than a circle. However, the voltage vector can be decomposed into a positive sequence component given by V_s^+ which rotates with the same angular frequency and in the same direction as V_s does; and a negative sequence component V_s^- which rotates in opposite direction of V_s. The module of grid voltage vector $\mathbf{v}_s$ experiences second order oscillations given by the third term in Eq. (3.1):

$$|\mathbf{v}_s| = \sqrt{\underbrace{(V_s^+)^2 + (V_s^-)^2}_{dc\ component} + \underbrace{2V_s^+V_s^-cos(2\omega t + \phi)}_{2\omega\ oscillations}} \tag{3.1}$$

Considering a dq reference control structure, the positive sequence component appears as dc quantity in dq^+ frame rotating in the same direction with grid angular frequency, while negative

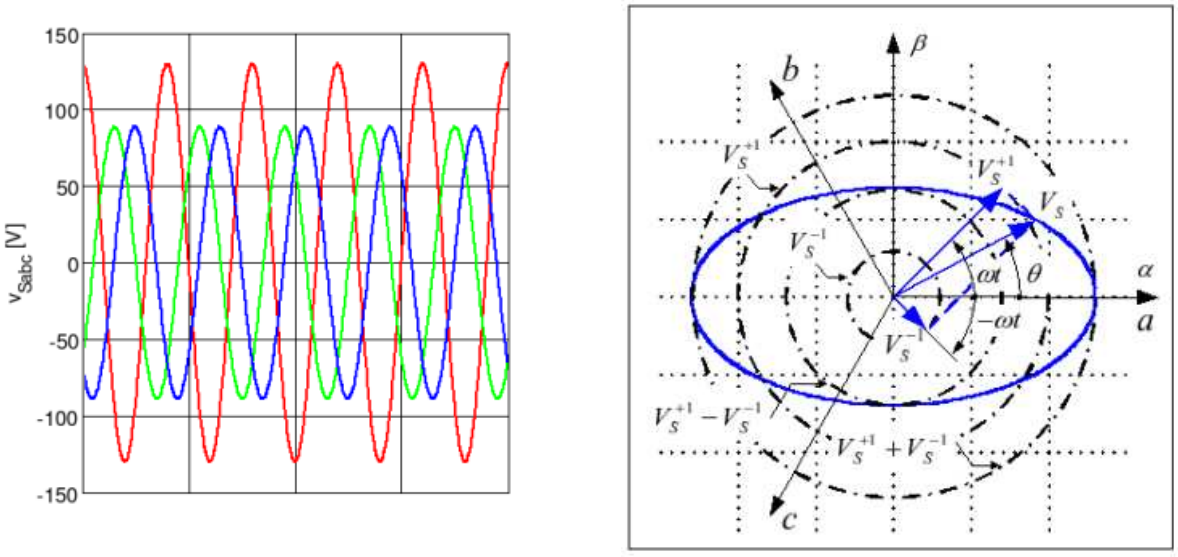

(a) (b)

Figure 3.1: *(a) Highly unbalanced grid voltages and (b) positive (V_s^{+1}) and negative (V_s^{-1}) sequence components of voltage (V_s) represented in stationary reference frame.*

sequence component appears as double frequency term. On the contrary, in the dq^- frame, rotating in opposite direction with the grid angular frequency, positive sequence component appears as double frequency quantity while the negative one appears as dc component.

As it is emphasized in Publication 5 on page 117, the presence of negative sequence has a negative impact on phase angle detection. Fig. 3.2 illustrates the phase angle estimation of conventional *dq PLL* (as depicted in Fig. 2(a) in Publication 5) in case of a fault situation. As shown in Fig. 3.2(a), a severe unbalanced grid fault occurs at time 0.3 seconds during which the negative sequence component rises considerably. Fig. 3.2(b) illustrates the synchronization angle produced by *dq PLL* while Fig. 3.2(c) shows the error between the real phase angle value and the one estimated by the PLL system. As it can be noticed, large oscillations at double fundamental frequency are present in both signals. The synchronization signal shown in Fig. 3.2(b) is directly contributing to the creation of current reference, hence is leading to non-

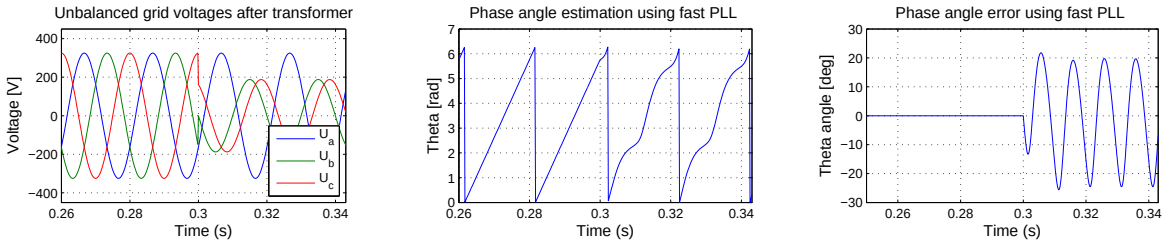

(a) (b) (c)

Figure 3.2: *Phase angle estimation during single phase grid fault: (a) voltages after the Δy transformer, (b) conventional PLL output and (c) the phase error between the real grid phase and estimated one by the PLL.*

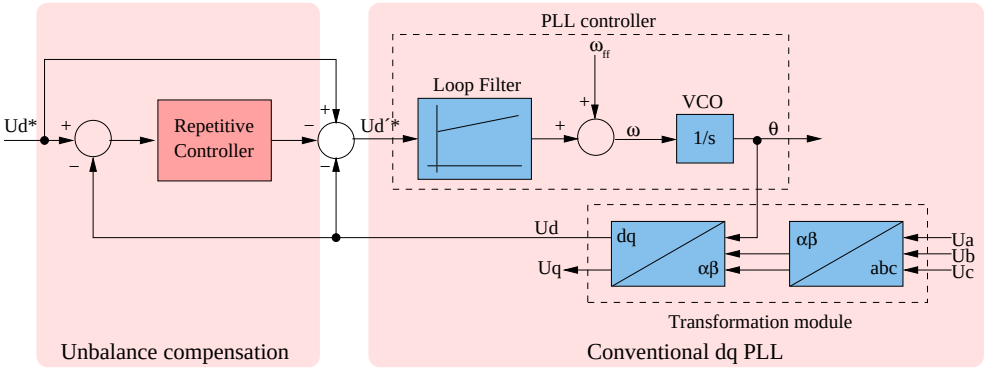

Figure 3.3: *Structure of proposed PLL system using a repetitive controller to eliminate the unbalance effect.*

sinusoidal current reference and thus to a poor quality of delivered power. As a consequence, a solution to mitigate the influence of negative sequence is necessary in order to obtain a clean synchronization signal for control.

Due to its low dynamics behavior, the zero crossing method is not further discussed in this work. In situation when `arctan` function is applied to sinusoidal waveforms, like is the case of $\alpha\beta$ coordinates, band pass filtering seems to be the appropriate solution [78, 79]. However, other filtering possibilities have been investigated in [72] where low pass, notch, space vector and Kalman filters are compared in respect to system response to a step phase angle deviation. A more advanced algorithm based on weighted least-squares is presented in [69] while an interesting approach based on employment of a PI controller to compensate for the delay introduced by filtering of $\alpha\beta$ voltages is introduced in [80].

3.2.2 Notches and higher order harmonics

Generally, notches and higher order harmonics (5^{th}, 7^{th}, etc.) do not represent a real problem[1] in phase angle detection if filtering techniques designed to combat unbalance are used. As such filters are having band pass properties for fundamental frequency or have a low cut off frequency to attenuate the double frequency oscillations, notches and higher order harmonics will also be filtered out, hence their influence on the phase angle estimation is diminished.

Publication 4 discusses the robustness of the above synchronization algorithms during grid voltage disturbances. Implementation of filtering techniques as well as a method to design slow dynamics PLL are detailed described. Based on presented experimental results for different grid disturbances, filtering of grid voltage prior phase angle detection is a necessity. However, precaution has to be payed due to the risk of creating a slow dynamics synchronization system. Although, filtering improves the behavior of synchronization algorithms when running on grid disturbances[2], does not provide robustness for all algorithms over a broad variation of grid disturbances. As a consequence, further research is necessary in order to obtain a synchronization algorithm having high dynamics and being robust to any kind of grid disturbance.

[1] Except for zero crossing detection method which may be seriously influenced by notches appearing at the moment of zero crossing.

[2] Table II in Publication 4 gives an overview of algorithms robustness to different grid disturbances.

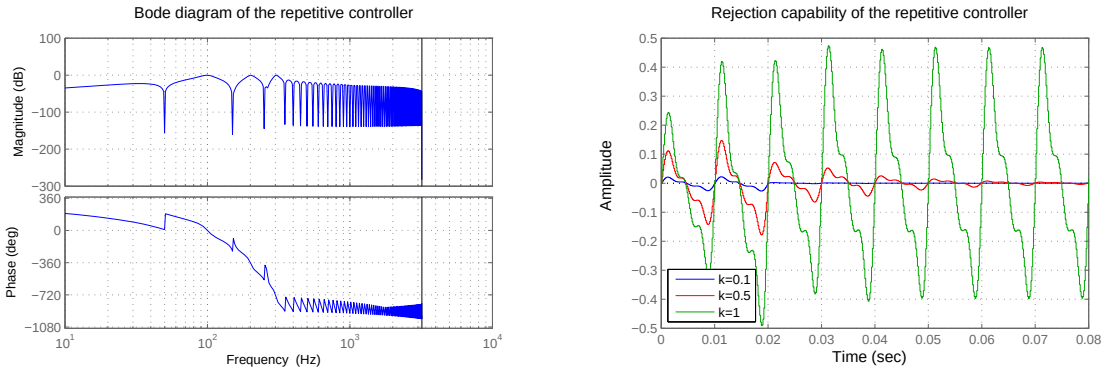

(a) (b)

Figure 3.4: *(a) Bode plot and (b) rejection capability (step in the error signal) for different gain values of repetitive controller.*

3.3 Proposed robust synchronization algorithms

As mentioned previously, unbalanced grid situations, especially unbalanced faults, are most challenging situations for synchronization algorithms, therefore the proposed solutions try to avoid the influence of the unbalance on the phase angle estimation. In other words, decomposition of grid voltage into its positive and negative sequence components and the allocation of positive sequence only as input to the locking loop would provide a synchronization system which will synchronize with the positive sequence component of grid voltage. This is advantageous because during grid conditions when unbalance does not exists, the grid voltage contains only the positive sequence component, hence the synchronization angle is identical for both grid voltage and its positive sequence. On the other hand, during unbalanced grid conditions, the algorithm would be able to provide a clean synchronization angle synchronized with the positive sequence component of grid voltage. This angle can be further used in control in order to provide sinusoidal current reference during unbalanced grid conditions and providing ride through capabilities of grid connected power generation systems.

Research towards a robust synchronization system which shall overcome every type of grid disturbance has been carried out on two directions. The first approach mitigates the effect of negative sequence in dq reference frame by means of a repetitive controller as discussed in Publication 5, while the second approach, detailed in Publication 6, uses a band pass filter based on second order generalized integrator (SOGI) to extract the voltage positive sequence component in $\alpha\beta$ reference frame.

3.3.1 Robust synchronization algorithm designed in synchronous rotating reference frame

The algorithm detailed in Publication 5 employs a repetitive controller to mitigate the effect of negative sequence onto the phase locking loop. As illustrated in Fig. 3.3, the repetitive controller is placed on the d-component of grid voltages and contributes to the new reference entering in the PLL controller. As Eq. (1) (recalled here as Eq. (3.2)) and Fig. 4 in Publication 5 show, the repetitive controller is based on Discrete Fourier Transform (DFT) algorithm, having in addition a gain and a feedback loop.

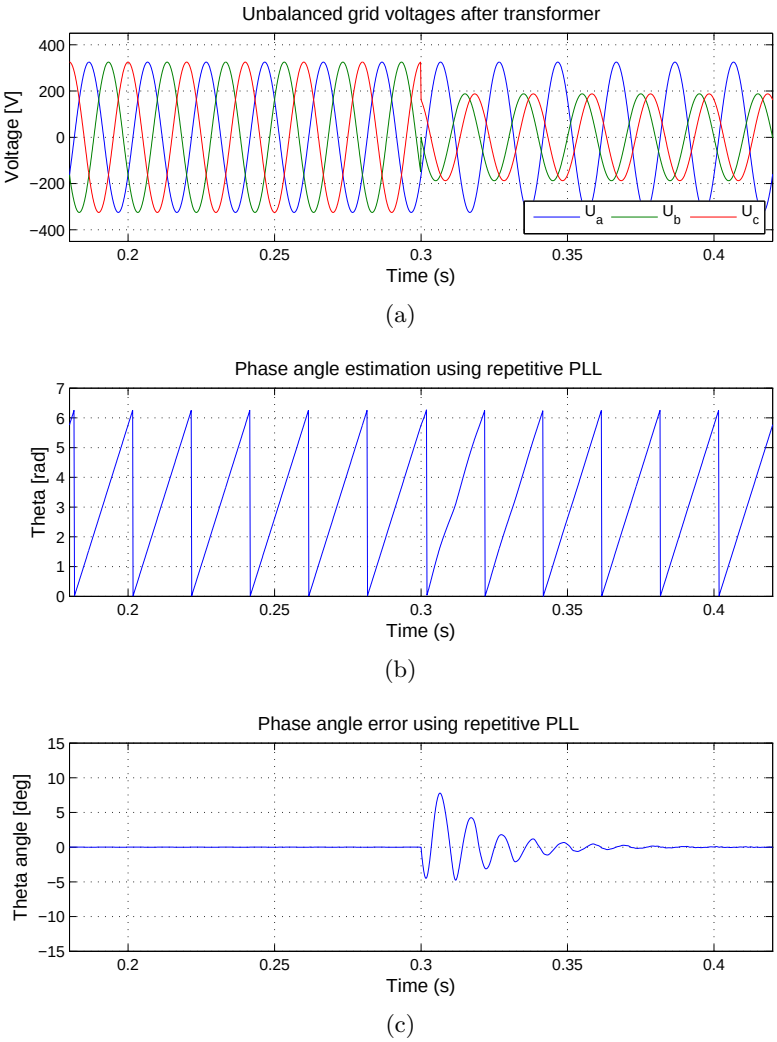

Figure 3.5: *Behavior of the proposed PLL based on repetitive controller under single phase fault at the PCC: (a) voltages after transformer, (b) repetitive PLL output and (c) the phase error between the real grid phase and estimated one by the proposed PLL.*

$$F_{DFT} = \frac{2}{N}\sum_{i=0}^{N-1}\left(\sum_{k\in N_h} cos\left[\frac{2\pi}{N}h(i+N_a)\right]\right)z^{-i} \tag{3.2}$$

The main objective of repetitive controller is to eliminate the influence of negative sequence component on the locking loop. As Fig. 3.4(a) illustrates, the behavior of the repetitive controller is similar to that of a bandpass filter designed to allow only even harmonics to pass through. Has been noticed that better results are obtained if the multiples of the second harmonic (4^{th} and 6^{th}) are also selected for compensation. Noticeable in Fig. 3.4(a) is the unity gain for the harmonics selected for compensation while the other harmonics are heavily filtered. Hence, the even harmonics are amplified due to the summation feedback inside the controller and they are passing through to contribute to the new reference for the PLL controller. These harmonics are then subtracted from the waveform of d-component voltage, resulting in a clean dc component which constitutes the input into the locking loop. Definitely, introducing the repetitive controller

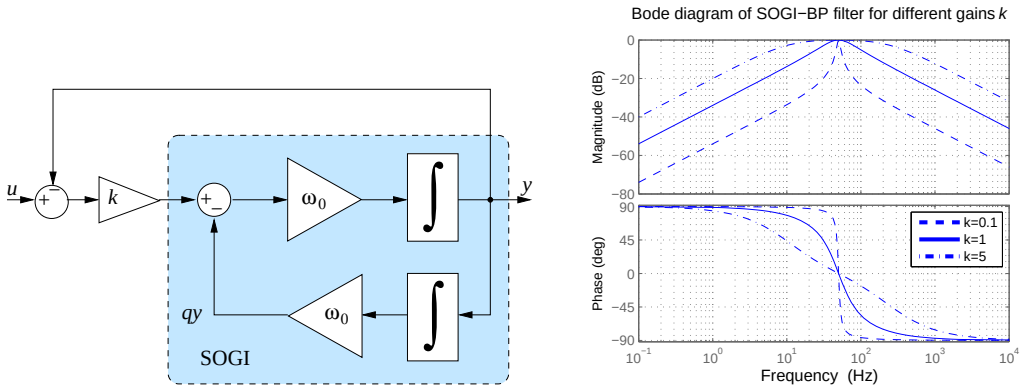

(a) (b)

Figure 3.6: *(a) Structure of band pass filter based on SOGI and (b) Bode diagram of this filter.*

in the PLL structure changes the system dynamics and its stability. Publication 5 discusses the influence of repetitive controller gain on these two issues. A final solution having fast dynamics, yet able to cancel out the influence of severe unbalance conditions has been developed.

Fig. 3.5 shows experimental results illustrating the behavior of proposed PLL system using repetitive controller in case of unbalanced fault. A clean synchronization angle is produced by the proposed PLL, no matter what the grid condition is, as depicted in Fig. 3.5(b). The phase angle error is quickly reduced to zero by the proposed algorithm, soon after the unbalance occurs in the grid voltage waveforms. These and other figures (Fig. 8, 9 and 11 in Publication 5) validate the robustness of the proposed synchronization algorithm when running on different grid disturbances and highlights the performance improvement in comparison with conventional PLL.

3.3.2 Robust synchronization algorithm based on SOGI filter

The second approach to obtain a clean synchronization angle in presence of grid disturbances is based on second order generalized integrator (SOGI) [40, 42, 43]. The transfer function of a band pass filter (BPF) based on SOGI is given by Eq. (3.3):

$$G(s) = \frac{k\omega_0 s}{s^2 + k\omega_0 s + \omega_0^2} \tag{3.3}$$

Studying the structure of BP-SOGI filter illustrated in Fig. 3.6(a), it should be noticed that beside notch filtering, this system also provides the quadrature signal of its output, e.g. the signal qy. This is particularly useful for calculating the positive and negative sequence components of grid voltage as described in Publication 6. The gain k controls the filtering band of BP-SOGI filter, and as Fig. 3.6(b) depicts, lower gain values produce more narrow filtering while high values enlarge the filtering band. Attention should be drawn on the fact that no phase delay is introduced by such filter structure, no matter what the value of k is, hence facilitating its use for phase estimation purposes.

Employment of two second order generalized integrator structures would allow the detection of positive sequence component of grid voltage, as Fig. 3 in Publication 6 illustrates. This can be calculated by:

$$|\mathbf{v}^+| = \sqrt{(v_\alpha^+)^2 + (v_\beta^+)^2} \tag{3.4}$$

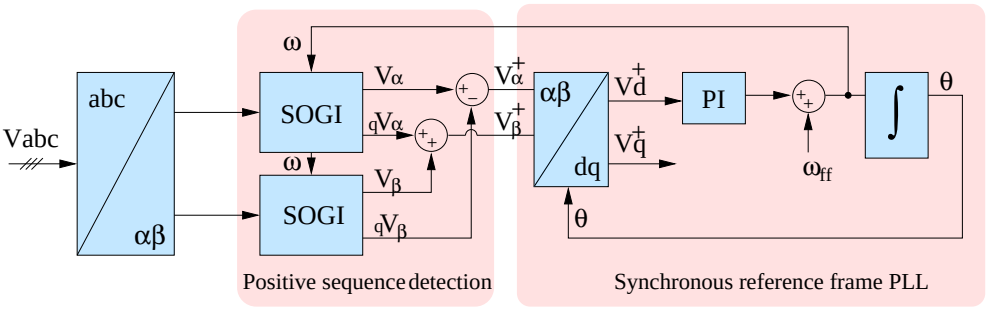

Figure 3.7: *Structure of robust grid synchronization system based on SOGI-BP filter and conventional synchronous reference frame PLL.*

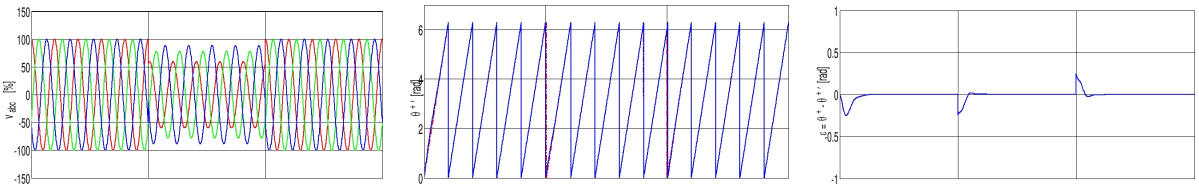

(a) (b) (c)

Figure 3.8: *Behavior of the proposed SOGI-PLL based on SOGI-BP filter under single phase fault at the PCC: (a) voltages after transformer, (b) synchronization signal estimated by the proposed system and (c) the phase error between the real grid phase and the one estimated by SOGI-PLL.*

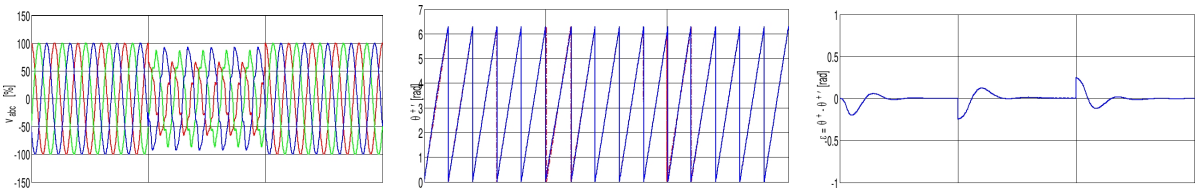

(a) (b) (c)

Figure 3.9: *Behavior of the proposed SOGI-PLL based on SOGI-BP filter during a very distorted voltages: (a) voltages after transformer, (b) synchronization signal estimated by the proposed system and (c) the phase error between the real grid phase and the one estimated by SOGI-PLL.*

Further on, the phase angle of the positive sequence can be estimated using a conventional PLL, as Fig. 3.7 shows.

In order to achieve best results, the resonance frequency of SOGI-BP filter, ω_0 needs to be identical with the grid fundamental frequency. In case the later deviates from its nominal value, SOGI-BP filter produces erroneous signals, leading to inaccuracy in estimation of phase angle. As a solution to this issue, the frequency signal provided by the locking loop can be fed back into the SOGI structure, this way resulting a self adapting algorithm, like is illustrated in Fig. 3.7.

The synchronization algorithm based on SOGI-BP filter has been tested under different unbalanced and distorted grid conditions in Publication 6. Fig. 3.9 reproduced here, shows an improved behavior of SOGI-PLL over the previous PLL based on repetitive controller. The SOGI-PLL is faster in reducing the phase angle error and does this with less overshoot. In a

situation of a very distorted and unbalanced voltage as presented in Fig. 9 in Publication 6, it is less than two fundamental periods that is necessary to asses the correct value for both positive sequence component and phase angle respectively. Based on these considerations, such structure is suitable for synchronizing distributed generation systems with the utility network even in very distorted grid conditions.

3.4 Summary

This chapter highlights the importance of a robust synchronization algorithm for control purposes of a grid connected power generation system. The research work carried out in this direction shows the necessity of filtering the grid voltage prior using it in the phase locking loop in order to obtain a robust synchronization algorithm. Particularly, negative sequence component has the largest impact on the phase angle detection accuracy, hence its influence has to be avoided by extracting it from the voltage signal which enter in the locking loop.

Several filtering techniques for extracting the grid voltage sequence components have been already described by previous works, however, two new schemes have been proposed and developed in this thesis. The first developed algorithm is implemented in dq frame and uses a repetitive controller based on DFT to mitigate the influence of negative sequence onto phase angle detection. The second algorithm developed is implemented in stationary $\alpha\beta$ frame and uses second order generalized integrator to deal with negative sequence influence onto synchronization. This algorithm is less demanding computationally and has increased performance as compared with the one based on DFT. Simulation and experimental results show that the proposed algorithms are robust to large range of grid disturbances.

Chapter 4

Grid monitoring

This chapter discusses the necessity of DPGS to monitor the grid parameters such as voltage amplitude, frequency and line impedance. First, the interconnection requirements related to operating margins in respect to grid voltage and frequency are briefly introduced. Next, the monitoring of grid frequency and voltage amplitude during the normal conditions as well as the positive and negative sequence voltage components during unbalanced network situation is addressed. This is followed by the discussion of algorithms proposed for identifying the value of grid impedance. The chapter ends up concluding the work developed for grid monitoring.

4.1 Interconnection requirements

Grid requirements applying to utility connected power generation units impose the operation conditions in respect to voltage and frequency values. The demands are country specific and vary also in respect to the generation system type, i.e. wind turbines (WT), photovoltaic (PV) systems, and power rating and grid connection level (LV, MV, HV). Considering grid monitoring demands for WT connected into MV Danish power system, a graphical representation of allowed operation area with regard to voltage amplitude and grid frequency is illustrated in Fig. 4.1 [62].

A normal operation area between 95 and 105% of the nominal grid voltage and ± 1 Hz around the nominal frequency is defined. Either frequency or voltage exceeds the predefined limits, the wind turbine should disconnect within the specified time interval. Therefore, in order to be able to disconnect in time, the wind turbine should accommodate a fast and reliable grid monitoring unit. Next section introduces a grid monitoring algorithm based on PLL structure implemented in synchronous rotating reference frame, using an unbalance compensation unit and a positive negative sequence detector to extract the grid frequency, the positive and negative sequence components of grid voltage and the phase angle of positive sequence voltage.

4.2 Voltage and frequency monitoring

Previous chapter discusses the detection of grid voltage phase angle and few algorithms have been presented. It has been mentioned in § 3.1 that the PLL system can give information about grid frequency and voltage amplitude as well, therefore the proposed algorithm for grid monitoring is based on PLL system. The structure of this system is illustrated in Fig. 4.3 and its features are detailed in Publication 7 on page 137. As it can be observed, the proposed system is composed of four major parts:

the transformation module is using equations (2.1b) and (2.2b) to transform the grid voltages from *abc* to *dq* synchronous rotating reference frame.

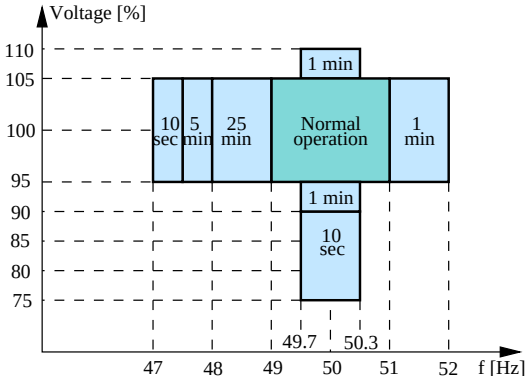

Figure 4.1: *Boundaries of operation and clearing times for both voltage and frequency according to the Danish grid operator [62].*

unbalance compensation algorithm which is based on the repetitive controller previously discussed in § 3.3.1 and detailed in Publication 5. The role of unbalance compensation unit is to allow only the positive sequence component to pass through the PLL controller, hence reducing the unbalance effect on the frequency and phase angle estimation.

PLL controller which employs a PI controller and an integrator to estimate both frequency and phase angle of the utility grid. Since its input is the positive sequence component of grid voltage, the estimated phase angle is corresponding to this component only.

positive negative sequence detector uses delay signal cancellation (DSC) filter [72] depicted in Fig. 4.2 and Eq. (4.1) to extract the positive and negative sequence components of grid voltage. Having the information about both positive and negative sequence components, the value of grid unbalance in term of negative sequence component can be further estimated.

$$U_{-} = \sqrt{U_d^2 + U_{osc}^2} \tag{4.1}$$

where U_d and U_{osc} are detailed in Publication 7 on page 137.

Using these four parts, the proposed system is able to estimate the phase angle of the positive sequence voltage component, the grid frequency and the magnitude of positive and negative sequence components. The algorithm has been extensively tested in Publication 7 where different grid disturbances have been considered. The performance of the monitoring system is reproduced in figures 4.4 and 4.5. Fig. 4.4(a) illustrates a voltage swell up to 137% of its nominal value and as observed in Fig. 4.4(b), the proposed algorithm quickly detects the change in the magnitude of grid voltage. Fig. 4.5 presents the response of the proposed monitoring system in case of grid frequency deviation. As illustrated in Fig. 4.5(b), fast detection of frequency

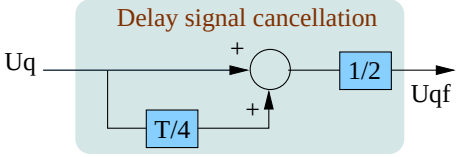

Figure 4.2: *The proposed filtering technique for cancellation of double frequency oscillations in the U_q signal.*

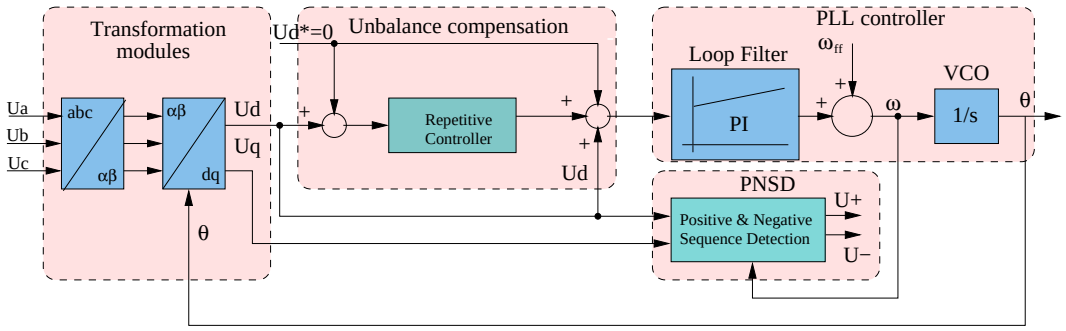

Figure 4.3: *The structure of the proposed system for grid monitoring based on PLL.*

deviation is noticed, the algorithm being able to detect the new frequency value in a bit more than two fundamental periods.

Publication 7 extends the tests to unbalanced voltage conditions. Again good performance is obtained in such situation, the algorithm being able to detect quickly and accurately the values of both positive and negative sequence components of grid voltage.

Comparing the response time of the proposed algorithm with the disconnection times suggested by the grid interconnection requirements, the algorithm is proving to be a suitable solution for grid monitoring in case of distributed power generation systems. Its output signals can be successfully used in the control scheme in order to decide whether or not the system should stay connected or disconnect from the utility network.

In addition to the algorithm shown in Fig. 4.3, the synchronization system based on SOGI-PLL illustrated in Fig. 3.7 on page 30 can also be employed for grid monitoring. The positive sequence detection unit can be adapted to extract also the negative sequence, providing in this case all the information that the system proposed in Fig. 4.3 provides.

4.3 Line impedance identification

The value of grid impedance is a beneficial information for achieving a robust control of DPGS and for the prediction of harmonic propagation into the power system. Moreover, with continuous connection and disconnection of loads in utility network, the line impedance value becomes vital for power system management.

For example, active filter control can be improved with the knowledge of line impedance value [81–83]. Better harmonic rejection as well as improved current controller response are obtained if the value of grid impedance is used in control [81]. Moreover, the gain of current controllers for grid tied converters could be adjusted according to the value of the grid impedance ensuring system stability over a broad range of line impedance values.

Estimation of grid impedance is one of the demands for photovoltaic (PV) systems connected into the power system of some European countries [84] and this is requested in order to detect islanding conditions. As photovoltaic industry registers an exponential growth worldwide, this demand was leading to an intensive research towards grid impedance identification [85–91]. Moreover, information about grid impedance would be useful for detection of grid faults and grid unbalance [58]. Additionally, grid impedance information combined with the information of the voltage at the point of common coupling can lead to identification of grid source voltage, hence the power system on which a DPGS is running can be completely characterized.

As grid impedance information could be a valuable information for the control of grid con-

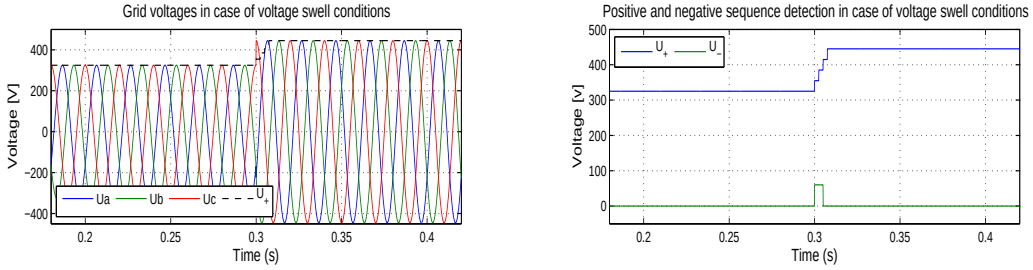

(a) (b)

Figure 4.4: *Response of monitoring algorithm to balanced voltage swell: (a) grid voltages having an amplitude increase up 137% of their nominal value and (b) positive and negative sequence detection using the proposed PLL system for grid monitoring.*

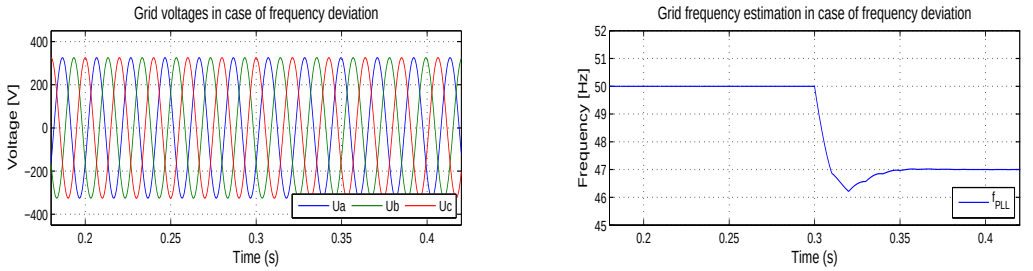

(a) (b)

Figure 4.5: *Simulation results in the case of frequency variations condition: (a) grid voltages and (b) grid frequency estimation using the proposed PLL system for grid monitoring.*

nected systems, this thesis proposes few methods for accurate estimation of both resistive and inductive part of grid impedance. An overview of state of the art methods for identification of grid impedance is briefly introduced, followed by the description of the proposed approaches.

4.3.1 Overview of methods

Generally, the methods for grid impedance detection can be classified in two main groups, i.e. passive and active methods.

Passive methods

Passive methods measure and monitor the grid distortions and based on them, the value of grid impedance is estimated. A major drawback of the passive methods is that the grid variations might not be sufficiently large to be accurately determined, hence failing to give an exact estimation of the grid impedance. Another issue related to passive methods is the time interval at which grid variations occur. It might be the case that no variations appear for a long time, hence no information about grid impedance is known during this time interval.

Active methods

Active methods deliberately create a disturbance at the point of common coupling (PCC) and the grid impedance calculation is based on grid response to the distortion. The most common

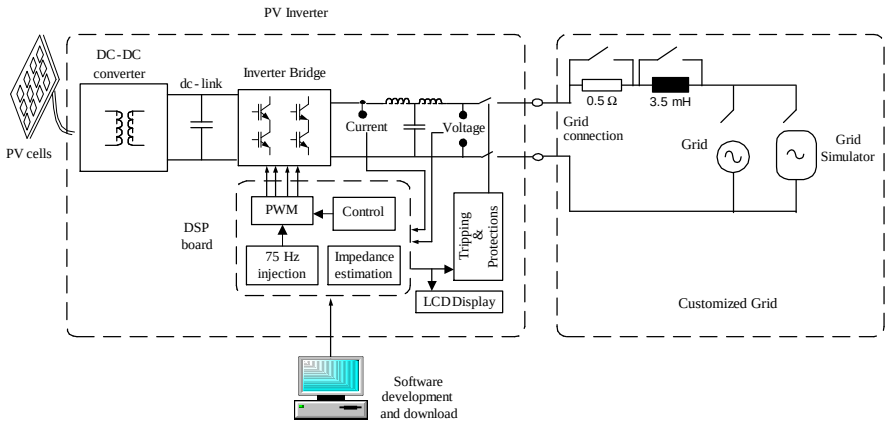

Figure 4.6: *Structure of PV inverter and setup for test on different grid conditions.*

disturbances can be summarized as consisting of [88]:

- *current pulse transient* usually applied at zero crossing of the voltage to produce a voltage transient in the grid based on which the grid impedance can be estimated.
- *noncharacteristic subharmonics (inter-harmonics)* injected into the utility network which give the possibility of calculating the line impedance at a particular frequency.
- *power variations* of both active and reactive power produce grid voltage variations based on which the line impedance can be estimated.

In [92, 93] a current spike is deliberately injected at the point of common coupling by a grid tied power converter. Based on the voltage response to this disturbance, the grid impedance value is determined using Fourier transform. The influence of non-linear loads connected close to the point of common coupling (PCC) is also addressed and as a consequence additional signal processing method is necessary in order to obtain accurate results.

In [85–88, 94] injection of non-characteristic inter-harmonic current is used to derived the grid impedance at that particular frequency. The value of inter-harmonic has to be chosen close to the fundamental grid frequency in order to assume that the identified value of grid impedance can be approximated for fundamental frequency too.

Although, active methods give better impedance identification, power system disturbance is not suitable when more than one power generation units are connected on the same grid. As discussed in Publication 10, because the injected inter-harmonic generated by DPGS is unique in the utility network, this particular method would allow the connection of more than one similar generation units on the same grid because synchronization in respect to the inter-harmonic injection is possible [88,95]. However, only a finite number of DPGS can be connected on the same feeder and this number is directly depending on the standard demands regarding disconnection time and the number of injections necessary to obtain accurate impedance identification.

4.3.2 Impedance identification based on inter-harmonic injection

Publication 8 discusses the problems of accurate impedance identification using the method presented in [85] when the power generation system is running on highly inductive grid conditions.

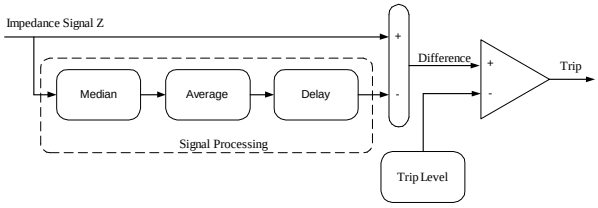

Figure 4.7: *ENS detection algorithm implemented in the PV inverter.*

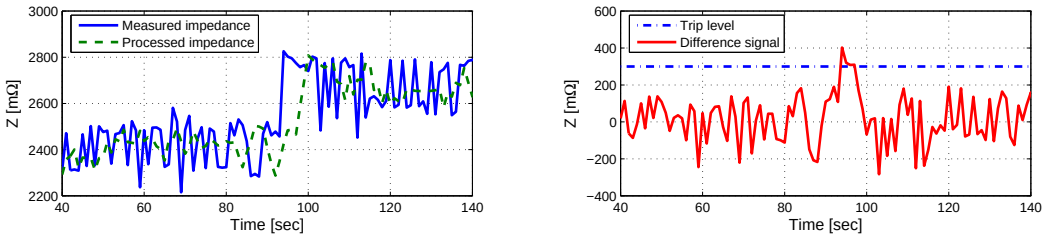

(a) (b)

Figure 4.8: *Islanding detection: (a) the behavior of the instantaneous and processed impedance signal when a change of 0.5 Ω is applied to the grid, (b) the difference between the signals and the trip level.*

The method in [85] uses a signal injection of 75 Hz to detect the line impedance as illustrated in Fig. 4.6. In order to do that, a 75 Hz resonant controller is used in addition to the main (50 Hz) current controller. In Publication 8, tuning of injection amplitude as well as its periodicity has been addressed to find a suitable injection amplitude which gives satisfactory accuracy for islanding detection. Even though the exact value of grid impedance is not identified, the method proposed in [85] can be used to detect islanding conditions, hence to comply with the ENS (VDE 0126) standard [84] for photovoltaic applications. Publication 9 details the signal processing work necessary to be used in conjunction with the impedance identification method in order to determine a 0.5 Ω resistive change in grid impedance, as requested by [84]. Simply using basic signal processing methodologies as shown in Fig. 4.7, the method for impedance estimation can provide islanding detection capabilities to the power generation system. The effectiveness of this method is illustrated in Fig. 4.8 where the estimated impedance signal and the processed one are used to detect islanding conditions. Fig. 4.8(b) illustrates the difference between the two signals crossing above the imposed islanding threshold, detecting this way islanding conditions and sending the trip signal to the power converter. The disconnection times presented in Table I in Publication 9 show the compliance of this method with the ENS standard regarding islanding conditions detection and ceasing power production within the requested time.

As highlighted above, an important issue which has to be considered in case of impedance estimation based on a signal injection is the influence of other similar power generation units using the same technique for impedance detection and which are connected on the same feeder. Concomitant inter-harmonic injection can occur in such situation leading to erroneous impedance identification. This issue is addressed in Publication 10 where a harmonic compensator (HC) tuned to resonate on the frequency of the injected inter-harmonic used for impedance determination has been found as an appropriate solution to alleviate the influence of other similar systems on the accuracy of impedance estimation. Consequently, synchronization of inter-harmonic in-

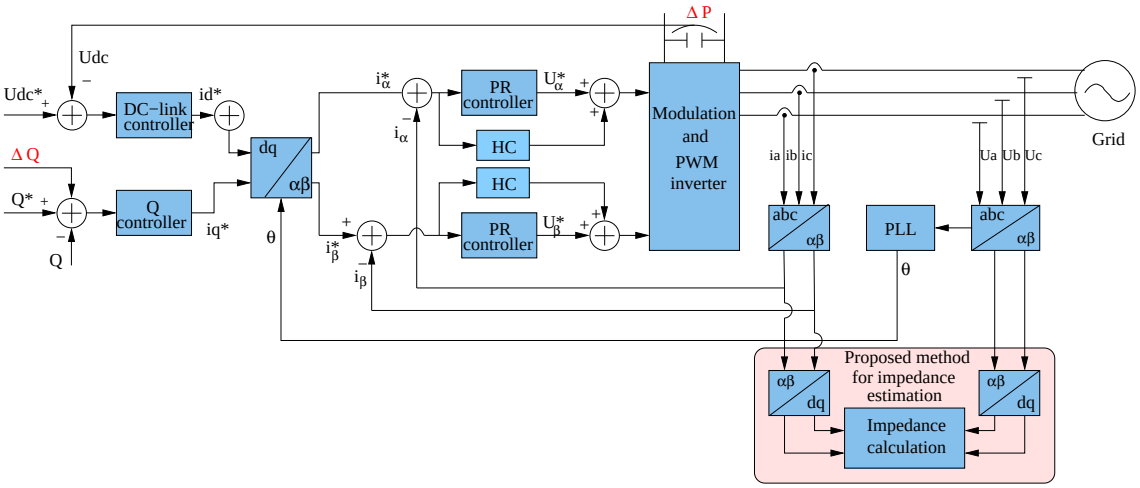

Figure 4.9: *Control structure of the grid side converter having an algorithm for line impedance estimation based on active and reactive power variations.*

jections as well as satisfactory impedance estimation when more DPGS are connected on the same feeder is achieved.

4.3.3 Impedance identification based on independent PQ variations

Another method for detecting the grid impedance proposed in this thesis uses both active and reactive power variations at PCC generated by a grid connected power generation system. Fig. 4.9 illustrates the control structure used for line impedance estimation using this method. Active power variations are generated in dc-link while reactive power fluctuations are summed up to the reactive power reference. The dc-link voltage controller sets up the reference for active current i_d^* while the output of reactive power controller is the reference for reactive current i_q^*. The current references are further transformed in $\alpha\beta$ stationary reference frame where a PR current controller is used for regulating the grid current.

As illustrated in Fig. 4.10(a), power variations at PCC would lead to different current and voltage values and based on the difference between two operating points, the grid impedance can be identified. Varying both active and reactive power (see Fig. 4.10(b)) it is possible to estimate the resistive and inductive parts of the impedance. Unlike the method presented in [85] which injects an inter-harmonic current in the power system, this method works at fundamental frequency, i.e. the fundamental component of the power (current) is varying. The proposed method derives the dq components of grid voltage and current respectively, which are further reported to an arbitrary rotating reference frame synchronized with the grid angular frequency. In case of practical implementation, the grid angular frequency can be obtained from a very slow PLL or a frequency locked loop (FLL) [76]. Consequently, the phase angle of the arbitrary reference frame can be derived from the grid frequency information like:

$$\theta = \int \omega \, dt \tag{4.2}$$

The voltage at the point of common coupling in two operating points can be written as:

$$\mathbf{v}_{pcc1} = \mathbf{v}_{s1} + Z \cdot \mathbf{i}_{pcc1} \tag{4.3a}$$

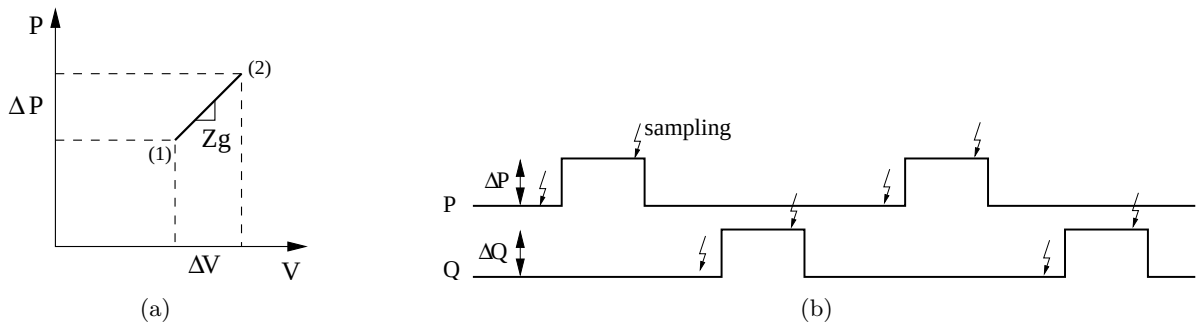

Figure 4.10: *Proposed method for line impedance identification using power variations in two working points: (a) the two necessary working points to apply the algorithm and (b) the active and reactive power variations and sampling instants to obtain the two working points.*

$$\mathbf{v}_{pcc2} = \mathbf{v}_{s2} + Z \cdot \mathbf{v}_{pcc2} \tag{4.3b}$$

where *1* and *2* are representing the two different sampling instants. The line impedance can be calculated using the variations in both current and voltage at the point of common coupling:

$$Z = \frac{\Delta \mathbf{v}_{pcc}}{\Delta \mathbf{i}_{pcc}} \tag{4.4}$$

where:

$$\Delta \mathbf{v}_{pcc} = \mathbf{v}_{pcc1} - \mathbf{v}_{pcc2} \tag{4.5a}$$

$$\Delta \mathbf{i}_{pcc} = \mathbf{i}_{pcc1} - \mathbf{i}_{pcc2} \tag{4.5b}$$

are the voltage and current variation respectively at the point of common coupling. It should be noted that the above equations are valid only if the source voltage and grid impedance Z are not changing between the two sample instants, e.g. $\mathbf{v}_{s1} = \mathbf{v}_{s2}$ and $Z_1 = Z_2 = Z$, constituting the main limitation of this method.

Further on, the module and phase angle of the voltage at the PCC can be calculated from its $\alpha\beta$ components:

$$|V_{pcc1,2}| = \sqrt{V_{\alpha 1,2}^2 + V_{\beta 1,2}^2} \tag{4.6a}$$

$$\theta_{V_{pcc1,2}} = tan^{-1}\left(\frac{V_{\beta 1,2}}{V_{\alpha 1,2}}\right) \tag{4.6b}$$

Based on the above equations, the dq components of the grid voltage for both sampling instants can be derived in relation to the arbitrary reference frame given by θ:

$$V_{d1,2} = |V_{pcc1,2}|\, cos(\theta_{V_{pcc1,2}} - \theta) \tag{4.7a}$$

$$V_{q1,2} = |V_{pcc1,2}|\, sin(\theta_{V_{pcc1,2}} - \theta) \tag{4.7b}$$

This way, the voltage at the point of common coupling is always referring to a general rotating reference frame provided by θ. Based on the dq components of both voltage and current, the resistive and inductive part of the impedance can be calculated like:

$$R = \frac{(V_{q1} - V_{q2}) \cdot (I_{q1} - I_{q2}) + (V_{d1} - V_{d2}) \cdot (I_{d1} - I_{d2})}{(I_{q1} - I_{q2})^2 + (I_{d1} - I_{d2})^2} \tag{4.8a}$$

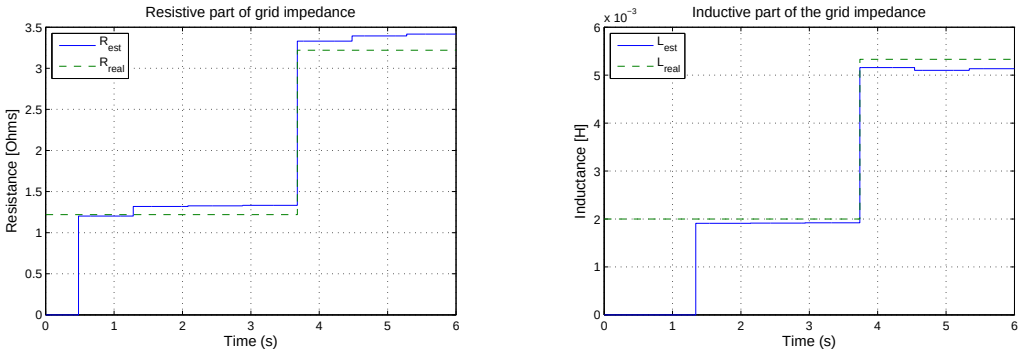

(a) (b)

Figure 4.11: *Estimation of both resistive (a) and inductive (b) parts of the grid impedance in the situation of 5% active power variations at PCC.*

$$\omega L = \frac{(V_{d1} - V_{d2}) \cdot (I_{q1} - I_{q2}) - (V_{q1} - V_{q2}) \cdot (I_{d1} - I_{d2})}{(I_{q1} - I_{q2})^2 + (I_{d1} - I_{d2})^2} \tag{4.8b}$$

Fig. 4.11 shows the estimation of both resistive and inductive parts of grid impedance in case when the active and reactive power varies 5% of its nominal value. The method is detailed described in Publication 11 where results in case of other power variations as well as large impedance variations are shown.

Table I in Publication 11 illustrates the accuracy of this method being around 5% which is comparable with that of a commercial product dedicated for impedance measurement available in laboratory.

Table 4.1: *Influence of power variation ΔP onto the accuracy of estimation*

ΔP	Accuracy R	Accuracy L
10 %	3.89 %	1.32 %
5 %	5.30 %	6.40 %
1 %	5.84 %	5.01 %
0.1 %	4.80 %	6.20 %

Although identification of grid impedance using this strategy is quite precise, in case of large power generation units such as wind turbines or wind farms, voltage variations at the point of common coupling caused by power variations necessary for impedance identification may produce flicker, hence the power generation unit will not comply with the related power quality standards [96]. Consequently, the above impedance estimation method necessitates improvement for better interconnection with the power system.

4.3.4 Impedance identification based on active power variations and grid voltage control

In order to overcome the voltage variations at the point of common coupling caused by the power fluctuations necessary for line impedance identification, the above method has been further developed by replacing the reactive power controller with a grid voltage controller. Modern wind turbines already integrate a voltage droop control function in their control structure, hence this

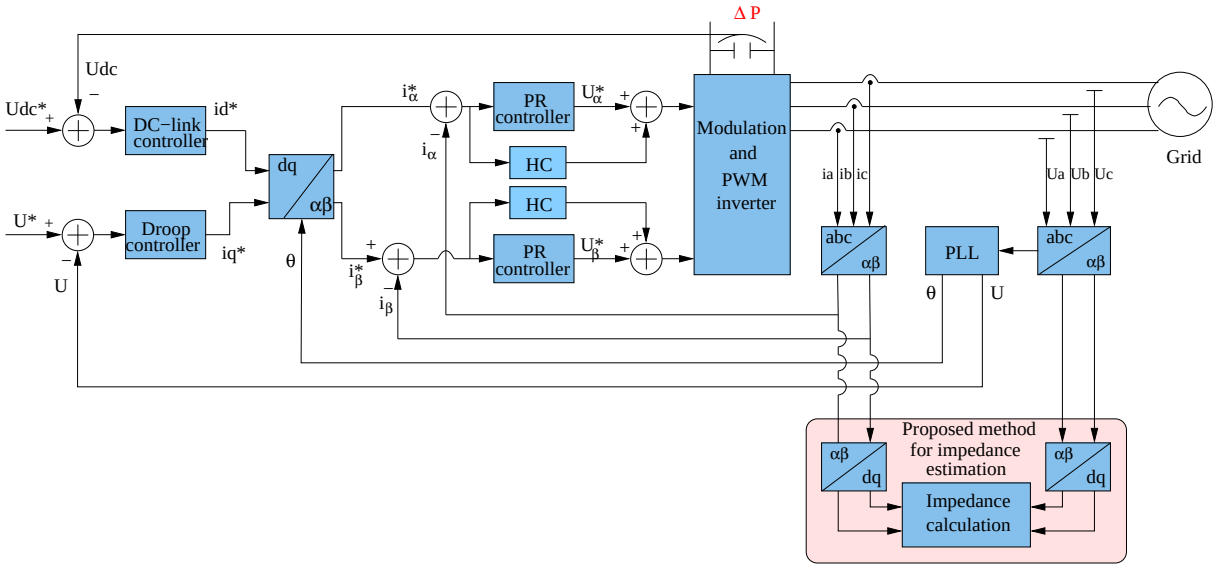

Figure 4.12: *Control structure using grid voltage control to regulate the reactive current in order to maintain constant the voltage magnitude at the point of common coupling.*

can be used for impedance identification as well. Impedance identification using grid voltage control is possible because the above algorithm uses the dq components of grid voltage and current referred to an arbitrary reference frame given by θ. Therefore, the voltage fluctuation $\Delta\vec{V}_{pcc}$ given by equation (4.5a) and illustrated in Fig. 4.10(a) can be mitigated to phase angle deviation using equations (4.7a) and (4.7b).

The control structure for the new method is illustrated in Fig. 4.12. In this case, the reactive current reference is not anymore provided by a reactive power controller but is given by a grid voltage controller instead. Therefore, in case active power variations necessary for impedance identification modify the grid voltage value, the voltage controller reacts by generating a reactive current reference which will keep constant the magnitude of voltage vector. Consequently, the reactive power variations occur at the same time with the active power oscillations, as opposite to the previous method (Fig. 4.10(b)).

Publication 12, describe in details the method, its implementation and the testing conditions. Signal processing of dq components of grid voltage and current respectively (illustrated

Table 4.2: *The effectiveness of the proposed method for impedance identification, validated by simulation results.*

Grid value	Estimated value
Normal grid	
Resistance $R_s = 1.3\ \Omega$	Resistance $R_{est} = 1.29\ \Omega$
Inductance $L_s = 6\ mH$	Inductance $L_{est} = 6\ mH$
Additional impedance	
Resistance $R_s = 1.55\ \Omega$	Resistance $R_{est} = 1.52\ \Omega$
Inductance $L_s = 9.3\ mH$	Inductance $L_{est} = 9.15\ mH$

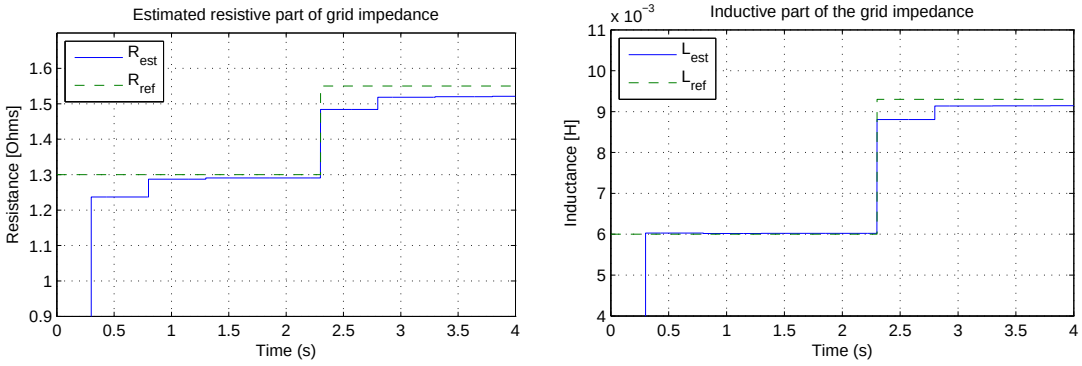

(a) (b)

Figure 4.13: *Simulation results of identification of (a) resistive and (b) inductive parts of grid impedance in situation of inductive grid conditions.*

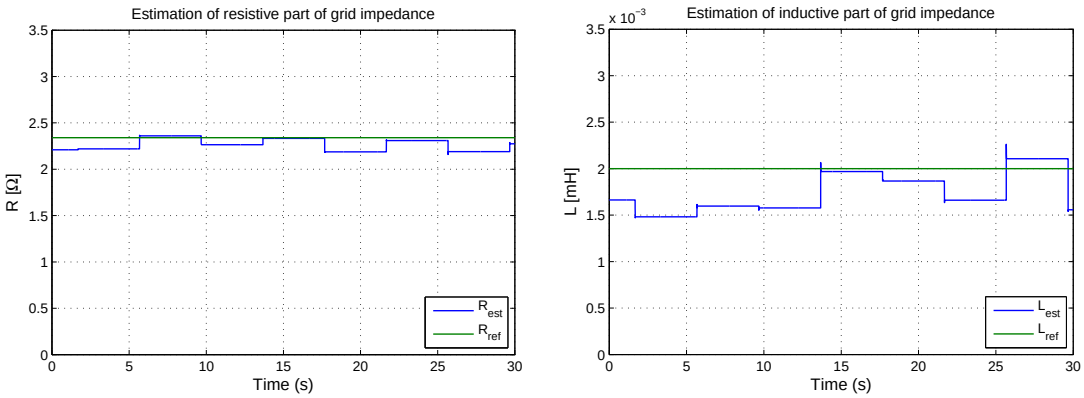

(a) (b)

Figure 4.14: *Experimental results of identification of (a) resistive and (b) inductive parts of grid impedance in situation of resistive grid conditions.*

in Fig. 7, Publication 12) plays an important role on the accuracy of impedance identification. The proposed method has been tested in simulation on inductive grid conditions. As Fig. 4.13 show, fast and accurate identification of both resistive and inductive parts of grid impedance is achieved. As highlighted in Table 4.2 recalled here from Publication 12, the proposed method based on active power variations and voltage control has an average accuracy of about 2% when implemented in simulation.

On the contrary, when the method has been implemented on experimental setup, it was tested on resistive grid conditions. Although the accuracy is not as high as in simulations, good agreement between the real[1] and identified values is also obtained in laboratory, as Fig. 4.14 illustrates.

[1]In laboratory, the line impedance has been measured using a Norma Unilap XE device, which is a dedicated apparatus for impedance measurement. The accuracy of this device is 5% for impedance measurement situated between 0.07 and 199 Ω.

4.3.5 Summary

This chapter discusses the possibilities to achieve fast and accurate monitoring of grid variables such as voltage amplitude, frequency and line impedance. An algorithm based on the robust synchronization system described in § 3.3.1 is proposed for monitoring the grid frequency and voltage amplitude. Additionally, the algorithm is further developed to extract the positive and negative sequences of grid voltage. The results presented in Publication 7 validate the high dynamics and accuracy of this algorithm to monitor the grid voltage amplitude and frequency even during sever grid disturbances.

Regarding the identification of grid impedance, two methods are detailed in this chapter. The first method uses active and reactive power oscillations at the terminals of a grid connected power generation system to identify both resistive and inductive parts of grid impedance. The results presented show a very good accuracy of this method, even when very low power variations are used.

The second method for line impedance identification is a further improvement of the first one. Due to the fact that voltage fluctuations at the point of common coupling can generate flicker, in the second method the reactive power variations are produced by a grid voltage controller which ensures that the amplitude of grid voltage is not changing when active power oscillations take place. Good agreement between reference and identified values of both resistive and inductive parts of line impedance has been obtained in this case too.

Chapter 5

Advanced control of grid converters

This chapter discusses few methodologies to improve the robustness of current controllers for grid connected power converters in situation of voltage disturbances in utility network. The development of an adaptive resonant controller with regard to grid frequency is first addressed, followed by the elaboration of an adaptive dead-beat controller regarding grid impedance variations. The chapter ends up with a description of several possibilities to control the active and reactive power during the fault, providing flexibility to the control of grid connected power generation systems.

5.1 Introduction

It has been mentioned previously that in situation when the control structure is implemented in stationary reference frames such as $\alpha\beta$ and *abc*, the use of PI controllers leads to unsatisfactory current regulation due to their limitations when controlling time varying quantities. As a consequence, PR, dead-beat and hysteresis controller gain acceptance in such situation, however, there are few issues to be considered when these controllers are employed for controlling grid connected power converters. The following sections address the influence of grid frequency deviation on the PR controller and the effect of grid impedance variation on dead-beat controller. The possibility of creating a robust dead beat controller by means of tuning one of its gain towards system stability is further discussed. Finally, several control possibilities for providing flexible active and reactive power during grid voltage faults are presented.

5.2 Adaptive resonant controller

Numerous works [39–43,97] reported good tracking capabilities of PR controller when controlling sinusoidal quantities. Inspecting the equation of the controller given by Eq. (5.1), it should be noticed the presence of resonant frequency ω_0 in its internal model:

$$G_c(s) = K_p + K_i \frac{s}{s^2 + \omega_0^2} \tag{5.1}$$

with: K_p the proportional gain, K_i integral gain and ω_0 the resonance frequency of the controller.

As emphasized in Publication 13, in case of grid connected power converters, the best performance of PR controller is obtained when the resonance frequency of the controller ω_0 is identical with the grid angular frequency ω. However, grid frequency can fluctuate around its nominal value, hence becoming different than the resonant frequency of the controller. The Bode-plot of the resonant controller for different integral gains K_i and ω_0 set to 50 Hz is shown in Fig. 5.1. As

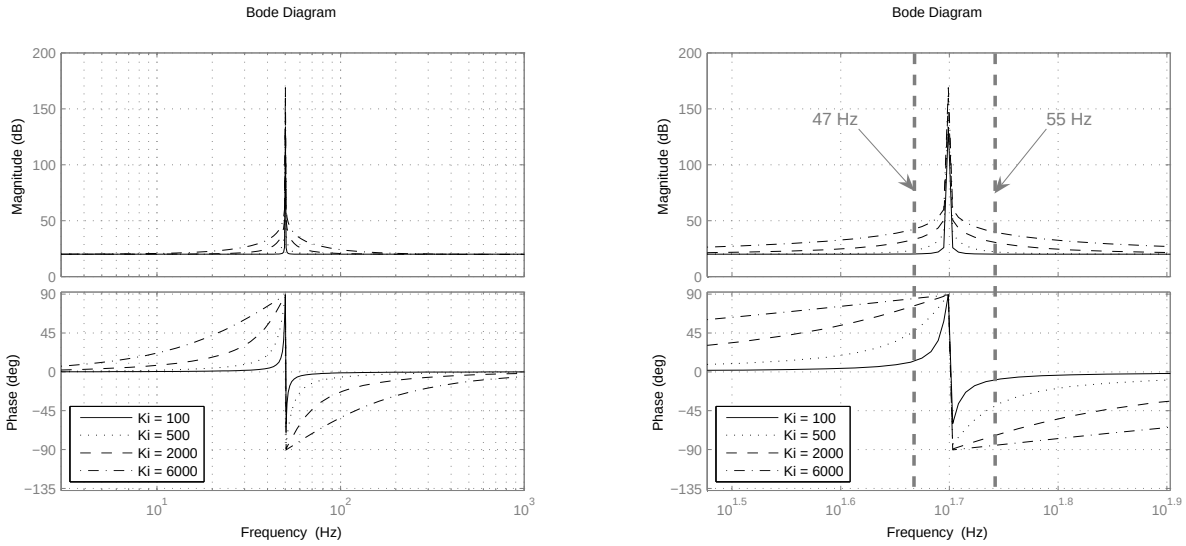

(a) (b)

Figure 5.1: *Bode-plot of resonant controller tuned for 50 Hz (a) having different integral gains and (b) zoom in around 50 Hz frequency.*

it can be observed, this controller achieves a very high gain in a narrow frequency band centered around the resonance frequency. The width of this frequency band depends on the integral time constant K_i. A low K_i leads to a very narrow band while a high value of K_i leads to a wider band. However, as § 4.1 on page 33 implies, distributed generation systems, especially wind turbines should be able to run on grid frequency deviation from 47 Hz up to 55 Hz. In case grid frequency changes to 55 Hz, (like the arrow points out in Fig. 5.1(b)), the performance of PR controller is drastically reduced due to the low gain at that frequency, hence will not be able to eliminate the steady state errors in such operation condition.

Fig. 3 and Fig. 4 in Publication 13 illustrate a satisfactory behavior of PR controller in case the grid frequency deviates ±1 Hz from its nominal value[1], hence an adaptive resonant controller is not a strict necessity in such situation. However, in case of wind turbines, the frequency band of operation is much larger, going from 47 Hz up to 55 Hz. As depicted in Fig. 5(b) and Fig. 6(b) in Publication 13, steady state error is registered in situation when grid frequency is deviating that much from its nominal value. As a consequence, adaptive resonant controller in respect to grid frequency is a necessity in this case. The solution proposed in Publication 13 and shown in Fig. 5.2, uses the frequency information provided by the PLL system as an additional input into the controller, leading to an adaptive resonant controller regarding the operational frequency. Fig. 5(c) and Fig. 6(c) in Publication 13 (recalled here as Fig. 5.3) depict an improved behavior of the adaptive resonant controller in situation of large frequency variations, validating the effectiveness of the proposed solution illustrated in Fig. 5.2.

[1]According to the grid interconnection requirements for photovoltaic systems [59, 61], ±1 Hz is the maximum frequency deviation allowed.

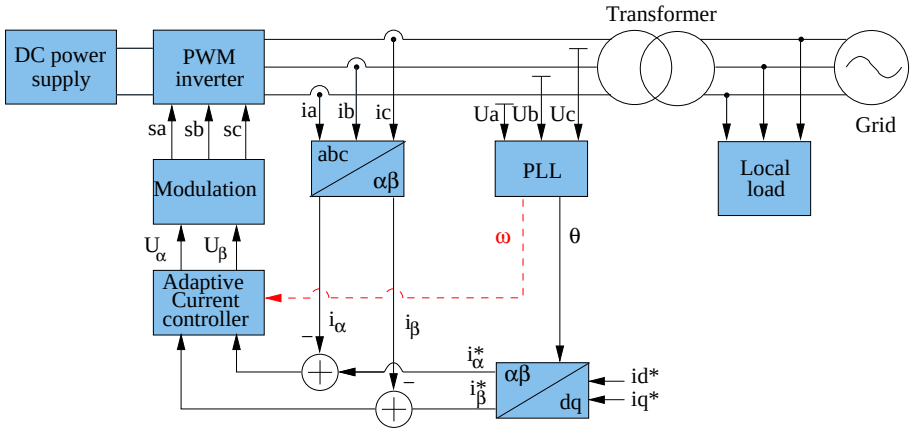

Figure 5.2: *Proposed control system using frequency information provided by the PLL to obtain an adaptive resonant controller.*

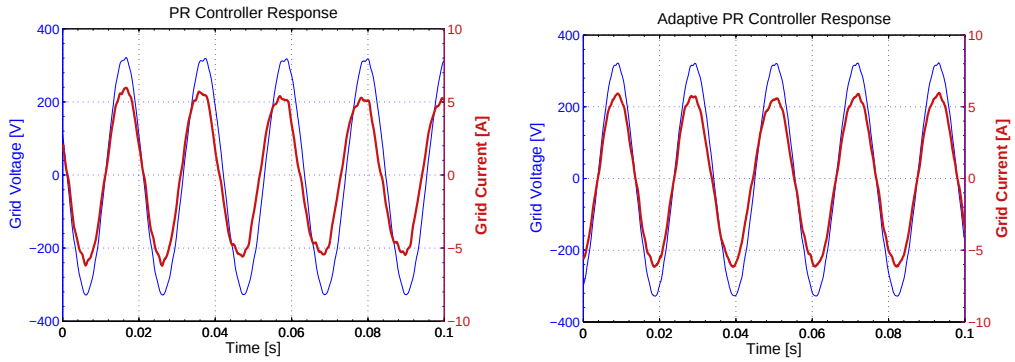

(a) (b)

Figure 5.3: *Experimental results for a frequency step from 50 Hz down to 47 Hz: (a) resonant controller and (b) adaptive resonant controller.*

5.3 Adaptive dead-beat controller

Both dead-beat and hysteresis controllers present the advantage of high dynamics which make them suitable for current control of grid converters. However, the necessity of high sampling and switching is not suitable for high power applications such as MW wind turbines. Additionally, their direct dependence on the plant parameters is another disadvantage when these controllers are employed for current regulation of grid connected power converters. Unlike drives applications where the motor impedance is not varying too much, in case of grid tied systems, the grid impedance can experience large variations due to the connection/disconnection of loads nearby the point of common coupling.

$$i_i((k+1)T_s) = e^{-\frac{R_T}{L_T}Ts} \cdot i_i(kT_s) - \frac{1}{R_T}\left(e^{-\frac{R_T}{L_T}Ts} - 1\right) \cdot (Ui(kT_s) - U_g(kT_s)) \qquad (5.2)$$

Examining Eq. (8) in Publication 2, recalled here for convenience as Eq. (5.2), the influence of both resistive (R_T) and inductive part (L_T) of the plant impedance onto dead-beat controller can be observed. Normally, the plant is considered to be formed by the output filter and the distribution transformer, thus tuning of current controller is realized without accounting for grid

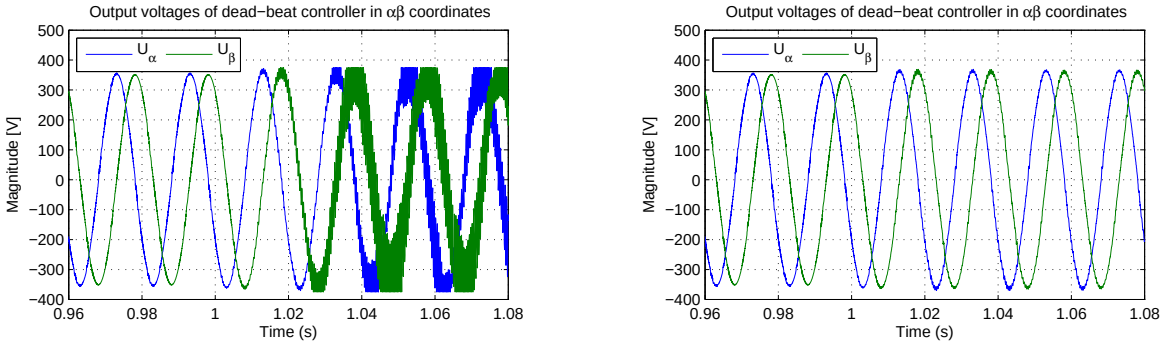

(a) (b)

Figure 5.4: *Output of dead-beat controller during grid impedance variation of Z=2+j0.02 Ω: (a) in situation when the grid impedance value is unknown to the controller and (b) in case of adaptive dead-beat controller.*

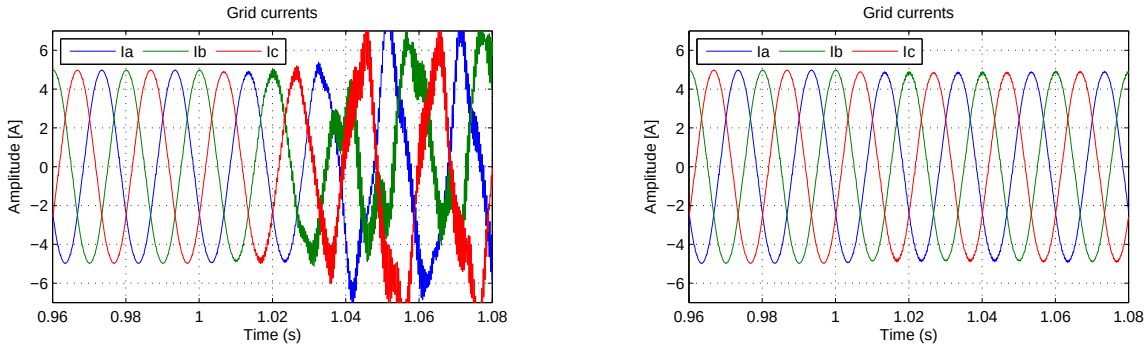

(a) (b)

Figure 5.5: *Behavior of dead-beat controller during grid impedance variation of Z=2+j0.02 Ω: (a) in situation when the grid impedance value is unknown to the controller and (b) in case of adaptive dead-beat controller.*

impedance. This is somehow reasonable because the value of grid impedance is small compared to the value of filter and transformer impedance and additionally, in case of high power DPGS, the transformer ratio is high, diminishing even more the contribution of grid impedance to the total impedance of the plant. However, in case of low power distributed generators connected to low voltage networks, the value of grid impedance can have larger contribution to the total impedance seen from the inverter output. Additionally, in situation when intentional islanding operation of DPGS is desired, the value of grid impedance plays an important role for system stability during such operation condition. Consequently, if dead beat or hysteresis controllers are used for current control, their tuning should be related to the variation of grid impedance in order to improve their behavior when operating in variable impedance conditions.

This thesis proposes a solution based on the use of grid impedance value, estimated by one of the algorithms described in § 4.3 on page 35. These estimation algorithms are able to identify both resistive and inductive part of grid impedance, making possible their use in dead-beat or hysteresis controller equations.

Fig. 5.4(a) shows the instability of dead-beat controller in case grid impedance varies with

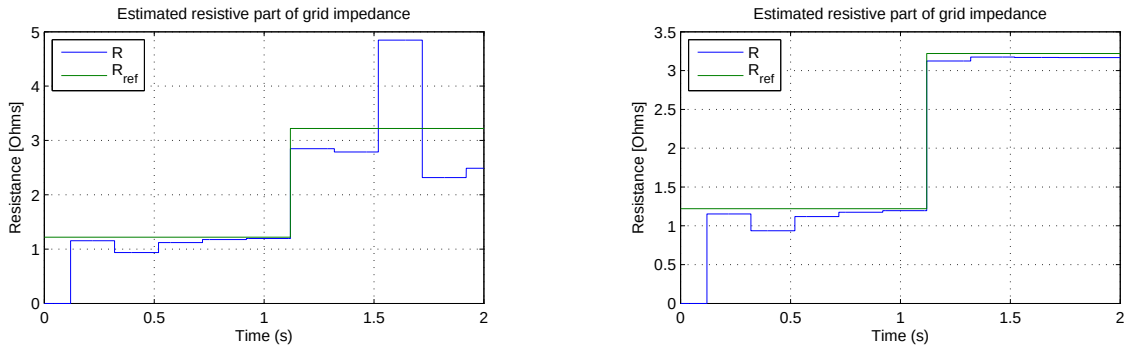

(a) (b)

Figure 5.6: *Estimation of grid resistance during grid impedance variation of Z=2+j0.02 Ω: (a) in situation when the grid impedance value is unknown to the controller and (b) in case of adaptive dead-beat controller.*

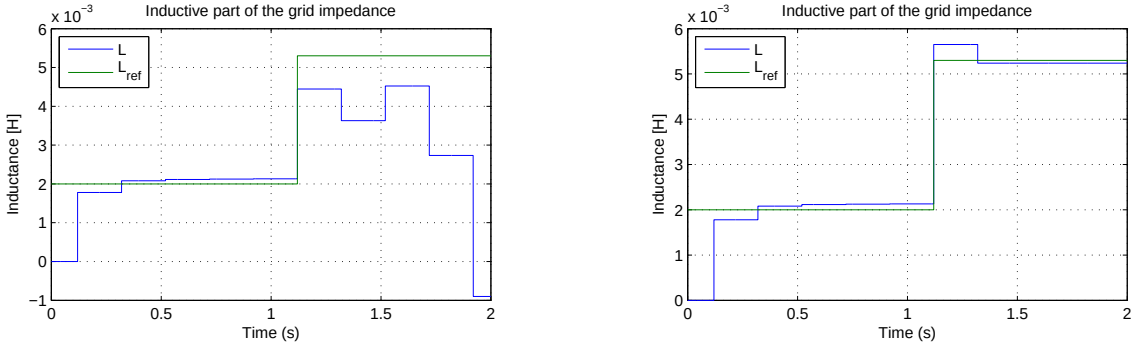

(a) (b)

Figure 5.7: *Estimation of grid inductance during grid impedance variation of Z=2+j0.02 Ω: (a) in situation when the grid impedance value is unknown to the controller and (b) in case of adaptive dead-beat controller.*

$Z = 2 + j0.02\ \Omega$. In this case, the output of the controller is saturating, hence control of grid current is lost as illustrated in Fig. 5.5(a). Consequently, the estimation of grid impedance is not anymore possible due to highly distorted current at the point of common coupling. As highlighted in Fig. 5.6(a) and Fig. 5.7(a) the inaccuracy in detecting the resistive and inductive part of grid impedance in such situation is high. However, in case when information about resistive and inductive part of grid impedance is forwarded to the controller, the variation of grid impedance does not influence the behavior of dead beat controller, as illustrated in Fig. 5.5(b). Thus, the identification of new value for grid impedance is possible as Fig. 5.6(b) and Fig. 5.7(b) show, and the controller is adapting with it.

5.4 Robust dead-beat controller

Sensitivity of dead beat controller to plant parameters have been always a major drawback for implementation of this controller in different application. It is not always the case when the power converter to be controlled has or needs an impedance estimation method which can

forward the information about changes in parameters of the plant.

During this study, a novel solution to improve the robustness of dead beat controller in situation of plant parameters change has been developed. Since this has not been yet published, the details are given in this thesis. The robustness of this controller has been previously addressed in [28, 32] where estimation of line voltage improves the robustness of the controller to the parameters mismatch. In [34], an improved dead beat controller using an adaptive self tuning load model is presented. In case of parameters mismatch, improved behavior is obtained as compared with the traditional controller. Although, these methods boost the robustness of dead beat controller in case of parameters mismatch, the solutions applied make the structure of the controller more complex.

As discussed in Publication 2, the design of dead beat controller is made considering the mathematical model of a single phase circuit as illustrated in Fig. 5 in Publication 2. In this case, the current equation can be derived as:

$$\frac{di(t)}{dt} = -\frac{R_T}{L_T} i(t) + \frac{1}{L_T}(u_i(t) - u_g(t)) \tag{5.3}$$

where $i(t)$ is the single phase grid current, $u_i(t)$ is the inverter voltage, $u_g(t)$ is the grid voltage and R_T and L_T are the total resistance and inductance upstream the distribution network. The discretized solution, considering one sample delay, is given by:

$$i((k+1)T_s) = e^{-\frac{R_T}{L_T}Ts} \cdot i(kT_s) - \frac{1}{R_T}\left(e^{-\frac{R_T}{L_T}Ts} - 1\right) \cdot (u_i(kT_s) - u_g(kT_s)) \tag{5.4}$$

Denoting a and b as follows:

$$a = e^{-\frac{R_T}{L_T}Ts} \tag{5.5}$$

$$b = -\frac{1}{R_T}\left(e^{-\frac{R_T}{L_T}Ts} - 1\right) \tag{5.6}$$

the controlled current can be expressed like:

$$i((k+1)T_s) = a \cdot i(kT_s) + b \cdot u(kT_s) \tag{5.7}$$

where $u(kT_s)$ is given by:

$$u(kT_s) = u_i(kT_s) - u_g(kT_s) \tag{5.8}$$

Considering that dead beat controller is designed to reach its reference in two sampling periods, the closed loop transfer function of the system becomes:

$$G_0(z) = z^{-2} \tag{5.9}$$

Applying Z transform to Eq. (5.7), the plant transfer function can be further derived:

$$I(z)z = aI(z) + bU(z) \tag{5.10a}$$

$$G_f(z) = \frac{I(z)}{U(z)} = \frac{bz^{-1}}{1 - az^{-1}} \tag{5.10b}$$

Hence, the mathematical model of the controller results in:

$$G_{DB}(z) = \frac{1}{G_f(z)} \frac{z^{-2}}{(1-z)} \tag{5.11}$$

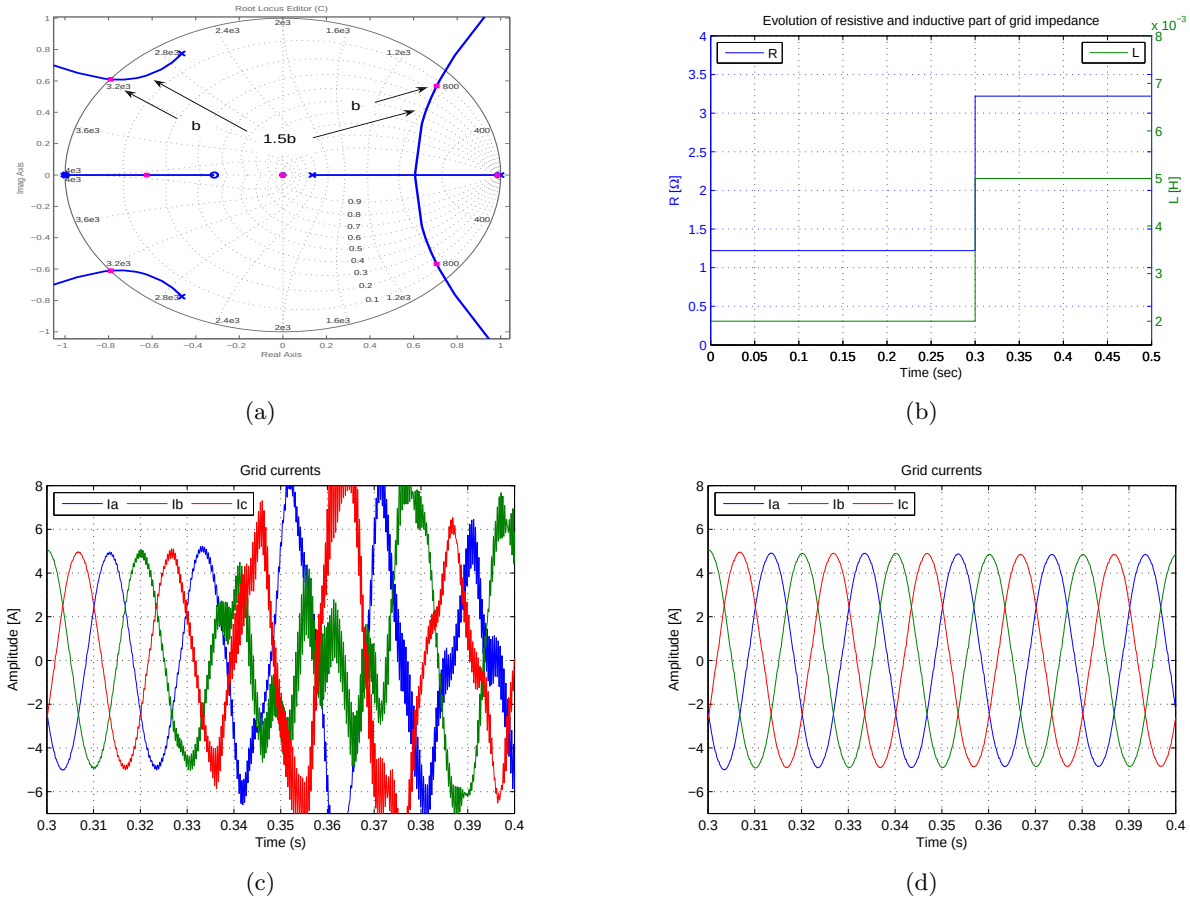

Figure 5.8: *Robustness evaluation of dead beat controller: (a) pole zero map used to derive the robust dead beat controller, (b) the variation of grid impedance, (c) behavior of conventional dead beat controller during the impedance change and (d) the behavior of robust dead beat controller during the impedance change.*

leading to the controller transfer function:

$$G_{DB}(z) = \frac{1}{b}\frac{1-az^{-1}}{(z-z^{-1})} \tag{5.12}$$

Consequently, the controller can be implemented using the following algorithm:

$$u_i((k+1)T_s) = u_i((k-1)T_s) + \frac{1}{b}\Delta i(kT_s) - \frac{a}{b}\Delta i((k-1)T_s) + u_g((k+1)T_s) - u_g((k-1)T_s) \tag{5.13}$$

The method for improving the robustness of dead beat controller proposed in this work increases artificially the gain b of the controller in respect to its initial value calculated by Eq. (5.6). As Fig. 5.8(a) illustrates, increasing b, the damping in the system is increased and additionally high frequency poles are moving inside the unity circle, ensuring the system stability. This method has been tested in many simulation models having different levels of parameters mismatch. In all cases, an increase of gain b with about 50% of its normal value initially calculated using Eq. (5.6) leads to a robust dead beat controller which is able to regulate the current even though the grid parameters have large variations from their initial values. Fig. 5.8(b) illustrates

the situation when grid impedance (both resistive and inductive parts) are registering large variations. In such case, the conventional dead beat controller having the gain b calculated by Eq. (5.6) encounters difficulties to control the current after the impedance value has changed, as depicted in Fig. 5.8(c). On the other hand, artificial increase of gain b leads to a robust dead beat controller able to operate over a large band of impedance values, as Fig. 5.8(d) shows.

5.5 Flexible power control during grid voltage faults

This section discusses the possibilities to control the power delivered at the point of common coupling during unbalanced grid faults. These possibilities apply to both active and reactive current control, however, for simplicity, only the active power control is discussed here. The implementation of these control strategies for reactive power is detailed in Publication 15.

As elaborated in § 3.2 on page 24, the appearance of negative sequence component challenges not only the synchronization algorithm but also the entire control structure. In this situation, a negative sequence current will flow uncontrolled through the grid side converter giving rise to oscillations in delivered power.

This issue has been addressed previously in case of rectifiers in [98, 99] where feed-forward terms comprising negative sequence information are introduced in the control structure. In [100, 101] the negative sequence current has been controlled towards cancellation of dc-link voltage ripple using negative sequence PI controller and hysteresis controller respectively. Implementation of dual PI controller [102], one for positive and one for negative sequence shows an improved control of power converters operating on unbalanced grid conditions. Consequently, these control strategies are able to cancel out the pulsating power coming from grid and to provide a stable dc-link voltage.

In situation of grid connected power generation units, [103] compares different options to structure the control of a power converter operating on unbalanced grid conditions. As a result of this study, in case of a control structure implemented in synchronous rotating reference frame, the best option is implementation of dual current controller, one for each sequence component. However, considering the equation of active power generated by a distribution system running on unbalanced conditions given by (5.14), there are more control possibilities to be investigated.

$$p = \mathbf{v} \cdot \mathbf{i} = \mathbf{v}^{+}\mathbf{i}^{+} + \mathbf{v}^{-}\mathbf{i}^{-} + \mathbf{v}^{+}\mathbf{i}^{-} + \mathbf{v}^{-}\mathbf{i}^{+} \tag{5.14}$$

with $\mathbf{v}$ being the grid voltage vector and $\mathbf{i}$ is the grid current vector, with superscripts "+" and "-" denoting the three-phase sinusoidal positive and negative sequence signals, respectively.

Based on this equation, there are several options to generate the active current reference $\mathbf{i}_p^*$ depending on which terms from the right side of Eq. (5.14) are selected to contribute to active power generation. Publications 14, 15 and 16 explain in detail the possibilities to control both active and reactive current during unbalanced faults. As a result of this study, five control strategies for grid connected power converters operating on voltage faults have been found to be interesting:

1. **Instantaneous active reactive control (IARC)**
   In this case the current reference vector is calculated to deliver the instantaneous active power $p = P^*$ to the grid. The equation for reference current would then become:

$$\mathbf{i}_p^* = g\mathbf{v}; \qquad \text{with:} \quad g = \frac{P}{|\mathbf{v}|^2} \tag{5.15}$$

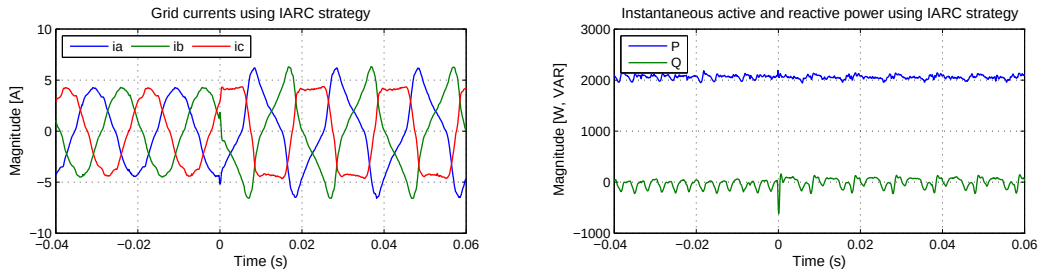

(a) (b)

Figure 5.9: *Experimental results in the case of single phase to ground fault using instantaneous active reactive control (IARC): (a) the grid currents and (b) the active and reactive power delivered to the utility network.*

where $|\mathbf{v}|$ denotes the module of the three-phase voltage vector $\mathbf{v}$, and g is the instantaneous conductance seen from the inverter output. Consequently, since P^* is a constant, the current injected during unbalanced faults is highly distorted, as Fig. 5.9 illustrates. Noticeable here is that the grid current is not sinusoidal and hence is hardly to predict the peak of the current during operation in such conditions. Therefore, caution has to be paid in order to not trip the power converter due to over-current protection. However, due to the fact that no oscillations are present in the output power, there would be no oscillation in dc-link voltage either. Additionally, in case of wind turbine having full scale power converter, grid voltage faults will not create oscillations on the generator side.

2. **Instantaneously controlled positive sequence (ICPS)**
In this situation, only the positive sequence current is controlled to produce the power $p = P^*$, whereas the reference for negative sequence current i_p^{*-} is set to zero.

$$\mathbf{v} \cdot \mathbf{i}_p^{*+} = P \tag{5.16a}$$

$$\mathbf{v} \cdot \mathbf{i}_p^{*-} = 0 \tag{5.16b}$$

Expression of (5.16b) makes negative-sequence current components equal zero, whereas the positive-sequence current reference can be calculated from (5.16a) as follows:

$$\mathbf{i}_p^* = \mathbf{i}_p^{*+} + \mathbf{i}_p^{*-} = g^+ \mathbf{v}^+; \tag{5.17a}$$

$$g^+ = \frac{P}{|\mathbf{v}^+|^2 + \mathbf{v}^+ \cdot \mathbf{v}^-} \tag{5.17b}$$

According to p-q theory [104], the instantaneous reactive power associated with the current vector of (5.17a) is given by:

$$q = \left|\mathbf{v} \times \mathbf{i}_p^{*+}\right| = \underbrace{\left|\mathbf{v}^+ \times \mathbf{i}_p^{*+}\right|}_{0} + \underbrace{\left|\mathbf{v}^- \times \mathbf{i}_p^{*+}\right|}_{\tilde{q}} \tag{5.18}$$

where the sign $\times$ denotes the cross product. It is possible to appreciate that current reference calculated by means of (5.18) gives rise to oscillations at twice the fundamental utility frequency in the instantaneous reactive power injected to the grid.

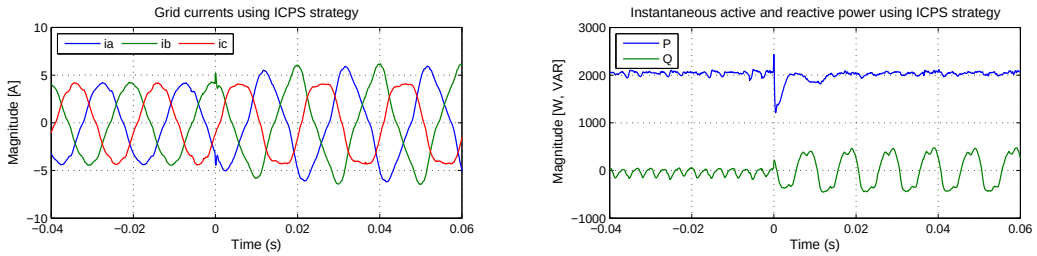

(a) (b)

Figure 5.10: *Experimental results in the case of single phase to ground fault using instantaneous controlled positive sequence (ICPS): (a) the grid currents and (b) the active and reactive power delivered to the utility network.*

In this case (as shown in Fig. 5.10), the active power is instantaneously constant while double frequency oscillations are present in the reactive power waveform due to the interaction of positive sequence current and negative sequence voltage. Again, the grid currents present high distortions leading to a non-sinusoidal waveform which can trip out the power converter.

3. **Positive negative sequence compensation (PNSC)**
With this control strategy, the negative sequence current is controlled in order to cancel out the oscillations present in the active power generated.

$$\mathbf{v}^{+} \cdot \mathbf{i}_p^{*+} + \mathbf{v}^{-} \cdot \mathbf{i}_p^{*-} = P \tag{5.19a}$$

$$\mathbf{v}^{+} \cdot \mathbf{i}_p^{*-} + \mathbf{v}^{-} \cdot \mathbf{i}_p^{*+} = 0 \tag{5.19b}$$

From (5.19b), the negative-sequence reference current can be written as:

$$\mathbf{i}_p^{*-} = -g^{-}\mathbf{v}^{-}; \qquad \text{where:} \qquad g^{-} = \frac{\mathbf{v}^{+} \cdot \mathbf{i}_p^{*+}}{|\mathbf{v}^{+}|^2} \tag{5.20}$$

Substituting (5.20) in (5.19a) and simplifying, the positive-sequence reference current can be calculated by:

$$\mathbf{i}_p^{*+} = g^{+}\mathbf{v}^{+}; \qquad \text{with:} \qquad g^{+} = \frac{P}{|\mathbf{v}^{+}|^2 - |\mathbf{v}^{-}|^2} \tag{5.21}$$

Adding (5.20) and (5.21), the final current reference becomes:

$$\mathbf{i}_p^{*} = \mathbf{i}_p^{*+} + \mathbf{i}_p^{*-} = g^{\pm}\left(\mathbf{v}^{+} - \mathbf{v}^{-}\right); \tag{5.22a}$$

$$\text{with:} \qquad g^{\pm} = \frac{P}{|\mathbf{v}^{+}|^2 - |\mathbf{v}^{-}|^2} \tag{5.22b}$$

The interaction between the current and voltage having different sequences is set to zero, only the components with the same sequence contribute to active power generation. As Fig. 5.11 depicts, the injected current at the point of common coupling is sinusoidal and unbalanced. In addition, the active power experiences no oscillations while the reactive power has large double frequency oscillations according to Eq. (11) in Publication 16. This control strategy presents the advantage of keeping a constant active power at PCC and yet injecting sinusoidal current into the network.

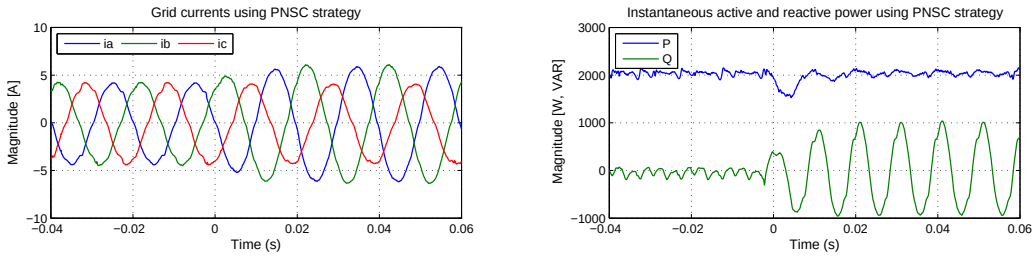

(a) (b)

Figure 5.11: *Experimental results in the case of single phase to ground fault using positive-negative-sequence control (PNSC): (a) the grid currents and (b) the active and reactive power delivered to the utility network.*

4. **Average active reactive control (AARC)**
Unlike the above described control strategies, the average active reactive control handles the current in an average way. The presence of second order component in the module of grid voltage given by Eq. (12) in Publication 16 give rise to high order harmonics in the grid current as presented in the IARC strategy. Since P has been assumed to be a constant, such harmonics come from the second-order component of $|\mathbf{v}|^2$, being:

$$|\mathbf{v}|^2 = \left|\mathbf{v}^+\right|^2 + \left|\mathbf{v}^-\right|^2 + 2\left|\mathbf{v}^+\right|\left|\mathbf{v}^-\right|\cos\left(2\omega\, t + \phi^+ - \phi^-\right) \tag{5.23}$$

High-order harmonics in the current references will be canceled if they are calculated by:

$$\mathbf{i}_p^* = G\ \mathbf{v}; \qquad \text{where:} \qquad G = \frac{P}{V_\Sigma^2} \tag{5.24}$$

where V_Σ is the collective rms value of the grid voltage, and it is defined by:

$$V_\Sigma = \sqrt{\frac{1}{T}\int_0^T |\mathbf{v}|^2\, dt} = \sqrt{|\mathbf{v}^+|^2 + |\mathbf{v}^-|^2} \tag{5.25}$$

In this case, instantaneous conductance is a constant under periodic conditions, namely $g = G$.

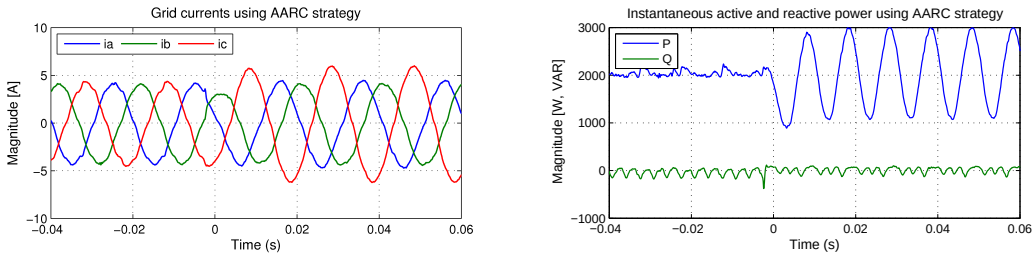

(a) (b)

Figure 5.12: *Experimental results in the case of single phase to ground fault using average active reactive control: (a) the grid currents and (b) the active and reactive power delivered to the utility network.*

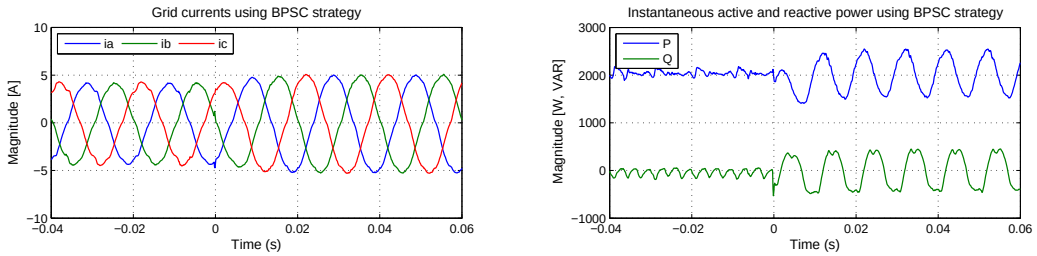

(a) (b)

Figure 5.13: *Experimental results in the case of single phase to ground fault using balanced positive-sequence control: (a) the grid currents and (b) the active and reactive power delivered to the utility network.*

As Fig. 5.12 illustrates, in this case the current is monotonously proportional to the grid voltage and large oscillations are present in the active power waveform .

5. **Balanced positive sequence control (BPSC)**
The last control strategy investigated is controlling the active current reference in respect to positive sequence component of grid voltage only.

$$\mathbf{i}_p^* = G^+\mathbf{v}^+; \qquad \text{where:} \qquad G^+ = \frac{P}{\left|\mathbf{v}^+\right|^2} \tag{5.26}$$

A current vector of (5.26) consists of a set of perfectly balanced positive-sequence sinusoidal waveforms. Under unbalanced operating conditions, the instantaneous active power delivered to the grid will differ from P because of the interaction between the positive-sequence injected current and the negative-sequence grid voltage. That is:

$$p = \mathbf{v}\cdot\mathbf{i}_p^* = \underbrace{\mathbf{v}^+\cdot\mathbf{i}_p^*}_{P} + \underbrace{\mathbf{v}^-\cdot\mathbf{i}_p^*}_{\tilde{p}} \tag{5.27}$$

where $\tilde{p}$ is the power oscillation at twice the fundamental utility frequency. Likewise, the instantaneous reactive power can be calculated as:

$$q = \left|\mathbf{v}\times\mathbf{i}_p^*\right| = \underbrace{\left|\mathbf{v}^+\times\mathbf{i}_p^*\right|}_{0} + \underbrace{\left|\mathbf{v}^-\times\mathbf{i}_p^*\right|}_{\tilde{q}} \tag{5.28}$$

where $\tilde{q}$ is also oscillating at twice the fundamental utility frequency.

As a consequence, the generated current towards the utility network is sinusoidal and balanced as shown in Fig. 5.13, while small double frequency oscillations are present in the active and reactive power waveforms. From the utility point of view, this control strategy may be advantageous when active power delivery is requested during grid fault conditions.

Discussion

Positive and negative-sequence vectors studied here can be considered as orthogonal seen over one grid period and represented on a Euclidean plane $\mathbb{R}^2$ since their scalar product throughout

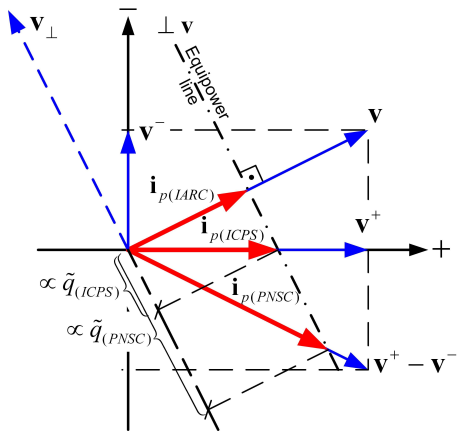

Figure 5.14: *Graphical representation of voltage and current vectors on a positive- negative-sequence Euclidean plane for different control strategies.*

the grid period is always equal to zero, that is:

$$\overline{\mathbf{x}^+ \cdot \mathbf{y}^-} = \frac{1}{T}\int_0^T \mathbf{x}^+ \cdot \mathbf{y}^- dt = 0 \tag{5.29}$$

This graphic representation of voltage and current vectors is shown in Fig. 5.14 and allows a better understanding of previous strategies for current reference generation. For a better visualization and understanding, only current vectors from IARC, ICPS, and PNSC strategies have been represented in Fig. 5.14 . Amplitude of all three current vectors is delimited by the *equi-power line*, which is perpendicular to $\mathbf{v}$. Amplitude of oscillations in the instantaneous reactive power associated to each strategy, $\tilde{q}$, is proportional to the projection of its current vector over the equi-power line. Current vectors from AARC and BPS strategies have the same direction that those vectors from IARC and ICPS strategies, respectively. However, their amplitudes are not instantaneously controlled, generating oscillations in the active power. None of these strategies give rise to a finite mean value in the reactive power injected to the grid.

At first sight, the control strategies providing smooth dc-link voltage waveform appear to be advantageous for distribution system during operation on unbalanced voltage conditions. However, the highly distorted current flowing through the power converter is a big disadvantage of these control strategy, putting stress on the current controller and increasing the risk of tripping out due to over-current protection.

Inspecting Fig. 5.11 and Fig. 5.12 it can be noticed that in one situation the current is direct proportional to the grid voltage while in the other case the current is inverse proportional to the grid voltage. This fact makes PNSC strategy to be useful to compensate for light unbalance of grid voltages, providing in this way ancillary service for the utility network.

However, the most convenient control strategy for DPGS running on unbalanced grid conditions appear to be BPSC. This is due to the fact that sinusoidal and balanced currents are delivered to the network. In addition, the dc-link voltage variations are not as high as in other cases (AARC), hence an over-dimensioned capacitor could facilitate smooth operation of DPGS using this control strategy.

As previously mentioned, these control strategies are treated above for active power delivering only, assuming no reactive power control is necessary at the point of common coupling. However, Publication 15 extends these control strategies to reactive power control as well. The

experimental results presented there validate different possibilities to control both active and reactive power during unbalanced voltage conditions.

5.6 Summary

This chapter discuses the improvement of control for grid connected power converters during grid faults operation conditions. Firstly, the necessity of having an adaptive PR controller with regard to grid frequency has been highlighted, especially when large frequency deviations take place in utility network. A method using the frequency information provided by the PLL algorithm has been proposed and as a consequence, improved behavior of PR controller running on a large frequency deviations has been obtained.

Secondly, the influence of grid impedance variation onto dead-beat controller has been addressed and a control scheme using impedance value imputed to the controller has been proposed. As a consequence, dead-beat controller becomes impedance adaptive, having a stable operation over a broad band of grid impedance variations. Additionally, a simple yet efficient way to design a robust dead beat controller has been developed by tuning its gain towards a more damped system.

Finally, different possibilities to control both active and reactive current during grid faults have been described. These strategies can offer the possibility to generate highly distorted grid currents, sinusoidal but unbalanced currents and sinusoidal and balanced currents, providing flexibility to the control strategies of power converters operating on grid fault conditions. Some of the strategies present advantages for the generation system whereas other can offer ancillary services useful to utility network.

Chapter 6

Conclusion

This chapter presents the conclusions of the work deposed during the thesis period. Although is not author's privilege to judge its own work, due to the fact that this report constitutes the basis of submission for the PhD degree in electrical engineering, the topics on which efforts for bringing novel and useful solutions for better interconnection of power generation systems with utility network are presented. At the end, the chapter points out future work which might be carried out using the knowledge of this study.

6.1 Summary

As pointed out in the beginning of the thesis, the work carried out in this project deals with three issues particular to grid connected power converters, i.e. *grid synchronization, grid monitoring* and *control of grid connected power converters*. Particular attention has been paid to the influence of grid faults, especially unbalanced grid faults, onto the above three listed issues.

Based on initial study about grid faults, the presence of negative sequence voltage component has been identified as one of the most challenging situations for grid connected power converters. The synchronization algorithm, along with the entire control structure, are heavily influenced by the appearance of negative sequence component during operation on unbalanced faults.

Consequently, the development of robust synchronization systems is done around the idea of eliminating the influence of negative sequence component onto the phase locking loop algorithm. As a result, two robust synchronization systems have been developed, one using a repetitive controller and another one using second order generalized integrator (SOGI) to combat the influence of negative sequence on the phase angle detection. Both algorithms have been extensively tested on different grid conditions and in all cases a clean phase angle signal synchronized with the positive sequence component of grid voltage has been achieved. If the algorithm using repetitive controller is computationally complex due to the involvement of DFT, the second algorithm based on second order generalized integrator is lighter and has a superior behavior on all the tests.

Further on, owing to the fact that PLL provides information about grid voltage amplitude and its frequency, grid monitoring systems based on the above robust synchronization algorithms can be further developed. The thesis treats in details a monitoring system based on robust synchronization algorithm using DFT. Along with the phase angle of positive sequence component, the grid frequency and positive and negative sequence components of grid voltage can be also determined, thus providing a detailed information about the status of grid voltage at the point of common coupling.

This information can be used in the control of grid connected power converters in order to

obtain more flexibility of power delivery. The thesis describes in details several control possibilities of both active and reactive power during normal and grid fault conditions. As a result, using the information from grid monitoring unit, the developed control strategies can shape the delivered power/current to meet the DPGS and/or power system needs. More precisely, the delivered power can be instantaneous controlled in order to minimize the oscillations in dc-link voltage, thus having a beneficial effect for the generation system when running on unbalanced grid conditions. Additionally, there is the possibility to control the active power in a way to compensate for light unbalance present in the utility voltage, providing in this way ancillary services for utility network. Moreover, even in the most unbalanced grid conditions caused by faults, there is possible to supply sinusoidal and balanced currents to the power system by using the positive sequence component information.

In addition to different control strategies, current controllers to be used for grid connected power converters control have been also studied in this thesis. Their strengths and weaknesses when running on grid fault conditions have been identified and solutions to improve their behavior have been proposed. Most of these solutions use information obtained from grid monitoring unit as input into the controller model in order to improve their robustness to parameters mismatch. The results presented confirm an improved behavior when the power generation system has to ride through different grid disturbances.

6.2 Thesis contributions

Although there is a large number of research articles and reports dealing with the interaction between distributed power generation systems and utility network, the work comprised in this thesis brings additional solutions for easy integration of DPGS.

- Regarding grid synchronization, the idea of filtering the grid voltages before estimating the phase angle has been widely described in previous publications. However, the filtering techniques applied are not facilitating robustness to severe grid disturbance such as those caused by unbalanced faults. Among the existent solutions, only two of them [73, 75] are robust to grid faults.

- In respect to grid monitoring, owing to already developed algorithm for grid synchronization, a self containing unit able to provide information of positive and negative voltage sequence components, grid frequency, voltage amplitude and positive sequence phase angle has been developed.

- Additionally, two methods for identifying the line impedance have been developed. Particular the method using active power variations and grid voltage control stands as an elegant way to identify the grid impedance in case of power generation systems having variable input power, such as wind turbines and photovoltaic systems. The method combines two of the already existent features of wind turbine control, i.e. output power variations due to wind speed variations and grid voltage control due to requirements from power system operators.

- Although the behavior of power converters running on unbalanced grid conditions has been previously discussed in other research works, the main goal there was to achieve a non-oscillatory dc-link voltage [98–101]. Few works [102, 103] treat the control of negative sequence current using a dedicated controller, however only one possibility is considered in these works. The work deposed in this thesis extends this to five possible control

strategies to be used during low voltage ride through (and not only) situations. Some of these strategies offer benefits for distribution generation system whereas other offer ancillary functions useful to utility network.

6.3 Author's contribution

As may be observed from the publications following this report, the author had a fruitful collaboration with his supervisors, colleagues and researchers from different academic and industrial institutions. Certainly, they influenced the research work done in this thesis and their contribution should be acknowledged.

The main subjects investigated in this thesis are not coming only from studies of previous works presented in literature but also from steering meetings and discussions with experienced researchers in the field such the supervisors, the steering meeting members and colleagues or guest researchers from within the institute.

However, the development of chosen algorithms, their implementation in simulation environment and experimental setup has been mainly done by the author. Moreover, with the exception of few publications (Publication 6 and 15), the author has been the leading force in preparing all the other publications.

6.4 Perspectives

Even though there has been a lot of intense research done in order to come up with the above solutions, there is still place for more improvements. Because only the grid side converter of a distributed power generation system has been considered in this work, would be interesting to test the behavior of the developed algorithms on a complete power generation unit such as wind turbine or photovoltaic system, involving also the input source and its control.

The impedance estimation method based on active power variations and grid voltage control claims that is complying with the power quality standards regarding flicker emission. Indeed, this method has been implemented into a simulation model of a 1 MW wind turbine connected through a full scale back to back converter to the utility network. The preliminary results showed a low flicker coefficient, however more investigations are necessary in order to validate that the method does not emit flicker in case of implementation into a real system.

Regarding the control possibilities during unbalanced grid conditions, would be interesting to investigate their effect on the input side converter and the generator in case of wind turbine system. Moreover, another interesting study can be the analysis of many DPGS forming a micro-grid/island making use of these control strategies in order to increase the power quality in the grid and/or to maintain it stable during disturbances.

Bibliography

[1] EWEA, "Wind power targets for Europe: 7500 MW by 2010," European Wind Energy Association, Tech. Rep., 2003. [Online]. Available: http://www.ewea.org/fileadmin/ewea_documents/documents/publications/75GW/13190_policy_briefing_4_01.pdf

[2] IEA-PVPS, "Installed PV power as of the end of 2005," http://www.iea-pvps.org/isr/01.htm, 2006.

[3] M. Shahidehpour and F. Schwartz, "Don't let the sun go down on PV," in *IEEE Power & Energy Magazine*, vol. 2, no. 3, 2004, pp. 40–48.

[4] J. P. Lyons and V. Vlatkovic, "Power electronics and alternative energy generation," in *Proc. of PESC'04*, 2004, pp. 16–19.

[5] T. Ackermann and L. Söder, "An overview of wind energy status - 2002," in *Renewable and Sustainable Energy Reviews 6*, 2002, pp. 67–128.

[6] S. Heier, *Grid Integration of Wind Energy Conversion Systems.* John Wiley & Sons, 1998.

[7] T. Ackermann, *Wind Power in Power Systems.* John Wiley & Sons, Ltd., 2005, ISBN: 0-470-85508-8.

[8] F. Blaabjerg, Z. Chen, and S. Kjaer, "Power electronics as efficient interface in dispersed power generation systems," *IEEE Trans. on Power Electronics*, vol. 19, no. 5, pp. 1184–1194, 2004.

[9] A. D. Hansen, F. Lov, F. Blaabjerg, and L. H. Hansen, "Review of contemporary wind turbine concepts and their market penetration," *Wind Engineering*, vol. 28, no. 3, pp. 247–263, 2004.

[10] Renewable Energy World, "Global wind market grows 32% in 2006," *Renewable Energy World*, vol. 10, no. 1, 2007. [Online]. Available: http://www.renewable-energy-world.com/display_article/283821/123/ARTCL/none/NEWS/Global-wind-market-grows-32-in-2006/

[11] P. Barbosa, L. Rolim, V. Tavares, E. Watanabe, and R. Hanitsch, "Novel control strategy for grid-connected DC-AC converters with load power factor," in *IEE Proc. in Generation, Transmission and Distribution*, vol. 145, no. 5, 1998, pp. 487–491.

[12] N. Jenkins, R. Allan, P. Croosley, D. Kirschen, and G. Strbac, *Embedded Generation.* IEE, 2000.

[13] MathWorks Inc., "MATLAB/Simulink," 2007. [Online]. Available: http://www.mathworks.com/

[14] Plexim GmbH, "PLECS Toolbox," http://www.plexim.com, 2007. [Online]. Available: http://www.plexim.com

[15] dSpace GmbH, "dSpace – Solutions for control," 2007. [Online]. Available: http://www.dspaceinc.com/ww/en/inc/start.cfm

[16] J. Carrasco, L. Franquelo, J. Bialasiewicz, E. Galvan, R. PortilloGuisado, M. Prats, J. Leon, and N. Moreno-Alfonso, "Power-electronic systems for the grid integration of renewable energy sources: A survey," *IEEE Trans. on Industrial Electronics*, vol. 53, no. 4, pp. 1002–1016, June 2006.

[17] C. Klumpner, F. Blaabjerg, and P. Thoegersen, "Alternate ASDs: evaluation of the converter topologies suited for integrated motor drives," *IEEE Industry Applications Magazine,*, vol. 12, no. 2, pp. 71–83, 2006.

[18] B. K. Bose, "An adaptive hysteresis-band current control technique of a voltage-fed PWM inverter for machine drive dystem," *IEEE Trans. on Industrial Electronics*, vol. 37, no. 5, pp. 402–408, 1990.

[19] L. Malesani and P. Tenti, "A novel hysteresis control method for current-controlled voltage-source PWM inverters with constant modulation frequency," *IEEE Trans. on Industry Applications*, vol. 26, pp. 88–92, 1990.

[20] L. Sonaglioni, "Predictive digital hysteresis current control," in *Proc. of IAS'95*, vol. 3, 1995, pp. 1879–1886.

[21] Q. Yao and D. Holmes, "A simple, novel method for variable-hysteresis-band current control of a three phase inverter with constant switching frequency," in *Proc. of IAS'93*, 1993, pp. 1122–1129.

[22] L. Malesani, P. Mattavelli, and P. Tomasin, "Improved constant-frequency hysteresis current control of VSI inverters with simple feedforward bandwidth prediction," *IEEE Trans. on Industry Applications*, vol. 33, no. 5, pp. 1194–1202, 1997.

[23] S. Buso, L. Malesani, and P. Mattavelli, "Comparison of current control techniques for active filter applications," *IEEE Trans. on Industrial Electronics*, vol. 45, no. 5, pp. 722–729, 1998.

[24] S. Buso, S. Fasolo, and P. Mattavelli, "Uninterruptible power supply multi-loop control employing digital predictive voltage and current regulators," in *Proc. of APEC 2001*, vol. 2, 2001, pp. 907–913.

[25] Y. Ito and S. Kawauchi, "Microprocessor based robust digital control for UPS with three-phase PWM inverter," *IEEE Trans. on Power Electronics*, vol. 10, no. 2, pp. 196–204, 1995.

[26] T. Kawabata, T. Miyashita, and Y. Yamamoto, "Dead beat control of three phase PWM inverter," *IEEE Trans. on Power Electronics*, vol. 5, no. 1, pp. 21–28, 1990.

[27] J. Kolar, H. Ertl, and F. Zach, "Analysis of on- and off-line optimized predictive current controllers for PWM converter systems," *IEEE Trans. on Power Electronics*, vol. 6, no. 3, pp. 451–462, July 1991.

[28] P. Mattavelli, G. Spiazzi, and P. Tenti, "Predictive digital control of power factor preregulators with input voltage estimation using disturbance observers," *IEEE Trans. on Power Electronics*, vol. 20, no. 1, pp. 140–147, 2005.

[29] S.-G. Jeong and M.-H. Woo, "DSP-based active power filter with predictive current control," *IEEE Trans. on Industrial Electronics*, vol. 44, no. 3, pp. 329–336, 1997.

[30] R. Wu, S. Dewan, and G. Slemon, "Analysis of a PWM AC to DC voltage source converter under the predicted current control with a fixed switching frequency," *IEEE Trans. on Industry Applications*, vol. 27, no. 4, pp. 756–764, 1991.

[31] K. Macken, K. Vanthournout, J. Van den Keybus, G. Deconinck, and R. Belmans, "Distributed control of renewable generation units with integrated active filter," *IEEE Trans. on Power Electronics*, vol. 19, no. 5, pp. 1353–1360, 2004.

[32] L. Malesani, P. Mattavelli, and S. Buso, "Robust dead-beat current control for PWM rectifiers and active filters," *IEEE Trans. on Industry Applications*, vol. 35, no. 3, pp. 613–620, 1999.

[33] G. Bode, P. C. Loh, M. Newman, and D. Holmes, "An improved robust predictive current regulation algorithm," *IEEE Trans. on Industry Applications*, vol. 41, no. 6, pp. 1720–1733, 2005.

[34] Y. A.-R. I. Mohamed and E. F. El-Saadany, "An improved deadbeat current control scheme with a novel adaptive self-tuning load model for a three-phase PWM voltage-source inverter," *IEEE Trans. on Industrial Electronics,*, vol. 54, no. 2, pp. 747–759, 2007.

[35] D. N. Zmood, D. G. Holmes, and G. H. Bode, "Frequency-domain analysis of three-phase linear current regulators," *IEEE Trans. on Industry Applications*, vol. 37, no. 2, pp. 601–610, 2001.

[36] E. Twining and D. G. Holmes, "Grid current regulation of a three-phase voltage source inverter with an LCL input filter," *IEEE Trans. on Power Electronics*, vol. 18, no. 3, pp. 888–895, 2003.

[37] M. Kazmierkowski and M. Dzieniakowski, "Review of current regulation methods for VS-PWM inverters," in *Proc. of ISIE'93*, 1993, pp. 448–456.

[38] ——, "Review of current regulation techniques for three-phase PWM inverters," in *Proc. of IECON '94*, vol. 1, 1994, pp. 567–575.

[39] S. Fukuda and T. Yoda, "A novel current-tracking method for active filters based on a sinusoidal internal model," *IEEE Trans. on Industrial Electronics*, vol. 37, no. 3, pp. 888–895, 2001.

[40] X. Yuan, W. Merk, H. Stemmler, and J. Allmeling, "Stationary-frame generalized integrators for current control of active power filters with zero steady-state error for current harmonics of concern under unbalanced and distorted operating conditions," *IEEE Trans. on Industry Applications*, vol. 38, no. 2, pp. 523–532, 2002.

[41] D. Zmood and D. G. Holmes, "Stationary frame current regulation of PWM inverters with zero steady-state error," *IEEE Trans. on Power Electronics*, vol. 18, no. 3, pp. 814–822, 2003.

[42] R. Teodorescu and F. Blaabjerg, "Proportional-resonant controllers. A new breed of controllers suitable for grid-connected voltage-source converters," in *Proc. of OPTIM'04*, vol. 3, 2004, pp. 9–14.

[43] R. Teodorescu, F. Blaabjerg, U. Borup, and M. Liserre, "A new control structure for grid-connected LCL PV inverters with zero steady-state error and selective harmonic compensation," in *Proc. of APEC'04*, vol. 1, 2004, pp. 580–586.

[44] M. Kazmierkowski, R. Krishnan, and F. Blaabjerg, *Control in Power Electronics – Selected Problems*. Academic Press, 2002.

[45] V. Blasko and V. Kaura, "A novel control to actively damp resonance in input LC filter of a three-phase voltage source converter," *IEEE Trans. on Industry Applications*, vol. 33, no. 2, pp. 542–550, 1997.

[46] I. Agirman and V. Blasko, "A novel control method of a VSC without AC line voltage sensors," *IEEE Trans. on Industry Applications*, vol. 39, no. 2, pp. 519–524, 2003.

[47] S.-H. Song, S.-I. Kang, and N.-K. Hahm, "Implementation and control of grid connected AC-DC-AC power converter for variable speed wind energy conversion system," in *Proc. of APEC '03*, vol. 1, 2003, pp. 154–158.

[48] R. Teodorescu, F. Iov, and F. Blaabjerg, "Flexible development and test system for 11 kW wind turbine," in *Proc. of PESC'03*, vol. 1, 2003, pp. 67–72.

[49] Q. Zeng, L. Chang, and P.Song, "SVPWM-based current controller with grid harmonic compensation for three-phase grid-connected VSI," in *Proc. of PESC04*, vol. 4, 2004, pp. 3494–3500.

[50] R. Teodorescu and F. Blaabjerg, "Flexible control of small wind turbines with grid failure detection operating in stand-alone and grid-connected mode," *IEEE Trans. on Power Electronics*, vol. 19, no. 5, pp. 1323–1332, 2004.

[51] M. Malinowski, M. Kazmierkowski, S. Hansen, F. Blaabjerg, and G. Marques, "Virtual-flux-based direct power control of three-phase PWM rectifiers," *IEEE Trans. on Industry Applications,*, vol. 37, no. 4, pp. 1019–1027, July-Aug. 2001.

[52] M. Malinowski, M. Kazmierkowski, and A. Trzynadlowski, "A comparative study of control techniques for PWM rectifiers in AC adjustable speed drives," *IEEE Trans. on Power Electronics*, vol. 18, no. 6, pp. 1390–1396, 2003.

[53] M. Prodanovic and T. C. Green, "Control of power quality in inverter based distributed generation," in *Proc. of IECON'02*, vol. 2, 2002, pp. 1185–1189.

[54] M. Prodanovic and T. Green, "Control and filter design of three-phase inverters for high power quality grid connection," *IEEE Trans. on Power Electronics*, vol. 18, no. 1, pp. 373–380, Jan. 2003.

[55] D. Candusso, L. Valero, and A. Walter, "Modelling, control and simulation of a fuel cell based power supply system with energy management," in *Proc. of IECON'02*, vol. 2, 2002, pp. 1294–1299.

[56] M. Malinowski, M. Jasinski, and M. Kazmierkowski, "Simple direct power control of three-phase PWM rectifier using space-vector modulation (DPC-SVM)," *IEEE Trans. on Industrial Electronics*, vol. 51, no. 2, pp. 447–454, April 2004.

[57] L. Xu and P. Cartwright, "Direct active and reactive power control of dfig for wind energy generation," *IEEE Trans. on Energy Conversion*, vol. 21, no. 3, pp. 750–758, Sept. 2006.

[58] M. H. J. Bollen, *Understanding Power Quality Problems: Voltage Sags and Interruptions.* IEEE Press, 2002.

[59] IEC Standard 61727, "Characteristic of the utility interface for photovoltaic (PV) systems," IEC, Tech. Rep., 2002.

[60] IEEE15471, "IEEE standard for interconnecting distributed resources with electric power systems," 2005.

[61] IEEE929, "IEEE recommended practice for utility interface of photovoltaic (PV) systems," 2000.

[62] Eltra and Elkraft, "Wind turbines connected to grids with voltage below 100 kV," http://www.eltra.dk, 2004.

[63] E.ON-Netz, "Grid code – high and extra high voltage," E.ON Netz GmbH, Tech. Rep., 2006. [Online]. Available: http://www.eon-netz.com/Ressources/downloads/ENENARHS2006eng.pdf

[64] F. M. Gardner, *Phase Lock Techniques.* New York: Wiley, 1979.

[65] P. V. Brennan, *Phase-locked loops : principles and practice.* Macmillan, 1996.

[66] D. R. Stephens, *Phase-locked loops for wireless communications : digital, analog and optical implementations.* Kluwer Academic, 2002.

[67] V. Kaura and V. Blasko, "Operation of a phase loop system under distorted utility conditions," *IEEE Trans. on Industry Applications*, vol. 33, no. 1, pp. 58–63, 1997.

[68] H.-S. Song, H.-G. Park, and K. Nam, "An instantaneous phase angle detection algorithm under unbalanced line voltage condition," in *Proc. of PESC'99*, vol. 1, 27 June-1 July 1999, pp. 533–537vol.1.

[69] H.-S. Song and K. Nam, "Instantaneous phase-angle estimation algorithm under unbalanced voltage-sag conditions," in *IEE Proceedings of Generation, Transmission and Distribution*, vol. 147, no. 6, Nov. 2000, pp. 409–415.

[70] S.-K. Chung, "A phase tracking system for three phase utility interface inverters," *IEEE Trans. on Power Electronics*, vol. 15, no. 3, pp. 431–438, 2000.

[71] ——, "Phase-Locked Loop for grid-connected three-phase power conversion systems," *IEE Proceedings on Electronic Power Applications*, vol. 147, no. 3, pp. 213–219, 2000.

[72] J. Svensson, "Synchronisation methods for grid-connected voltage source converters," in *IEE Proc. Generation, Transmission and Distribution*, vol. 148, no. 3, 2001, pp. 229–235.

[73] M. Karimi-Ghartemani and M. Iravani, "A method for synchronization of power electronic converters in polluted and variable-frequency environments," *IEEE Trans. on Power Systems*, vol. 19, no. 3, pp. 1263–1270, 2004.

[74] P. Rodriguez, J. Pou, J. Bergas, I. Candela, R. Burgos, and D. Boroyevich, "Double synchronous reference frame PLL for power converters," in *Proc. of PESC'05*, 2005, pp. 1415–1421.

[75] M. C. Benhabib and S. Saadate, "A new robust experimentally validated Phase-Looked Loop for power electronic control," *EPE Journal*, vol. 15, no. 3, pp. 36–48, August 2005.

[76] P. Rodriguez, A. Luna, M. Ciobotaru, R. Teodorescu, and F. Blaabjerg, "Advanced grid synchronization systems for power converters under unbalanced and distorted operating conditions," in *Proc. of IECON'06*, 2006, pp. 5173–5178.

[77] P. Rodriguez, J. Pou, J. Bergas, J. I. Candela, R. P. Burgos, and D. Boroyevich, "Decoupled double synchronous reference frame PLL for power converters control," *IEEE Trans. on Power Electronics*, vol. 22, no. 2, pp. 584–592, March 2007.

[78] H. Kim, S.-J. Lee, and S.-K. Sul, "Reference wave generator in dynamic voltage restorers by use of PQR power theory," *Proc. of APEC'04*, vol. 3, pp. 1452–1457, 2004.

[79] S.-J. Lee, H. Kim, S.-K. Sul, and F. Blaabjerg, "A novel control algorithm for static series compensators by use of PQR instantaneous power theory," *IEEE Trans. on Power Electronics*, vol. 19, no. 3, pp. 814–827, 2004.

[80] C. Klumpner, M. Liserre, and F. Blaabjerg, "Improved control of an active-front-end adjustable speed drive with a small DC-link capacitor under real grid conditions," in *Proc. of PESC'04*, vol. 2, no. 1156-1162, 2004.

[81] A. Tarkiainen, R. Pollanen, M. Niemela, and J. Pyrhonen, "Identification of grid impedance for purposes of voltage feedback active filtering," *IEEE Power Electronics Letters*, vol. 2, no. 1, pp. 6–10, 2004.

[82] M. Sumner, B. Palethorpe, and D. Thomas, "Impedance measurement for improved power quality-Part 2: a new technique for stand-alone active shunt filter control," *IEEE Trans. on Power Delivery*, vol. 19, no. 3, pp. 1457–1463, 2004.

[83] V. Diana, M. Sumner, P. Zanchetta, and M. Marinelli, "Non-invasive power system impedance monitoring for improved power quality," in *Proc. of Power Electronics, Machines and Drives*, vol. 1, 2004, pp. 265–268.

[84] DIN and VDE, "Automatic disconnection device between a generator and the public low-voltage grid," Standard, 2005.

[85] L. Asiminoaei, R. Teodorescu, F. Blaabjerg, and U. Borup, "A new method of on-line grid impedance estimation for PV inverters," in *Proc. of APEC'04*, vol. 3, 2004, pp. 1527–1533.

[86] ——, "A digital controlled PV-inverter with grid impedance estimation for ENS detection," *IEEE Trans. on Power Electronics*, vol. 20, no. 6, pp. 1480–1490, 2005.

[87] A. V. Timbus, R. Teodorescu, F. Blaabjerg, and U. Borup, "Online grid measurement and ENS detection for PV inverter running on highly inductive grid," *IEEE Power Electronics Letters*, vol. 2, no. 3, pp. 77–82, 2004.

[88] F. Bertling and S. Soter, "A novel converter integrable impedance measuring method for islanding detection in grids with widespread use of decentral generation," in *Proc. of Power Electronics, Electrical Drives, Automation and Motion*, 2006, pp. 503–507.

[89] IEA-PVPS, "Evaluation of islanding detection methods for photovoltaic utility interactive power systems," IEA-PVPS, http://www.iea-pvps.org, Online report T5-09, March 2002. [Online]. Available: http://www.oja-services.nl/iea-pvps/products/download/rep5_09.pdf

[90] F. De Mango, M. Liserre, A. Dell'Aquila, and A. Pigazo, "Overview of anti-islanding algorithms for PV systems. Part I: Passive methods," in *Proc. of Power Electronics and Motion Control Conference*, 2006, pp. 1878–1883.

[91] F. De Mango, M. Liserre, and A. Dell'Aquila, "Overview of anti-islanding algorithms for PV systems. Part II: Active methods," in *Proc. of Power Electronics and Motion Control Conference*, Aug. 2006, pp. 1884–1889.

[92] B. Palethorpe, M. Sumner, and D. Thomas, "Power system impedance measurement using a power electronic converter," in *Proc. of Harmonics and Quality of Power*, vol. 1, 2000, pp. 208–213.

[93] ——, "System impedance measurement for use with active filter control," in *Proc. of Power Electronics and Variable Speed Drives*, 2000, pp. 24–28.

[94] A. V. Timbus, R. Teodorescu, F. Blaabjerg, and U. Borup, "ENS detection algorithm and its implementation for PV inverters," *IEE Proceedings of Electric Power Applications*, vol. 153, no. 2, pp. 206–212, 2006.

[95] ——, "Online grid impedance measurement suitable for multiple PV inverters running in parallel," in *Proc. of APEC '06*, 2006, pp. 907–911.

[96] IEC Standard, "Electromagnetic compatibility (EMC) - Part 4: Testing and measurement techniques, Section 15: Flickermeter - Functional and design specifications," International Electrotechnical Commission, Tech. Rep. 61000-4-15, 1997.

[97] Y. Sato, T. Ishizuka, K. Nezu, and T. Kataoka, "A new control strategy for voltage-type PWM rectifiers to realize zero steady-state control error in input current," *IEEE Transactions on Industry Applications*, vol. 34, no. 3, pp. 480–486, May-June 1998.

[98] P. Enjeti and S. Choudhury, "A new control strategy to improve the performance of a PWM AC to DC converter under unbalanced operating conditions," *IEEE Trans. on Power Electronics*, vol. 8, no. 4, pp. 493–500, Oct. 1993.

[99] D. Vincenti and H. Jin, "A three-phase regulated PWM rectifier with on-line feedforward input unbalance correction," *IEEE Trans. on Industrial Electronics*, vol. 41, no. 5, pp. 526–532, Oct. 1994.

[100] P. Rioual, H. Pouliquen, and J.-P. Louis, "Regulation of a PWM rectifier in the unbalanced network state using a generalized model," *IEEE Trans. on Power Electronics*, vol. 11, no. 3, pp. 495–502, May 1996.

[101] A. Stankovic and T. Lipo, "A novel control method for input output harmonic elimination of the PWM boost type rectifier under unbalanced operating conditions," *IEEE Trans. on Power Electronics*, vol. 16, no. 5, pp. 603–611, 2001.

[102] H.-S. Song and K. Nam, "Dual current control scheme for PWM converter under unbalanced input voltage conditions," *IEEE Trans. on Industrial Electronics*, vol. 46, no. 5, pp. 953–959, 1999.

[103] G. Saccomando, J. Svensson, and A. Sannino, "Improving voltage disturbance rejection for variable-speed wind turbines," *IEEE Trans. on Energy Conversion*, vol. 17, no. 3, pp. 422–428, 2002.

[104] H. Akagi, Y. Kanazawa, and A. Nabae, "Instantaneous reactive power compensator comprising switching devices without energy storage components," *IEEE Trans. on Industry Application*, vol. IA-20, pp. 625–630, 1984.

Part II

Publications

Publication 1

Overview of control and grid synchronization for distributed power generation systems

by F. Blaabjerg, R. Teodorescu, M. Liserre and A. Timbus
Article published in IEEE Transactions on Industrial Electronics, Vol. 53, No. 5, pages 1398 – 1409, 2006

Overview of Control and Grid Synchronization for Distributed Power Generation Systems

Frede Blaabjerg *Fellow, IEEE,* Remus Teodorescu *Senior Member, IEEE,* Marco Liserre, *Member, IEEE,* and Adrian V. Timbus, *Student Member, IEEE,*

***Abstract*—Renewable energy sources like wind, sun and hydro are seen as a reliable alternative to the traditional energy sources such as oil, natural gas or coal. Distributed Power Generation Systems (DPGS) based on renewable energy sources experience a large development worldwide, with Germany, Denmark, Japan, US as leaders in the development in this field. Due to the increasing number of DPGS connected to the utility network, new and stricter standards in respect to power quality, safe running, islanding protection are issued. As a consequence, the control of distributed generation systems should be improved in order to meet the requirements for grid interconnection. This paper gives an overview of the structures for the DPGS based on fuel cell (FC), photovoltaic (PV) and wind turbines (WT). In addition, control structures of the grid side converter are presented and the possibility of compensation for low order harmonics is also discussed. Moreover, control strategies when running on grid faults are treated. The paper ends up with an overview of synchronization methods and a discussion about their importance in the control.**

***Index Terms*—Distributed power generation, grid converter control, grid disturbances, control strategies, grid synchronization.**

I. Introduction

NOWADAYS fossil fuel is the main energy supplier of the worldwide economy, but the recognition of it as being a major cause of environmental problems makes the mankind to look for alternative resources in power generation. Moreover, the day-by-day increasing demand for energy can create problems for the power distributors, like grid instability and even outages. The necessity of producing more energy combined with the interest in clean technologies yields in an increased development of power distribution systems using renewable energy [1].

Among the renewable energy sources, hydro power and wind energy have the largest utilization nowadays. In countries with hydro power potential, small hydro turbines are used at the distribution level, in order to sustain the utility network in dispersed or remote locations. The wind power potential in many countries around the world has led to a large interest and fast development of wind turbine (WT) technology in the last decade [2]. A total amount of nearly 35 GW wind power has been installed in Europe by the end of 2004, as Fig. 1(a) shows.

A.V. Timbus, F. Blaabjerg and R. Teodorescu are with the Institute of Energy Technology, Aalborg University, DK-9220 Aalborg, Denmark. Email: avt@iet.aau.dk, fbl@iet.aau.dk, ret@iet.aau.dk

M. Liserre is with the Polytechnic of Bari, Dept. of Electrotechnical and Electronic Engineering, 70125-Bari, Italy. Email: liserre@poliba.it

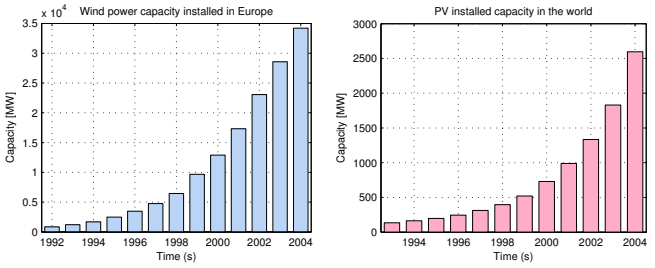

(a) (b)

Fig. 1. Installed capacity at the end of 2004: (a) wind energy in Europe [2] and (b) PV power in the world [3].

Another renewable energy technology which gains acceptance as a way of maintaining and improving living standards without harming the environment is the photovoltaic technology. As shown in Fig. 1(b), the number of photovoltaic (PV) installations has an exponentially growth, mainly due to the governments and utility companies that support programs which focus on grid connected PV systems [3], [4].

Besides their low efficiency, the controllability of the DPGS based on both wind and sun are their main drawback [5]. As a consequence, their connection to the utility network can lead to grid instability or even failure, if these systems are not properly controlled. Moreover, the standards for interconnecting these systems to the utility network are stressing more and more the capability of the DPGS to run over short grid disturbances. In this case, both synchronization algorithm and the current controller play an major role. Therefore, the control strategies applied to distributed systems become of high interest.

This paper gives an overview of the main DPGS structures, photovoltaic and fuel cell systems being first discussed. A classification of wind turbine systems regarding the use of power electronics follows. This is continued by a discussion of control structures for grid side converter and the possibilities of implementation in different reference frames. Further on, the main characteristics of control strategies under grid fault conditions are discussed. The overview of grid synchronization methods and their influence in control conclude the paper.

II. DPGS structure

A general structure for distributed systems is illustrated in Fig. 2. The input power is transformed into electricity by means of a power conversion unit whose configuration is closely related to the input power nature. The electricity produced can be delivered to the local loads or can be delivered

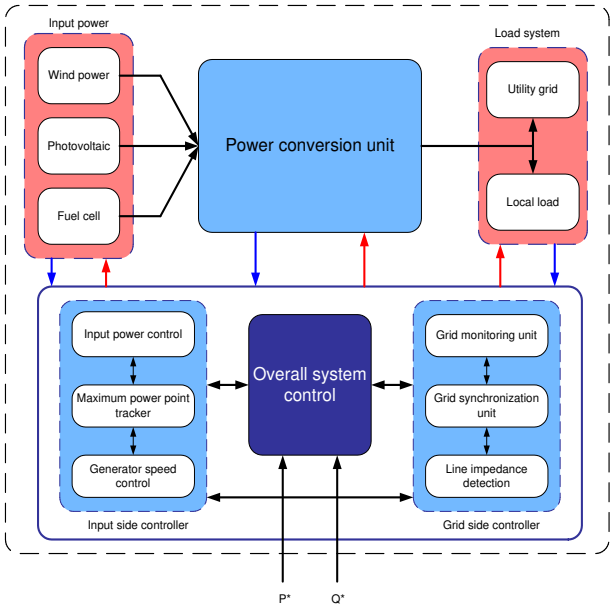

Fig. 2. General structure for distributed power system having different input power sources.

to the utility network, depending where the generation system is connected.

One important part of the distributed system is its control. The control tasks can be divided into two major parts:

- *input side controller* with the main property to extract the maximum power from the input source. Naturally, protection of the input side converter is also considered in this controller.
- *grid side controller* which can have the following tasks
  - control of active power generated to the grid
  - control of reactive power transfer between the DPGS and the grid
  - control of dc-link voltage
  - ensure high quality of the injected power
  - grid synchronization

The items listed above for the grid side converter are the basic features this converter should have. Additionally, ancillary services like local voltage and frequency regulation, voltage harmonic compensation or active filtering might be requested by the grid operator.

As previously pointed out, the power conversion unit has different hardware structures which are close related to the input power nature. The following section is revising the technologies most used today in fuel cell (FC) and PV systems as well as WT systems.

III. Hardware Topologies for DPGS

A detailed description of the hardware structure for many types of DPGS is given in [5]. Noticeable is that the PV and FC systems have a similar hardware structure while different hardware topologies can be found for WT systems, depending on the type of the generator used. A brief introduction into the structure of these systems is given below.

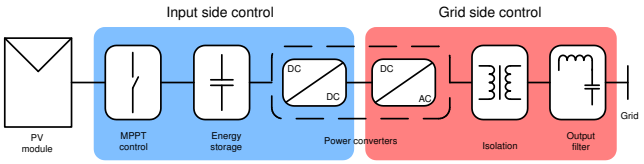

Fig. 3. Hardware structure for a PV system using a dc-dc stage to boost up the input voltage.

A. Photovoltaic and fuel cell systems

As mentioned above, the hardware structures of a PV and FC system are quite similar. Although, both FC and PV systems have a low voltage input provided by the fuel cell and the photovoltaic panels, more such units can be connected together to obtain the required voltage and power. Usually power conditioning systems, including inverters and dc-dc converters, are often required in order to supply normal customer load demand or send electricity into the grid, as shown in Fig. 3. The voltage boosting can be done in the dc or ac stage of the system [5]–[11]. For smoothing the output current, an LCL filter is normally used between these systems and the utility network. In addition, isolation between the input and output power is required in many countries where such systems are installed. Again, there are two ways to achieve isolation, one is using the dc-dc converter and other is using an isolation transformer after the dc-ac stage.

B. Wind turbine systems

In this section a classification of WT systems in those using and those not using power electronics as interface to the utility network is given. Hardware structures in each cases will be illustrated in order to distinct the systems.

1) Wind turbine systems without power electronics: Most of these topologies are based on squirrel-cage induction generator (SCIG) which is directly connected to the grid. A soft-starter is usually used to reduce the inrush currents during start up [5], [12], [13]. Moreover, a capacitor bank is necessary to compensate for the reactive power necessary to the machine as it is shown in Fig. 4(a).

2) Wind turbines systems with power electronics: By adding power electronics units into the WT systems, the complexity of the system is increased. In addition, the solution becomes more expensive. Anyway, better control of the input power and grid interaction are obtained. For example, maximum power for a large interval of wind speeds can be extracted while control of both active and reactive power into the grid is achieved by means of power electronics.

The usage of power electronics into WT systems can be further divided into two categories: systems using partial scale power electronics units and systems using full scale power electronics units. A particular structure is using an induction generator with a wounded rotor. An extra resistance controlled by power electronics is added in the rotor, which gives a variable speed range of 2% to 4%. The power converter for the rotor resistance control is for low voltage but high currents. Anyway, this solution also needs a soft starter and a reactive power compensator [5].

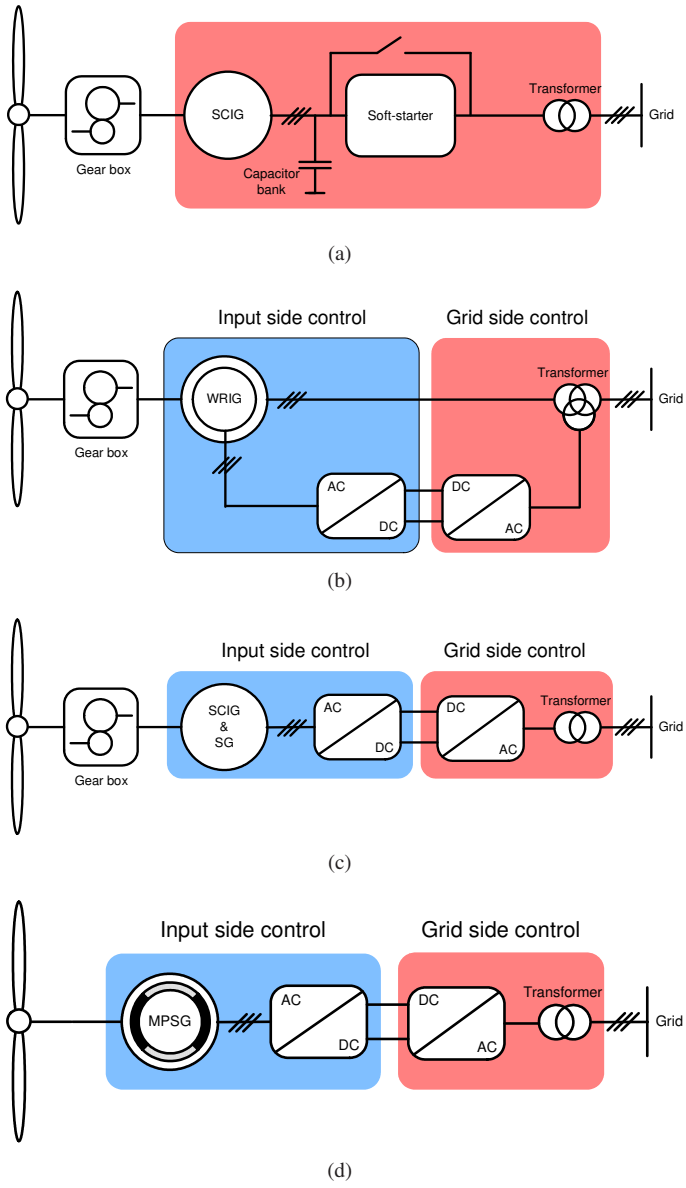

Fig. 4. Wind turbine systems using power electronics: (a) minimum electronics unit, (b) partial power converter, (c) full scale power converter structure with gearbox and (d) full scale power converter structure without gearbox and using multi-pole synchronous generator (MPSG).

Additionally, another solution is using a medium scale power converter with a wounded rotor induction generator (WRIG) as shown in Fig. 4(b). In this case, a power converter connected to the rotor through slip rings controls the rotor currents. If the generator is running super-synchronously, the electrical power is delivered through both the rotor and the stator. If the generator is running sub-synchronously the electrical power is only delivered into the rotor from the grid. A speed variation of 60% around synchronous speed may be obtained by the use of a power converter of 30% of nominal power [5].

By implementing a full scale power converter between the generator and the utility grid, additional technical performances of the WT system can be achieved, with the payback in losses in the power conversion stage. Normally, as Fig. 4(c) shows, SCIG is used in this configuration but an advantage to eliminate the gear-box can be obtained by using multi-pole wound rotor synchronous generator (WRSG) or permanent magnet synchronous generator (PMSG) as depicted in Fig. 4(d).

Noticeable is that for interacting with the power system, all the structures presented above are using two level PWM voltage source inverters (VSI) as this is the state of the art technology used today by all manufactures of wind systems. The possibility of high switching frequencies combined with a proper control makes these converters suitable for grid interface in the case of distributed generation, having a large contribution to the improvement of generated power quality.

Yet, three level neutral point clamped (NPC) VSI is an option for high power WT systems (5 MW) in order to avoid high voltage power devices. Attempts of using multilevel [14] or matrix converters [15], [16] have been made but those technologies have not convinced yet in the field of distributed generation.

Therefore, the next section is discussing the control structures and strategies applied to two level VSI PWM driven converters, focusing on the grid side converter control. Control structures implemented in different reference frames are presented and the possibility of compensating for low order harmonics is also discussed. Moreover, control strategies when grid faults occur are considered.

IV. Control Structures for Grid Connected DPGS

The control strategy applied to the grid side converter consists mainly of two cascaded loops. Usually, there is a fast internal current loop which regulates the grid current and an external voltage loop which controls the dc-link voltage [17]–[22]. The current loop is responsible for power quality issues and current protection, thus harmonic compensation and dynamics are the important properties of the current controller. The dc-link voltage controller is designed for balancing the power flow in the system. Usually, the design of this controller aims for system stability having slow dynamics.

In some works, the control of grid side controller is based on a dc-link voltage loop cascaded with an inner power loop instead of current loop. In this way, the current injected into the utility network is indirectly controlled [23].

Moreover, control strategies employing an outer power loop and an inner current loop are also reported [24].

In the following, a division of the control strategies in respect to the reference frame they are implemented in is given and the main properties of each structure are highlighted.

A. Synchronous reference frame control

Synchronous reference frame control, also called *dq control*, uses a reference frame transformation module, e.g. $abc \rightarrow dq$, to transform the grid current and voltage waveforms into a reference frame which rotates synchronously with the grid voltage. By means of this, the control variables become dc values, thus filtering and controlling can be easier achieved [25].

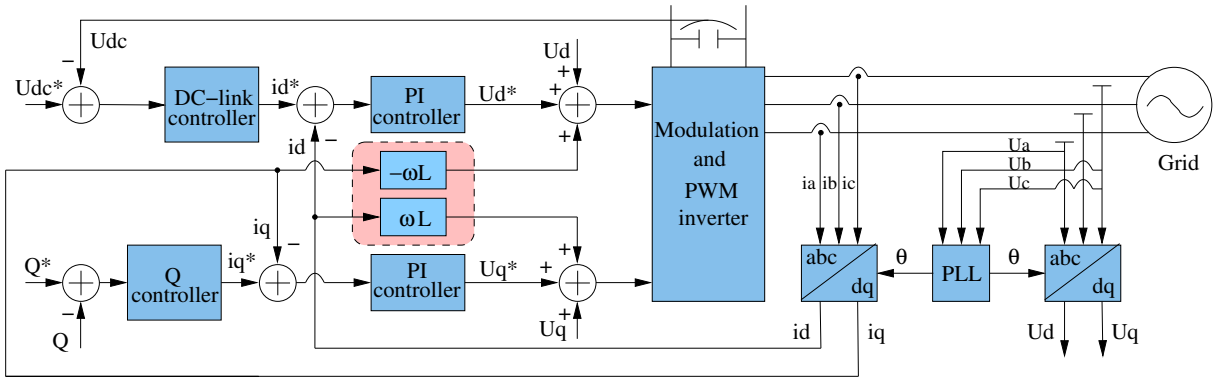

Fig. 5. General structure for synchronous rotating frame control structure.

A schematic of the dq control is represented in Fig. 5. In this structure, the dc-link voltage is controlled accordingly to the necessary output power. Its output is the reference for the active current controller while the reference for the reactive current is usually set to zero, if the reactive power control is not allowed. In the case that the reactive power has to be controlled, a reactive power reference must be imposed to the system.

The dq control structure is normally associated with PI controllers since they have a satisfactory behavior when regulating dc variables. The matrix transfer function of the controller in dq coordinates can be written as:

$$G_{PI}^{(dq)}(s) = \begin{bmatrix} K_p + \frac{K_i}{s} & 0 \\ 0 & K_p + \frac{K_i}{s} \end{bmatrix} \quad (1)$$

where K_p is the proportional gain and K_i is the integral gain of the controller.

Since the controlled current has to be in phase with the grid voltage, the phase angle used by the $abc \rightarrow dq$ transformation module has to be extracted from the grid voltages. As a solution, filtering of the grid voltages and using arc-tangent function to extract the phase angle can be a possibility [26]–[28]. In addition, the Phase-Looked Loop (PLL) technique [29]–[33] became a state of the art in extracting the phase angle of the grid voltages in the case of distributed generation systems.

For improving the performance of PI controller in such a structure as depicted in Fig. 5, cross coupling terms and voltage feed forward is usually used [17], [19], [25], [34], [35]. Anyway, with all these improvements, the compensation capability of the low order harmonics in the case of PI controllers is very poor, standing as a major drawback when using it in grid connected systems.

B. Stationary reference frame control

Another possibility to structure the control loops is using the implementation in stationary reference frame, as Fig. 6 shows. In this case, the grid currents are transformed into stationary reference frame using $abc \rightarrow \alpha\beta$ module. Since the control variables are sinusoidal in this situation and, due to the known drawback of PI controller in failing to remove the steady state error when controls sinusoidal waveforms, employment of other controller types is necessary. Proportional Resonant (PR) controller [36]–[39] gained a large popularity in the last decade in current regulation of grid tied systems.

In the PR case, the controller matrix in stationary reference frame is given by:

$$G_{PR}^{(\alpha\beta)}(s) = \begin{bmatrix} K_p + \frac{K_i s}{s^2+\omega^2} & 0 \\ 0 & K_p + \frac{K_i s}{s^2+\omega^2} \end{bmatrix} \quad (2)$$

where: ω is the resonance frequency of the controller, K_p is the proportional gain and K_i is the integral gain of the controller.

Characteristic to this controller is the fact that achieves a very high gain around the resonance frequency, thus being

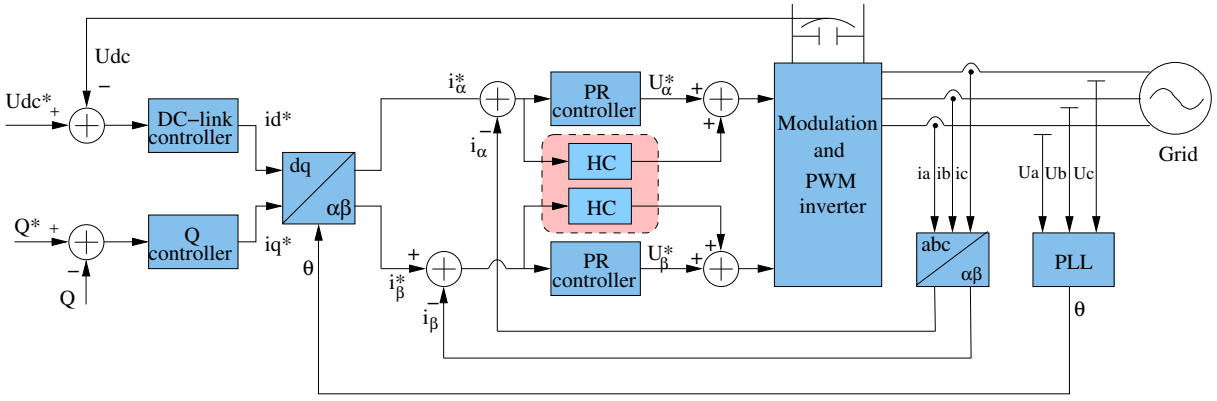

Fig. 6. General structure for stationary reference frame control strategy.

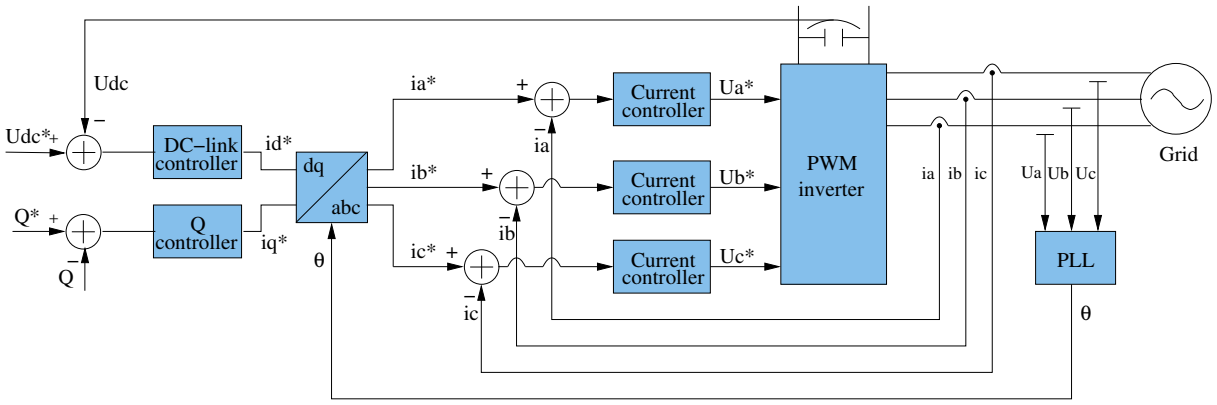

Fig. 7. General structure for natural reference frame control strategy.

$$G_{PI}^{(abc)}(s) = \frac{2}{3} \cdot \begin{bmatrix} K_p + \frac{K_i s}{s^2+\omega_0^2} & -\frac{K_p}{2} - \frac{K_i s+\sqrt{3}K_i\omega_0}{2\cdot(s^2+\omega_0^2)} & -\frac{K_p}{2} - \frac{K_i s-\sqrt{3}K_i\omega_0}{2\cdot(s^2+\omega_0^2)} \\ -\frac{K_p}{2} - \frac{K_i s-\sqrt{3}K_i\omega_0}{2\cdot(s^2+\omega_0^2)} & K_p + \frac{K_i s}{s^2+\omega_0^2} & -\frac{K_p}{2} - \frac{K_i s+\sqrt{3}K_i\omega_0}{2\cdot(s^2+\omega_0^2)} \\ -\frac{K_p}{2} - \frac{K_i s+\sqrt{3}K_i\omega_0}{2\cdot(s^2+\omega_0^2)} & -\frac{K_p}{2} - \frac{K_i s-\sqrt{3}K_i\omega_0}{2\cdot(s^2+\omega_0^2)} & K_p + \frac{K_i s}{s^2+\omega_0^2} \end{bmatrix} \tag{3}$$

capable to eliminate the steady state error between the controlled signal and its reference [38]. The width of the frequency band around the resonance point depends on the integral time constant K_i. A low K_i leads to a very narrow band while a high K_i leads to a wider band.

Moreover, high dynamic characteristics of PR controller have been reported in different works [39], [40].

C. Natural frame control

The idea of *abc* control is to have an individual controller for each grid current but however, the different ways to connect the three phase systems, i.e. delta, star with or without isolated neutral, etc. is an issue to be considered when designing the controller. In the situation of isolated neutral systems, the phases interact one to each other, hence only two controllers are necessary since the third current is given by the Kirchhoff current law. Anyway, the possibility of having three independent controller is possible by having extra considerations in the controller design as usually is the case for hysteresis and dead beat control.

Normally, *abc* control is a structure where nonlinear controllers like hysteresis or dead beat are preferred due to their high dynamics. It is well known that the performance of these controllers is proportional to the sampling frequency, hence the rapid development if digital systems such as Digital Signal Processors (DSP) or Field-Programmable Gate Array (FPGA) is an advantage for such an implementation.

A possible implementation of *abc* control is depicted in Fig. 7, where the output of dc-link voltage controller sets the active current reference. Using the phase angle of the grid voltages provided by a PLL system, the three current references are created. Each of them are compared with the corresponding measured current and the error goes into the controller. If hysteresis or dead beat controllers are employed in the current loop, the modulator is not anymore necessary. The output of these controllers are the switching states for the switches in the power converter. In the case that three PI or PR controllers are used, the modulator is necessary to create the duty cycles for the PWM pattern.

1) PI controller: PI controller is very much used in conjunction with *dq* control but its implementation in *abc* frame is also possible as [35] describes. The transfer function of the controller in this case becomes as (3) and noticeable is the complexity of the controller matrix in this case due to the significant off-diagonal terms representing the cross coupling between the phases.

2) PR controller: The implementation of PR controller in *abc* is straight forward since the controller is already in stationary frame and implementation of three controllers as illustrated by (4) is possible. Again, in this case, the influence of the isolated neutral in the control has to be accounted, hence the third controller is not necessary in (4). However, it is worth to notice that the complexity of the controller in this case is considerably reduced compared to (3).

$$G_{PR}^{(abc)}(s) = \begin{bmatrix} K_p + \frac{K_i s}{s^2+\omega_0^2} & 0 & 0 \\ 0 & K_p + \frac{K_i s}{s^2+\omega_0^2} & 0 \\ 0 & 0 & K_p + \frac{K_i s}{s^2+\omega_0^2} \end{bmatrix} \tag{4}$$

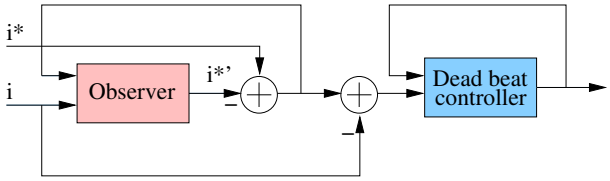

Fig. 9. Structure of the dead beat controller using an observer to compensate for the delay introduced by the controller.

3) Hysteresis controller: It is worth to note that in the case of hysteresis control implementation, an adaptive band of the controller has to be designed in order to obtain fixed switching frequency. In [41]–[44], different methods and algorithms to obtain fixed switching frequency are presented.

Since the output of the hysteresis controller is the state of the switches, considerations about the isolated neutral are again necessary. In [43], a $a^{'}$ term is introduced in the formula of the hysteresis band in order to account for the load (transformer) connection type as Eq. (5) shows.

$$HB = \frac{0.25a^{'}U_{dc}}{f_{sw}L_T}\left[1 - \frac{L_T^2}{a^{'2}U_{dc}}\left(\frac{U_g}{L_T} + \frac{di^*}{dt}\right)^2\right] \quad (5)$$

In [45] a similar approach is used, but here the current error is split into its non-interacting part ζ and the interacting part γ to resolve the equation for the variable hysteresis band.

4) Dead beat controller: The dead-beat controller attempts to null the error with one sample delay. The controller in its digital implementation is:

$$G_{DB}^{(abc)} = \frac{1}{b} \cdot \frac{1 - az^{-1}}{1 - z^{-1}} \quad (6)$$

where a and b are denoted as following:

$$\begin{aligned} a &= e^{-\frac{R_T}{L_T}Ts} \\ b &= -\frac{1}{R_T}\left(e^{-\frac{R_T}{L_T}Ts} - 1\right) \end{aligned} \quad (7)$$

Since dead beat controller regulates the current such that this reaches its reference at the end of next switching period, the controller is introducing one sample time delay. In order to compensate for this delay, an observer can be introduced in the structure of the controller, with the aim to modify the current reference in order to compensate for the delay [46], as Fig. 9 shows.

The discrete transfer function of the observer is given by:

$$F_{DB}^{(abc)} = \frac{1}{1 - z^{-1}} \quad (8)$$

thus, the new current reference becomes:

$$i^{*'} = F_{DB}^{(abc)}\left(i^* - i\right) \quad (9)$$

As a consequence, a very fast controller containing no delay is finally obtained. Moreover, the algorithm of both dead beat controller and the observer are not complicated, being suitable for microprocessor based implementation [47].

In addition, in the case of abc control, two modalities of implementing the PLL are possible. First possibility is to use three single phase PLL systems [33], thus the three phase angles are independently extracted from the grid voltages. In this case, the transformation module $dq \rightarrow abc$ is not anymore necessary, the active current reference being multiply with the sine of the phase angles. Second possibility is to use one three phase PLL [31], [32], [48], [49]. In this case, the current references are created as shown in Fig. 7. A discussion about the influence of the PLL in the control loop is given in § VII.

D. Evaluation of control structures

The necessity of voltage feed-forward and cross coupling terms is the major drawbacks of the control structure implemented in synchronous reference frame. Moreover, the phase angle of the grid voltage is a must in this implementation. In the case of control structure implemented in stationary reference frame, if PR controllers are used for current regulation, the complexity of the control becomes lower compared to the structure implemented in dq frame. Additionally, the phase angle information is not a necessity, filtered grid voltages can be used as template for the reference current waveform.

In the case of control structure implemented in natural frame, the complexity of the control can be high if an adaptive band hysteresis controller is used for current regulation. A simpler control scheme can be achieved by implementing a dead beat controller instead. Again, as in the case of stationary frame control, the phase angle information is not a must. Noticeable for this control structure is the fact that independent control of each phase can be achieved, if grid voltages or three single phase PLLs are used to generate the current reference.

V. Power Quality Considerations

One of the demands present in all standards regarding grid tied systems is the quality of the distributed power. According to the standards in this field [13], [50]–[53] the injected current in the grid should not have a total harmonic distortion (THD) larger than 5%. A detailed image of the harmonic distortion regarding each harmonic is given in Table I.

TABLE I
Distortion Limits for Distributed Generation Systems Set by IEC Standard [50].

Odd harmonics	Distortion limit
3^{rd} – 9^{th}	< 4.0 %
11^{th} – 15^{th}	< 2.0 %
17^{th} – 21^{st}	< 1.5 %
23^{rd} – 33^{rd}	< 0.6 %

As it was mentioned previously, one of the responsibilities of the current controller is the power quality issue. Therefore, different methods to compensate for the grid harmonics in order to obtain an improved power quality are addressed in the following.

A. Harmonics compensation using PI controllers

Since PI controllers typically are associated with dq control structure, the possibilities for harmonic compensation are based on low-pass (LP) and high-pass (HP) filters [54]. If

the current controller has to be immune to the grid voltage harmonic distortion (mainly 5^{th} and 7^{th} in three-phase systems), harmonic compensator for each harmonic order should be designed. Fig. 8 shows the dq control structure having a harmonic compensator for the positive sequence of the 5^{th} harmonic. In addition, under unbalance conditions, harmonic compensators for both positive and negative sequence of each harmonic order are necessary. As a consequence, four compensators like the one depicted in Fig. 8 are necessary to compensate for the 5^{th} and 7^{th} harmonics. Noticeable is in this case the complexity of the control algorithm.

B. Harmonics compensation using PR controllers

In the case of PR control implementation, the things are different. Harmonic compensation can be achieved by cascading several generalized integrators (GI) tuned to resonate at the desired frequency. In this way, selective harmonic compensation at different frequencies is obtained. In [38], the transfer function of a typical harmonic compensator (HC) designed to compensate the 3^{rd}, 5^{th} and 7^{th} harmonics is given as:

$$G_h(s) = \sum_{h=3,5,7} K_{ih} \frac{s}{s^2 + (\omega \cdot h)^2} \tag{10}$$

In this case it is easy to extend the capabilities of the scheme adding harmonic compensation features simply with more resonant controllers in parallel to the main controller as Fig. 10 illustrates. The main advantage in this situation is given by the fact that the harmonic compensator works on both positive and negative sequence of the selected harmonic, thus only one HC is necessary for a harmonic order.

An interesting feature of the HC is that it does not affect the dynamics of the PR controller, as it only reacts to the frequencies very close to the resonance frequency. This characteristic makes the PR controller a successful solution in applications

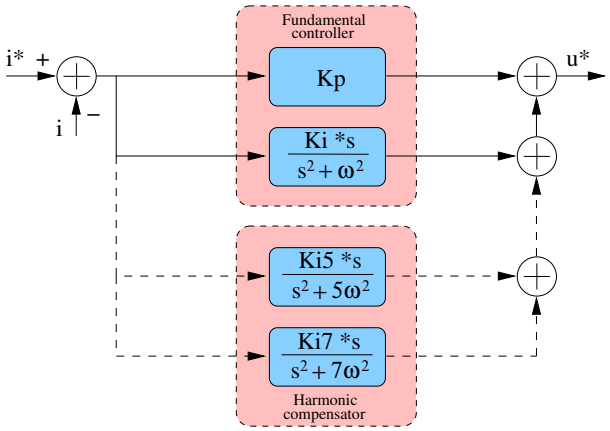

Fig. 10. Structure of the harmonic compensator attached to the resonant controller of the fundamental current.

where high dynamics and harmonics compensation, especially low order harmonics, are required, as it is the case of DPGS.

C. Harmonics compensation using non-linear controllers

Since both hysteresis and dead beat controller have very fast dynamics, there is no concern about the low order harmonics when the implemented control structure uses such controllers. Anyway, it should be noticed that the current waveform will contain harmonics at switching and sampling frequencies order. Another issue is the necessity of fast sampling capabilities of the hardware used.

D. Evaluation of harmonic compensators

The necessity of using two filters, two transformation modules and one controller to compensate for the positive sequence of one harmonic only, makes the harmonic compensator implemented in dq frame to not be a practical solution. On the other

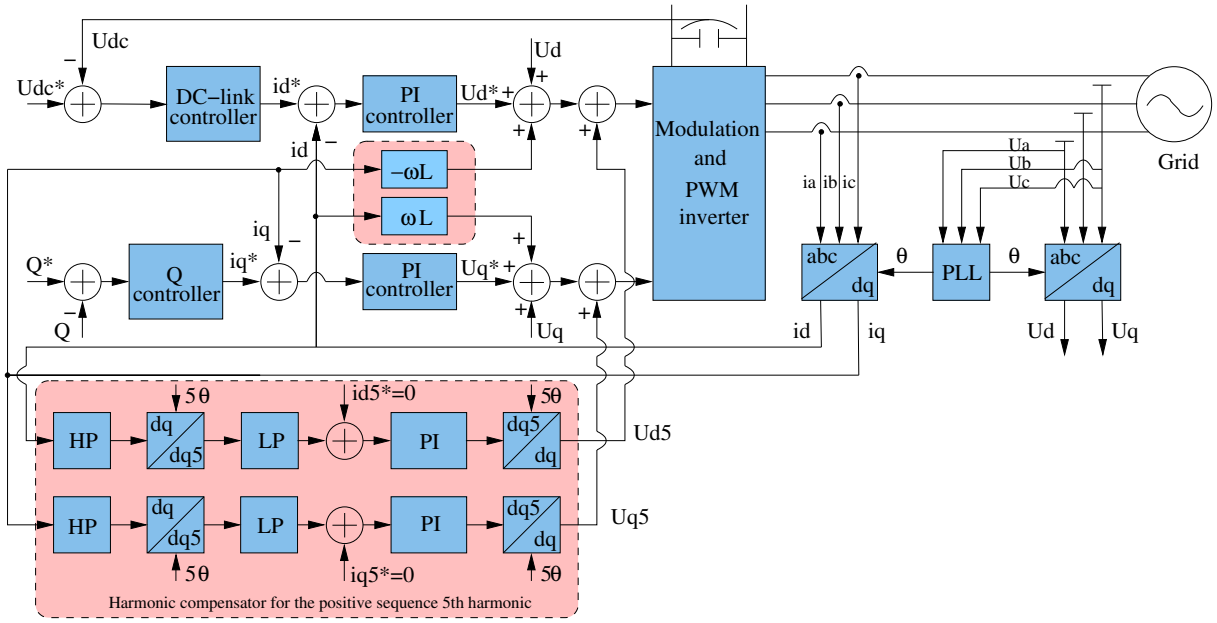

Fig. 8. Method for compensating the positive sequence of the 5^{th} harmonic in dq control structure.

hand, easier implementation is observed in the situation when the control structure is implemented in stationary reference frame, since the structure of the compensator is reduced and it acts on both positive and negative sequence.

VI. Control Strategy under Grid Faults

Due to the large amount of distributed power generation connected to the utility networks in some countries, instability of the power system may arise. As a consequence, more stringent demands for interconnecting the DPGS to the grid are issued. Among all the requests, more and more stress is put on the ability of DPGS to ride through short grid disturbances such as voltage and frequency variations.

The grid faults can be classified in two main categories [55]:

- *symmetrical fault* – when all three grid voltages register the same amplitude drop but the system remain balanced (no phase shifting is registered). This type of fault is very seldom in the power systems.
- *unsymmetrical fault* – when the phases register an unequal amplitude drop together with phase shifting between them. This type of fault occurs due to one or two phases shorted to ground or to each other.

By considering the DPGS connected to the utility network as shown in Fig. 11, where a distribution transformer is used by the generation system to interface the power system, the propagation of a voltage fault occurring at the bus 1 appears different at the bus 2. For example, if a severe grid fault like single phase shorted to ground take place at bus 1, two of the voltages at the DPGS terminals (after the Δ/Y transformer) experience a voltage drop which is dependent on the impedance of the line between the fault and DPGS transformer value. As a consequence, the voltages at bus 2 will register both amplitude and phase unbalance [55].

Since this case is an unsymmetrical fault, the negative sequence appear in the grid voltages. This creates second harmonic oscillations which propagates in the system, appearing in the dc-link voltage as a ripple [56]. Moreover, the control variables are also affected by this phenomenon. In [57]–[59] has been shown that the PLL system can be designed to filter out the negative sequence, producing a clean synchronization signal. If the three phase PLL system is not designed to be robust to unbalance, second harmonic oscillations will appear in the phase angle signal, thus in the current reference.

In addition, the second harmonic ripple present in the dc-link voltage will also have a negative influence in generation of the current reference. As a consequence, in order to provide ride through capabilities for DPGS, the influence of the unbalance should be minimized when running under faulty conditions.

Regarding the control strategy under faults, four major possibilities are available.

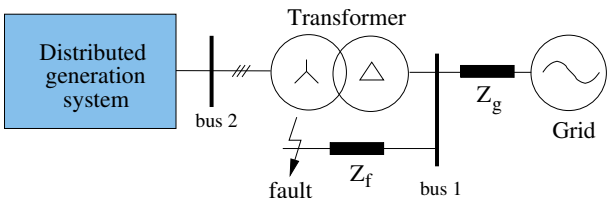

Fig. 11. Distributed generation system connected through a Δ/Y transformer to the utility network.

A. Unity power factor control strategy

One of the control strategies that a DPGS can adopt on grid faults is to maintain unity power factor during the fault. The most efficient set of currents delivering the instantaneous active power P to the grid can be calculated as follow:

$$\mathbf{i} = g\mathbf{v}; \qquad \text{where: } g = \frac{P}{|\mathbf{v}|^2} \tag{11}$$

is the instantaneous conductance seen from the inverter output and $|\mathbf{v}|$ denotes the module of the three-phase voltage vector $\mathbf{v}$. Its value is a constant in balanced sinusoidal conditions but under grid faults however, the negative-sequence component gives rise to oscillations at twice the fundamental frequency in $|\mathbf{v}|$. Consequently, the injected currents will not keep their sinusoidal waveform and high order components will appear in their waveform. Current vector of (11) is instantaneously proportional to the voltage vector and therefore does not have any orthogonal component in relation to the grid voltage, hence gives rise to the injection of no reactive power to the grid. Thus, in this situation, both active and reactive instantaneous power are kept constant during the fault time.

B. Positive sequence control strategy

Another control strategy that can be applied under fault is to follow the positive sequence of the grid voltages. Contrary to the unity power factor control, in this case a PLL system that can detect the unbalance is necessary in the control structure. Moreover, this system should be robust to unbalance and should be capable of detecting the positive sequence of the grid voltages. Synchronous reference frame PLL is suited for this purpose. In [57]–[60], the detection of both positive and negative sequence of the utility voltage by modifying the conventional dq PLL, has been demonstrated.

Because the extracted phase angle is following the positive sequence of the grid voltages, the reference currents can easily be obtained for all control structures, i.e. dq control, stationary reference frame ($\alpha\beta$) control and abc control, since there is no difference between the synchronization angle during the fault and the one during normal operating conditions. The only problem in this situation is the ripple of the dc-link voltage which has an influence on the active current reference. Using a digital filter such as Delay Signal Cancellation (DSC) [17], this can be filtered out without introducing any delay in the system. Anyway, the dc-link capacitor should be rated such as it overcomes the second harmonic ripple present during a fault, otherwise device failure can occur.

In the case of this control strategy, the grid currents will remain sinusoidal and balanced during the fault, only registering an increase in amplitude due to the amplitude drop of the grid voltages. Anyway, both active and reactive power will register double frequency oscillations over the whole fault period.

C. Constant active power control strategy

Another control strategy that might be adopted under faulty grid conditions is to keep the active power constant. As previously mentioned, in the case of unbalance the grid voltages will comprise both positive and negative sequence. Similar, the grid current will became unbalanced, thus both the active and reactive power will experience double harmonic oscillations. In [61]–[63] has been demonstrated that injecting an amount of negative sequence in the current reference defined by (12), compensation for the double harmonic can be obtained, thus the active power can be kept constant during the fault.

$$I_n = -\frac{U_n}{U_p} I_p \tag{12}$$

where p and n denote the positive and negative sequence component of both current and voltage. In the case this control strategy is applied to a control structure which uses PI controllers for current regulation, additional controllers for the negative sequence current are necessary [17], [61].

In the case of a control structure based on PR controller, the negative component of the current can be introduced in the current reference since this controller can regulated both $+\omega$ and $-\omega$, presenting a clear advantage from the implementation point of view.

It is worth to note that in the case of constant power control strategy, the grid currents are not balanced during the fault. Moreover, the reactive power experiences large oscillations.

D. Constant reactive power control strategy

Like in the constant active power control case, similar expression can be derived for the reactive power in order to cancel the double frequency oscillations. Additionally, a current vector orthogonal to the grid voltage vector can be found and this can give access to independent control of reactive power if for example the DPGS should exchange some amount of reactive power to the grid. In this case the reference for the reactive power should be changed from zero to the desired value when the grid fault is detected.

As a consequence, the upcoming grid codes can be fulfilled by using one of the control strategies presented, depending on what the power system operator imposes when the DPGS is connected to the utility network.

VII. Overview of Grid Synchronization Methods

The injected current into the utility network has to be synchronized with the grid voltage as the standards in the field request that [50]–[53]. Therefore, grid synchronization algorithms play an important role for distributed power generation systems. The synchronization algorithm mainly outputs the phase of the grid voltage vector which is used to synchronize the control variables, e.g. grid currents with the grid voltages using different transformation modules like $abc \rightarrow dq$.

Different methods to extract the phase angle have been developed and presented in many works up to now. In [32] a comparison of the main techniques used for detection of the phase angle of the grid voltages on different grid conditions is carried out. Advantages and disadvantages as well as an evaluation of performance are presented.

In this paper, a brief description of the main methods is given and a discussion about detection of grid unbalance is given.

A. Zero crossing method

Among all technique, the zero crossing method has the simplest implementation, but also poor performances are reported when using it, mainly if grid voltages register variations such as harmonics or notches.

B. Filtering of grid voltages

Filtering of the grid voltages in different reference frame such as dq [32] or $\alpha\beta$ [26]–[28] is another possibility. Improved performance over the zero crossing method is reported but still the filtering technique encounters difficulty to extract the phase angle when grid variations or faults occur in the utility network [32]. The method requires the use of the arctangent function in order to obtain the phase angle of the utility voltage. It is well known that using filtering, a delay is introduced in the processed signal. In the case when it is used for extracting the grid voltage angle, this is unacceptable. Thus a proper filter design is a necessity.

In the case when the current controller is implemented in the stationary reference frame like Fig. 6 shows, the knowledge of the grid voltage angle θ is not needed, hence it is not necessary to calculate the arctangent function. In fact, the filtered $\alpha\beta$ components can be directly used as template for the reference current signal in order to have synchronization [64].

C. Phase-Looked Loop technique

Nowadays, the PLL technique is the state of the art method to extract the phase angle of the grid voltages [31], [33], [48], [49]. The PLL is implemented in dq synchronous reference frame and its schematic is illustrated in Fig. 13. As it can be noticed, this structure needs the coordinate transformation form $abc \rightarrow dq$ and the lock is realized by setting the reference V_d^* to zero. A regulator, usually PI, is used to

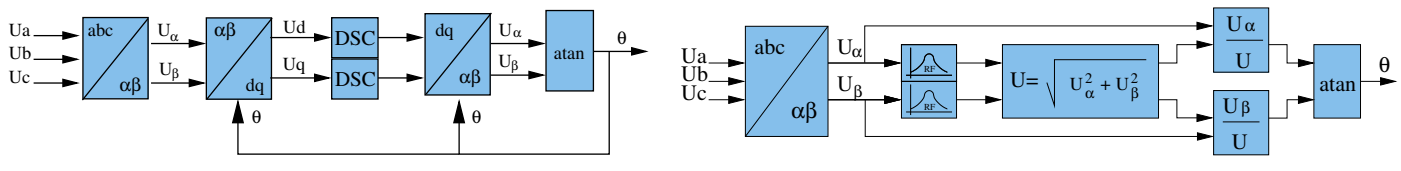

Fig. 12. Synchronization method using (a) filtering on the dq synchronous rotating reference frame and (b) filtering on $\alpha\beta$ stationary frame.

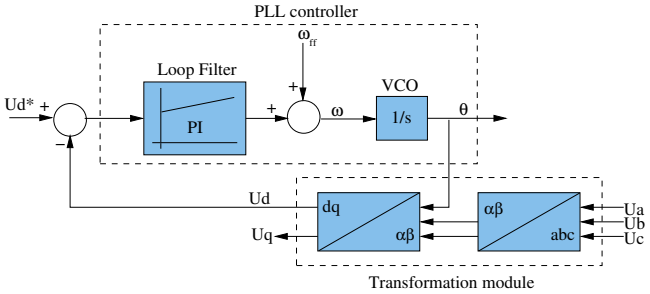

Fig. 13. General structure of three phase dq PLL.

control this variable and the output of this regulator is the grid frequency. After the integration of the grid frequency, the utility voltage angle is obtained, which is fed back into the $\alpha\beta \rightarrow dq$ transformation module in order to transform into the synchronous rotating reference frame.

This algorithm has a better rejection of grid harmonics, notches and any other kind of disturbances but additional improvements have to be done in order to overcome grid unbalance [57]–[59], [65], [66]. In the case of unsymmetrical voltage faults, the second harmonics produced by the negative sequence will propagate through the PLL system and will be reflected in the extracted phase angle. In order to overcome this, different filtering techniques are necessary such that the negative sequence is filtered out. As a consequence, during unbalance conditions, the three phase dq PLL structure can estimate the phase angle of the positive sequence of the grid voltages.

VIII. Conclusion

This paper discusses the control of distributed power generation systems. Hardware structures for DPGS, control structures for the grid side converter and control strategies under faults are primary addressed. Different implementation structures like dq, stationary and natural frame control structures are presented and their major characteristics are pointed out. A discussion about different controllers and their ability to compensate for low order harmonics presented in the utility network is given. In addition, four different control strategies that a DPGS can use during an unbalanced grid fault are discussed.

Finally, an overview of grid synchronization algorithms is given. Their influence and role in the control of DPGS on normal and faulty grid condition is discussed.

IX. Acknowledgments

The authors want to acknowledge the financial support for this project offered by Risø National Lab, Eltra and the Danish Research Councils under the contract number 2058-03-0003.

References

[1] R. Lawrence and S. Middlekauff, "The new guy on the block," in *IEEE Industry Applications Magazine*, vol. 11, no. 1, Jan-Feb 2005, pp. 54–59.
[2] EWEA, "www.ewea.org/documents," Online Documentation, October 2005.
[3] IEA-PVPS, "Cumulative Installed PV power," www.iea-pvps.org, October 2005.
[4] M. Shahidehpour and F. Schwartz, "Don't let the sun go down on PV," in *IEEE Power & Energy Magazine*, vol. 2, no. 3, 2004, pp. 40–48.
[5] F. Blaabjerg, Z. Chen, and S. Kjaer, "Power electronics as efficient interface in dispersed power generation systems," *IEEE Trans. on Power Electronics*, vol. 19, no. 5, pp. 1184–1194, 2004.
[6] R. W. Erickson and D. Maksimovic, *Fundamentals of Power Electronics*, 2nd ed. Kluwer Academic Publishers, 2001.
[7] M. Todorovic, L. Palma, and P. Enjeti, "Design of a wide input range DC-DC converter with a robust power control scheme suitable for fuel cell power conversion," in *Proc. of APEC'04*, vol. 1, 2004, pp. 374–379.
[8] G. K. Andersen, C. Klumpner, S. B. Kjaer, and F. Blaabjerg, "A new green power inverter for fuel cells," in *Proc. of PESC'02*, vol. 2, 2002, pp. 727–733.
[9] M. Tanrioven and M. Alam, "Modeling, control and power quality evaluation of a PEM fuel cell based power supply system for residential use," in *Proc. of IAS'04*, vol. 4, 2004, pp. 2808–2814.
[10] R. Caceres and I. Barbi, "A boost DC-AC converter: analysis, design, and experimentation," *IEEE Trans. on Power Electronics*, vol. 14, no. 1, pp. 134–141, 1999.
[11] C. Cecati, A. Dell'Aquila, and M. Liserre, "A novel three-phase single-stage distributed power inverter," *IEEE Trans. on Power Electronics*, vol. 19, no. 5, pp. 1226–1233, 2004.
[12] S. Heier, *Grid Integration of Wind Energy Conversion Systems*. John Wiley & Sons, 1998.
[13] T. Ackermann, *Wind Power in Power Systems*. John Wiley & Sons, Ltd., 2005, ISBN: 0-470-85508-8.
[14] L. Helle and S. Munk-Nielsen, "Comparison of converter efficiency in large variable speed wind turbines," *Proc. of APEC'01*, vol. 1, pp. 628–634, 2001.
[15] A. V. Rebsdorf and L. Helle, "Variable wind turbine having a matrix converter," United States Patent, May 2003.
[16] S. Barakati, M. Kazerani, and X. Chen, "A new wind turbine generation system based on matrix converter," in *IEEE Power Engineering Society General Meeting*, 2005, pp. 218 – 224.
[17] G. Saccomando and J. Svensson, "Transient operation of grid-connected voltage source converter under unbalanced voltage conditions," in *Proc. of IAS'01*, vol. 4, Chicago, IL, 2001, pp. 2419–2424.
[18] I. Agirman and V. Blasko, "A novel control method of a VSC without AC line voltage sensors," *IEEE Trans. on Industry Applications*, vol. 39, no. 2, pp. 519–524, 2003.
[19] R. Teodorescu and F. Blaabjerg, "Flexible control of small wind turbines with grid failure detection operating in stand-alone and grid-connected mode," *IEEE Trans. on Power Electronics*, vol. 19, no. 5, pp. 1323–1332, 2004.
[20] R. Teodorescu, F. Blaabjerg, U. Borup, and M. Liserre, "A new control structure for grid-connected LCL PV inverters with zero steady-state error and selective harmonic compensation," in *Proc. of APEC'04*, vol. 1, 2004, pp. 580–586.
[21] S.-H. Song, S.-I. Kang, and N.-K. Hahm, "Implementation and control of grid connected AC-DC-AC power converter for variable speed wind energy conversion system," in *Proc. of APEC '03*, vol. 1, 2003, pp. 154–158.
[22] H. Zhu, B. Arnet, L. Haines, E. Shaffer, and J-S.Lai, "Grid synchronization control without AC voltage sensors," in *Proc. of APEC'03*, vol. 1, 2003, pp. 172–178.
[23] C. Ramos, A. Martins, and A. Carvalho, "Current control in the grid connection of the double-output induction generator linked to a variable speed wind turbine," in *Proc. of IECON'02*, vol. 2, 2002, pp. 979–984.
[24] D. Candusso, L. Valero, and A. Walter, "Modelling, control and simulation of a fuel cell based power supply system with energy management," in *Proc. of IECON'02*, vol. 2, 2002, pp. 1294–1299.
[25] M. Kazmierkowski, R. Krishnan, and F. Blaabjerg, *Control in Power Electronics – Selected Problems*. Academic Press, 2002.
[26] J. Svensson, "Synchronisation methods for grid-connected voltage source converters," in *IEE Proc. Generation, Transmission and Distribution*, vol. 148, no. 3, 2001, pp. 229–235.
[27] H. Kim, S.-J. Lee, and S.-K. Sul, "Reference wave generator in dynamic voltage restorers by use of PQR power theory," *Proc. of APEC'04*, vol. 3, pp. 1452–1457, 2004.
[28] S.-J. Lee, H. Kim, S.-K. Sul, and F. Blaabjerg, "A novel control algorithm for static series compensators by use of PQR instantaneous power theory," *IEEE Trans. on Power Electronics*, vol. 19, no. 3, pp. 814–827, 2004.
[29] F. M. Gardner, *Phase Lock Techniques*. New York: Wiley, 1979.
[30] G. C. Hsieh and J. C. Hung, "Phase-Locked Loop Techniques - A Survey," *IEEE Trans. on Industrial Electronics*, vol. 43, no. 6, pp. 609–615, 1996.

[31] S.-K. Chung, "A phase tracking system for three phase utility interface inverters," *IEEE Trans. on Power Electronics*, vol. 15, no. 3, pp. 431–438, 2000.
[32] A. V. Timbus, M. Liserre, R. Teodorescu, and F. Blaabjerg, "Synchronization methods for three phase distributed power generation systems. An overview and evaluation," in *Proc. of PESC'05*, 2005, pp. 2474–2481.
[33] L. N. Arruda, S. M. Silva, and B. Filho, "PLL structures for utility connected systems," in *Proc. of IAS'01*, vol. 4, 2001, pp. 2655–2660.
[34] R. Teodorescu, F. Iov, and F. Blaabjerg, "Flexible development and test system for 11 kW wind turbine," in *Proc. of PESC'03*, vol. 1, 2003, pp. 67–72.
[35] E. Twining and D. G. Holmes, "Grid current regulation of a three-phase voltage source inverter with an LCL input filter," *IEEE Trans. on Power Electronics*, vol. 18, no. 3, pp. 888–895, 2003.
[36] S. Fukuda and T. Yoda, "A novel current-tracking method for active filters based on a sinusoidal internal model," *IEEE Trans. on Industrial Electronics*, vol. 37, no. 3, pp. 888–895, 2001.
[37] X. Yuan, W. Merk, H. Stemmler, and J. Allmeling, "Stationary-frame generalized integrators for current control of active power filters with zero steady-state error for current harmonics of concern under unbalanced and distorted operating conditions," *IEEE Trans. on Industry Applications*, vol. 38, no. 2, pp. 523–532, 2002.
[38] R. Teodorescu and F. Blaabjerg, "Proportional-resonant controllers. A new breed of controllers suitable for grid-connected voltage-source converters," in *Proc. of OPTIM'04*, vol. 3, 2004, pp. 9–14.
[39] D. Zmood and D. G. Holmes, "Stationary frame current regulation of PWM inverters with zero steady-state error," *IEEE Trans. on Power Electronics*, vol. 18, no. 3, pp. 814–822, 2003.
[40] M. Ciobotaru, R. Teodorescu, and F. Blaabjerg, "Control of single-stage single-phase PV inverter," in *Proc. of PELINCEC'05*, 2005, CDROM.
[41] L. Malesani, P. Mattavelli, and P. Tomasin, "Improved constant-frequency hysteresis current control of VSI inverters with simple feed-forward bandwidth prediction," *IEEE Trans. on Industry Applications*, vol. 33, no. 5, pp. 1194–1202, 1997.
[42] L. Sonaglioni, "Predictive digital hysteresis current control," in *Proc. of IAS'95*, vol. 3, 1995, pp. 1879–1886.
[43] B. K. Bose, "An adaptive hysteresis-band current control technique of a voltage-fed PWM inverter for machine drive dystem," *IEEE Trans. on Industrial Electronics*, vol. 37, no. 5, pp. 402–408, 1990.
[44] L. Malesani and P. Tenti, "A novel hysteresis control method for current-controlled voltage-source PWM inverters with constant modulation frequency," *IEEE Trans. on Industry Applications*, vol. 26, pp. 88–92, 1990.
[45] Q. Yao and D. Holmes, "A simple, novel method for variable-hysteresis-band current control of a three phase inverter with constant switching frequency," in *Proc. of IAS'93*, 1993, pp. 1122–1129.
[46] P. Mattavelli, G. Spiazzi, and P. Tenti, "Predictive digital control of power factor preregulators with input voltage estimation using disturbance observers," *IEEE Trans. on Power Electronics*, vol. 20, no. 1, pp. 140–147, 2005.
[47] Y. Ito and S. Kawauchi, "Microprocessor based robust digital control for UPS with three-phase PWM inverter," *IEEE Trans. on Power Electronics*, vol. 10, no. 2, pp. 196–204, 1995.
[48] S.-K. Chung, "Phase-Locked Loop for grid-connected three-phase power conversion systems," *IEE Proceedings on Electronic Power Applications*, vol. 147, no. 3, pp. 213–219, 2000.
[49] V. Kaura and V. Blasko, "Operation of a phase loop system under distorted utility conditions," *IEEE Trans. on Industry Applications*, vol. 33, no. 1, pp. 58–63, 1997.
[50] IEC Standard 61727, "Characteristic of the utility interface for photovoltaic (PV) systems," IEC, Tech. Rep., 2002.
[51] IEEE15471, "IEEE standard for interconnecting distributed resources with electric power systems," 2005.
[52] Eltra and Elkraft, "Wind turbines connected to grids with voltage below 100 kV," http://www.eltra.dk, 2004.
[53] E.ON-Netz, "Grid code – high and extra high voltage," E.ON Netz GmbH, Tech. Rep., 2003. [Online]. Available: http://www.eon-netz.com/Ressources/downloads/enenarhseng1.pdf
[54] M. Newman, D. Zmood, and D. Holmes, "Stationary frame harmonic reference generation for active filter systems," *IEEE Trans. on Industry Applications*, vol. 38, no. 6, pp. 1591–1599, 2002.
[55] M. H. J. Bollen, *Understanding Power Quality Problems: Voltage Sags and Interruptions*. IEEE Press, 2002.
[56] L. Moran, P. Ziogas, and G. Joos, "Design aspects of synchronous PWM rectifier-inverter systems under unbalanced input voltage conditions," *IEEE Trans. on Industry Applications*, vol. 28, no. 6, pp. 1286–1293, 1992.
[57] M. Karimi-Ghartemani and M. Iravani, "A method for synchronization of power electronic converters in polluted and variable-frequency environments," *IEEE Trans. on Power Systems*, vol. 19, no. 3, pp. 1263–1270, 2004.
[58] P. Rodriguez, J. Pou, J. Bergas, I. Candela, R. Burgos, and D. Boroyevich, "Double synchronous reference frame PLL for power converters," in *Proc. of PESC'05*, 2005, pp. 1415–1421.
[59] M. C. Benhabib and S. Saadate, "A new robust experimentally validated Phase-Looked Loop for power electronic control," *EPE Journal*, vol. 15, no. 3, pp. 36–48, August 2005.
[60] A. V. Timbus, M. Liserre, F. Blaabjerg, R. Teodorescu, and P. Rodriguez, "PLL algorithm for power generation systems robust to grid faults," in *Proc. of PESC'06*, 2006, pp. 1360–1366.
[61] H.-S. Song and K. Nam, "Dual current control scheme for PWM converter under unbalanced input voltage conditions," *IEEE Trans. on Industrial Electronics*, vol. 46, no. 5, pp. 953–959, 1999.
[62] A. Stankovic and T. Lipo, "A novel control method for input output harmonic elimination of the PWM boost type rectifier under unbalanced operating conditions," *IEEE Trans. on Power Electronics*, vol. 16, no. 5, pp. 603–611, 2001.
[63] A. V. Timbus, P. Rodriguez, R. Teodorescu, M. Liserre, and F. Blaabjerg, "Control strategies for distributed power generation systems operating on faulty grid," in *Proc. of ISIE'06*, 2006, pp. 1601–1607.
[64] P. Verdelho, "Voltage type reversible rectifiers control methods in unbalanced and nonsinusoidal conditions," in *Proc. of IECON '98*, vol. 1, 1998, pp. 479–484.
[65] S. Lee, J. Kang, and S. Sul, "A new phase detection method for power conversion systems considering distorted conditions in power system," in *Proc. of IAS'99*, vol. 4, 1999, pp. 2167–2172.
[66] H.-S. Song, H.-G. Park, and K. Nam, "An instantaneous phase angle detection algorithm under unbalanced line voltage condition," in *Proc. of PESC'99*, vol. 1, 27 June-1 July 1999, pp. 533–537vol.1.

Publication 2

Linear and nonlinear control of distributed power generation systems

by A. Timbus, M. Liserre, R. Teodorescu, P. Rodriguez, and F. Blaabjerg
Article published in Proceedings of IAS'06, pages 1015-1023, 2006

Linear and Nonlinear Control of Distributed Power Generation Systems

Adrian V. Timbus, *Student Member, IEEE*, Marco Liserre, *Member, IEEE*, Remus Teodorescu, *Senior Member, IEEE*, Pedro Rodriguez, *Member, IEEE* and Frede Blaabjerg, *Fellow, IEEE*

***Abstract*—In this paper, different control structures applied to distributed power generation system are discussed. Implementation of proportional-integral (PI), proportional-resonant (PR), hysteresis and dead beat controller in different reference frames is also treated. An evaluation in terms of current harmonic distortion when running in steady state condition is made. Additionally, the controllers behavior in transient operation such as step in current reference and single phase fault in the utility grid has also been studied. Experimental results are presented for their evaluation.**

I. Introduction

DISTRIBUTED Power Generation Systems (DPGS) based on renewable energies are not anymore regarded as one of the engineering challenges today but as a potential player which can have a major contribution to the total energy production around the world. Exponential growth of both wind turbines (WT) and photovoltaic (PV) power generation systems are registered in the last decade [1], [2].

Anyway, due to the stochastic behavior of the input power for both WT and PV systems, their controllability is an important issue to be considered when these systems are connected to the utility network [3]. Due to the large penetration of renewable systems in some of the European countries, more stringent interconnection demands are requested by the power system operators. The power quality and robustness to the grid voltage and frequency variations are two of the main points demanded in the latest issues of grid codes for wind turbines in Germany, Denmark and Spain. Thus, there is a large interest in studying the control capabilities of distributed systems when having faulty grid conditions.

This paper discusses the control issues of the DPGS in order to fulfill the grid demands regarding power quality and grid faults ride through. Since the demands are more stringent in the WT case, focus is set on these systems rather than PV systems.

Firstly, a general structure of a DPGS is described, highlighting the possible control tasks. Secondly, the grid converter control is detailed analyzed, possible control loops and considerations in case of grid faults are given. Further on, some linear and nonlinear controllers are investigated and evaluated in terms of power quality, input power variations and grid faults ride through. Finally, experimental results are presented to validate the evaluation of the controllers and control structures discussed in this work.

A.V. Timbus, R. Teodorescu and F. Blaabjerg are with the Institute of Energy Technology, Aalborg University, DK-9220 Aalborg, Denmark. Email: avt@iet.aau.dk, ret@iet.aau.dk, fbl@iet.aau.dk

M. Liserre is with the Dept. of Electrotechnical and Electronic Engineering, Polytechnic of Bari, 70125-Bari, Italy. Email: liserre@ieee.org

P. Rodriguez is with the Dept. of Electrotechnical and Electronic Engineering, Technical University of Catalonia, Spain. Email: prodriguez@ee.upc.edu

II. DPGS structure and control

A. DPGS structure

A general structure of a distributed generation system is depicted in Fig. 1. Depending on the input power nature, i.e. wind, sun, hydrogen, different hardware configurations are possible [3]. Here, a system having a back-to-back converter configuration is considered. In this situation, there is an *input side controller* which controls the input side converter and a *grid side controller* which takes care of the DPGS interaction with the utility grid.

B. DPGS control

Normally, the input side controller ensures the maximum power extraction from the input power source and transmits the information about available power to the grid side controller. In the case of grid failure, this controller should also protect the input power source. In the case of wind turbine systems, the input side controller has different tasks, depending on the generator type used. On the other hand, the grid side controller normally regulates the dc-link voltage in order to maintain the power balance and takes care about the quality of the generated power by controlling the output current. Synchronization with the grid voltage and grid monitoring is also an important task of this controller. Since in the considered topology, the output power is completely decoupled from the input power by the dc-link, the grid side converter is the one responsible for the fault tolerance of the power distribution system.

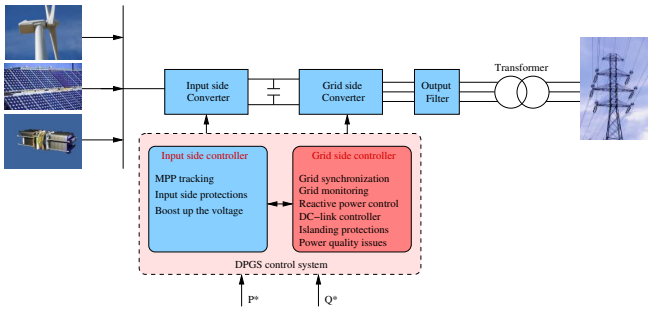

Fig. 1. General structure of a renewable energy DPGS.

III. Grid demands

Due to the exponentially increase of WT and PV systems connected to the utility network, more restrictive demands imposed by the Transmission System Operators (TSOs) are issued in order to maintain a proper functionality of the power system.

A. Power quality issues

For both WT and PV systems, the maximum limit for the total harmonic distortion (THD) of the output current is set to 5% according to the IEEE 1574 standard [4]. In order to comply with this, the current controller should have a very good harmonic rejection, especially for low order harmonics which have a higher content in the power system.

Table I shows the maximum allowed distortion limits for the first 33 current harmonics.

TABLE I
DISTORTION LIMITS FOR DPGS SYSTEMS WHEN INTERCONNECTING THE UTILITY NETWORK.

Odd harmonics	Distortion limit
3^{rd} – 9^{th}	< 4.0 %
11^{th} – 15^{th}	< 2.0 %
17^{th} – 21^{st}	< 1.5 %
23^{rd} – 33^{rd}	< 0.6 %

B. Voltage variation issues

Additionally to the power quality demands, the TSOs also require the capability of the generation systems to ride through short grid voltage variations. Considering an installation of a WT system into the Danish utility grid, the voltage variations and corresponding ride through times published in [5] and depicted in Fig. 2 should be fulfilled. As it may be noticed, the WT should have a ride through capability of 0.1 seconds when the grid voltage amplitude register a dip down to 25% of its nominal value. On the other hand, the generation system should also ride through for a voltage being 120% of its nominal value. As a consequence, the grid side controller should be prepared for such situations in order to avoid the disconnection of the generation unit and to comply with the demands.

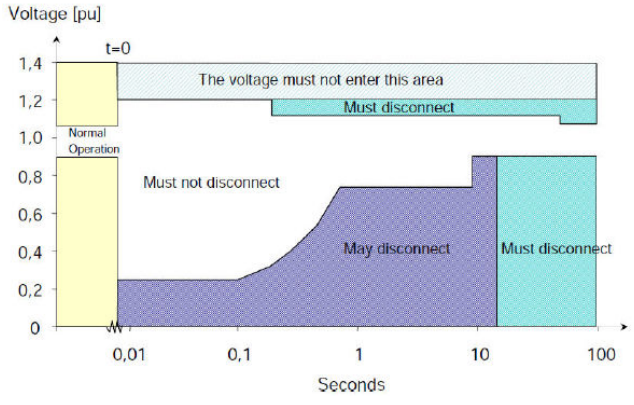

Fig. 2. Illustration of the grid voltage variations and the disconnection boundaries for wind turbines connected to the Danish power system.

Depending on the number of phases that register such a dip, the power system can remain balanced if all three phases are dropping with the same amplitude, or it can become unbalanced if one or two phases experience such a fault.

In addition to the power quality and voltage variations, there are many other requirements stated in the grid codes for WT systems, i.e. grid frequency variations, reactive power control, etc. but their discussion here is less relevant for the purpose of this work.

IV. Control structures for grid converter

In the following, a few control structures for the grid converter are discussed. The implementation of the control strategy for a distributed generation system can be done in different reference frames such as synchronous rotating (dq), stationary ($\alpha\beta$) or natural (abc) reference frame. The focus is set on different controller types and their implementation in different reference frames.

A. dq control

The dq control structure is using the $abc \rightarrow dq$ transformation module to transform the control variables from their natural frame abc to a frame which synchronously rotates with the frequency of the grid voltage. As a consequence, the control variables are becoming dc signals. Specific to this control structure is the necessity of information about the phase angle of utility voltage in order to perform the transformation. Normally, PI controllers are associated with this control structure. A typical transfer function of a PI controller is given by:

$$G_{PI}(s) = K_p + \frac{K_i}{s} \tag{1}$$

where K_p is the proportional and K_i is the integral gain of the controller. The structure of dq control involving cross coupling and feed forward of the grid voltages is depicted in Fig. 3. Since grid voltage feed-forward is used in this control structure, the dynamics of the control is expected to be high during grid voltage fluctuations. Every deviation of the grid voltage amplitude will be reflected into the d- and q-axis component of the voltage, leading to a fast response of the control system.

B. Stationary frame control

Since in the case of stationary reference frame control, the control variables, e.g. grid currents, are time varying waveforms, PI controllers encounter difficulties in removing the steady state error. As a consequence, another type of controller should be used in this situation.

Proportional resonant controller (PR) gained a large popularity in the last decade due to its capability of eliminating the steady state error when regulating sinusoidal signals, as is the case of grid connected DPGS control. Moreover, easily implementation of harmonic compensator for low order harmonics without influencing the controller dynamics, makes

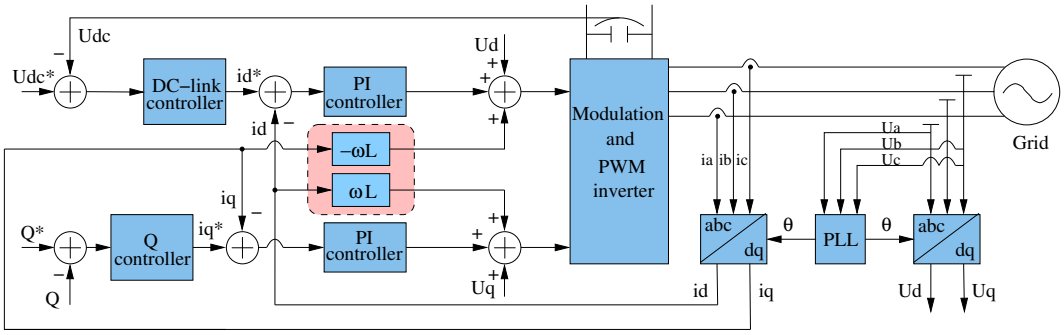

Fig. 3. General structure for synchronous rotating frame control using cross coupling and voltage feed-forward terms.

this controller well suited for grid tied systems [6]. The transfer function of resonant controller is defined as:

$$G_{PR}(s) = K_p + K_i \frac{s}{s^2 + \omega^2} \tag{2}$$

Because this controller acts on a very narrow band around its resonant frequency ω, the implementation of harmonic compensator for low order harmonics is possible without influencing at all the behavior of the current controller [6]. The transfer function of the harmonic compensator is given by:

$$G_{HC}(s) = \sum_{h=3,5,7} K_{ih} \frac{s}{s^2 + (\omega \cdot h)^2} \tag{3}$$

where *h* denotes the harmonic order the compensator is implemented for. A general structure of a stationary reference frame control using resonant controllers and harmonics compensator is illustrated in Fig. 4. Noticeable is that both Eq. (2) and Eq. (3) use information about the resonant frequency at which the controller operates. For the best performance of the resonant controller, this frequency has to be identical to the grid frequency. Hence, it should be remarked that an adaptive adjustment of the controller frequency is necessary if grid frequency variations are registered in the utility network, as reported in [7].

C. Natural frame control

Historically, the control structure implemented in *abc* frame is one of the first structures used for PWM driven converters [8]. Usually, implementation of nonlinear controllers such hysteresis controller has been used. The main disadvantage of these controllers was the necessity of high sampling rate in order to obtain improved behavior. Nowadays, due to the fast development of digital devices such as micro controllers (MC) and digital signal processors (DSP), implementation of nonlinear controllers for grid tied applications become very actual.

In this paper, the *abc* control is divided into *nonlinear control*, which discusses implementation issues of hysteresis controller on one hand, and *linear control* which treats the implementation and portability of PI, PR and dead beat controllers to the *abc* frame on the other hand.

It is worth to remark that in the situation of an isolated neutral transformer, as is the case of DPGS using a Δy transformer as grid interface, only two of the grid currents can be independently controlled, the third one being the negative sum of the other two, according to Kirchhoff law. Hence, the implementation of two controllers only is necessary in this situation [9].

1) Linear control: However, not only nonlinear controllers can be used in the natural frame but linear controllers such as PI controllers can also be ported to the stationary or natural frame, as demonstrated in [9].

a) PI controller: In [9], the portability of the PI controller to other reference frame like stationary frame has been derived using transformation modules between the frames. Moreover, in [10], the equivalent of PI controller in *abc* frame has been derived as (4). Noticeable in this case is the complexity of the controller matrix due to the off-diagonals terms owed to the cross coupling terms between the phases.

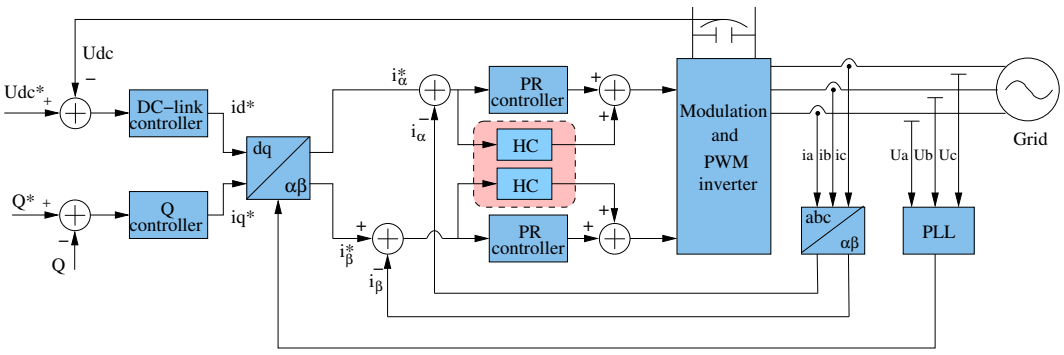

Fig. 4. General structure for stationary reference frame control strategy using resonant controller and harmonic compensator.

$$G_{PI}^{(abc)}(s) = \frac{2}{3} \cdot \begin{bmatrix} K_p + \frac{K_i s}{s^2+\omega_0^2} & -\frac{K_p}{2} - \frac{K_i s+\sqrt{3}K_i\omega_0}{2\cdot(s^2+\omega_0^2)} & -\frac{K_p}{2} - \frac{K_i s-\sqrt{3}K_i\omega_0}{2\cdot(s^2+\omega_0^2)} \\ -\frac{K_p}{2} - \frac{K_i s-\sqrt{3}K_i\omega_0}{2\cdot(s^2+\omega_0^2)} & K_p + \frac{K_i s}{s^2+\omega_0^2} & -\frac{K_p}{2} - \frac{K_i s+\sqrt{3}K_i\omega_0}{2\cdot(s^2+\omega_0^2)} \\ -\frac{K_p}{2} - \frac{K_i s+\sqrt{3}K_i\omega_0}{2\cdot(s^2+\omega_0^2)} & -\frac{K_p}{2} - \frac{K_i s-\sqrt{3}K_i\omega_0}{2\cdot(s^2+\omega_0^2)} & K_p + \frac{K_i s}{s^2+\omega_0^2} \end{bmatrix} \quad (4)$$

b) Resonant controller: Since the PR controller is already defined in stationary reference frame, its portability to natural frame is a straight solution. The controller matrix in this case is given by Eq. (5). As there is no cross-coupling terms to account for phases interaction in this case, Eq. (5) cannot be used when the neutral of the transformer is isolated, in this situation only two controllers being necessary as [9] describes.

c) Dead beat controller: The equation of predictive dead beat (DB) controller can be derived using Kirchhoff's law on the single phase circuit. In this case, the equation for the current through the inverter i_i (controlled current) can be expressed as:

$$\frac{di_i(t)}{dt} = -\frac{R_T}{L_T} i_i(t) + \frac{1}{L_T}(U_i(t) - U_g(t)) \quad (6)$$

where L_T is the total inductance and R_T is the total resistance upstream of the grid converter, $U_i(t)$ and $U_g(t)$ is the inverter and grid voltage respectively. The discretized form of Eq. (6) is given by:

$$\begin{aligned} i_i((k+1)T_s) &= e^{-\frac{R_T}{L_T}Ts} \cdot i_i(kT_s) \\ &- \frac{1}{R_T}\left(e^{-\frac{R_T}{L_T}Ts} - 1\right) \cdot (Ui(kT_s) - U_g(kT_s)) \end{aligned} \quad (7)$$

Solving (7), the controller equation can be derived as:

$$G_{DB}^{(abc)} = \frac{1}{b} \cdot \frac{1 - az^{-1}}{1 - z^{-1}} \quad (8)$$

where a and b are denoted as:

$$a = e^{-\frac{R_T}{L_T}Ts}; \qquad b = -\frac{1}{R_T}\left(e^{-\frac{R_T}{L_T}Ts} - 1\right) \quad (9)$$

Again, because the controller equation in this case has been derived considering a single phase circuit, implementation of only two such controllers are necessary in the situation of a isolated neutral transformer, the third grid current being given by the Kirchhoff's law.

Since DB controller controls the current such that this reaches its reference at the end of next switching period, the controller is introducing one sample time delay. In order to compensate for this delay and the plant nonlinearities, an observer can be introduced in the structure of the controller [11]. Moreover, a fuzzy logic controller tuned on the basis of dead beat theory and then modified on-line in order to take into account the unmodeled nonlinearities is also possible [12].

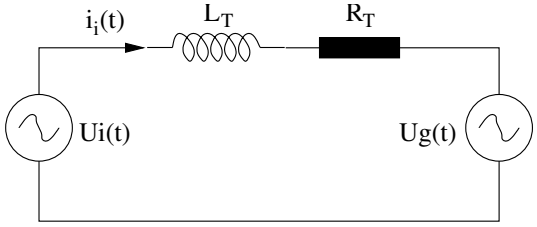

Fig. 5. Representation of single phase circuit used to derived the dead beat controller equation where $L_T = L_i + L_g$ and $R_T = R_i + R_g$.

D. Nonlinear control

d) Hysteresis controller: Besides the necessity of high sampling, another drawback of the hysteresis controller is the compulsion of an adaptive hysteresis band in order to obtain fixed switching frequency. In [13], [14], different methods and algorithms to obtain fixed switching frequency are presented. Depending on the method used, the complexity of the controller can be increased considerably. This paper treats an implementation based on [14] where the hysteresis band can be calculated as:

$$HB = \frac{0.25a' U_{dc}}{f_{sw} L_T}\left[1 - \frac{L_T^2}{a'^2 U_{dc}}\left(\frac{U_g}{L_T} + \frac{di^*}{dt}\right)^2\right] \quad (10)$$

with a' typically varying between $1/3$ and $2/3$, U_{dc} being the dc-link voltage, L_T the total phase inductance comprising the filter inductance L_i and the grid inductance L_g, e.g. ($L_T = L_i + L_g$), f_{sw} the modulation frequency and U_g the grid voltage.

Normally, the output of the hysteresis comparator is the state of the switches in the power converter, hence three hysteresis controllers are required (one for each leg of the inverter) in the case of a three phase converter. Therefore, once again the coupling of the transformer needs to be considered when designing the controller. In Eq. (10), the term a' accounts for an isolated neutral connection, allowing in this case the implementation of three controllers.

Normally, the term $\frac{di^*}{dt}$ is neglected as it is considerably smaller as compared to the term $\frac{U_g}{L}$ hence leading to an easier implementation of Eq. (10).

$$G_{PR}^{(abc)}(s) = \begin{bmatrix} K_p + \frac{K_i s}{s^2+\omega_0^2} & 0 & 0 \\ 0 & K_p + \frac{K_i s}{s^2+\omega_0^2} & 0 \\ 0 & 0 & K_p + \frac{K_i s}{s^2+\omega_0^2} \end{bmatrix} \quad (5)$$

V. Design of linear controllers

In the above paragraphs, the equations for nonlinear controllers, i.e. hysteresis and dead-beat, lead to the direct implementation of this controllers without further tuning. As it can be observed in Eq. (10) and (9), the parameters of these controllers are directly depending on the plant parameters R_T and L_T. Since these parameters are known, the implementation and tuning of these nonlinear controllers is a straight solution.

Anyway, in the situation of PI and PR controllers these should be tuned according to some rules in order to get the desired response of the controller and normally the tuning of these controllers is related to the plant to be controlled.

A. Model of the plant

The considered plant in this application is the LCL filter attached to the power converter. In this case, only an LC filter is physically implemented, while the second L is the inductance of the transformer, as Fig. 9 shows.

The filter transfer function has been derived using the single phase electrical diagram of the filter, as depicted in Fig. 6.

The relation for the currents flowing through the filter is given by:

$$i_i - i_c - i_g = 0 \tag{11}$$

while based on Fig. 7, the voltages can be described as:

$$U_i = i_i L_i s + U_c \tag{12a}$$

$$U_g = -i_g L_i s + U_c \tag{12b}$$

$$U_c = i_c(\frac{1}{C_f s} + R_d) \tag{12c}$$

Deriving the current values yields:

$$i_i = \frac{1}{L_i s}(U_i - U_c), \quad i_g = \frac{1}{L_g s}(U_c - U_g) \tag{13}$$

Rewriting in terms of impedances, the voltages can derived as

$$\begin{aligned} U_i &= z_{11} i_i + z_{12} i_g \\ U_g &= z_{21} i_i + z_{22} i_g \end{aligned} \tag{14}$$

where:

$$\begin{aligned} z_{11} &= L_i s + \tfrac{1}{C_f s} + R_d, \quad z_{12} = -(\tfrac{1}{C_f s} + R_d) \\ z_{22} &= -(L_g s + \tfrac{1}{C_f s} + R_d), \quad z_{21} = \tfrac{1}{C_f s} + R_d \end{aligned} \tag{15}$$

Finally, the transfer function between the grid current and the inverter voltage is:

$$\begin{aligned} H(s) = \frac{i_g}{U_i} &= \frac{z_{21}}{z_{12} z_{21} - z_{11} z_{22}} \\ &= \frac{R_d C_f \cdot s + 1}{L_i L_g C_f \cdot s^3 + R_d C_f (L_i + L_g) \cdot s^2 + (L_i + L_g) \cdot s} \end{aligned} \tag{16}$$

The LCL filter parameters are listed in Table II. As previously mentioned, the grid side parameters L_g and R_g are representing the transformer.

TABLE II
LCL output filter parameters.

Inverter side impedance	Capacitance	Grid side impedance
L_i = 10 mH	C_f = 0.7μF	L_g = 2 mH
R_i = 0.4 Ω	R_d = 0 Ω	R_g =0.6 Ω

B. Resonant controller design

The PR controller is tuned based on the root-locus theory. Using the controller transfer function as given in (2) and the plant transfer function from (16), the close loop transfer function is derived in discrete form like:

$$CL(z) = \frac{PR(z) \cdot H(z)}{1 + PR(z) \cdot H(z)} \tag{17}$$

where $PR(z)$ and $H(z)$ are the discrete forms of the Eq. (2) and (16) respectively, derived using *c2d* facility in MATLAB®. The root loci of the close loop system shown in Fig. 8(a) is used to tune the resonant controller. The controller has been designed for having a damping of $\zeta = 1/\sqrt{2}$ and in this case the proportional gain of the controller has been obtained as $K_p = 30$. The value for the integral gain of the controllers K_i has been obtained using Bode plot of the open loop system shown in Fig. 8(b), where from the value of $K_i = 6000$ has been selected for implementation which provides a very high gain at the resonant frequency of the controller (50 Hz in this case), hence having a good steady state error rejection.

C. PI controller design

Because the values of the controller gains are not changing when the controller is transformed in different reference frames [9], the same values for K_p and K_i are used for the PI controllers as well (in both *dq* and *abc* implementations).

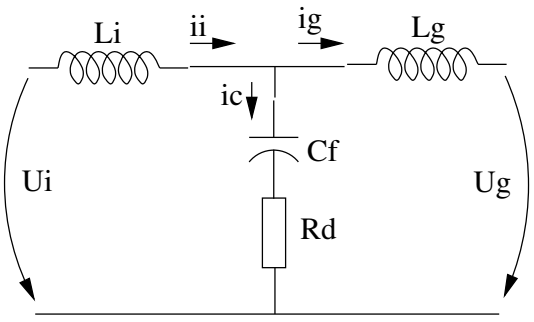

Fig. 6. Single phase representation of the LCL filter layout.

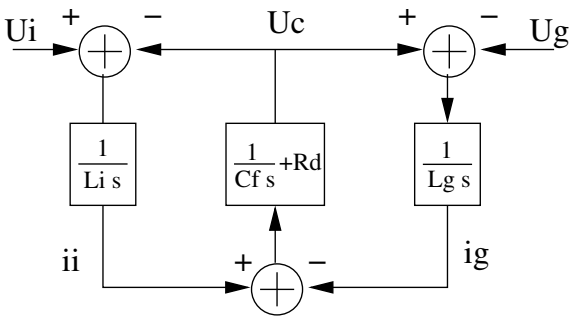

Fig. 7. Representation in terms of transfer function of the LCL filter.

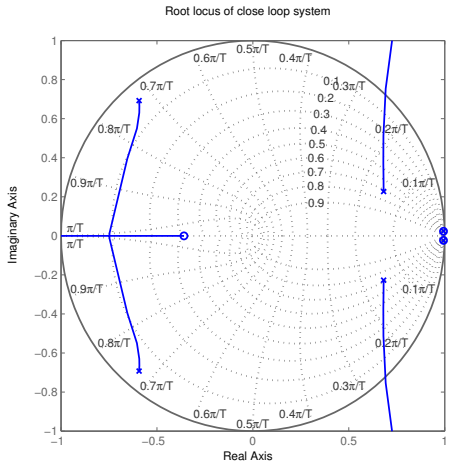

(a)

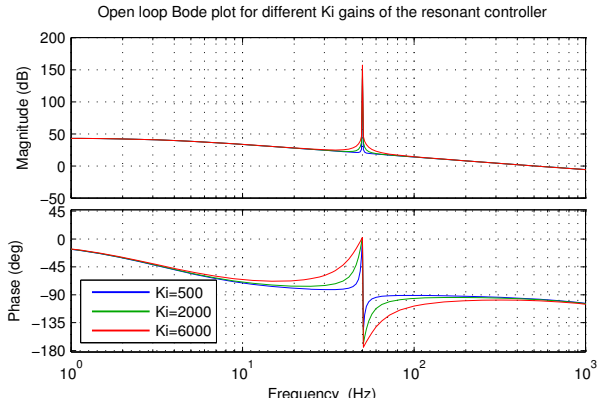

(b)

Fig. 8. Tuning methods for resonant controller (a) root loci of the closed loop system and (b) bode plot of the open loop in the case of different values for the integral gain K_i.

VI. Laboratory Implementation

To be able to evaluate the behavior of the different control structures and controllers, an experimental setup having the schematic as depicted in Fig. 9 has been implemented in laboratory. The filter parameters are as described in § V-A and the power converter is a Danfoss VLT 5000 series rated for 400 V and 5 A. Since the grid simulator cannot accept power in, a local load is connected in the circuit. The load is sized in the way that the current through the load is the sum of the converter current and the grid current. The grid currents and voltages as well as the dc-link voltage are sampled and used in the control structures described in § IV, as Fig. 9 shows.

The controllers and the control structures are implemented

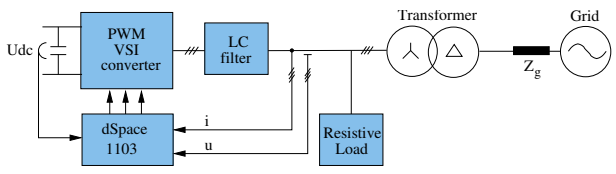

Fig. 9. Schematic of the laboratory setup connected to a grid simulator through a Δy transformer and having a resistive load.

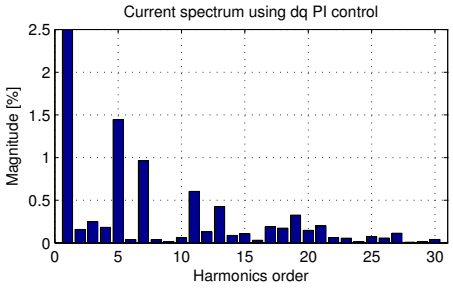

(a)

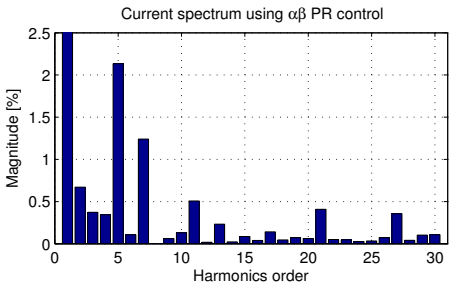

(b)

Fig. 10. Harmonic spectrum of the grid current in the case of: (a) dq PI control and (b) stationary control using PR controller.

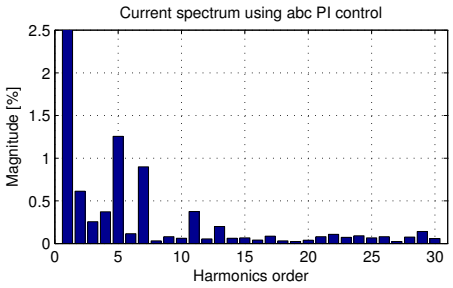

(a)

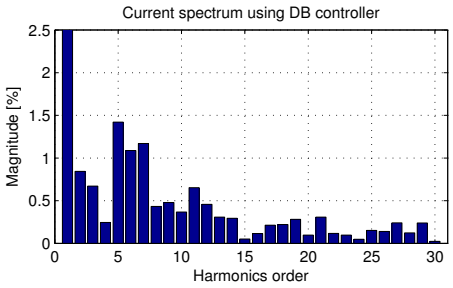

(b)

Fig. 11. Harmonic spectrum of the grid current in the case of: (a) equivalent of PI used in abc frame and (b) dead beat control.

using a dSpace 1103 board having a 333 MHz Power PC (PPC) processor. Due to the limitations of this board, the nonlinear controllers, e.g. dead beat are not implemented using high sampling rate, thus all control structures are implemented at a sampling and switching frequency of 13 kHz. In this work, experimental result for four control structures are presented, i.e. PI controllers implemented in dq frame (Eq. (1)), PR implemented in $\alpha\beta$ stationary frame (Eq. (2)), the equivalent of PI in abc frame (Eq. (4)) and dead beat controller implemented

in abc frame (Eq. (8)). For a fair evaluation of the controllers only the current loop is considered, hence the influence of the dc-link controller or any other outer loop control is eliminated.

VII. Experimental results

The evaluation of the control structures and controllers is made in two situations, i.e. steady state and transient operation. In steady state situation, the quality of the controlled current is discussed while in the transient operation conditions the controller response to a step increase of the current reference and to a single phase grid fault is studied.

A. Steady state operation

The pollution rate of the controllers is determined in the situation of ideal grid conditions. The grid simulator is programed to provide a perfect sinusoidal output voltage containing no harmonics, hence the harmonics of the grid current are owing to the current controller. In all the cases, the total harmonic distortion (THD) of the current is measured using a three phase Voltech PM3000 power meter.

1) Synchronous rotating frame control: The THD of the grid current in the case of dq control employing PI controllers for current regulation is shown in Fig. 10(a). The first 30 harmonics are shown and as can be observed, the 5^{th} and 7^{th} harmonics are having the larger contribution to the grid current THD, which in this case was measured to be 1.77%. It is worth noticing that no filtering has been used for the voltage feed-forward terms U_d and U_q which are provided by the transformation module $abc \rightarrow dq$, as Fig. 3 illustrates.

2) Stationary frame control: As previously mentioned, in the case of stationary frame control, resonant controller is used for current regulation. In order to have a fair comparison between the structures and controllers, the harmonic compensator has not been considered here. As a consequence, a larger magnitude for the 5^{th} and 7^{th} harmonics is registered in this case, as can be observed in Fig. 10(b). The THD value of the delivered current in this situation is 2.6%.

3) Natural frame control: In the case of natural frame control, two controller types are implemented, i.e. equivalent of PI in abc and predictive dead beat controller.

a) Equivalent of PI in abc frame: The grid current harmonic spectrum using the implementation of (4) is depicted in Fig. 11(a). A slightly lower magnitude for all harmonic orders can be observed compared to the dq implementation of the same controller. This is also proved by the THD value which in this situation is 1.72%.

b) Dead beat controller: Fig. 11(b) illustrates the harmonic spectrum of the grid current in the case when dead beat controller is used for current regulation. The total harmonic distortion in this situation measured by the power meter is 2.4%.

B. Transient operation conditions

The tests for transient operation conditions are divided into two types. Firstly, a step in the current reference is generated such that the output power of the converter increases from 2kW up to 3kW. The dynamics of the controllers are pursued during this experiment. Secondly the behavior of the current controller in the case of single phase grid fault is examined.

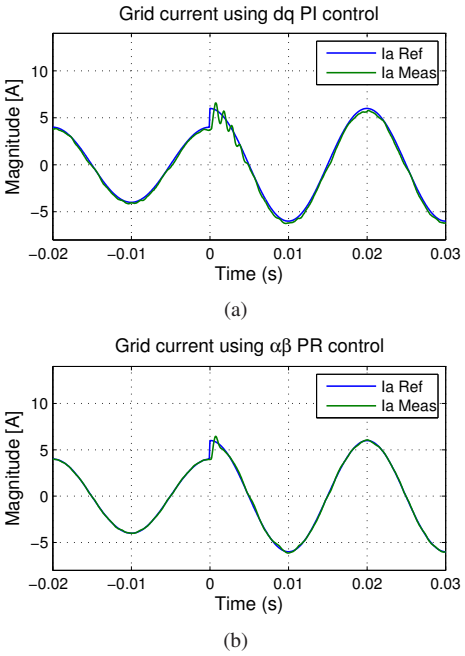

Fig. 12. Dynamics of the controllers in the case of 2A current reference step: (a) PI controller implemented in dq frame and (b) PR controller in stationary frame.

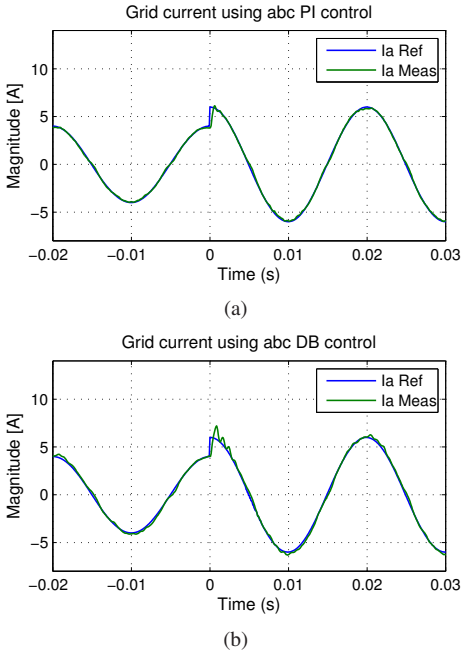

Fig. 13. Dynamics of the controllers in the case of 2A current reference step: (a) equivalent of PI in abc frame and (b) DB controller in abc frame.

1) Step in reference current: Fig. 12(a) depicts the response of the PI controller implemented in dq synchronous frame when a step in the current reference is issued. As it might be observed, the controller has very high dynamics, following closely the imposed reference. The responses of the other controllers are shown in Fig. 12(b) – 13(b). Noticeable is that

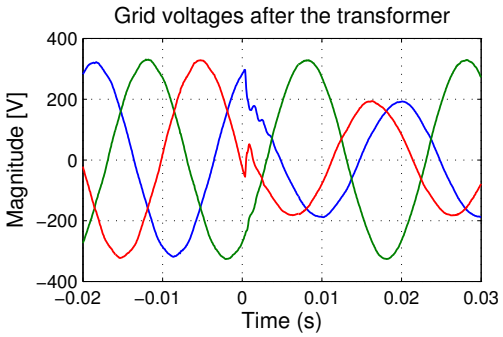

Fig. 14. Grid voltages after the Δy transformer in the case of single phase fault at the point of common coupling.

all controllers have a good and fast transient response in this situation.

2) Single phase grid fault: In [15] it has been shown that in the case of single phase fault in the grid, the voltages after the Δy transformer (at the converter terminals) behave as illustrated in Fig. 14. The grid simulator has been programmed to produce zero voltage on one phase at the time instant 0 seconds. As a consequence, amplitude drop and phase jump in two of the phases is registered, as Fig. 14 illustrates. Under such unbalanced grid conditions, the synchronization algorithm has an important role in the control. A Phase-Looked Loop (PLL) system which is able to extract the positive sequence of the grid voltages has been used [16], hence the phase angle provided by the algorithm during the fault is synchronized to the positive sequence component of the grid voltages. In this situation, the current references remain sinusoidal and balanced, as [17] describes.

a) dq control structure: Looking at the controlled current using dq control structure (Fig. 15(a)), a small disturbance can be observed in the current waveform when the fault occurs, but this is fast regulated according with the imposed reference. The grid voltage feed-forward terms used in this control structure play an important role here, enhancing the dynamics of the controller in the situation of grid voltage variations.

b) Stationary frame control structure: The behavior of the PR controller implemented in stationary frame is depicted in Fig. 15(b). As it might be noticed in this case, the controller has a larger overshoot in its response when the grid fault take place. Anyway, this is not too large to trip out the current protection of the system and the current is fast controlled according to its reference within one fundamental period. Noticeable is that in this case no grid voltage feed-forward terms is used in the controller.

c) Equivalent of PI in abc frame: A similar behavior is registered by the equivalent of PI controller implemented in natural reference frame. Anyway, the overshoot in this case is not as large as in the case of PR controller and the current is also fast regulated soon after the fault.

d) Dead beat control: The response of the dead beat controller in the case of grid fault is shown in Fig. 16(b). Comparing to all previous behaviors, the DB controller has the highest robustness in a situation of a grid fault. A small transient in the controlled current waveform can be observed

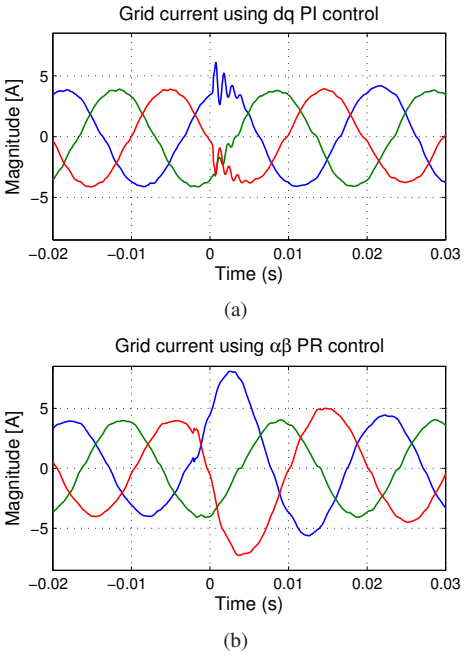

Fig. 15. Response of the controller in the case of single phase fault: (a) PI controller implemented in dq frame and (b) PR controller in stationary frame.

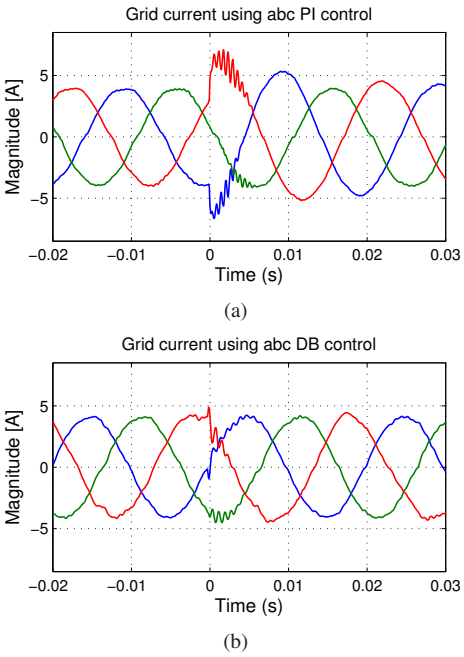

Fig. 16. Response of the controller in the case of single phase fault: (a) equivalent of PI in abc frame and (b) DB controller in abc frame.

when the fault occurs, but the current value does not exhibits any overshoot, following closely the imposed reference.

VIII. Conclusion

This paper gives a description of some possible control structures for distributed power generation systems connected to utility network. The traditional synchronous reference frame structure as well as stationary reference frame and natural reference frame structures are addressed in this work. The

control structures are illustrated and their major characteristics are described.

Additionally, five types of controllers have been introduced, namely PI controllers implemented in *dq* frame, resonant controller, PI controller implemented in *abc* frame, hysteresis controller and finally the dead beat predictive controller. An evaluation in terms of harmonic distortion when running in steady state conditions and dynamics in the case of reference current step up and a single phase fault situation has been carried out. All controllers prove to have an satisfactory behavior in all situations but dead beat controller proves to be superior to the others especially during grid fault.

REFERENCES

[1] EWEA, "www.ewea.org/documents," Online Documentation, October 2005.

[2] IEA-PVPS, "Cumulative Installed PV power," www.iea-pvps.org, October 2005.

[3] F. Blaabjerg, Z. Chen, and S. Kjaer, "Power electronics as efficient interface in dispersed power generation systems," *IEEE Trans. on Power Electronics*, vol. 19, no. 5, pp. 1184–1194, 2004.

[4] IEEE15471, "IEEE standard for interconnecting distributed resources with electric power systems," 2005.

[5] Eltra and Elkraft, "Wind turbines connected to grids with voltage below 100 kV," http://www.eltra.dk, 2004.

[6] R. Teodorescu and F. Blaabjerg, "Proportional-resonant controllers. A new breed of controllers suitable for grid-connected voltage-source converters," in *Proc. of OPTIM'04*, vol. 3, 2004, pp. 9–14.

[7] A. V. Timbus, M. Ciobotaru, R. Teodorescu, and F. Blaabjerg, "Adaptive resonant controller for grid-connected converters in distributed power genaration systems," in *In Proc. of APEC'06*, 2006, pp. 1601–1606.

[8] S. Buso, L. Malesani, and P. Mattavelli, "Comparison of current control techniques for active filter applications," *IEEE Trans. on Industrial Electronics*, vol. 45, no. 5, pp. 722–729, 1998.

[9] D. N. Zmood, D. G. Holmes, and G. H. Bode, "Frequency-domain analysis of three-phase linear current regulators," *IEEE Trans. on Industry Applications*, vol. 37, no. 2, pp. 601–610, 2001.

[10] E. Twining and D. G. Holmes, "Grid current regulation of a three-phase voltage source inverter with an LCL input filter," *IEEE Trans. on Power Electronics*, vol. 18, no. 3, pp. 888–895, 2003.

[11] P. Mattavelli, G. Spiazzi, and P. Tenti, "Predictive digital control of power factor preregulators with input voltage estimation using disturbance observers," *IEEE Trans. on Power Electronics*, vol. 20, no. 1, pp. 140–147, 2005.

[12] A. Dell'Aquila, A. Lecci, and M. Liserre, "Microcontroller-based fuzzy logic active filter for selective harmonic compensation," in *Proc. of IAS'03*, 2003.

[13] L. Malesani, P. Mattavelli, and P. Tomasin, "Improved constant-frequency hysteresis current control of VSI inverters with simple feed-forward bandwidth prediction," *IEEE Trans. on Industry Applications*, vol. 33, no. 5, pp. 1194–1202, 1997.

[14] B. K. Bose, "An adaptive hysteresis-band current control technique of a voltage-fed PWM inverter for machine drive dystem," *IEEE Trans. on Industrial Electronics*, vol. 37, no. 5, pp. 402–408, 1990.

[15] M. H. J. Bollen, *Understanding Power Quality Problems: Voltage Sags and Interruptions*. IEEE Press, 2002.

[16] A. V. Timbus, M. Liserre, F. Blaabjerg, R. Teodorescu, and P. Rodriguez, "PLL algorithm for power generation systems robust to grid faults," in *Proc. of PESC'06*, 2006, pp. 1360–1366.

[17] A. V. Timbus, P. Rodriguez, R. Teodorescu, M. Liserre, and F. Blaabjerg, "Control strategies for distributed power generation systems operating on faulty grid," in *Proc. of ISIE'06*, 2006, pp. 1601–1607.

Publication 3

Independent synchronization and control of three phase grid converters

by A. Timbus, M. Liserre, R. Teodorescu, F. Blaabjerg and A. Dell'Aquila
Article published in proceedings of SPEEDAM'06, pages 1246 – 1251, 2006

Independent Synchronization and Control of Three Phase Grid Converters

Adrian V. Timbus, *Student Member, IEEE*, Marco Liserre, *Member, IEEE*, Remus Teodorescu, *Senior Member, IEEE*, Frede Blaabjerg, *Fellow, IEEE* and A. Dell'Aquila *Senior Member, IEEE*

***Abstract*—This paper deals with independent control and synchronization for three phase grid connected converters. Two different implementations of Phase-Locked Loop (PLL), i.e. the conventional three phase PLL denoted here as $dqPLL$ and the single phase PLL are discussed. The difference between these two algorithms and their influence on the current reference are highlighted. Additionally, the implementation of two linear controllers, namely proportional-integral (PI) and proportional-resonant (PR) in order to obtain independent control is also discussed. Equations of the controllers in both cases are derived. Finally, simulation results are presented in each case.**

***Index Terms*—independent current control, grid synchronization, PI controller, resonant controller**

I. Introduction

IN THE LAST decade, Distributed Power Generation Systems (DPGS) based on renewable energies contribute more and more to the total amount of energy production on the globe [1], [2]. Wind Turbines (WT) as well as Photovoltaics (PV) systems are seen as reliable energy sources which should be further explored in order to get maximum efficiency and overcome the increasing power demand in the world. Fig. 1 shows the installed capacity of wind and photovoltaic power in the last decade, where an exponential increase is observed in both cases. It is worth noting that the majority of this power is connected to the utility network.

Owed to the uncertainty of the availability of input power, controllability of these systems is a challenge [3]. Moreover, the increased amount of distributed systems connected to the utility network can create instability of the power systems, even leading to outages. As a consequence, the Transmission System Operators (TSOs) issue more stringent demands regarding [4] grid connection of the DPGS. One of the most severs demand nowadays is the ability of the DPGS to run over short grid disturbances such as voltage sags and frequency variations. As a consequence, the control of DPGS needs to be improved.

The presence of a delta-star isolation transformer in most of the distributed generation systems connected to utility network transforms one of the most severe fault (e.g. one phase short circuited with the ground) into a situation more affordable (two phases reduce their amplitude and change the phase)

A.V. Timbus, R. Teodorescu and F. Blaabjerg are with the Institute of Energy Technology, Aalborg University, DK-9220 Aalborg, Denmark. Email: avt@iet.aau.dk, ret@iet.aau.dk, fbl@iet.aau.dk

M. Liserre and A. Dell'Aquila are with the Dept. of Electrotechnical and Electronic Engineering, Polytechnic of Bari, 70125-Bari, Italy. Email: liserre@ieee.org

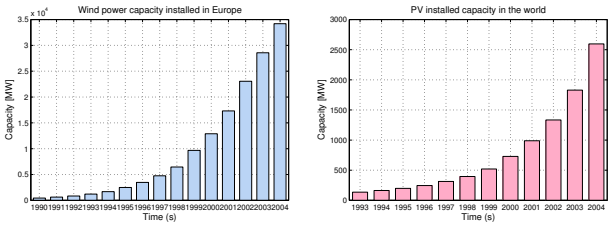

(a) (b)

Fig. 1. Installed capacity at the end of 2004: (a) wind energy in Europe [1] and (b) PV power in the world [2].

[5]. Hence, more than the reduction of amplitude of one or two phases what is affecting the performance of the system controller is the phase jump due to the unbalance. In these situation it could be better to have a system characterized by independent control of each phase of the converter. Moreover, the new release of the German standard VDE 0126-1-1 offers now an alternative to the grid impedance estimation feature of the photovoltaic systems installed in Germany. According to the new standard, the three phase systems can use individual monitoring of the three grid voltages to detect islanding situation, but in this case the control of the PV inverter needs to be independent for each phase.

However the control of the current in abc could lead to steady-state errors if done with PI controllers. Moreover, the use of one Phase-Looked Loop (PLL) for the overall system allows the control to operate only as a whole, no matter happens with the grid voltages. The two above mentioned problems can be solved, as described in the paper, with the use of resonant controllers and three different PLL's.

This paper discusses a control strategy implemented in natural reference frames abc. An introduction to control strategies for grid converters is first given, followed by a description of the proposed system. The current controller implementation in different reference frames is further discussed. Finally, simulation and experimental results when the power generation system runs under normally and faulty grid conditions are presented.

II. Grid converter control under faults

In the case of DPGS using a back-to-back converter topology, the control strategies applied to the grid converter are usually consisting of two cascaded loops. An inner current loop, which regulates the output current and an outer loop which in most of the cases regulates the dc-link voltage [6],

[7]. The dynamics of the current loop are normally high in order to be able to fast regulate the current in transient conditions so that the system will not trip out due to the over-current protection. In addition, the quality of the output current should also be considered when designing the current controller. On the other hand, the dc-link voltage controller is usually designed for optimum regulation and stability. Its dynamics are normally slower than those of current controller. The output of the dc-link controller sets the reference for the active current to be injected in the grid.

Another alternative is to use a power controller [8]–[10] instead of dc-link voltage controller. The references for the active and reactive current are calculated from the active and reactive power references. In [11], a combination between these two strategies is used. The reference for the current controller is calculated from the power reference and dc-link voltage. In addition, a dc-link controller determines the dynamic behavior of the dc voltage. As reported in all the works above, these control strategies are well performing under normal grid conditions.

Anyway, when grid faults occur in the utility network, more considerations should be made when designing the controllers. Grid unbalance, due to voltage or phase angle variations, can cause serious problems to the control algorithm of DPGS. A common phenomenon which happens under unbalance is the appearance of the negative sequence in the grid voltages [5]. The negative sequence will create double frequency oscillations in the system, which will be reflected in the dc-link capacitor. As a consequence, the dc-link controller should be designed to reject these oscillations in order to ensure a constant current reference for the current loop.

Another weak point of the control when the system is running on grid faults is the synchronization algorithm. In [12]–[14] it has been highlighted that improvements have to be made to the conventional three phase PLL algorithm in order to overcome grid faults and provide a clean synchronization signal for the current reference.

III. Proposed control algorithm

The control strategy depicted in Fig. 2 is proposed in this work. The system comprises a PWM driven Voltage Source Inverter (VSI) supplied by a controllable dc power supply. As it can be observed, the control algorithm is implemented in natural reference frames (abc) where resonant controllers (RC) are employed for current regulation. The current reference is derived from the power reference of the system. The dc-link voltage is controlled by a PI regulator and its output is feed-forwarded to the current reference. For systems where reference power P^* is not directly available (wind turbine systems typically), the control can be implemented without the power feed forward term. In this case, the dc-link voltage controller sets the current reference. In order to decouple all three phases and to have independent control of them, three PLL systems are used. These are implemented such as the first algorithm detects the phase angle of the grid voltage V_a, the second detects that of V_b and finally the third algorithm estimates the phase angle of V_c.

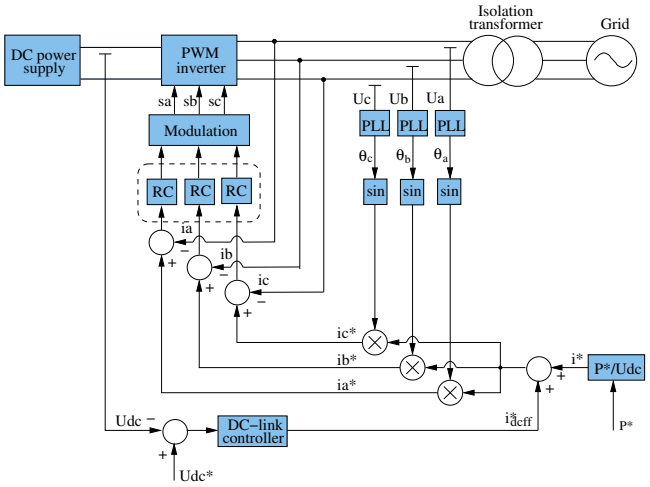

Fig. 2. Proposed control structure for independent control of the grid current.

Anyway, in the case of a system having a Δy transformer with isolated neutral as interface to the utility network, the three grid current cannot be controlled individually as one of them has to fulfill the condition [15]:

$$i_a + i_b + i_c = 0 \tag{1}$$

In the case that all three grid currents want to be controlled, the neutral point of the transformer has to be connected to the midpoint of the dc-link.

A. Dc-link controller

A PI controller is employed for the dc-link voltage regulation. Its design aims for system stability and optimal power conversion, yielding in low dynamics characteristics. As mentioned in § II, the dc-link controller needs special design in order to cancel the oscillations due to the negative sequence appearing in the grid when an unbalance fault occur. This feature of the controller is beyond the scope of this paper and has not been implemented here. A filtering technique based on delay signal cancellation (DSC) [16] is applied to the current reference instead. This filter is able to eliminate the double frequency oscillations with almost no delay, canceling in this way the effect of the oscillations to the current reference. Noticeable is that this will not cancel the oscillations in the dc-link voltage, thus appropriate size of the dc-link capacitor is necessary.

IV. PLL system

As mentioned in § II, another affected part of the control when the power generation system is running on grid faults is the PLL. Two possible PLL algorithms and their influence on having independent control of each phase current are discussed in the following.

A. dq PLL

The most common PLL technique applied to three phase grid connected systems is based on an algorithm implemented in synchronous reference frame (dq) [17]. The structure of the

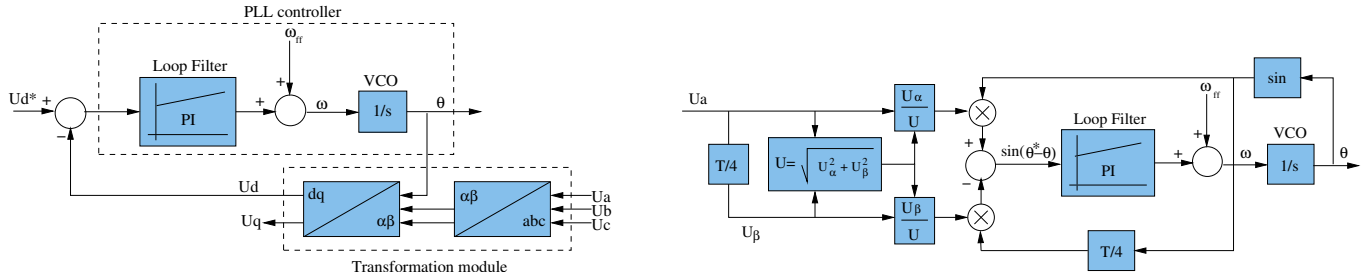

Fig. 3. Structure of: (a) three phase $dqPLL$ algorithm and (b) single phase PLL using a quarter of the mains period delay to create the quadrature voltage.

$dqPLL$ is depicted in Fig. 3(a). The grid voltages are the input into the algorithm and they are transformed into synchronous reference frame by means of $abc \rightarrow dq$ transformation module. The phase locking is realized by controlling the $d-$voltage to be zero. In this way, the phase angle of grid voltage a is detected and this is the output of the algorithm.

Anyway, in the case of unbalanced grid faults, this structure is not able to provide a clean synchronization signal for the current reference due to the appearance of the negative sequence in the grid voltages. Hence, improvements have to be added to this algorithm in order to be able to filter out the negative sequence [13], [14]. As a consequence, the phase angle provided when advanced algorithms are used is following the positive sequence of the grid voltages.

In the situation of independent control and synchronization of each phase current, the structure presented in Fig. 3(a) has a major drawback, e.g. cannot detect the phase angle of each grid voltage, thus independent synchronization of each current cannot be realized with this algorithm. In the case of grid unbalance, even if three such algorithms are used, the resulting phase angles are always balanced (120 degrees displaced) due to the capability of this algorithm to provide a clean synchronization angle of the positive sequence only. As a consequence, the current references will always be balanced when such an algorithm is used in control.

Fig. 4 shows the phase angle estimation when three $dqPLL$ algorithms are used in the control. At the simulation time 0.2 seconds, the voltages at the point of common coupling experience a single phase fault as depicted in Fig. 7(a). Due to this fault, a negative sequence voltage appears in the grid, e.g. $U = U^+ + U^-$. The implemented PLLs are able to extract the positive sequence of the voltages and to provide their corresponding phase angles, hence the synchronization signals are also balanced after the fault.

B. Single phase PLL

The structure of the single phase PLL is depicted in Fig. 3(b). This algorithm artificially creates the orthogonal component of the grid voltage used to obtain the phase error between the phase of the real grid voltage and the estimated one by the PLL. In [18], a few methods to create the orthogonal component are presented. Here, the delay with a quarter of the fundamental period $T = 0.02\ s$ is chosen for implementation.

In the case of three phase grid converters, three such PLL structures (one for each phase) are necessary. The output of the three systems will follow their respective grid voltage phase angle and, as a consequence, the reference currents will be in phase to their corresponding voltages. Hence, independent synchronization can be implemented using three such PLLs.

Fig. 5 illustrates the estimation of the phase angle for each phase voltage. Contrary to $dqPLL$, single phase PLL is not able to discern the unbalance in the grid, therefore cannot see if there is a negative sequence or not. An extra algorithm which derives the positive and negative sequence from the magnitude of each voltage can be employed in this situation. Anyway, the single phase PLL algorithm closely tracks the phase variation of its corresponding voltage with disregard of the other two grid voltages. As it can be observed in Fig. 5, the phase angles in this situation are unbalanced leading to a creation of an unbalance current reference.

V. Current Controller in Natural Reference Frame

One of the controllers most used in applications involving power converter is the proportional-integral (PI) controller. It is well known the necessity of transformation of control variables into a reference frame where these become dc signals, in order to have a proper utilization of PI controller [6]. In the case of

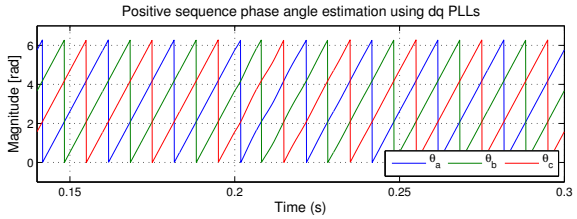

Fig. 4. Positive sequence phase angle estimation using three $dqPLL$ systems in the case of a single phase fault.

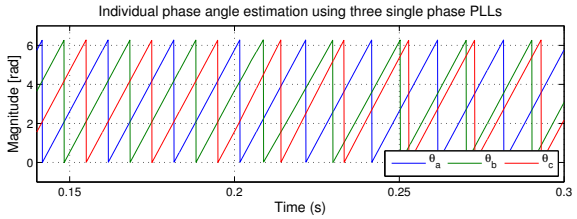

Fig. 5. Phase angle estimation using three single phase PLLs systems in the case of a single phase fault in the utility network.

$$G_c^{(a,b,c)}(s) = \frac{2}{3} \cdot \begin{bmatrix} K_p + \frac{K_i s}{s^2+\omega_0^2} & -\frac{K_p}{2} - \frac{K_i s + \sqrt{3} K_i \omega_0}{2\cdot(s^2+\omega_0^2)} & -\frac{K_p}{2} - \frac{K_i s - \sqrt{3} K_i \omega_0}{2\cdot(s^2+\omega_0^2)} \\ -\frac{K_p}{2} - \frac{K_i s - \sqrt{3} K_i \omega_0}{2\cdot(s^2+\omega_0^2)} & K_p + \frac{K_i s}{s^2+\omega_0^2} & -\frac{K_p}{2} - \frac{K_i s + \sqrt{3} K_i \omega_0}{2\cdot(s^2+\omega_0^2)} \\ -\frac{K_p}{2} - \frac{K_i s + \sqrt{3} K_i \omega_0}{2\cdot(s^2+\omega_0^2)} & -\frac{K_p}{2} - \frac{K_i s - \sqrt{3} K_i \omega_0}{2\cdot(s^2+\omega_0^2)} & K_p + \frac{K_i s}{s^2+\omega_0^2} \end{bmatrix} \quad (2)$$

individual control of each phase current in applications such as grid tied converters, it has no sense to use such a reference frame. As in this situation the grid current is sinusoidal, the current controller needs to be able to track sinusoidal signals. In the followings, two different controllers to be used in the proposed control structure are discussed.

A. PI controller

As stated above, PI controllers are widely used in control of PWM VSI converters. Due to their characteristic of better regulating dc signals, the implementation of these controllers is usually done in a rotating reference frame where the control variables are becoming dc signals. Cross coupling terms as well as feed-forward of the utility voltage are additionally used to improve the behavior of these controllers. In the hypothesis that the PI transfer function is given by the first equation of (3) and neglecting the cross-coupling terms the controller matrix in dq frames becomes as the second part of (3)

$$PI(s) = K_p + \frac{K_i}{s};\ G_c^{(d,q)} = \begin{bmatrix} K_p + \frac{K_i}{s} & 0 \\ 0 & K_p + \frac{K_i}{s} \end{bmatrix} \quad (3)$$

This transfer function of the controller can also be rotated in a stationary reference frame as described in [19]. Therefore, in the case of independent control in abc reference frame, a matrix transfer function as expressed in (2) has to be used for the controller. The complexity of the matrix, due to the appearance of the cross coupling terms is a drawback when implementing PI controllers in abc reference frame. Noticeable are the main diagonal terms. These terms are representing the transfer function of the proportional-resonant (PR) controller as defined in [20].

B. Proportional-Resonant controller

It is well established that such type of controller has an improved behavior when regulating sinusoidal signals. The transfer function of this controller is given by [20]:

$$G_c(s) = K_p + K_i \frac{s}{s^2 + \omega^2} \quad (6)$$

where: K_p – proportional gain, K_i – the integral gain, and ω – the resonance frequency.

As this controller is already in stationary reference frame, implementation of individual current control is straight forward and in the situation of a star with isolated neutral transformer the relation for the currents can be written like (4), while the third current is given by:

$$i_c(t) = -i_a(t) - i_b(t) \quad (7)$$

As a consequence, the final controller matrix can be derived as (5) and one third of the sum of all three controllers has to be subtracted from the output of each controller in this case.

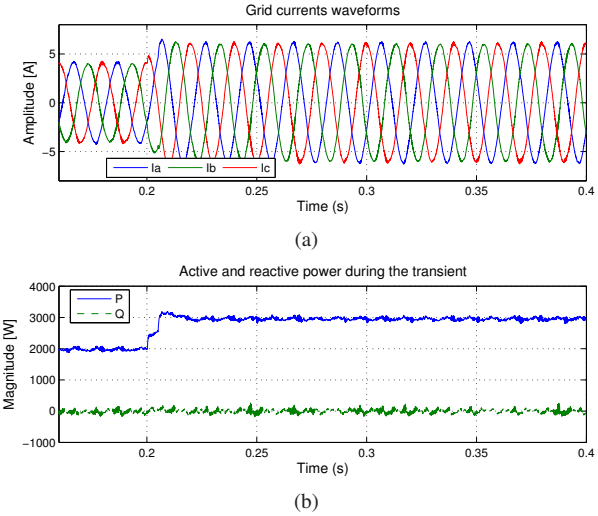

Fig. 6. Simulation results using implementation of (5) as the controller matrix in the case of step change in the reference power: (a) controlled grid currents and (b) active and reactive power transmitted to the utility grid.

VI. Simulation Results

Simulation results showing the control behavior when $dqPLL$ and three single phase PLLs are used are presented in the following. The PWM inverter was controlled with a switching frequency $f_{sw} = 10$ kHz and an LCL filter ($L_i = 10mH,\ C = 0.7\mu F,\ L_g = 2mH$) has been used between the inverter and the grid. As no difference between implementing (2) or (5) for the current controller has been observed, the results presented here are using (5) as the controller matrix. In [15] the similar behavior of the two implementations has been analytically proved.

Results for two simulation cases are presented in the followings. Firstly, the dynamic behavior of the current controller when sudden jump in the input power occurs is pursued. Secondly, the influence of the PLLs in the current reference and the controller response in the situation of a grid fault is presented.

A. Input power variations

Firstly, input power fluctuation conditions are simulated, where the input power reference registers a step change from 2 kW up to 3 kW at the simulation time 0.2 seconds. The transient and steady state results at the new operating point for the current controller implementation using (5) are presented in Fig. 6. A good transient behavior of the controller can be noticed in this situation. The current is controlled according to its new reference and the output power of the converter smoothly reaches its new operating point.

As mentioned above, implementation of (2) leads to similar results.

$$\frac{d}{dt}\begin{bmatrix} i_a(t) \\ i_b(t) \end{bmatrix} = \frac{1}{L}\begin{bmatrix} -R & 0 \\ 0 & R \end{bmatrix} \cdot \begin{bmatrix} i_a(t) \\ i_b(t) \end{bmatrix} + \begin{bmatrix} 1 & 0 \\ 0 & -1 \end{bmatrix} \cdot \begin{bmatrix} v_a(t) \\ v_b(t) \end{bmatrix} \tag{4}$$

$$G_{c1}^{(a,b,c)}(s) = \begin{bmatrix} K_p + \frac{K_i s}{s^2+\omega_0^2} & 0 & 0 \\ 0 & K_p + \frac{K_i s}{s^2+\omega_0^2} & 0 \\ 0 & 0 & K_p + \frac{K_i s}{s^2+\omega_0^2} \end{bmatrix} \tag{5}$$

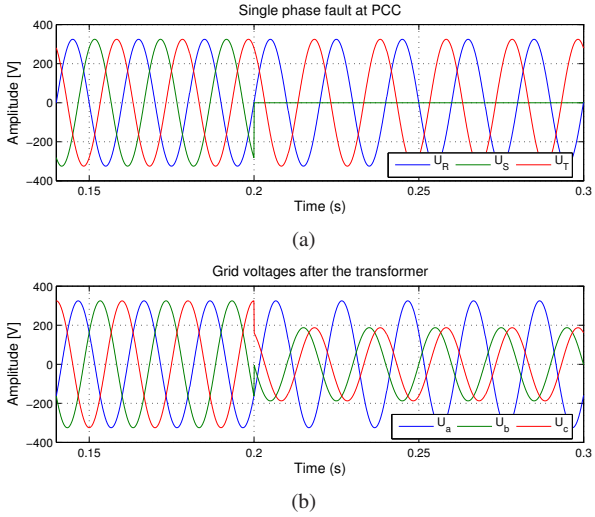

Fig. 7. Single phase voltage fault: (a) voltages at PCC and (b) voltages after the Δy isolation transformer.

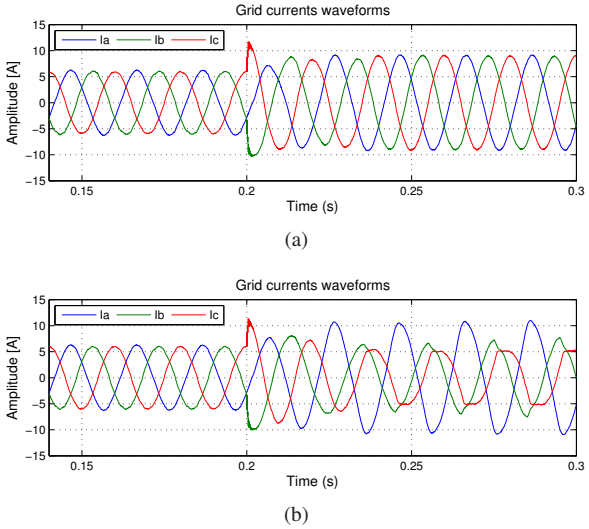

Fig. 8. Behavior of the current controller under single phase grid fault conditions: (a) using $dqPLL$ and (b) using three single phase PLLs for synchronization.

B. Grid voltage variation

In order to observe the behavior of the implementations under grid variations, a single phase fault at the point of common coupling (PCC) was simulated. The voltage waveforms before and after the transformer are shown in Fig. 7.

1) Using dq PLL: The control behavior using three $dqPLL$ is further discussed. The grid current waveforms in the situation of a grid fault are depicted in Fig. 8(a). Since the $dqPLL$ outputs the phase angle pf the positive sequence, the current references are sinusoidal and balanced, only the amplitude is increased due to the drop in the grid voltages amplitude.

2) Using three single phase PLLs: Grid currents waveforms in the situation when three single phase PLLs are used for synchronization are depicted in Fig. 8(b). As it can be observed, in this case the grid currents are not sinusoidal nor balanced. Since the current references follow the phase angles outputted by each PLL as they are depicted in Fig. 5, unbalance exists in their waveform. Due to this unbalance, a negative sequence which affects the controller is occurring. In [16] it has been proved that better current regulation is obtained if the controller accounts for both positive and negative sequence of the current is this kind of situation.

VII. Conclusion

This paper discusses the possibility of implementing an independent current control and synchronization for three phase grid converters. In the case of synchronization, two possibilities, i.e. using $dqPLL$ or three single phase PLLs are discussed. It has been found out that using $dqPLL$, the current reference will always be sinusoidal and balanced, no matter happens in the grid. Contrary, when using three single phase PLLs, an unbalance current reference is created under unsymmetrical grid faults. The negative sequence that occurs in this case influences the current controller, therefore this has to be considered in the control.

In the case of the current controller, implementation of PI and PR controllers in abc frame is investigated. A major issue in the case of the systems connected through a Δy transformer is that only two of the grid currents can be controlled individually, the third current being given by (1). Moreover, the controller matrix in the case of PI controller is much more complex due to the presence of cross coupling terms.

VIII. Acknowledgment

This research work has been carried out at the Department of Electrotechnical and Electronic Engineering, Polytechnic of Bari, Italy. A.V. Timbus wants to thank to Associate Professor Marco Liserre, for his support and contribution to this work.

References

[1] EWEA, "www.ewea.org/documents," Online Documentation, October 2005.

[2] IEA-PVPS, "Cumulative Installed PV power," www.iea-pvps.org, October 2005.

[3] F. Blaabjerg, Z. Chen, and S. Kjaer, "Power electronics as efficient interface in dispersed power generation systems," *IEEE Trans. on Power Electronics*, vol. 19, no. 5, pp. 1184–1194, 2004.
[4] T. Ackermann, *Wind Power in Power Systems*. John Wiley & Sons, Ltd., 2005, ISBN: 0-470-85508-8.
[5] M. H. J. Bollen, *Understanding Power Quality Problems: Voltage Sags and Interruptions*. IEEE Press, 2002.
[6] M. Kazmierkowski, R. Krishnan, and F. Blaabjerg, *Control in Power Electronics – Selected Problems*. Academic Press, 2002.
[7] Q. Zeng, L. Chang, and P.Song, "SVPWM-based current controller with grid harmonic compensation for three-phase grid-connected VSI," in *Proc. of PESC04*, vol. 4, 2004, pp. 3494–3500.
[8] M. Prodanovic and T. C. Green, "Control of power quality in inverter based distributed generation," in *Proc. of IECON'02*, vol. 2, 2002, pp. 1185–1189.
[9] D. Candusso, L. Valero, and A. Walter, "Modelling, control and simulation of a fuel cell based power supply system with energy management," in *Proc. of IECON'02*, vol. 2, 2002, pp. 1294–1299.
[10] M. Marei, E. El-Saadany, and M. Salama, "A novel control algorithm for the DG interface to mitigate power quality problems," *IEEE Trans. on Power Delivery*, vol. 19, no. 3, pp. 1384–1392, 2004.
[11] R. Teodorescu and F. Blaabjerg, "Flexible control of small wind turbines with grid failure detection operating in stand-alone and grid-connected mode," *IEEE Trans. on Power Electronics*, vol. 19, no. 5, pp. 1323–1332, 2004.
[12] A. V. Timbus, M. Liserre, R. Teodorescu, and F. Blaabjerg, "Synchronization methods for three phase distributed power generation systems. An overview and evaluation," in *Proc. of PESC'05*, 2005, pp. 2474–2481.
[13] P. Rodriguez, J. Pou, J. Bergas, I. Candela, R. Burgos, and D. Boroyevich, "Double synchronous reference frame PLL for power converters," in *Proc. of PESC'05*, 2005, pp. 1415–1421.
[14] M. C. Benhabib and S. Saadate, "A new robust experimentally validated Phase-Looked Loop for power electronic control," *EPE Journal*, vol. 15, no. 3, pp. 36–48, August 2005.
[15] E. Twining and D. G. Holmes, "Grid current regulation of a three-phase voltage source inverter with an LCL input filter," *IEEE Trans. on Power Electronics*, vol. 18, no. 3, pp. 888–895, 2003.
[16] G. Saccomando and J. Svensson, "Transient operation of grid-connected voltage source converter under unbalanced voltage conditions," in *Proc. of IAS'01*, vol. 4, Chicago, IL, 2001, pp. 2419–2424.
[17] S.-K. Chung, "Phase-Locked Loop for grid-connected three-phase power conversion systems," *IEE Proceedings on Electronic Power Applications*, vol. 147, no. 3, pp. 213–219, 2000.
[18] L. N. Arruda, S. M. Silva, and B. Filho, "PLL structures for utility connected systems," in *Proc. of IAS'01*, vol. 4, 2001, pp. 2655–2660.
[19] D. N. Zmood, D. G. Holmes, and G. H. Bode, "Frequency-domain analysis of three-phase linear current regulators," *IEEE Trans. on Industry Applications*, vol. 37, no. 2, pp. 601–610, 2001.
[20] R. Teodorescu and F. Blaabjerg, "Proportional-resonant controllers. A new breed of controllers suitable for grid-connected voltage-source converters," in *Proc. of OPTIM'04*, vol. 3, 2004, pp. 9–14.

Publication 4

Synchronization methods for three phase distributed power generation systems. An overview and evaluation

by A. Timbus, R. Teodorescu, F. Blaabjerg and M. Liserre
Article published in Proceedings of PESC'05, pages 2474-2481, 2005

Synchronization Methods for Three Phase Distributed Power Generation Systems. An Overview and Evaluation

Adrian V. Timbus, *Student Member, IEEE*, Marco Liserre, *Member, IEEE*, Remus Teodorescu, *Senior Member, IEEE* and Frede Blaabjerg, *Fellow, IEEE*

***Abstract*—Nowadays, it is a general trend to increase the electricity production using Distributed Power Generation Systems (DPGS) based on renewable energy resources such as wind, sun or hydrogen. If these systems are not properly controlled, their connection to the utility network can generate problems on the grid side. Therefore, considerations about power generation, safe running and grid synchronization must be done before connecting these systems to the utility network. This paper is mainly dealing with the grid synchronization issues of distributed systems. An overview of the synchronization methods as well as their major characteristics is given. New solutions to optimize the synchronization methods when running on distorted grid conditions are discussed. Simulation and experimental results are used to evaluate the behavior of the synchronization methods under different kind of grid disturbances such as voltage dips, harmonics and notches.**

***Index Terms*—Distributed Generation Systems, renewable energy, grid synchronization, Phase-Looked Look (PLL), voltage dips, notches**

I. Introduction

THE worldwide economy is mainly running on fossil fuels which is largely recognized as a major cause of environmental problems. As a consequence, an overall growth in alternative energy generation technologies and markets has been registered in the last decade. The demand for alternative and renewable energy generation systems has been growing about 25% per year. This is mainly due to a general increasing demand for electricity, a rising interest in clean technologies and the saturation of oil resources [1].

Among the renewable energy sources (RES), the wind energy knows the largest utilization nowadays. The wind potential in some countries like Denmark, Germany, Spain, US led to a large interest and fast development of wind turbines technology in the last decade. Today, a total capacity of 39294 MW wind power is installed around the world, with 8133 MW installed in 2003 only [2].

Another renewable energy technology which gains acceptance as a way of maintaining and improving living standards without harming the environment is the photovoltaic technology. The annual number of PV installations knows an increasing growth, mainly due to the government or utility companies, that support programs which focus on grid connected PV systems [3]. The advances in solar cell technology also sustain this continuous growth of PV systems. Most systems today use sliced crystalline or polycrystalline silicon wafers that can have an efficiency up to 20 % but with the pay of quite large production cost. A new trend in this field is the production of ribbon silicon which can have the same efficiency but with a lower production cost. Actually, a large interest is payed on PV systems based on organic materials. One type of organic device is the dye sensitized solar cell which uses an organic dye to absorb the solar radiation and generate electronic carriers [1].

Fuel-cell technology is also under many companies and governmental interest as an alternative energy source and this is mainly due to its potential of high efficiency (around 70%) which is higher related to the wind energy transformation (around 45%) and photovoltaic (around 20% using the new technologies of polycrystalline silicon wafers) [1].

Due to the increased number of distributed power systems connected to utility network, instability of the these system and of the grid itself can occur. As a consequence, new and more stringent standards are issued in respect to power distribution.

One of the most important issue of the DPGS connected to the utility network is the synchronization with the grid voltage vector. The synchronization algorithm mainly outputs the phase of the grid voltage vector. The phase angle of the utility voltage is a critical piece of information for grid connected systems. This information can be used to synchronize the turning on/off of the power devices, calculate and control the flow of active/reactive power or transform the feedback variables to a reference frame suitable for control purposes [4].

The content of this paper describes the structures and main characteristics of grid synchronization algorithms used for distributed generation systems. An evaluation in terms of precision of estimating the grid voltage angle as well as influence of the grid disturbances on this precision will be given. Capability of the algorithms to keep synchronization over short grid faults will be discussed as well. It has to be mentioned here that only three phase systems are under investigation.

II. Grid synchronization methods for three phase DPGS

Among the literature papers for grid synchronization of distributed generation systems, a few methods are noticed.

A.V. Timbus, R. Teodorescu and F. Blaabjerg are with the Institute of Energy Technology, Aalborg University, DK-9220 Aalborg, Denmark. Email: avt@iet.aau.dk, ret@iet.aau.dk, fbl@iet.aau.dk

M. Liserre is with the Dept. of Electrotechnical and Electronic Engineering, Polytechnic of Bari, 70125-Bari, Italy. Email: liserre@ieee.org

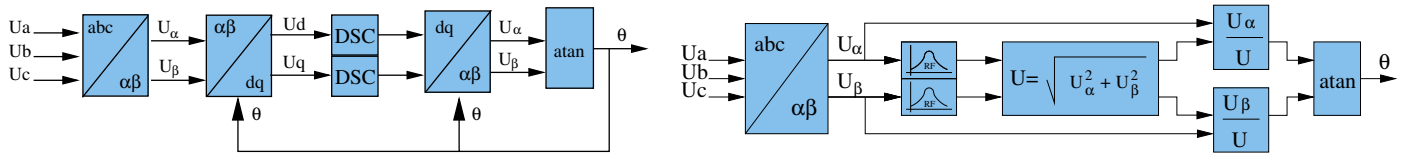

Fig. 1. Synchronization method using (a) filtering on the dq synchronous rotating reference frame and (b) filtering on $\alpha\beta$ stationary frame.

In the following, an overview of their structure and main characteristics are given.

A. Zero crossing method

One of the simplest methods for obtaining the phase information is to detect the zero crossing of the utility voltages [5]. However, the zero crossing points can only be detected at every half cycle of the utility voltage frequency; thus the dynamic performance of this technique is quite low. Hence, its discussion has been considered less relevant for this overview.

B. $\alpha\beta$ Filter algorithm

The phase angle of the utility grid voltage can also simply be obtained by filtering the input signals, i.e. the three phase voltages (U_a, U_b, U_c). Depending on the reference frame where the filtering is applied, two structures can be obtain:

- filtering in $\alpha\beta$ stationary reference frame
- filtering in dq synchronous rotating reference frame

Fig. 1(b) depicts one way to obtain the phase angle of the utility network in stationary reference frame. After the three phase voltages are transformed in $\alpha\beta$ reference frame using a proper matrix transform, filtering is applied for both components of the grid voltage. In [6], different filter types such as low pass filter, notch filter, space vector filter, etc. are investigated and their effectiveness when implemented in a stationary reference frame is discussed. It is well known that using filtering, delays will be introduced in the signal which is unacceptable in the case of grid voltage angle; therefore a proper filter design has to be made. An other alternative, as suggested in [7], is to compensate for the filter delay. A PI controller, monitoring the q component of the voltage can be used to correct the displacement introduced by the filter. One more method can be the use of band-pass filters as explained in [8] and [9]. In order to obtain satisfactory results under the unbalanced grid conditions, the authors implemented a "wave shaping and normalization module" which keeps the α and β components of the voltage sinusoidal and in quadrature.

In this paper, a resonant filter is proposed to be used to filter the $\alpha\beta$ voltages. The resonant filter has a similar characteristic as a band-pass filter but is not introducing delay.

C. $dqFilter$ algorithm

Another synchronization algorithm, this time implemented in the dq reference frame is shown in Fig. 1(a). Since the U_d and U_q voltage components are dc variables, more filtering techniques can be applied to obtain clear signals, i.e. notch filter, low-pass filter, band-stop filter, etc. [10].

In this work, the delay signal cancellation method described in [10] and [11] is used. When applied to $\alpha\beta$ reference frame, the method is described by:

$$e^{\alpha\beta}_{pos}(t) = 0.5 \cdot \left(e^{\alpha\beta}(t) + je^{\alpha\beta}(t - T/4) \right) \quad (1)$$

$$e^{\alpha\beta}_{neg}(t) = 0.5 \cdot \left(e^{\alpha\beta}(t) - je^{\alpha\beta}(t - T/4) \right) \quad (2)$$

where T is the period of the fundamental frequency. The method implies a delay with $T/4$ of the signals which makes the method vulnerable if the fundamental frequency experience variations due to different grid faults. Experimental results will validate this later.

D. $dqPLL$

The third method for synchronization is the phase locked loop (PLL) technique. The PLL can be defined as a device which causes one signal to track another. It keeps an output signal synchronizing with a reference input signal in frequency as well as in phase [12].

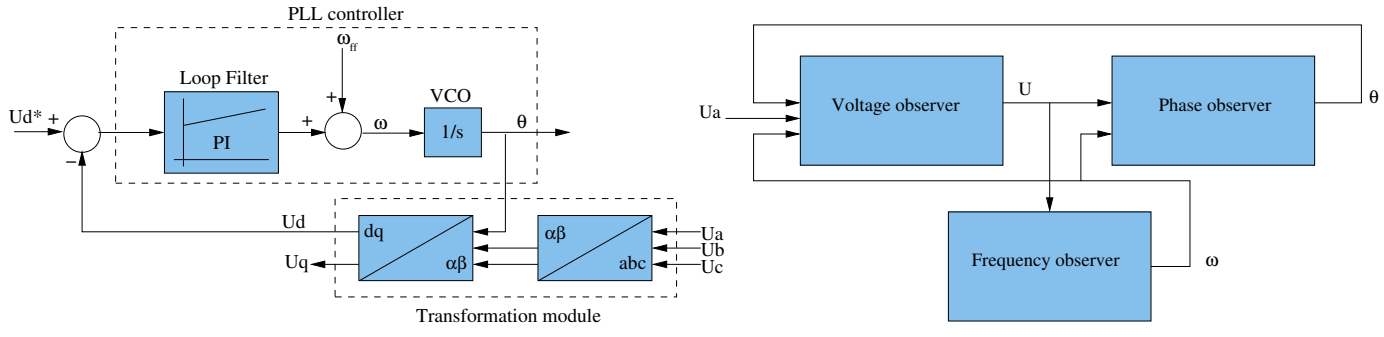

Fig. 2. (a) General structure of dq PLL method and (b) adaptive PLL comprising a voltage observer, a frequency observer and a phase angle observer.

A common structure for grid synchronization used nowadays [4], [13]–[16] is the phase locked loop implemented in dq synchronous reference frame and its schematic is illustrated in Fig. 2(a).

As it can be noticed, this structure uses the coordinate transformation form $abc \rightarrow dq$ and the lock is realized by setting the V_d^* to zero. A regulator, usually PI, can be used to control this variable and the output of this regulator is the grid frequency. After the integration of the grid frequency, the utility voltage angle is obtained, which is fed back into the $\alpha\beta \rightarrow dq$ transformation module in order to transform into the synchronous rotating reference frame.

This structure of PLL consists of two major parts, the phase detection and the loop filter. The phase detection can be readily implemented by using $abc \rightarrow dq$ transform in the three phase system. On the other hand, the loop filter determines the dynamics of the system. Therefore, the bandwidth of the filter is a trade off between the filtering performance and the time response. As a consequence, parameters of the loop filter have a significant influence on the lock quality and the PLL dynamics.

E. Adaptive PLL

A more advanced PLL structure, based on adaptive algorithm is presented in [17] and it is shown in Fig. 2(b). The author suggests that three PLL systems (one for each phase) will have better performance than one common system for all phases. The adaptive PLL consists of three control units that individually control the frequency, phase angle and voltage magnitude. The disadvantage of this structure can be the large algorithm necessary to implement (3x3 controllers) and the fact that controllers involve a moving average algorithm that is computationally heavy but very precise. Anyway, one of the advantages is that it provides the information about each phase amplitude, frequency and phase. This issue makes this method suitable for grid monitoring, and thus islanding detection and safety improvement.

III. Design of the $dqPLL$ system

The PLL system, when used for grid connected applications, can be influenced by the distortions taking place in the utility network [4], [10], [16], [18]. As noticed, the synchronization algorithm dynamic is closely related to the bandwidth of its filter. As a consequence, a low dynamic filter will produce a very filtered and stable output but with a longer synchronization time. On the other hand, a design for fast dynamics will produce an output which is able quick to synchronize to the input but distortions in the input signal will pass through the filter and become part of the output signal. Therefore, when designing a synchronization system, one should be aware of the purpose of this system. If the algorithm is only used for synchronizing the control variables to the utility voltage vector in order to have a precise synchronization necessary for control, then a slow dynamic algorithm can be used. If the synchronization algorithm is employed in grid monitoring (to detect grid faults), a fast dynamic system needs to be used.

In the following, a tuning method for the $dqPLL$ controller is given. The method gives access to the settling time T_s and damping ratio ζ of the system. Thus, one can design a low dynamics or fast dynamics system by accordingly selecting these two parameters. The tuning method is derived from the transfer function of dqPLL shown in Fig. 2(a).

The time domain transfer function of the $dqPLL$ system depicted in Fig. 2(a) can be derived as:

$$H(s) = \frac{K_p \cdot s + \frac{K_p}{T_i}}{s^2 + K_p \cdot s + \frac{K_p}{T_i}} \tag{3}$$

This expression is similar to the standard second order transfer function having a zero:

$$G(s) = \frac{2\zeta\omega_n \cdot s + \omega_n^2}{s^2 + 2\zeta\omega_n \cdot s + \omega_n^2} \tag{4}$$

therefore the controller gains can be derived from (3) and (4) as follows:

$$K_p = \frac{9.2}{T_s}, \qquad T_i = \frac{T_s\zeta^2}{2.3}, \qquad where \;\; \omega_n = \frac{4.6}{\zeta T_s} \tag{5}$$

Considering a damping factor $\zeta = 0.707$, which should give an overshoot of 5% in the case of step response [19], and selecting a desired settling time of $T_s = 0.02$, the step response and Bode diagram of (3) is shown in Fig. 3.

As it can be noticed from the Fig. 3(a), the overshoot is increased to 20% and this is due to the zero exhibited by the transfer function in (3), which is neglected when doing the design. In order to eliminate this effect, a compensator (lag term) can be introduced in the loop [20]. The step response

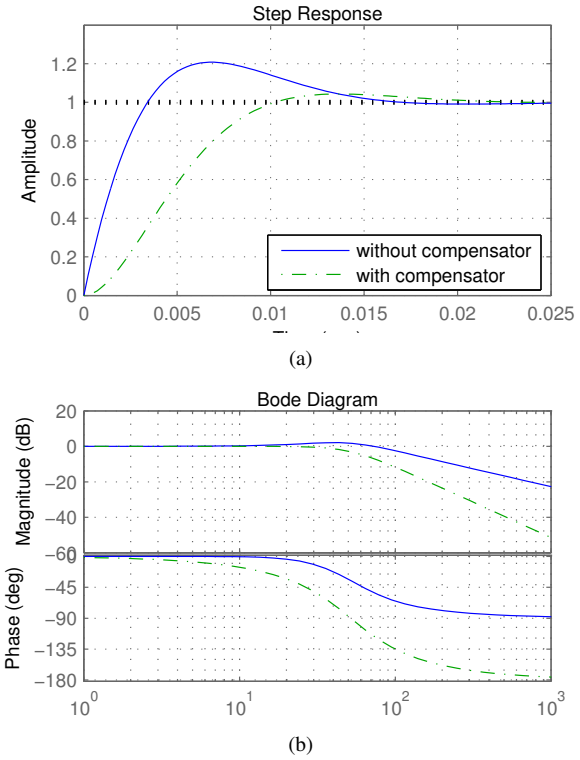

Fig. 3. (a) Step response and (b) Bode plot of the dqPLL system with and without a lag compensator.

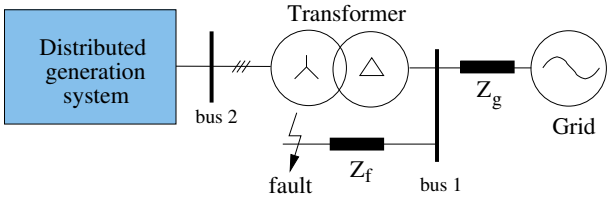

Fig. 4. Distributed system connected to the utility network using a Δ/Y transformer.

of the system having the compensator term included is shown with dotted line in Fig. 3(a). As it can be observed, the effect of the compensator diminishes the overshoot to 5%, maintaining the imposed settling time of the system. From the Bode plot shown in Fig. 3(b), for the case with and without compensator, it can be concluded that both systems have considerably phase margin in order to ensure system stability.

IV. Grid faults

No matter how stiff the transmission and distribution system is, grid faults can occur due to different reasons. As the synchronization algorithms used by the distributed systems have the grid voltages as input, it is expected that the grid faults will have a significant influence on the behavior of the synchronization algorithms.

Considering the distributed system connected to the utility network as shown in Fig. 4, the grid behavior due to the short circuit faults should be discussed.

Assuming a grid fault taking place at the bus 1, the voltage here will be directly proportional to the grid (Z_g) and the fault impedance (Z_f). Moreover, if the X/R ratio of the two impedances differs, the voltage will also experience a phase jump [21]. It has been analyzed in [22] that usually six types of faults can occur due to the short circuit fault. These faults are graphically expressed in Fig. 5.

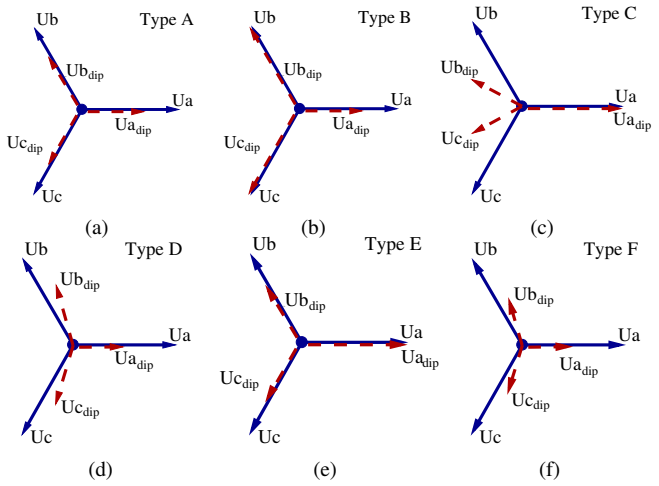

Fig. 5. Classification of voltage dips due to short circuit. Solid lines represent the voltage before the dip and dotted lines represent the voltage after the dip.

If the distributed system is connected to the utility network through the standard distribution transformer Δ/Y, the voltage dips at bus 2 are as listed in Table I.

TABLE I
Propagation of voltage dips through Δ/Y transformer.

Fault type	Dips seen at bus 1	Dips seen at bus 2
3 phase fault	type A	type A
1 phase fault	type B	type C
2 phase to ground	type E	type F
phase-to-phase	type C	type D

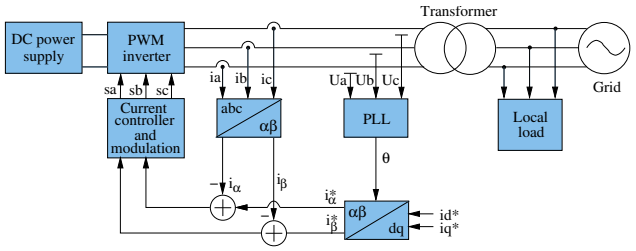

Fig. 6. Schematic of the experimental system used for testing.

In Fig. 5 it can be noticed that only three of the grid faults are symmetrically (120^0 shifted), the other three, i.e. C, D, F experiencing both amplitude and phase variations. Moreover, from Table I it can be observed that only one fault out of four is symmetrical at bus 2.

Due to the use of $abc \rightarrow \alpha\beta$ transformation module in the synchronization algorithms, which is only valid for symmetrical systems, it will be interesting to observe the behavior of these algorithms under different kind of unsymmetrical faults.

V. Experimental system

In order to test the PLL structures and observe their behavior under different grid conditions, an experimental system was built in laboratory, as shown in Fig. 6.

The system comprises the PWM inverter supplied by a DC power source which ensures the DC-link voltage necessary for the application. The connection to the grid is made through an isolation transformer. The three phase voltages are sampled and used by the synchronization algorithm which provides the grid voltage vector angle. Using this angle, the reference currents in the stationary reference frame are constructed using a $dq \rightarrow \alpha\beta$ transformation module. In this way, the control of active and reactive current reference is ensured. The sampled phase currents are transformed into $\alpha\beta$ reference frame as well and subtracted from their reference. The resonant current controller implemented in stationary reference frame controls the input error to zero and sets the PWM pattern for the inverter.

VI. Evaluation of the synchronization algorithms

In the following, an evaluation of the synchronization algorithms described above is made. The following tests, since they are most common to occur in the utility network, were chosen to be done:

- 6% total harmonic distortion (THD) of the grid voltages
- 30% notches
- 30% voltage dip type A
- 40% voltage dip type C

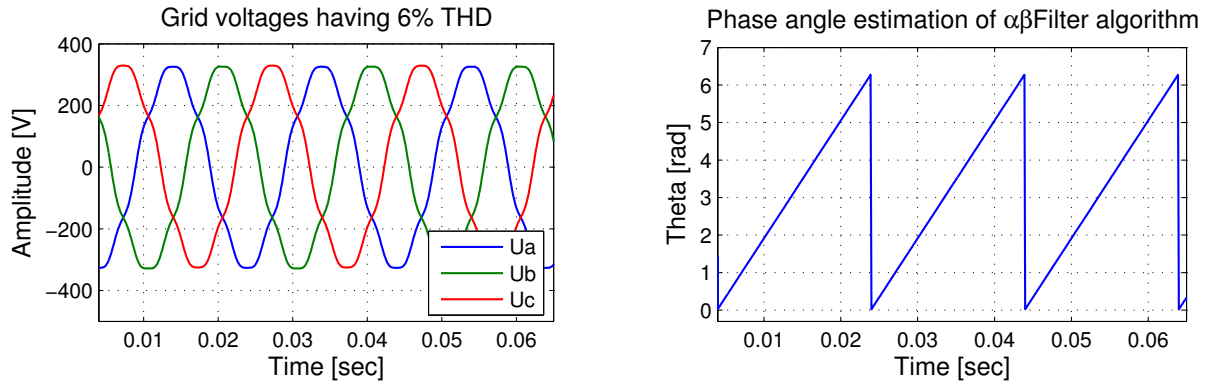

(a) (b)

Fig. 7. The behavior of $\alpha\beta Filter$ algorithm under 6% THD of the utility grid: (a) the voltage waveforms and (b) estimation of the phase angle.

In order to achieve all the disturbances in the grid voltages, a grid power simulator, e.g. California Instruments has been used in laboratory setup. The grid simulator can be controlled from the computer and voltage dips, sags, harmonics or frequency shift can be programed to appear in the outputted waveforms. Anyway, in case of voltage dip type C, simulations results are provided since the grid simulator is not able to create phase shift of the output voltages.

Since the adaptive PLL is implemented for each phase, some of the above listed test, will not have a big influence on its behavior. Moreover, this algorithm is able to estimate the voltage amplitude, its frequency and its phase. As a consequence, the adaptive PLL will be investigated separately.

A. Harmonics test

As mentioned above, 6% THD of the voltage has been set for the harmonic test. As a consequence, the voltage input into the synchronization algorithms look as shown in Fig. 7(a). Since all algorithms make use of a filter in one way or another, it is expected that the harmonics content shown in Fig. 7(a) to be filtered out. In Fig. 8(c), the output of the $\alpha\beta Filter$ algorithm is shown. As expected, the resonant filter only pass through the 50 Hz component of the grid voltages, a clean synchronization signal being provided. The other two algorithms, i.e. $dqFilter$ and $dqPLL$ behave similarly. It has to be mentioned here that for the $dqPLL$ system, a settling time of $T_{set} = 0.2$ seconds has to be set inside the PI controller in order to be able to filter out the harmonics. A drawback in this case will be the low dynamics of the system.

B. Notches test

It is not likely that the utility network is always polluted by notches, but when a distributed system is connected in the immediate vicinity of an industrial park, where lots of high power switching devices (mostly thyristors) are running, notches can appear into the grid voltages. Thus, it is worth to investigate the behavior of synchronization algorithms under such conditions.

The grid simulator has been programmed to output the grid voltages as shown in Fig. 8(a). Since notches have even higher frequencies than the harmonics inserted in the previous test, a proper behavior of the synchronization algorithms is expected. As it can be observed in Fig. 8(b), the $\alpha\beta Filter$ algorithm provides a clean synchronization signal. Similar behavior has been registered in the case of $dqPLL$ having again a settling time of 0.2 seconds. In Fig. 8(c), the output of $dqFilter$ is shown. Small oscillations can be observed in the synchronization signal. This is caused by the settings of notches to occur close to zero crossing, modifying the fundamental period. The Delay Signal Cancellation (DSC), which uses a fixed delay of $T/4$, is not able to reject the oscillation due to the disagreement of the fundamental period of the two signals it compares. As an alternative to the DSC used for filtering purposes here, other types of filters can be used as suggested in [6].

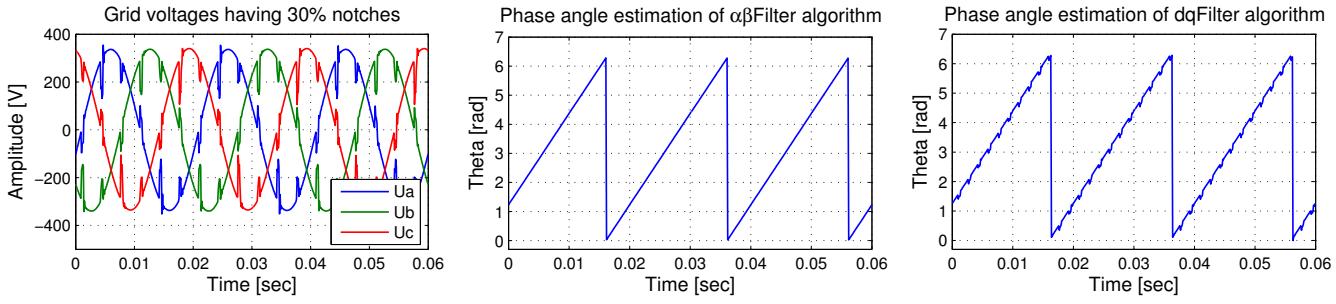

(a) (b) (c)

Fig. 8. The behavior of $dqFilter$ and $\alpha\beta Filter$ filtering algorithm with 30% notches distortion of the utility grid.

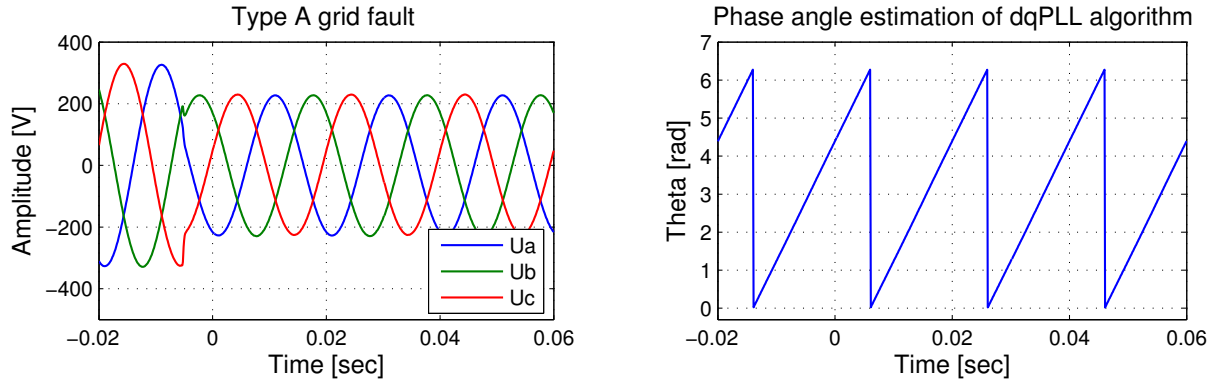

(a) (b)

Fig. 9. The behavior of $dqPLL$ under 30% type A voltage dip: (a) grid voltages and (b) phase angle estimation.

C. Voltage dip type A

As described in §IV, the type A voltage dip manifests a suddenly drop in voltage magnitude in all three phases at the same time. No phase or frequency variations take place during this type of dip. In Fig. 9(a), the grid voltages register a 30% amplitude drop. Since the resulting voltages are still balanced (120^o shifted), no negative sequence is appearing in the line voltages. This makes the synchronization algorithms to behave normally, all of them producing a clean output signal (e.g. $dqPLL$ output shown in Fig. 9(b)).

D. Voltage dip type C

This type of fault is maybe the most demanding one for the synchronization algorithms. Beside the amplitude drop in two of the grid phases, these will also suffer a phase shift. To simulate this situation, the amplitude of b and c phases are diminished 40% of their nominal value and a phase shift of 30 degrees is registered for both these phases. The resulting grid voltages are shown in Fig. 10(a) and the output of the $dqPLL$ system in Fig. 10(b). As it can be observed, the low dynamics of the PI controller is able to filter out the negative sequence of the d axis voltage, keeping the system synchronized with the positive sequence of the voltages. The power factor of the system will not be unity anymore under the fault but the great advantage is that if the grid recovers, the $dqPLL$ is able to resynchronize the system with the positive sequence of the grid voltages. This issue provides the distributed system with the so called *ride through* capability. Similar behavior has been noticed for the $dqFilter$ algorithm.

In Fig. 10(c), the synchronization signal of the $\alpha\beta Filter$ algorithm is shown. As it can be noticed, this fails to provide a clean signal. The 100 Hz frequency of the negative sequence is filtered out by the resonant filter but differences in amplitudes of α and β voltages are occurring. This difference will produce variations in the synchronization signal. This issue can be avoided by iterating the algorithm few times, as it is explained in [8] and [9].

E. Testing the adaptive PLL

Due to the different structure and behavior of the adaptive PLL, this is treated separately. The first major difference between this algorithm and all the previous ones presented is that the adaptive PLL is implemented for one phase. Therefore, in a three phase system, three such algorithms have to be implemented in order to synchronize the injected currents with their corresponding grid voltages. Of course, there is possibility to implement only one algorithm and then shift the obtained phase angle with 120 and 240 degrees respectively, in order to obtain the phase angle for the other two voltages. Anyway, when the grid become slightly unbalanced, the unity power factor of the distributed system will be lost, thus this solution in not recommended. Fig. 11 depicts a possible way of using the adaptive PLL in a three phase control structure of the DPGS.

As it is mentioned above, the adaptive PLL is able to track the amplitude of the grid voltage, its frequency and its phase. In the tests below, simulation results for only one phase are presented.

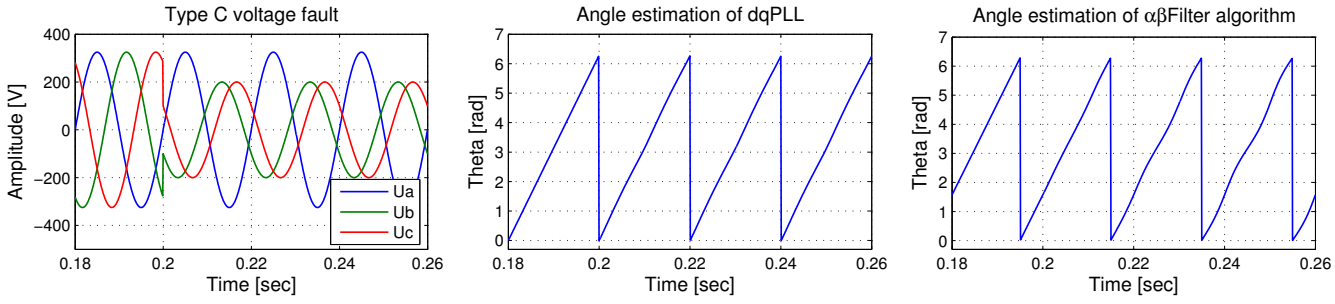

(a) (b) (c)

Fig. 10. Dip fault type C: (a) the grid voltages, (b) the output of $dqPLL$ and (c) output of $\alpha\beta Filter$ algorithm.

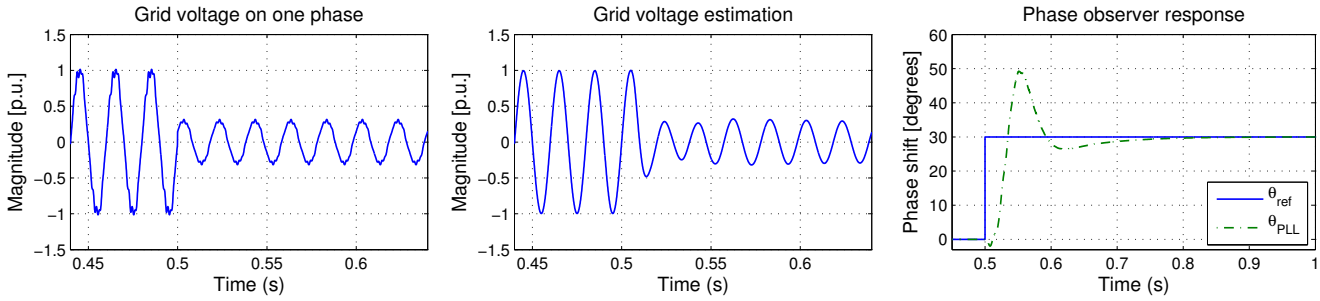

(a) (b) (c)

Fig. 12. Adaptive PLL behavior under the fault: (a) 8% THD of grid voltages, (b) voltage estimation, and (c) phase angle detection.

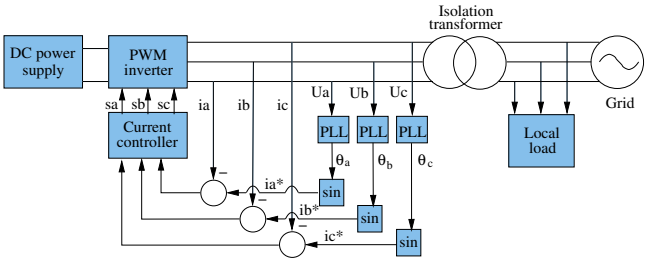

Fig. 11. Possible use of the adaptive PLL in a three phase control structure.

Since the adaptive PLL is implemented for each phase the effect of unbalance should be minimal in this case. As a consequence, in order to test this structure, the following fault was created (Fig. 12(a)):

- 8% THD in the grid voltages was set
- 70% voltage drop at time instant 0.5 s
- 30^o phase shift at the same time instant

As can be noticed in Fig. 12(b), the voltage observer needs one and a half fundamental periods to correctly detect the voltage dip taking place in the utility network. This is fast enough according to the grid codes for wind turbines as described in [23]. In Fig. 12(c), the phase observer response to the fault conditions is shown. Its output is able to follow the new phase angle of the grid voltage within 0.35 seconds. The overshoot occurring during the fault is due to the interaction of all three controllers of this structure, i.e. voltage controller, frequency controller and phase controller. If these controllers are designed slower, the overshoot will be reduced but also a slower dynamic will be achieved. This will influence on the detection time of the grid variables, exceeding maybe the standard demands in the field.

In Table II, a comparison in respect to the robustness and simplicity of the presented synchronization algorithms is done. It can be concluded that some of the simple algorithms can experience problems when running on different kind of distorted grid. Having a proper tuning, the more complex structures manage to keep synchronization even when the grid is severely distorted.

VII. Conclusion

This paper gives an overview of the synchronization algorithms and their structure for grid connected distributed systems. The ability of the synchronization algorithms to overcome the grid fault and provide a clean synchronization signal is closely related to its filter design. Filtering methods already existing in the literature as well as new filter procedures such as resonant filters have been introduced and described.

A controller design in the case of $dqPLL$ have been made in a way that gives access to the dynamics of the system. The algorithms have been tested under different grid conditions and the results are commented.

As a result of the experimental tests, the $dqFilter$ algorithm using delay signal cancellation has problems when the grid frequency varies, as was the case in the notches test. Anyway, using another filter may improve the situation.

In order to properly work under unbalanced grid conditions, the $\alpha\beta Filter$ necessitates few iterations of the normalizing and wave shaping stage.

The low dynamic designed $dqPLL$ and adaptive PLL prove to overcome all the test conditions. This make them suitable for grid connected applications, such as wind turbines, PV or fuel cell systems.

TABLE II
Comparison of the Presented Synchronization Algorithms.

Algorithm	Strong points	Weak points
$dqFilter$ (with DSC)	simplicity	on frequency shift variations
$\alpha\beta Filter$	simplicity	on unbalanced grid
$dqPLL$	works on every grid type, provides ride through capability	slow dynamics
$adaptivePLL$	estimates amplitude, frequency and phase angle	complex structure

References

[1] J. P. Lyons and V. Vlatkovic, "Power electronics and alternative energy generation," in *Proc. of PESC'04*, 2004, pp. 16–19.
[2] EWEA, "www.ewea.org/documents," Online Documentation, October 2005.
[3] M. Shahidehpour and F. Schwartz, "Don't let the sun go down on PV," in *IEEE Power & Energy Magazine*, vol. 2, no. 3, 2004, pp. 40–48.
[4] V. Kaura and V. Blasko, "Operation of a phase loop system under distorted utility conditions," *IEEE Trans. on Industry Applications*, vol. 33, no. 1, pp. 58–63, 1997.
[5] F. M. Gardner, *Phase Lock Techniques*. New York: Wiley, 1979.

[6] J. Svensson, "Synchronisation methods for grid-connected voltage source converters," in *IEE Proc. Generation, Transmission and Distribution*, vol. 148, no. 3, 2001, pp. 229–235.

[7] C. Klumpner, M. Liserre, and F. Blaabjerg, "Improved control of an active-front-end adjustable speed drive with a small DC-link capacitor under real grid conditions," in *Proc. of PESC'04*, vol. 2, no. 1156-1162, 2004.

[8] H. Kim, S.-J. Lee, and S.-K. Sul, "Reference wave generator in dynamic voltage restorers by use of PQR power theory," *Proc. of APEC'04*, vol. 3, pp. 1452–1457, 2004.

[9] S.-J. Lee, H. Kim, S.-K. Sul, and F. Blaabjerg, "A novel control algorithm for static series compensators by use of PQR instantaneous power theory," *IEEE Trans. on Power Electronics*, vol. 19, no. 3, pp. 814–827, 2004.

[10] G. Saccomando and J. Svensson, "Transient operation of grid-connected voltage source converter under unbalanced voltage conditions," in *Proc. of IAS'01*, vol. 4, Chicago, IL, 2001, pp. 2419–2424.

[11] H. Awad, J. Svensson, and M. Bollen, "Tuning software Phase-Locked Loop for series-connected converters," *IEEE Trans. on Power Delivery*, vol. 20, no. 1, pp. 300–308, 2005.

[12] G. C. Hsieh and J. C. Hung, "Phase-Locked Loop Techniques - A Survey," *IEEE Trans. on Industrial Electronics*, vol. 43, no. 6, pp. 609–615, 1996.

[13] S.-K. Chung, "A phase tracking system for three phase utility interface inverters," *IEEE Trans. on Power Electronics*, vol. 15, no. 3, pp. 431–438, 2000.

[14] ——, "Phase-Locked Loop for grid-connected three-phase power conversion systems," *IEE Proceedings on Electronic Power Applications*, vol. 147, no. 3, pp. 213–219, 2000.

[15] L. N. Arruda, S. M. Silva, and B. Filho, "PLL structures for utility connected systems," in *Proc. of IAS'01*, vol. 4, 2001, pp. 2655–2660.

[16] S. Lee, J. Kang, and S. Sul, "A new phase detection method for power conversion systems considering distorted conditions in power system," in *Proc. of IAS'99*, vol. 4, 1999, pp. 2167–2172.

[17] D. Jovcic, "Phase Locked Loop system for FACTS," *IEEE Trans. on Power Systems*, vol. 18, no. 3, pp. 1116–1124, 2003.

[18] H.-S. Song, H.-G. Park, and K. Nam, "An instantaneous phase angle detection algorithm under unbalanced line voltage condition," in *Proc. of PESC'99*, vol. 1, 27 June-1 July 1999, pp. 533–537vol.1.

[19] G. F. Franklin, J. D. Powell, and A. Emami-Naeini, *Feedback Control of Dynamic Systems – Third Edition*. Addison Wesley, 1995.

[20] W. Leonhard, *Control of Electric Drives*. Springer, 1996.

[21] G. Saccomando, J. Svensson, and A. Sannino, "Improving voltage disturbance rejection for variable-speed wind turbines," *IEEE Trans. on Energy Conversion*, vol. 17, no. 3, pp. 422–428, 2002.

[22] M. H. J. Bollen, *Understanding Power Quality Problems: Voltage Sags and Interruptions*. IEEE Press, 2002.

[23] J. Matevosyan, T. Ackermann, S. Bolik, and L. Söder, "Comparison of international regulations for connection of wind turbines to the network," in *Proc. of NPWC'04*, Goteborg, Sweden, 2004, (CDROM).

Publication 5

PLL algorithm for power generation systems robust to grid voltage faults

by A. Timbus, M. Liserre, R. Teodorescu, P. Rodriguez and F. Blaabjerg
Article published in Proceedings of PESC'06, pages 1-7, 2006

PLL Algorithm for Power Generation Systems Robust to Grid Voltage Faults

Adrian V. Timbus, *Student Member, IEEE*, Marco Liserre, *Member, IEEE*, Remus Teodorescu, *Senior Member, IEEE*, Pedro Rodriguez, *Member, IEEE* and Frede Blaabjerg, *Fellow, IEEE*

***Abstract*—In the case of unbalanced grid faults, one of the main problems for the Distributed Power Generation Systems (DPGSs) controller is the second harmonic ripple in the control, consequence of the phase unbalance caused by the fault. The second harmonic propagates into different sections of the controller and can have a negative influence on the controller even leading to trip out of the system.**

This paper proposes a novel Phase-Looked Loop (PLL) algorithm which is able to filter out the negative sequence and to provide a clean synchronization signal. Along with the conventional PI controller in the PLL structure, the proposed algorithm employs a repetitive controller to deal with the second harmonic. The purpose of the repetitive controller is to amplify the second harmonic in the reference of the PI controller, so that this can be better rejected. Simulation and experimental results are used to validate the robustness of the proposed system when running on grid faults.

***Index Terms*—Distributed generation, positive and negative sequence, robust PLL, fault ride-through**

I. Introduction

DUE to the lack of harmful emissions and inexhaustible resources Distributed Power Generation Systems (DPGS) based on renewable energies are more and more seen as an alternative to the traditional power sources. However, due to the uncertainty of the input power, the controllability of these systems is their main drawback [1]. The new issued grid codes in some of the European countries put more and more stress on the capability of the DPGS in general and Wind Turbine Systems (WTSs) in particular to be able to run over short grid disturbances. This, so called *fault ride-through* feature of the wind turbines, should be capable to maintain the system running when short voltage or frequency variations occur in the utility network.

An overview of the voltage and frequency ranges as well as reactive power exchange with the utility network for different European countries is given in [2]. Taking the example of Denmark, which is the country with the largest penetration of wind power in the power system, the grid code is provided by the Transmission System Operator (TSO) in [3]. In this case, the grid voltage variations which a wind turbine should handle are illustrated in Fig. 1. As it can be noticed, the wind turbine should run for about 0.1 seconds when the grid voltage is 25% of its nominal value. Considering that only one or two of the grid voltages experience such a drop in magnitude, the power system will become unbalanced [4].

The negative sequence and unbalance has been the subject of many research studies until now [5]–[8]. In the case of DPGS, one way to deal with the negative sequence is to use the Phase-Locked Loop (PLL) algorithm to filter it out, so that the phase angle used in generating the grid current reference is a clean signal, synchronized with the positive sequence of the voltages. Regarding this, in [5], it is suggested that having a slow dynamic design of the PLL controller, the negative sequence of the grid voltages can be filtered out. Anyway, noticeable is that a constant oscillation of few degrees appears in the estimated phase angle of the PLL system, in this case. In [6], a multi-variable filter is used on $\alpha\beta$ voltages in order to eliminate the unbalance effects. A more advanced structure, involving a conventional PLL structure and a decoupling network used to eliminate the negative sequence appearing under unbalance grid conditions is presented in [7]. A positive sequence extractor used in combination with three single phase PLLs is proposed in [8] for elimination of unbalance effect in three phase systems.

Additionally to the variation of the voltage amplitude, the utility network can register frequency oscillations or phase jumps as well. The new grid codes for wind turbines are demanding a functionality of the turbine for a frequency deviation of ± 3 Hz [2]. Thus, it is important for DPGS to have a synchronization algorithm which is able to run on

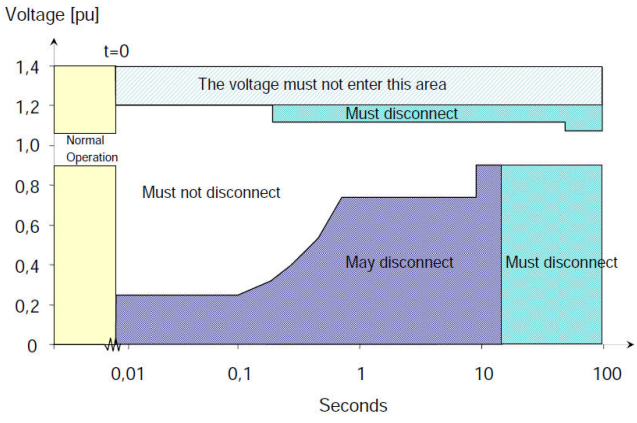

Fig. 1. Illustration of the grid voltage variations and the disconnection boundaries for wind turbines connected to the Danish power system (Source: Energinet.dk).

A.V. Timbus, R. Teodorescu and F. Blaabjerg are with the Institute of Energy Technology, Aalborg University, DK-9220 Aalborg, Denmark. Email: avt@iet.aau.dk, ret@iet.aau.dk, fbl@iet.aau.dk

P. Rodriguez is with the QUPER, Dept. of Electrotechnical and Electronic Engineering, Technical University of Catalonia, Spain. Email: prodriguez@ee.upc.edu

M. Liserre is with the Dept. of Electrotechnical and Electronic Engineering, Polytechnic of Bari, 70125-Bari, Italy. Email: liserre@ieee.org

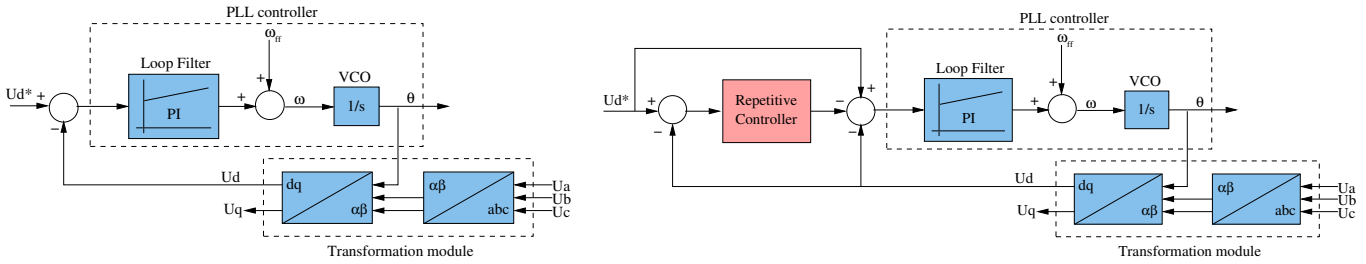

Fig. 2. PLL structure: (a) conventional PLL system implemented in dq reference frame and (b) proposed PLL using a repetitive controller to eliminate the unbalance effect.

such frequency band. Phase jump of the all three phases or just one phase of the utility network can occur due to different transients (e.g. large single of three phase loads connection/disconnection). Characteristic to single or two phases phase angle jump is the appearance of unbalance, hence there is a necessity for an advanced synchronization algorithm.

This paper proposes a novel PLL structure which employs a repetitive controller to cope with the negative sequence present in the PLL system under unbalanced grid conditions. The controller is placed on the reference of the d-axis voltage, with the purpose of modifying the reference V_d in order to improve the rejection capability of the PI controller inside the PLL structure.

In this paper, the conventional synchronous reference frame PLL is firstly introduced and its drawback when running on unbalanced grid is highlighted. Secondly, the novel proposed system using a repetitive controller to cope to the unbalance effect is introduced. The structure and tuning method of this controller is further described. The proposed algorithm is then evaluated under the same unbalance conditions and an improved behavior is noted. Moreover, the novel PLL is also tested in the situation of grid frequency deviations and phase jump situation. Simulation and experimental results are finally presented in order to validate the theory and simulation models.

II. Conventional PLL system

The conventional PLL system implemented in synchronous reference frame is shown in Fig. 2(a). This uses a PI controller to track the phase angle of the grid voltages and the lock is realized by setting the reference of the d-axis voltage to zero. The controller parameters are the trade-off between a fast dynamic system providing quick synchronization and slow system providing filtered output [9]–[11]. Therefore, under ideal grid conditions, this PLL structure performs satisfactory. When higher order harmonics or notches are present in the grid voltages, the bandwidth of the PLL controller should be reduced in order to provide a good synchronization signal. In the case of unbalance, due to the second harmonic present in the grid voltages, the bandwidth of the PLL controller should be further reduced, yielding into a system with slow dynamics.

The unsatisfactory behavior of the conventional PLL system having fast dynamics (locking time of the controller is 0.06 seconds) is outlined in Fig. 3. In the case of a single phase fault at the point of common coupling (PCC), the voltages at the generation system terminals become unbalanced. As it can be observed in Fig. 3(c), the synchronization signal has a 100 Hz ripple and the phase error reported in Fig. 3(d) is as large as 20 degrees. The signal depicted in Fig. 3(c) cannot be used in the control because will produce a non-sinusoidal current reference. Therefore, if a sinusoidal current reference is desired in a ride through situation when the utility grid is unbalanced, improvements to the conventional three phase PLL are necessary.

III. Proposed PLL system

In order to improve the behavior of the conventional PLL system under unbalance conditions, a new PLL algorithm is proposed. This employs a closed loop *repetitive controller* to cope with the second harmonic present in the system when having unbalance. The schematic of the proposed algorithm is depicted in Fig. 2(b). The repetitive controller is cascaded with the PLL controller participating in the settings of the new reference for the PI controller.

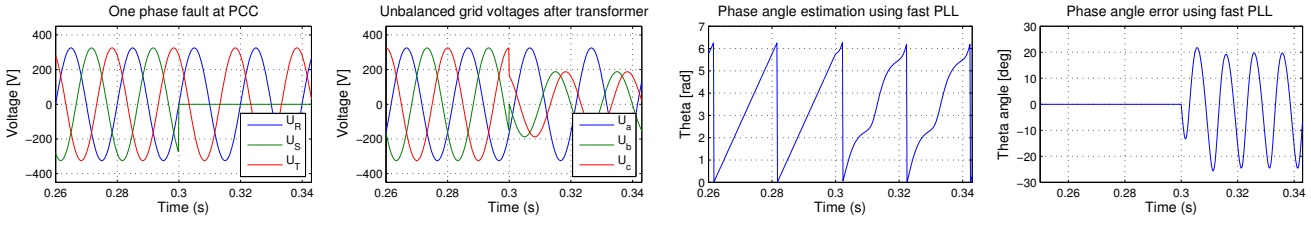

Fig. 3. Single phase grid fault: (a) voltages at PCC, (b) voltages after the Δy transformer, (c) conventional PLL output using fast dynamics and (d) the phase error between the real grid phase and estimated one by the PLL.

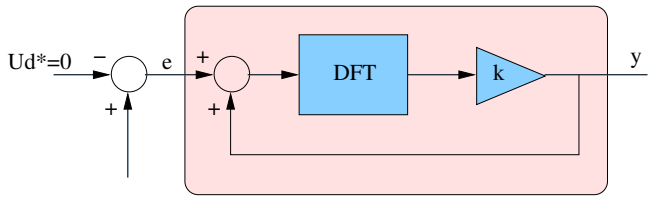

Fig. 4. Structure of the close loop repetitive controller based on FIR filter.

Repetitive controller

The main objective of the repetitive controller is to eliminate the second harmonic oscillations from the locking loop. As observed in Fig. 5(a), the repetitive controller behaves as a bandpass filter where the even harmonics have no attenuation while the odd harmonics are filtered out. In the unbalanced case, when even harmonics appear, they pass through the filter and they are added to the reference of the d-axis voltage. In this way, the proportional gain of PI controller is artificially increased at that particular frequency, thus better rejection of these harmonics can be achieved.

1) Structure: The structure of the repetitive controller is outlined in Fig. 4. Its model is based on a DFT algorithm, where compensation for different harmonics is possible [12].

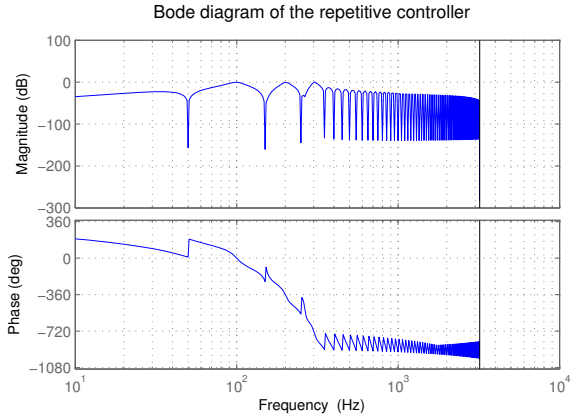

(a)

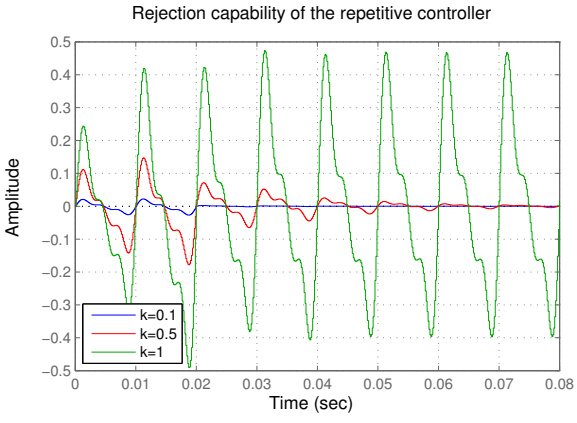

(b)

Fig. 5. Bode plot (a) and rejection capability (step in the error signal) for different gain values (b) of the repetitive controller.

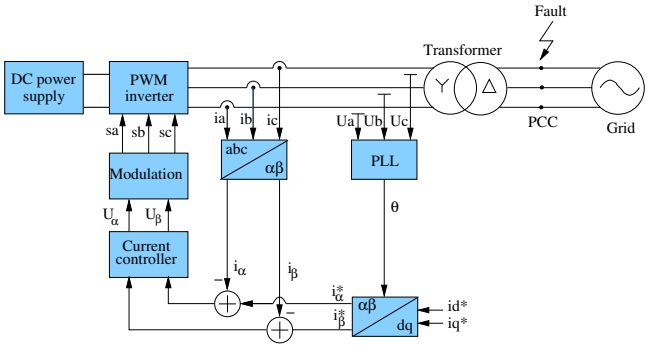

Fig. 6. The schematic of the system used to test the proposed PLL algorithm.

The discrete transfer function of the controller is given by (1):

$$F_{DFT} = \frac{2}{N}\sum_{i=0}^{N-1}\left(\sum_{k\in N_h} cos\left[\frac{2\pi}{N}h(i+N_a)\right]\right)z^{-i} \quad (1)$$

where N_h is the set of selected harmonics, and N_a is the number of the leading steps determined by the system stability. As it can be observed, (1) can be seen as a Finite-Impulse Response (FIR) filter of N taps with unity gain on all selected harmonics h.

2) Frequency response: Better results are obtained if the multiples of the second harmonic (4^{th} and 6^{th}) are also selected for compensation. The Bode plot of the repetitive controller used to compensate for the above mentioned harmonics is shown in Fig. 5(a). Noticeable is the unity gain for the harmonics selected for compensation while the other harmonics are heavily filtered. Hence, the even harmonics are amplified due to the summation feedback inside the controller and they are passing through to contribute to the new reference for the PLL controller.

3) Dynamics: Before talking about the gain of the repetitive controller, it is worth to note that the locking time of the PI controller has been set to be three fundamentals periods, e.g. 0.06 seconds. As it can be noticed in Fig. 4, the repetitive controller has also a gain, k. The value of the gain has influence on the PLL system stability, therefore considerations should be made when selecting its value. Moreover, this gain also sets the dynamics of the repetitive controller, therefore selecting its value becomes a trade of between fast harmonics compensation and system stability [12].

Since the repetitive controller is cascaded with the PI controller and contributes to its reference setting, the repetitive controller dynamic should be slower than the PI controller one. The rejection capability (step in error signal e) of the repetitive controller is shown in Fig. 5(b). As observed, a value of 1 for the gain k makes the repetitive controller unstable. Moreover, for the value of $k = 0.1$, the repetitive controller becomes faster than the PI controller of the PLL system, making the whole system unstable. As a consequence, a gain of 0.5 has been selected for the repetitive controller. With this gain, the settling time of the repetitive controller is 0.08 seconds, being slower than the PI controller and ensuring system stability.

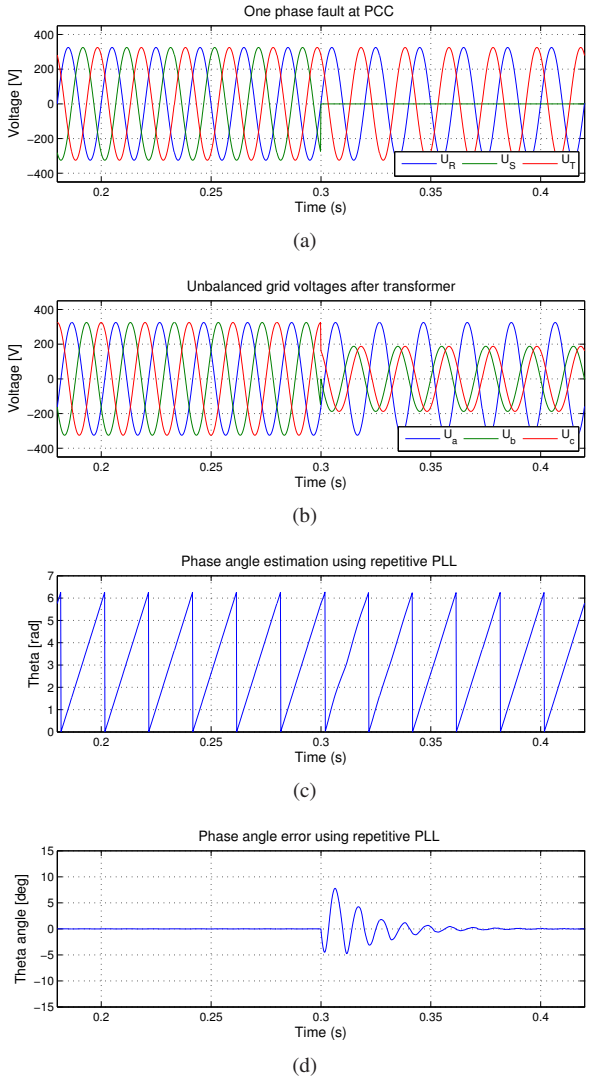

Fig. 7. Behavior of the proposed PLL system under single phase fault at the PCC: (a) voltages at PCC, (b) voltages after transformer, (c) repetitive PLL output and (d) the phase error between the real grid phase and estimated one by the proposed PLL.

IV. Evaluation of the Proposed PLL System

In order to evaluate the behavior of the PLL system under different grid faults, a setup having the diagram as in Fig. 6 has been used. A grid simulator is employed for grid faults generation at the point of common coupling. The PWM inverter supplied by a dc power source is switched at 12800 kHz. An LC filter ($L_i = 10\ mH,\ C = 0.7\mu F$) and an Δy transformer ($L_t = 2mH$) are used between the inverter and the ac power supply which emulates the grid. Due to the presence of the Δy transformer, the voltage fault at the point of common coupling appears differently at the inverter terminals. As it is illustrated in Fig 3(a) and Fig. 3(b) a single phase fault to ground is transformed into a more convenient situation where two of the phases drop in amplitude and register a phase shift. A detailed study about the propagation of the voltages through Δy transformer is done in [4].

A. Simulation results

In order to see the effectiveness of the proposed PLL in reducing the phase error under unbalanced grid conditions, simulation results, providing access to the initial phase angle of the grid, are presented. The same fault as depicted in Fig. 3(a) has been considered. As it can be observed in Fig. 7(c), the proposed algorithm has a much better performance under fault. The 100 Hz ripple in the synchronization signal can be observed for one single period, while the phase error in Fig. 7(d) is reduced to zero in about 0.08 seconds, as it was previously designed. This result proves the effectiveness of the proposed algorithm to eliminate the unbalance effect on the synchronization algorithm, providing a clean synchronization signal during an imbalanced fault. This signal represents the phase angle of the positive sequence of grid voltages and can be further used in the control strategy for current synchronization.

B. Experimental results

Voltage faults

Firstly, the proposed PLL system it is experimentally tested against voltage faults. Three types of faults, i.e. single phase sag, two phase sag and three phase sag, are considered. Due to the large amount of unbalance in the situation of single and two phase sag, these two cases are considered to be the worst case scenario this PLL can run on.

Additionally, the novel proposed PLL is also tested against high content of harmonics in the utility grid. The ac power source is programmed to inject a large amount of harmonics in its output voltages, and the behavior of the proposed algorithm is pursued. The experimental results for each particular situation are presented in the following.

1) Single phase sag: As mentioned above, a grid simulator is used in the laboratory to generate the voltage faults. The experimental results for one phase fault in the grid are shown in Fig. 8. The voltage waveforms after the transformer are depicted in Fig. 8(a). One of the grid voltages register a drop from 230 V_{RMS} down to 100 V_{RMS}. As it can be noticed in Fig. 8(b), the phase angle estimation under such unbalanced conditions is still satisfactory. The proposed PLL algorithm is able to reject the unbalance effect, generating a clean synchronization signal.

2) Two phase sag: The voltage waveforms after the Δy transformer in the situation of two phase sag are illustrated in Fig. 9(a). In this case, two of the grid voltages at the point of common coupling (Fig. 6) register a drop down to 100 V_{RMS}. Looking at the repetitive PLL response depicted in Fig. 9(b), the estimated phase angle is again satisfactory. No 100 Hz ripple is noticed in the estimated signal, the proposed PLL system being able to cancel the effect of the negative sequence, outputting a clean synchronization signal for the control.

3) Three phase sag: Another type of the grid fault that appears very seldom in the power system is the three phase sag situation. In this case, all three phases register the same amplitude drop. Characteristic to this fault is that the grid voltages are balanced during the fault, i.e. no negative sequence occurs.

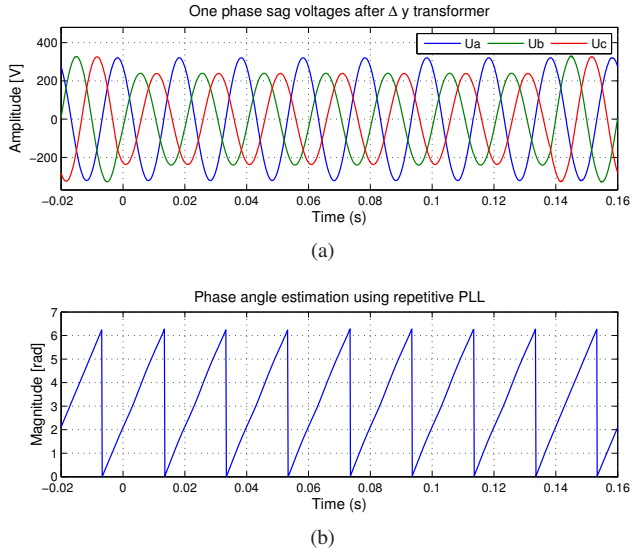

Fig. 8. Experimental results in the case of one phase voltage sag in the grid: (a) the voltages after the transformer and (b) the estimation of the phase angle using the proposed repetitive PLL.

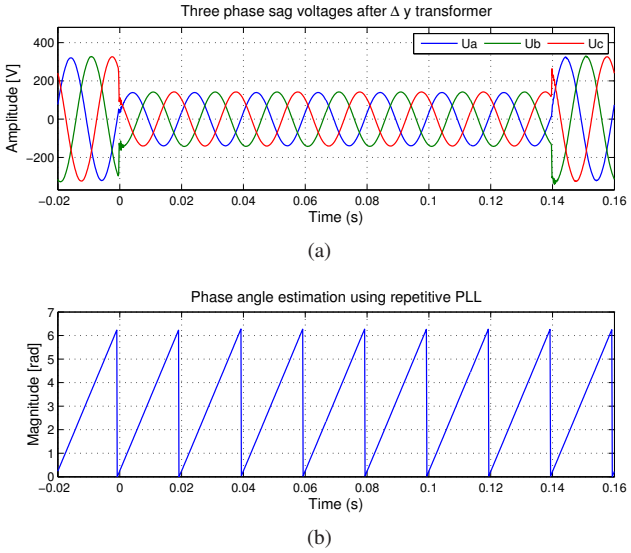

Fig. 10. Experimental results in case of tree phase voltage sag in the grid: (a) the voltages after the transformer and (b) the estimation of the phase angle using the proposed repetitive PLL.

The voltage waveforms in the case of a three phase sag are presented in Fig. 10(a). As it can be observed, the amplitude of the all three voltages drops down to 100 V_{RMS} but no phase jump is registered.

Since there is no negative sequence present in the voltages in this situation, the proposed PLL system behaves as a conventional PLL system. In this case, the repetitive controller does not influence the system behavior.

4) Harmonics: In [5] it has been proved that traditional dq PLL system is not influenced by the harmonics content in the grid. Since a repetitive controller which rejects the odd order harmonics is added to the proposed algorithm, it is expected that the new system will perform better when harmonics are present in the grid voltages. In order to demonstrate this, experimental results are presented in Fig. 11. The grid simulator has been programed to inject the content of harmonics stated in Table I in the grid voltages. All voltage harmonics have a phase angle displacement of 180^o with respect to the fundamental.

TABLE I
AMPLITUDE OF THE HARMONICS INJECTED IN THE GRID VOLTAGES.

Harmonic order	*Amplitude*
5^{th}	5%
7^{th}	4%
9^{th}	3%
11^{th}	3%

As the lower plot of Fig. 11 shows, the proposed algorithm is robust to the high content of harmonics in the grid voltages,

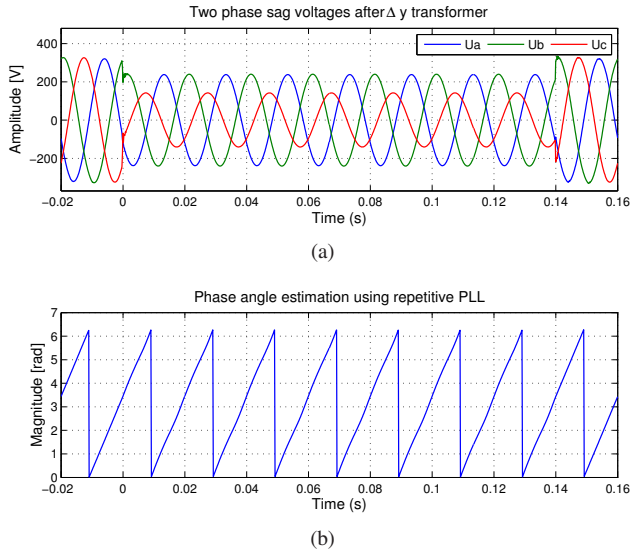

Fig. 9. Experimental results in case of two phase voltage sag in the grid: (a) the voltages after the transformer and (b) the estimation of the phase angle using the proposed repetitive PLL.

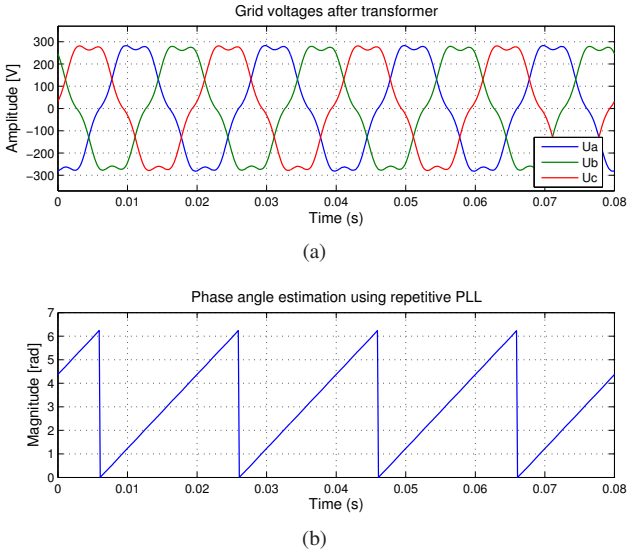

Fig. 11. Experimental results in case of harmonic content in the grid voltages: upper plot: the voltages after the transformer and lower plot: the estimation of the phase angle using the proposed repetitive PLL.

the estimated synchronization signal being a clean one.

Frequency deviations

Additionally to the voltage faults, the novel proposed PLL system has been also tested against grid frequency variations. As stated before, most of the grid codes demand the wind turbines to run when frequency deviations occur in the utility grid. Thus, the synchronization algorithm should be capable to provide a good signal to be used in the control structure.

The behavior of the proposed PLL system when the grid frequency deviates with 3 Hz from its nominal value is depicted in Fig. 12. As shown in Fig. 12(a), the proposed algorithm is able to detect and to follow the new grid frequency within three fundamental cycles. Therefore, the estimated phase angle illustrated in Fig. 12(b) is still synchronized with the grid after the frequency deviation occurrence at simulation time 0.3 seconds. This result proves the robustness of the novel PLL to the grid frequency deviations.

Phase angle jump

Finally, the proposed synchronization algorithm is tested against phase angle jumps. Two different cases can be distinguished in this situation.

- Firstly, is the situation when the whole grid experience a phase jump of several degrees. In this case, there is a short transient in the grid but the grid voltages remain balanced during the fault. Thus, being no negative sequence in the grid voltages, the proposed PLL will provide a synchronization signal synchronized with phase a of the grid.
- Secondly, it is the case when only one or two of the grid voltages experience a phase jump. In this situation, the grid becomes unbalanced, thus the repetitive controller tries to eliminate the effect of the unbalance and to provide the phase angle of the positive sequence of the grid.

Fig. 13 illustrates the behavior of proposed PLL in the situation of a grid phase jump of 60 degrees. As it can be observed in Fig. 13(a), the proposed system is able to track the new phase angle in about 4 fundamental periods , with a small overshoot when the transient occurs. As Fig. 13(b) depicts, the phase angle becomes again synchronized with the phase angle a of the utility grid.

The situation when only one phase (phase a) of the utility network registers a phase jump of 60 degrees is illustrated in Fig. 14. Noticeable is in this case that the phase angle estimated by the PLL does not coincide with the one of the phase a but with the one of the positive sequence of the grid, as Fig. 14(a) shows.

V. Conclusion

This paper discusses a novel synchronization algorithm robust to grid faults. The novelty of the proposed Phase-Looked Loop system consists in the employment of a repetitive controller to eliminate the unbalance effect when this exists in the grid voltages. Analogies and differences with the conventional PLL system have been highlighted. The design of the repetitive controller regarding locking time and system stability has been discussed. Frequency domain and step response plot have been presented to validate the design.

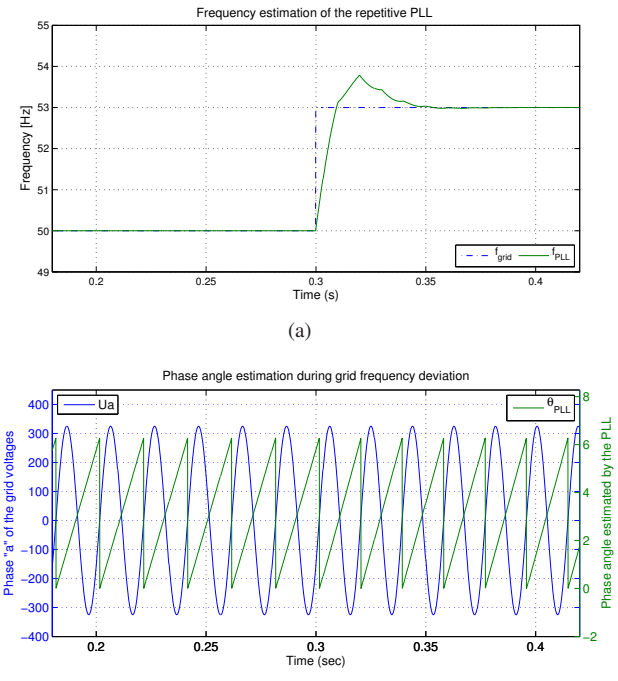

(a)

(b)

Fig. 12. Experimental results in the case of grid frequency deviation: (a) the estimated frequency by the proposed PLL algorithm and (b) the phase angle signal synchronized with phase a of the grid voltages.

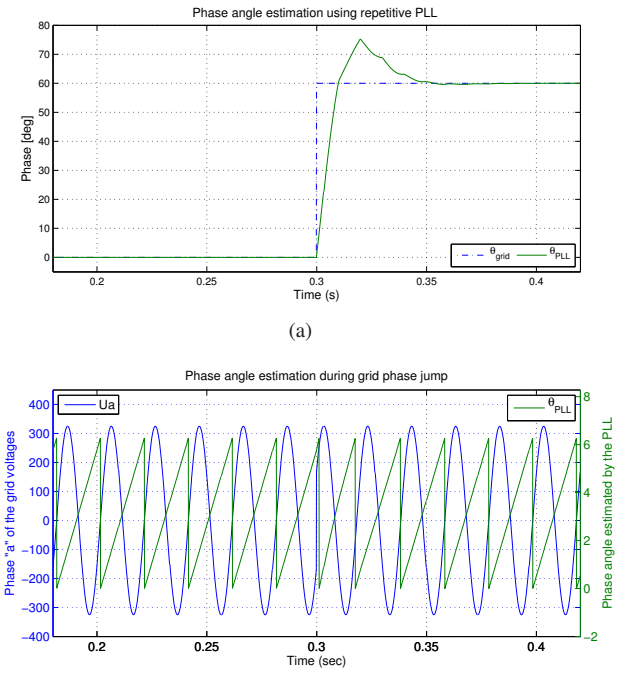

(a)

(b)

Fig. 13. Experimental results in the case of grid phase angle jump: (a) the grid and estimated phase angle by the PLL in the case of a 60^0 phase jump and (b) the phase angle signal synchronized with the grid voltage phase a.

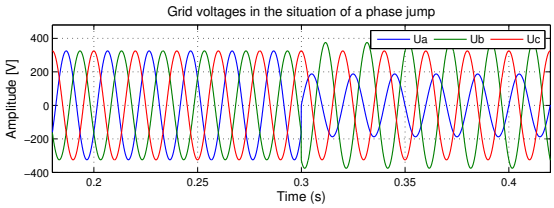

(a)

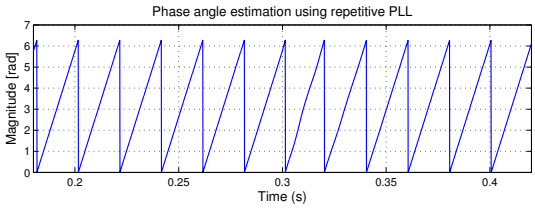

(b)

Fig. 14. Experimental results in the case of single phase angle jump: (a) the grid and estimated phase angle by the PLL in the case of a 60^0 phase jump of phase *a* and (b) the phase angle signal synchronized with the positive sequence of the utility grid.

The proposed PLL has been tested against different grid faults, both symmetrical and unsymmetrical. Simulation and experimental results prove a better behavior of the proposed system when running on unbalanced grid faults as compared to the conventional algorithm. The proposed algorithm is able to reject the effect of unbalance from the grid voltages, providing a clean synchronization signal and, in the same time, keeping a high dynamics of the system. Moreover, the proposed PLL proves to be robust to grid frequency variations as well as to phase angle jumps.

REFERENCES

[1] F. Blaabjerg, Z. Chen, and S. Kjaer, "Power electronics as efficient interface in dispersed power generation systems," *IEEE Trans. on Power Electronics*, vol. 19, no. 5, pp. 1184–1194, 2004.

[2] T. Ackermann, *Wind Power in Power Systems*. John Wiley & Sons, Ltd., 2005, ISBN: 0-470-85508-8.

[3] Eltra and Elkraft, "Wind turbines connected to grids with voltage below 100 kV," http://www.eltra.dk, 2004.

[4] M. H. J. Bollen, *Understanding Power Quality Problems: Voltage Sags and Interruptions*. IEEE Press, 2002.

[5] A. V. Timbus, M. Liserre, R. Teodorescu, and F. Blaabjerg, "Synchronization methods for three phase distributed power generation systems. An overview and evaluation," in *Proc. of PESC'05*, 2005, pp. 2474–2481.

[6] M. C. Benhabib and S. Saadate, "A new robust experimentally validated Phase-Looked Loop for power electronic control," *EPE Journal*, vol. 15, no. 3, pp. 36–48, August 2005.

[7] P. Rodriguez, J. Pou, J. Bergas, I. Candela, R. Burgos, and D. Boroyevich, "Double synchronous reference frame PLL for power converters," in *Proc. of PESC'05*, 2005, pp. 1415–1421.

[8] M. Karimi-Ghartemani and M. Iravani, "A method for synchronization of power electronic converters in polluted and variable-frequency environments," *IEEE Trans. on Power Systems*, vol. 19, no. 3, pp. 1263–1270, 2004.

[9] V. Kaura and V. Blasko, "Operation of a phase loop system under distorted utility conditions," *IEEE Trans. on Industry Applications*, vol. 33, no. 1, pp. 58–63, 1997.

[10] L. N. Arruda, S. M. Silva, and B. Filho, "PLL structures for utility connected systems," in *Proc. of IAS'01*, vol. 4, 2001, pp. 2655–2660.

[11] S.-K. Chung, "Phase-Locked Loop for grid-connected three-phase power conversion systems," *IEE Proceedings on Electronic Power Applications*, vol. 147, no. 3, pp. 213–219, 2000.

[12] P. Mattavelli and F. Marafao, "Repetitive-base control for selective harmonic compensation in active power filters," *IEEE Trans. on Industrial Electronics*, vol. 51, no. 5, pp. 1018–1024, 2004.

Publication 6

New positive-sequence voltage detector for grid synchronization of power converters under faulty grid conditions

by P. Rodriguez, R. Teodorescu, I. Candela, A. Timbus, M. Liserre and F. Blaabjerg
Article published in Proceedings of PESC'06, pages 1-7, 2006

New Positive-sequence Voltage Detector for Grid Synchronization of Power Converters under Faulty Grid Conditions

P. Rodríguez[⋏], R. Teodorescu[⋆], I. Candela[⋏], A.V. Timbus[⋆], M. Liserre[✱] and F. Blaabjerg[⋆]

[⋏] Technical University of Catalonia
Department of Electrical Engineering
Barcelona – Spain
prodriguez@ee.upc.edu

[⋆] Aalborg University
Institute of Energy Technology
Aalborg – Denmark
ret@iet.aau.dk

[✱] Polytechnic of Bari
Dept. of Electrotechnical and Electronic Eng.
Bari – Italy
liserre@poliba.it

Abstract— This paper deals with a fundamental aspect in the control of grid-connected power converters, i.e., the detection of the positive-sequence component at fundamental frequency of the utility voltage under unbalanced and distorted conditions. Accurate and fast detection of this voltage component under grid faults is essential to keep the control over the power exchange with the grid avoiding to trip the converter protections and allowing the ride-through of the transient fault.

In this paper, the systematic use of well known techniques conducts to a new positive-sequence voltage detection system which exhibits a fast, precise, and frequency-adaptive response under faulty grid conditions. Three fundamental functional blocks make up the proposed detector, these are: *i)* the quadrature-signals generator (QSG), *ii)* the positive-sequence calculator (PSC), and *iii)* the phase-locked loop (PLL). A key innovation of the proposed system is the use of a dual second order generalized integrator (DSOGI) to implement the QSG. For this reason, the proposed positive-sequence detector is called DSOGI-PLL. A detailed study of the DSOGI-PLL and verification by simulation are performed in this paper. From the obtained results, it can be concluded that the DSOGI-PLL is a very suitable technique for characterizing the positive-sequence voltage under grid faults.

I. INTRODUCTION

Grid synchronization is one the most important issues in the integration of power converter into power systems. In particular, this aspect becomes crucial in the connection of wind turbines (WT) to power systems. In recent years, rapid development of WT and increasing penetration of wind power generation have resulted in the reformulation of the grid connection requirements (GCR) for wind power [1]. CGR of the most of the countries with a high rate of wind power penetration state that WT have to ride-through of transient faults to sustain generation. In such grid faults, the amplitude, phase and frequency of the utility voltages can show significant transient variations. Therefore the fast and accurate detection of the positive-sequence component of the utility voltage is necessary in order to keep generation up according to the GCR.

When it is assumed that the frequency of the utility is a constant and well-known magnitude, an algorithm based on the instantaneous symmetrical components (ISC) method can be easily implemented for effective detection of the positive-sequence component [2]. In Europe the frequency is usually 50±0.1 Hz and falls out of the 49-50.3 range very seldom [3]. However, during a transient fault, the system frequency can show significant fluctuations. Regarding the GCR for wind power, the control system of the grid connected converter must ensure its fast adaptation to the faulty conditions, improving the fault tolerance of the wind generation system and avoiding the post-fault collapse of the power system because wind generators are lost.

On the other hand, when the utility frequency is not constant, the positive-sequence detection system uses closed-loop adaptive methods in order to render it insensitive to input frequency variations. The use of a phase-locked loop (PLL) is indeed the most representative example of such frequency adaptive methods. In three-phase systems, the PLL's are usually based on the synchronous reference frame (SRF-PLL) [4]. Under ideal utility conditions, i.e., neither imbalance nor harmonic distortion, the SRF-PLL yields good results. In case the utility voltage is distorted with high-order harmonics, the SRF-PLL can still operate satisfactorily if its bandwidth is reduced in order to reject and cancel out the effect of these harmonics on the output. But under voltage unbalance however, the bandwidth reduction is not an acceptable solution since the overall dynamic performance of the PLL system would become unacceptably deficient [5]. This drawback can be overcome by using a PLL based on the decoupled double synchronous reference frame (DSRF-PLL) [6]. In the DSRF-PLL, a decoupling network permits a proper isolation of the positive- and negative-sequence components. An alternative technique for frequency-adaptive positive-sequence detection is presented in [7]. Such technique uses a single-phase enhanced phase-locked loop (EPLL) for each phase of the three-phase system allowing fundamental frequency adaptation. The phase voltages and its respective 90-degree shifted versions detected by the EPLL are used by the ISC method in order to detect the positive-sequence voltages of the three-phase system. Finally, a fourth single-phase EPLL is applied to the output of the ISC method to estimate the phase-angle of the positive-sequence voltage.

This work presents a new frequency-adaptive positive-sequence detection technique, namely the 'Dual Second Order Generalized Integrator PLL' (DSOGI-PLL). This technique translates the three-phase voltage from the *abc* to the $\alpha\beta$ reference frames. A dual SOGI-based quadrature-signals generator (QSG) is used for filtering and obtaining the 90-degree shifted versions from the $\alpha\beta$ voltages. These signals act as inputs to the positive-sequence calculator (PSC) which lies on the ISC method on the $\alpha\beta$ domain. Finally, the positive-sequence $\alpha\beta$ voltages are translated to the *dq* synchronous reference frame and a PLL (SRF-PLL) is employed to make the system frequency-adaptive.

II. POSITIVE-SEQUENCE CALCULATION ON THE $\alpha\beta$ REFERENCE FRAME

At early 30's, *Lyon* extended the use of the *Fortescue*'s symmetrical components method to the time-domain [8]. Using that principle, the instantaneous positive-sequence component $\mathbf{v}^+_{abc}$ of a generic three-phase voltage vector $\mathbf{v}_{abc}=\begin{bmatrix}v_a & v_b & v_c\end{bmatrix}^T$ is given by:

$$\mathbf{v}^+_{abc}=\begin{bmatrix}v^+_a & v^+_b & v^+_c\end{bmatrix}^T=[T_+]\,\mathbf{v}_{abc},$$
$$[T_+]=\frac{1}{3}\begin{bmatrix}1 & a^2 & a\\ a & 1 & a^2\\ a^2 & a & 1\end{bmatrix},\quad a=e^{-j\frac{2\pi}{3}}. \tag{1}$$

Using the non-normalized *Clarke* transformation, the voltage vector can be translated from the *abc* to the $\alpha\beta$ reference frames as follow:

$$\mathbf{v}_{\alpha\beta}=\begin{bmatrix}v_\alpha & v_\beta\end{bmatrix}^T=[T_{\alpha\beta}]\,\mathbf{v}_{abc},$$
$$[T_{\alpha\beta}]=\frac{2}{3}\begin{bmatrix}1 & -\frac{1}{2} & -\frac{1}{2}\\ 0 & \frac{\sqrt{3}}{2} & -\frac{\sqrt{3}}{2}\end{bmatrix}. \tag{2}$$

Therefore, the instantaneous positive-sequence voltage on the $\alpha\beta$ reference frame can be calculated by:

$$\mathbf{v}^+_{\alpha\beta}=[T_{\alpha\beta}]\,\mathbf{v}^+_{abc}=[T_{\alpha\beta}][T_+]\,\mathbf{v}_{abc}$$
$$=[T_{\alpha\beta}][T_+][T_{\alpha\beta}]^{-1}\,\mathbf{v}_{\alpha\beta}=\frac{1}{2}\begin{bmatrix}1 & -q\\ q & 1\end{bmatrix}\mathbf{v}_{\alpha\beta},\quad q=e^{-j\frac{\pi}{2}}, \tag{3}$$

where q is a phase-shift operator in the time-domain which obtains the quadrature-phase waveform (90-degrees lag) of the original in-phase waveform.

Transformation of (3) is implemented in the PSC of the proposed DSOGI-PLL and its right operation depends on the precision of the quadrature-phase signal provided to its input. It is worth to remark that the time-delay introduced by the q operator is dynamically set according the fundamental frequency of the input voltage. Therefore, the positive-sequence component calculated from the n^{th}-order harmonic at the input voltage is given by:

$$\mathbf{v}^+_{\alpha\beta}=\frac{1}{2}\begin{bmatrix}1 & -|n|q\\ |n|q & 1\end{bmatrix}\mathbf{v}^n_{\alpha\beta}, \tag{4}$$

where the positive –negative sign of n represents the positive –negative-sequence of the input voltages. From (4), the harmonic rejection capability of the PSC on the $\alpha\beta$ reference frame can be summarized as in Table I, where cells for characteristic harmonics have been highlighted. The PSC does not act as a sequence changer. Consequently, if negative-sequence signals are applied to the PSC input they will arrive to its output with the same sequence but multiplied by the complex factor specified in Table I. In this sense, positive-sequence calculation of (3) is better than that shown in (1) since this second transformation is transparent for characteristic harmonics propagation.

TABLE I

HARMONIC PROPAGATION IN THE PSC ($\mathbf{v}^+_\alpha$ WHEN $\mathbf{v}^n_\alpha=1\angle 0^\circ$)

Order	Input signals sequence	
n	+	-
1st	$1\angle 0^\circ$	0
2nd	$1/\sqrt{2}\angle -45^\circ$	$1/\sqrt{2}\angle 45^\circ$
3rd	0	$1\angle 0^\circ$
4th	$1/\sqrt{2}\angle 45^\circ$	$1/\sqrt{2}\angle -45^\circ$
5th	$1\angle 0^\circ$	0
…	…	…

A relevant aspect to be analyzed in the PSC is the error made in the positive-sequence estimation when the frequency setting the time-delay of the q operator, ω', differs from the actual center grid frequency, ω. In such unsynchronized conditions, the complex factor affecting to an n^{th}-order harmonic at the input of the PSC is given by:

$$\mathbf{v}^+_\alpha=\mathbf{C}^n\cdot\mathbf{v}^n_\alpha \begin{cases} |\mathbf{C}^n|=\sqrt{\frac{1}{2}\left[1+\sin\left(n\frac{\omega}{\omega'}\frac{\pi}{2}\right)\right]} \\ \angle\mathbf{C}^n=\mathrm{sgn}(n)\tan^{-1}\dfrac{\cos\left(n\frac{\omega}{\omega'}\frac{\pi}{2}\right)}{2|\mathbf{C}^n|^2}\end{cases} \tag{5}$$

For the sake of clarifying, a numerical example is presented here. In this example, the frequency determining the time-delay of the q operator is $\omega'=50\text{Hz}$ whereas the actual grid frequency is $\omega=40\text{Hz}$. In such conditions, if the components of the grid voltage are $\mathbf{v}^{+1}_\alpha=80\angle 0^\circ$, $\mathbf{v}^{-1}_\alpha=20\angle -10^\circ$ and $\mathbf{v}^{-5}_\alpha=10\angle 30^\circ$, the $\mathbf{v}^+_\alpha$ voltage at the PSC output is composed by $\mathbf{C}^{+1}\mathbf{v}^{+1}_\alpha=79\angle 9^\circ$, $\mathbf{C}^{-1}\mathbf{v}^{-1}_\alpha=3.13\angle -91^\circ$, and $\mathbf{C}^{-5}\mathbf{v}^{-5}_\alpha=7.07\angle -15^\circ$. The amplitude of $\mathbf{v}^+_\beta$ is the same that of $\mathbf{v}^+_\alpha$ but its phase-angle is either 90-degrees lag or lead when the input voltage sequence is either positive or negative, respectively. This numerical example has been illustrated in Fig. 1, where the grid frequency changes from ω=50Hz to ω=40Hz at t=0.15s with ω'=50Hz permanently.

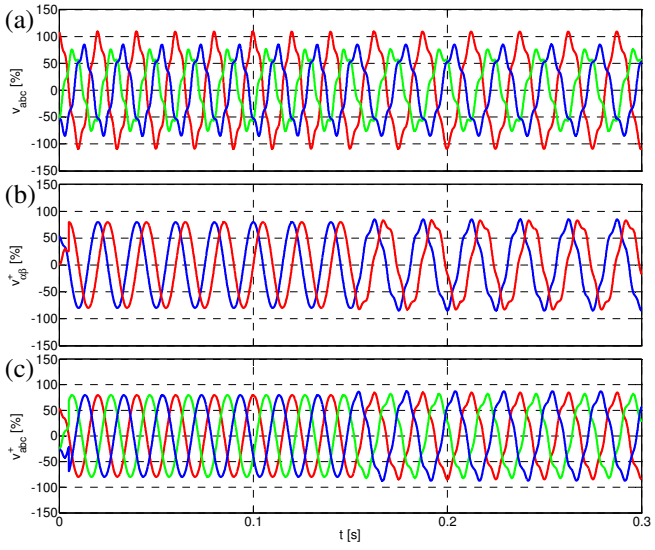

Fig. 1. PSC output when grid frequency changes (ω=40Hz, ω'=50Hz).

III. SECOND ORDER GENERALIZED INTEGRATOR FOR QUADRATURE-SIGNALS GENERATION

A transport delay buffer was used to easily achieve the 90-degrees shifted version of v_α and v_β signals in simulation of Fig. 1. Another simple quadrature-signals generator (QSG) can be implemented by means of a first-order all-pass filter. However, such techniques are not frequency-adaptive, which could give rise to errors in the positive-sequence estimation, e.g. in Fig. 1. Moreover, these simple techniques do not block harmonics from the input signals. To overcome these drawbacks, the use of a single-phase EPLL is proposed in [7]. The EPLL is actually an adaptive notch-filter based on minimizing the product of quadrature-signals [9] and whose frequency moves based on the fundamental frequency of the grid. Other advanced methods for frequency adaptive quadrature-signals generation have been reported in the literature, e.g., the *Hilbert* transformation-based PLL (HT-PLL) [10] or the inverse *Park* transformation-based PLL (IPT-PLL) [11], however they become also complex. With the aim of simplifying, this work proposes the use of a second order generalized integrator (SOGI) [12]-[13] for quadrature-signals generation. The SOGI-QSG scheme is shown in Fig. 2(a) and its characteristic transfer functions are given by :

$$D(s) = \frac{v'}{v}(s) = \frac{k\omega' s}{s^2 + k\omega' s + \omega'^2} \tag{6a}$$

$$Q(s) = \frac{qv'}{v}(s) = \frac{k\omega'^2}{s^2 + k\omega' s + \omega'^2} \tag{6b}$$

where ω' and k set resonance frequency and damping factor of the SOGI-QSG respectively. Bode plots from transfer functions of (6) are shown in Fig. 2(b) and 2(c) for several values of k. These plots show how the lower value of k the more selective filtering response, but the longer stabilization time as well. A critically-damped response is achieved when $k = \sqrt{2}$. This value of gain results an interesting selection in terms of stabilization time and overshot limitation.

If v is a sinusoidal signal with frequency ω, it can be expressed as a phasor $\mathbf{v}$. Therefore the SOGI-QSG outputs can be calculated from (6) as follow:

$$\mathbf{v}' = \mathbf{D}\mathbf{v} \begin{cases} |\mathbf{D}| = \dfrac{k\omega\omega'}{\sqrt{\left(k\omega\omega'\right)^2 + \left(\omega^2 - \omega'^2\right)^2}} \\ \underline{|\mathbf{D}} = \tan^{-1}\left(\dfrac{\omega'^2 - \omega^2}{k\omega\omega'}\right) \end{cases} \tag{7a}$$

$$\mathbf{qv}' = \mathbf{Q}\mathbf{v} \begin{cases} |\mathbf{Q}| = \dfrac{\omega'}{\omega}|\mathbf{D}| \\ \underline{|\mathbf{Q}} = \underline{|\mathbf{D}} - \dfrac{\pi}{2} \end{cases} \tag{7b}$$

It is worth to remark from (7), that qv' is always 90-degrees lag respect to v', independently of the value of k, ω and ω'. This is a very interesting feature for implementing

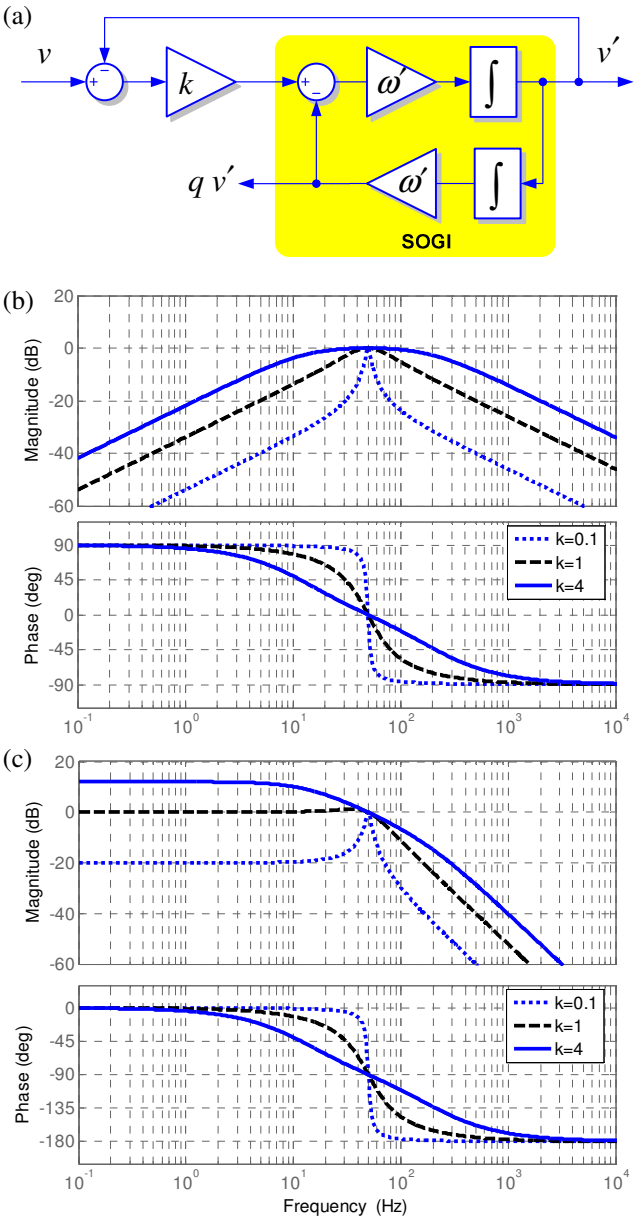

Fig. 2. SOGI-QSG. (a) SOGI-QSG scheme, (b) Bode plot of $D(s)$, (c) Bode plot of $Q(s)$.

the 90-degrees phase-shifting of the q operator. However, (7) also evidences that the SOGI-QSG output signals will be wrong in both amplitude and phase when the SOGI-QSG resonant frequency, ω', does not match up to the input signal frequency, ω. The consequence of these errors will be analyzed in the next section.

IV. POSITIVE-SEQUENCE DETECTOR USING A DUAL SOGI-QSG

The essential structure of the proposed positive-sequence detection system is shown in Fig. 3 where a dual SOGI-QSG (DSOGI-QSG) provides the input signals to the PSC on the $\alpha\beta$ reference frame. To evaluate the response of the system it will be supposed that the grid voltage suddenly experiments a complex voltage sag (dip) type D as a

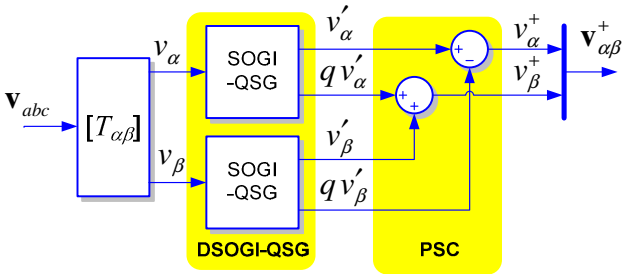

Fig. 3. Positive sequence calculation based on DSOGI-QSG

consequence of a fault condition which is cleared after 100ms [14]. In this dip, the characteristic voltage is $0.6\angle\underline{-20^\circ}$ and the positive-negative factor is $0.9\angle\underline{-10^\circ}$, both of them expressed in p.u. respect to the perfectly balanced pre-fault voltage $\mathbf{v}^+_{pf} = 1\angle\underline{0^\circ}$. Consequently, the positive and negative sequence fault voltages are given by $\mathbf{v}^+ = 0.747\angle\underline{-14^\circ}$ and $\mathbf{v}^- = 0.163\angle\underline{8.63^\circ}$ respectively. In this simulation, it is assumed that the DSOGI-QSG resonance frequency perfectly matches up with the grid frequency, that is $\omega = \omega' = 2\cdot\pi\cdot 50$ rad/s. In addition, the gain of the DSOGI-QSG has been set at $k = \sqrt{2}$. Fig. 4 shows the response of the PSC under such operating conditions when the DSOGI-QSG is perfectly synchronized. The faulty phase-voltages are shown in Fig. 4(a) and the estimated positive-sequence phase-voltages in the natural *abc* reference frame are shown in Fig. 4(e).

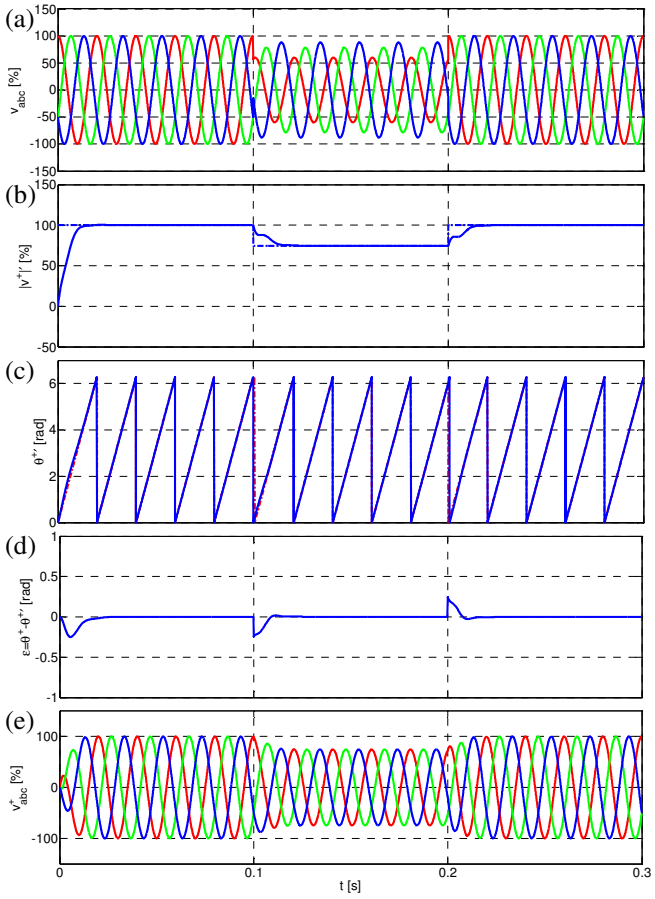

Fig. 4. Response of the PSC in presence of unbalanced voltage sag.

Fig. 4(b) shows the actual and estimated amplitude for the positive-sequence component, $\mathbf{v}^+$, whereas its actual and estimated phase angle are shown in Fig. 4(c). These waveforms are calculated as follows:

$$\left|\mathbf{v}^+\right|' = \sqrt{\left(v^+_\alpha\right)^2 + \left(v^+_\beta\right)^2} \quad ; \quad \theta^{+\prime} = \tan^{-1}\frac{v^+_\beta}{v^+_\alpha}. \tag{8}$$

Fig. 4(d) shows the error in phase-angle estimation. Plots of Fig. 4 confirm the good behavior of the proposed system, which is canceling the steady-state error after one cycle of the grid voltage.

As studied in Section III, when the grid frequency differs from the DSOGI-QSG resonance frequency, the input signals to the PSC show amplitude and phase errors. Nevertheless such signals are always orthogonal. This last characteristic makes easy to analyze how DSOGI-QSG errors are propagated through the PSC. Expressing the n^{th} harmonic of v_α as the phasor $\mathbf{v}^n_\alpha$, it can be concluded from (3) and (7) that the output of the PSC is given by:

$$\mathbf{v}^+_\alpha = \mathbf{P}^n\mathbf{v}^n_\alpha \begin{cases} \left|\mathbf{P}^n\right| = \dfrac{k\omega'}{2}\sqrt{\dfrac{(n\omega+\omega')^2}{(kn\omega\omega')^2+\left(n^2\omega^2-\omega'^2\right)^2}} \\ \underline{\mathbf{P}^n} = \operatorname{sgn}(n)\tan^{-1}\left(\dfrac{\omega'^2-n^2\omega^2}{kn\omega\omega'}\right) \\ \qquad -\dfrac{\pi}{2}\left(1-\operatorname{sgn}\left(n^2\omega+n\omega'\right)\right) \end{cases}, \tag{9a}$$

$$\left|\mathbf{v}^+_\beta\right| = \left|\mathbf{v}^+_\alpha\right| \quad ; \quad \underline{\mathbf{v}^+_\beta} = \underline{\mathbf{v}^+_\alpha} - \operatorname{sgn}(n)\frac{\pi}{2}, \tag{9b}$$

where ω is the fundamental grid frequency, ω' is the DSOGI-QSG resonance frequency, and positive –negative sign of n represents positive –negative-sequence of the input voltage. Magnitude calculation of (9a) is plotted in Fig. 5 for $k = \sqrt{2}$. This plot evidences that the system of Fig. 3 acts as both a low-pass filter for positive-sequence and a notch filter for negative-sequence. Another remarkable aspect in this plot is the high-order harmonics attenuation, which is a very convenient feature to make the detection technique more robust in front of grid voltage distortion. Expressions of (9) accurately quantify the error in the positive-sequence calculation when the DSOGI-QSG

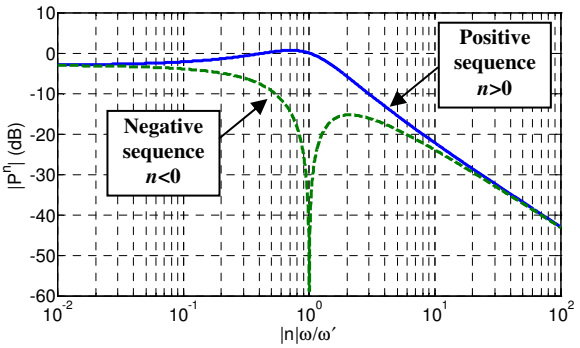

Fig. 5. Frequency response of the PSC based on DSOGI-QSG

resonance frequency does not match up with the grid frequency. These equations can be used to compensate the estimation error when the actual grid frequency is properly detected by an additional mechanism such as a PLL. In this work, although a PLL is employed for grid frequency detection, its output is not used to calculate and compensate the error of (9). In this case however, the output of the PLL dynamically modifies the resonance frequency of the DSOGI-QSG in order to achieve the frequency-adaptive functionality in the proposed positive-sequence detector.

V. POSITIVE-SEQUENCE DETECTOR USING A FREQUENCY-ADAPTIVE DSOGI

To ensure that the proposed positive-sequence detector gives rise to precise results under grid frequency variations it is necessary to implement some kind of close-loop system which allows proper adaptation of the DSOGI-QSG resonance frequency to the actual network conditions. One way to achieve this is by using a single-phase EPLL, HT-PLL, or IPT-PLL on v_α^+–or v_β^+–to detect the grid frequency and dynamically modify the DSOGI-QSG resonance frequency. The EPLL brings to the simplest single-phase implementation among previous three options. However the EPLL is not employed in this work because its filtering characteristic provides the same functionality as the SOGI-QSG. Although the joint action of both filtering stages improves the steady state response of the detection system in presence of high levels of voltage distortion, it also increases output oscillations and extends the stabilization period when the grid experiments voltage sags.

In the proposed system, the well known SRF-PLL structure is used instead of the single-phase PLL for grid frequency detection and subsequent DSOGI-QSG resonance frequency adaptation. The structure of this DSOGI-based PLL (DSOGI-PLL) is presented in Fig. 7, where the positive-sequence voltage vector is translated from the $\alpha\beta$ stationary reference frame to the dq rotating reference frame by means of *Park*'s transformation, that is:

$$\mathbf{v}_{dq}^{+} = \begin{bmatrix} v_d^+ \\ v_q^+ \end{bmatrix} = \left[T_{dq}\right]\mathbf{v}_{\alpha\beta}^{+} \quad ; \quad \left[T_{dq}\right] = \begin{bmatrix} \cos\theta^+ & \sin\theta^+ \\ -\sin\theta^+ & \cos\theta^+ \end{bmatrix}. \quad (10)$$

In the system of Fig. 7, the feedback loop regulating the q component to zero is controlling the angular position of the dq reference frame and estimating the grid frequency.

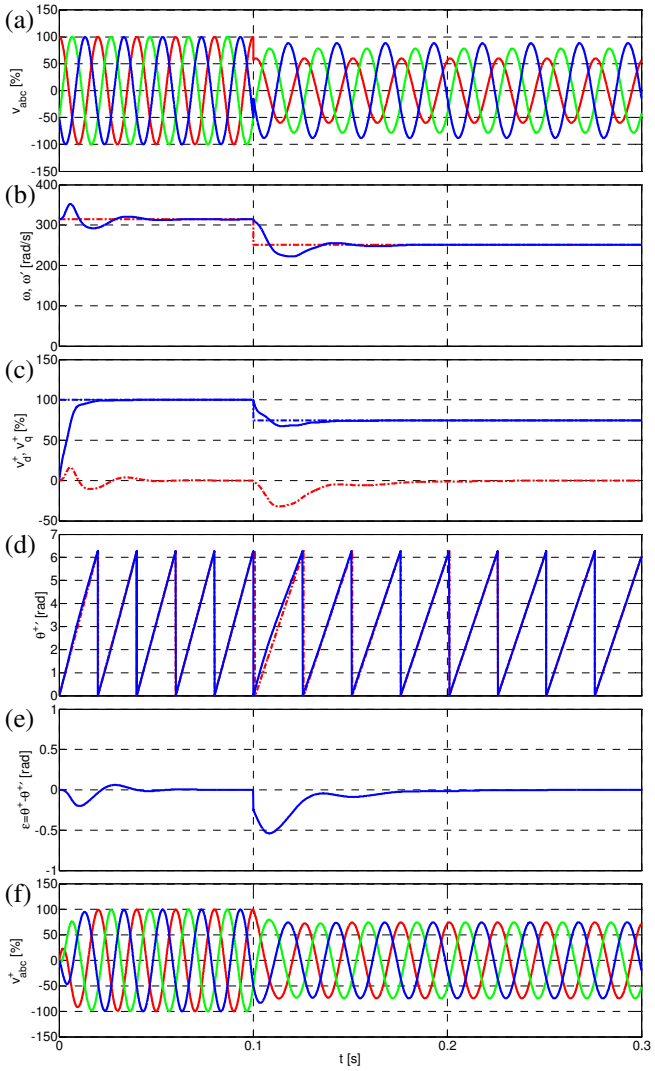

Fig. 6: Characteristic signals of the DSOGI-PLL under a frequency step (50Hz to 40Hz) with k=1.41, k_p=2.22, and k_i=61.69.

The estimated grid frequency, ω', is used by the outer feedback loop to dynamically adapt the DSOGI-QSG resonant frequency.

Fig. 6 shows the DSOGI-PLL response when the grid frequency hypothetically changes from 50 Hz to 40 Hz during an unbalanced sag. Parameters of the SRF-PLL PI controller were calculated according to [5], i.e., k_p=2.22 and k_i=61.69 which implies that cut-off frequency and damping factor are $\omega_c = 2\pi \cdot 12.5$ and $\xi = \sqrt{2}$, respectively.

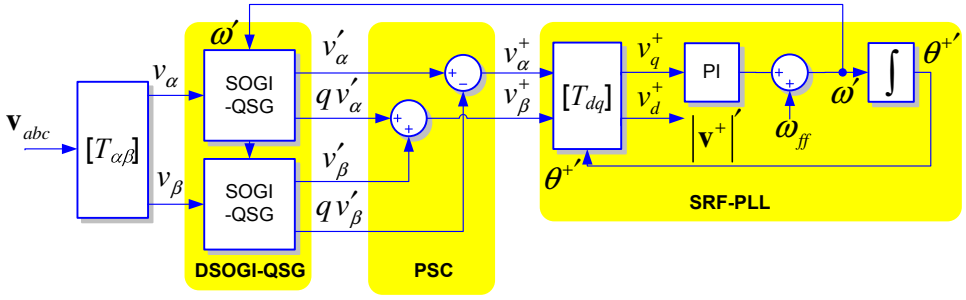

Fig. 7. Block diagram of the DSOGI-PLL

Fig. 6(b) shows the grid frequency step (-20%) and how the SRF-PLL evolutions toward the new frequency value. It is worth to remark that, in front of this big frequency jump, the response of the positive-sequence detector is in steady state again after a stabilization period shorter than 100 ms.

To evaluate the effect of the SRF-PLL on the dynamics of the detection system, the faulty voltages used in Section IV are now applied to the input of the DSOGI-PLL of Fig. 7. The most significant signals from this simulation are shown in Fig. 8, where it is possible to observe the good behavior of the proposed frequency-adaptive positive-sequence detector. Regarding simulation results shown in Fig. 4, the additional delay due to the SRF-PLL is small and the response of the system is completely stabilized after about two grid cycles.

The robustness of the DSOGI-PLL in presence of distorted grid voltages is finally evaluated. In this simulation, the unbalanced and distorted grid voltage during the fault consisted of $\mathbf{v}^{+1} = 0.747\angle\underline{-14^\circ}$, $\mathbf{v}^{-1} = 0.163\angle\underline{8.63^\circ}$, $\mathbf{v}^{-5} = 0.07\angle\underline{-60^\circ}$ and $\mathbf{v}^{+7} = 0.05\angle\underline{30^\circ}$, being $\mathbf{v}_{pf}^{+1} = 1\angle\underline{0^\circ}$ the pre-fault grid voltage. Fig. 9 illustrates the behavior of the DSOGI-PLL in such operating conditions and verifies its harmonics rejection capability. Positive-sequence voltage of Fig. 9(e) is practically sinusoidal and balanced, and its harmonic components are given by $\mathbf{P}^{-5}\mathbf{v}^{-5} = 0.008\angle\underline{-113^\circ}$ and $\mathbf{P}^{+7}\mathbf{v}^{+7} = 0.0057\angle\underline{-48^\circ}$.

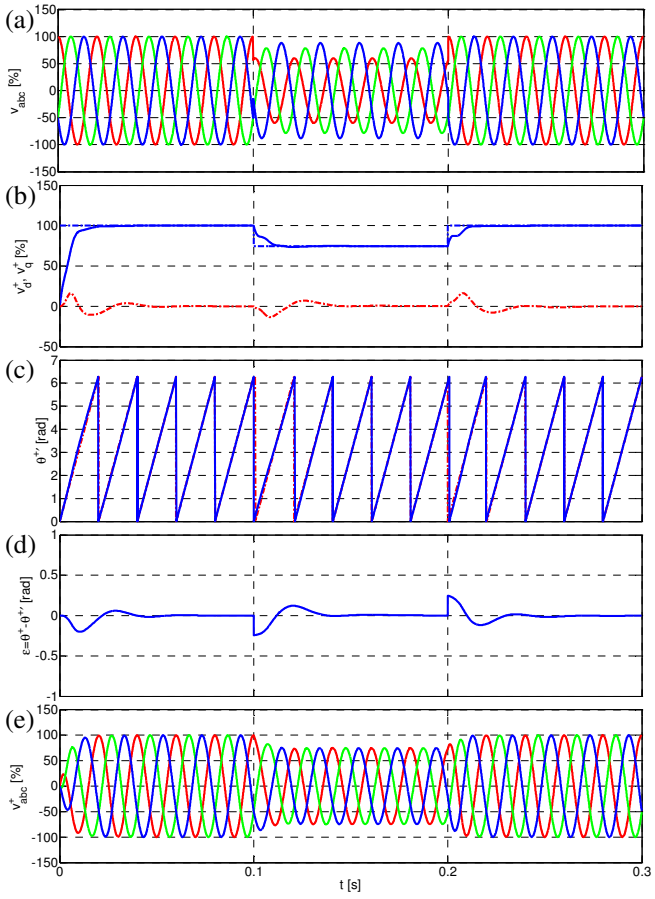

Fig. 8: Characteristic signals of the DSOGI-PLL in presence of an unbalanced voltage sag with k=1.41, k_p=2.22, and k_i=61.69.

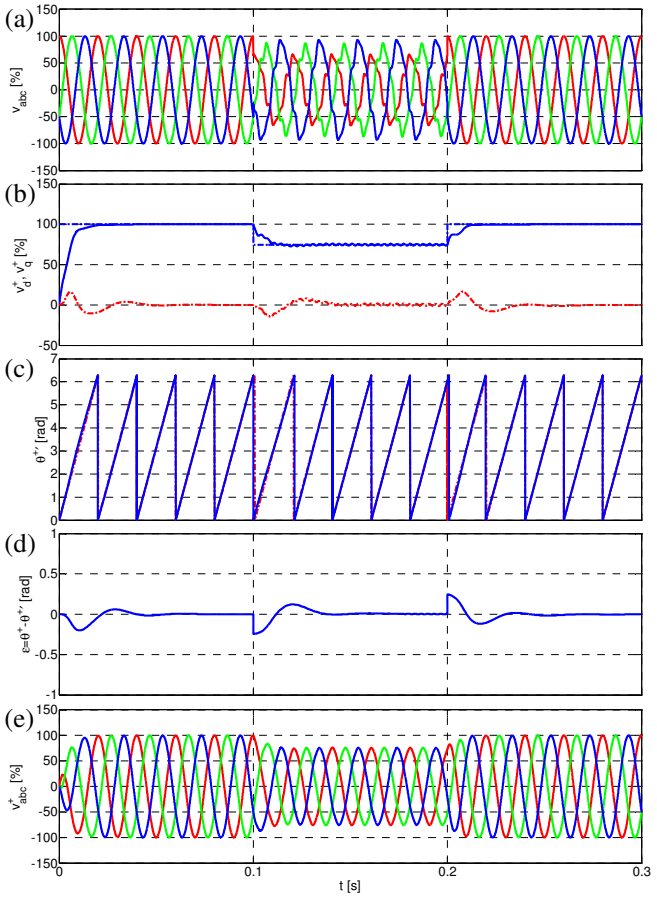

Fig. 9: Characteristic signals of the DSOGI-PLL in presence of distorted and unbalanced grid voltages with k=1.41, k_p=2.22, and k_i=61.69.

VI. CONCLUSION

From the study and results presented in this paper, it can be concluded that the proposed DSOGI-PLL provides an effective solution for grid synchronization of power converters under grid faulty conditions.

The DSOGI-PLL is based on a systematic use of well known techniques. The SOGI is the building block of the QSG and offers harmonic blocking capability to the system. The ISC method on the $\alpha\beta$ reference frame provides an effective mechanism to easily calculate the positive-sequence voltage component. The SRF-PLL makes the detection system frequency-adaptive. The joint action of such techniques converts the DSOGI-PLL to a high-performance detection system which allows fast and precise characterization of the positive-sequence voltage component even under extreme unbalanced and distorted grid operating conditions. Conclusions drawn from the theoretical study of the DSOGI-PLL are ratified by simulation.

ACKNOWLEDGMENT

This work was supported by Ministerio de Ciencia y Tecnologia of Spain under Project ENE2004-07881-C03-02.

REFERENCES

[1] C. Jauch, J. Matevosyan, T. Ackermann, and S. Bolik, "International comparison of requirements for connection of wind turbines to power systems," *Wind Energy*, vol. 8, pp. 295-306, Jul. 2005.

[2] A. Ghosh and A. Joshi, "A new algorithm for the generation of reference voltages of a DVR using the method of instantaneous symmetrical components," *IEEE Power Eng. Review*, vol. 22, pp. 63-65, Jan. 2002.

[3] T. Ackermann, *Wind Power in Power Systems*, England: John Wiley & Sons, Ltd., 2005.

[4] V. Kaura and V. Blasco, "Operation of a phase locked loop system under distorted utility conditions," *IEEE Trans. Ind. Applicat.*, vol. 33, pp. 58-63, Jan./Feb. 1997.

[5] S. Chung, "A phase tracking system for three phase utility interface inverters," *IEEE Trans. Power Electron.*, vol. 15, pp. 431-438, May 2000.

[6] P. Rodríguez, J. Pou, J. Bergas, I. Candela, R. Burgos, and D. Boroyevich, "Double synchronous reference frame PLL for power converters," *in Proc. IEEE Power Electron. Spec. Conf. (PESC'05)*, 2005, pp. 1415-1421.

[7] M. Karimi-Ghartemani and M.R. Iravani, "A method for synchronization of power electronic converters in polluted and variable-frequency environments," *IEEE Trans. Power Systems*, vol. 19, pp. 1263-1270, Aug. 2004.

[8] W. V. Lyon, *Application of the Method of Symmetrical Components*, New York: McGraw-Hill, 1937.

[9] S. Luo and Z. Hou, "An adaptive detecting method for harmonic and reactive currents," *IEEE Trans. on Ind. Electron.*, vol. 42, pp. 85-89, Feb. 1995.

[10] M. Saitou, N. Matsui, and T. Shimizu, "A control strategy of single-phase active filter using a novel d-q transformation," *in Proc. IEEE Ind. Applicat. Conf. (IAS'03)*, 2003, vol. 2, pp. 1222-1227.

[11] S.M. Silva, B.M. Lopes, B.J.C. Filho, R.P. Campana, and W.C. Bosventura, "Performance evaluation of PLL algorithms for single-phase grid-connected systems," *in Proc. IEEE Ind. Applicat. Conf. (IAS'04)*, 2004, vol. 4, pp. 2259-2263.

[12] X. Yuan, W. Merk, H. Stemmler, J. Allmeling, "Stationary-frame generalized integrators for current control of active power filters with zero steady-state error for current harmonics of concern under unbalanced and distorted operating conditions," *IEEE Trans. on Ind Applicat.*, vol. 38, pp.523 – 532, Mar./Apr. 2002.

[13] R. Teodorescu, F. Blaabjerg, U. Borup, and M. Liserre, "A new control structure for grid-connected LCL PV inverters with zero steady-state error and selective harmonic compensation," *in Proc. IEEE App. Power Electron. Conf. and Exp. (APEC'04)*, 2004, vol.1, pp. 580-586.

[14] L.D. Zhang, M.H.J. Bollen, "Characteristic of voltage dips (sags) in power systems," *IEEE Trans. Power delivery*, vol. 15, pp. 827-832, Apr. 2000.

Publication 7

Grid monitoring for distribution power generation systems to comply with grid codes

by A. Timbus, P. Rodriguez, R. Teodorescu and F. Blaabjerg
Article published in Proceedings of ISIE'06, pages 1608-1612, 2006

Grid Monitoring for Distributed Power Generation Systems to Comply with Grid Codes

Adrian V. Timbus, *Student Member, IEEE*, Pedro Rodriguez, *Member, IEEE*, Remus Teodorescu, *Senior Member, IEEE* and Frede Blaabjerg, *Fellow, IEEE*

***Abstract*—This paper investigates the possibility of using the Phase-Looked Loop (PLL) algorithms for grid monitoring. The main interest is on the ability of the PLL to determine accurately other grid variables except the phase angle. The main focus is set on the voltage amplitude and frequency estimation but other attributes of the PLL systems such as the possibility to detect unbalance and to extract the positive and negative sequence from the grid voltages are also discussed. A detailed description of standards for wind turbine (WT) and photovoltaic (PV) systems regarding grid monitoring is given and the simulation results of the proposed PLL are compared with the values stated in these standards. Based on this comparison, it can be concluded that PLL system can be used with success for grid monitoring.**

***Index Terms*—Distributed generation systems, grid monitoring, grid codes, PLL, positive and negative sequence.**

I. Introduction

DISTRIBUTED Power Generation Systems (DPGS) based on renewable energy are more and more contributing to the energy production everywhere around the world. A total capacity of 50 GW wind power has been installed at the end of 2005 worldwide, with Germany, Denmark and Spain sharing 80% of this capacity. Nearly 20% of the Danish electricity production is generated by the wind systems which indicates a growth of the grid integration of such systems.

Due to the increased number of grid connected systems, more restrictive standard demands are requested by the Transmission System Operators (TSO) in order to ensure a proper functionality of the utility network. Boundaries of operation for both voltage and frequency are specified in order to protect both the utility and the generation system. In the case when these boundaries are exceeding, the distribution system should cease to energize the utility network. Therefore, the DPGS should have a monitoring unit which continuously measures or estimates the grid voltage amplitude and frequency in order to be able to disconnect in the requested time.

This paper discusses the possibility of using the PLL system already present in most of the modern DPGS for detection of grid voltage magnitude and frequency. Focus will be put on the time of detection and how fast this is compared to the requested disconnection time specified in the grid codes. Additionally, the capability of the PLL system to extract the positive and negative sequence of the unbalanced grid is also addressed in this work.

A.V. Timbus, R. Teodorescu and F. Blaabjerg are with the Institute of Energy Technology, Aalborg University, DK-9220 Aalborg, Denmark. Email: avt@iet.aau.dk, ret@iet.aau.dk, fbl@iet.aau.dk

P. Rodriguez is with the Dept. of Electrotechnical and Electronic Engineering, Technical University of Catalonia, Spain. Email: prodriguez@ee.upc.edu

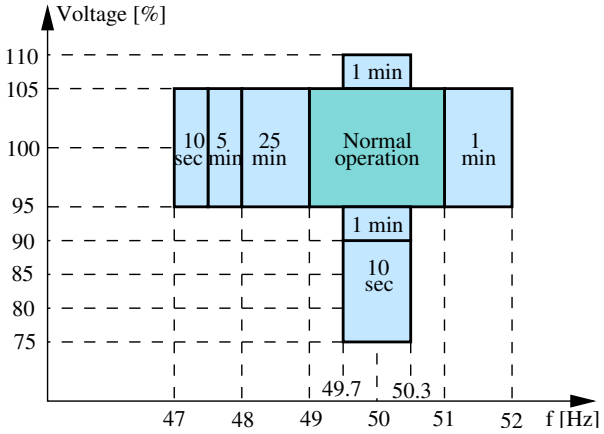

Fig. 1. Boundaries of operation and clearing times for both voltage and frequency according to the Danish grid operator [3].

A description of the PLL algorithms which can be used for grid monitoring is first given and one of them is selected to be treated in this work. This is followed by the grid monitoring demands requested by different grid operators or standards, where the voltage amplitude and frequency boundaries as well as the disconnection time is emphasized. Further on, the proposed PLL system is detailed described and the results for different grid situations are finally presented.

II. PLL in Grid Monitoring

In [1], different PLL algorithms for three phase DPGS are investigated and evaluated in respect to the phase angle estimation. Among the synchronization algorithms presented there, only two of them are able to additionally estimate both amplitude and frequency of the grid voltage, i.e. the PLL implemented in synchronous reference frame denoted as *dq PLL* and the *adaptive PLL*.

The latest is well described in [2] where the structure, design and results of this algorithm in respect to grid variables variations are presented. This structure employs three different controllers to detect the amplitude, frequency and phase angle of each grid voltage. Therefore, in the situation of a three phase system, nine such controllers are necessary, having a considerable contribution to the complexity of the monitoring unit. Anyway, it should be noticed that this PLL algorithm provides information about each voltage of the utility grid, i.e. voltage amplitude, frequency and phase angle. Due to the detailed information and results presented in [2], this structure is not considered here.

The most common PLL technique used for three phase grid tied converters is the algorithm implemented in synchronous reference frame [4], [5]. Regarding phase angle estimation, this technique behaves satisfactory in the situation of normal grid conditions. Anyway, when grid faults occur, especially in the case of unbalanced faults, this algorithm necessitates additional improvements in order to provide a clean synchronization signal [6]–[8]. The improvements normally consists in different filtering techniques which are able to filter out the negative sequence voltage which appears in the situation of unbalanced faults. Taking advantage of the additional filters, the *dq PLL* is able to generate an output signal which is synchronized with the positive sequence of the grid voltages.

Anyway, additionally to the phase angle, the synchronous reference frame PLL is capable to track the magnitude and the frequency of its input signals, e.g. the grid voltages. This additional features as well as a proposed algorithm for detecting the positive and the negative sequence attached to the *dq PLL* is the subject of this work.

III. Grid demands

As previously mentioned, grid monitoring demands are requested for the power generation system interconnecting the utility network. The demands country specific and are varying in respect to the generation system type, i.e. wind turbines (WT), photovoltaic (PV) systems. In this work, grid monitoring demands for WT connected into the Danish power system are considered along to the demands for the PV systems connected in Europe and North America.

A. Grid demands for wind turbines

A graphical representation of the allowed operation range in respect to the grid voltage and frequency for WT connected into the Danish utility is illustrated in Fig. 1. A normal operation area between 95 and 105% of the nominal grid voltage and ± 0.3 Hz around the nominal frequency is defined. Either frequency or voltage amplitude exceeds the stated limits, the wind turbine should disconnect within the specified time interval. Therefore, in order to be able to disconnect in time, the wind turbine should monitor both voltage amplitude and its frequency.

TABLE I
VOLTAGE BOUNDARIES AND DISCONNECTION TIMES FOR PV SYSTEMS.

Voltage (at PCC)		Trip time
	V < 50%	6 cycles
50% <	V < 88%	120 cycles
88% <	V < 110%	normal operation
110% <	V < 127%	120 cycles
137% <	V	2 cycles

B. Grid demands for PV systems

Regarding the frequency range that a PV system can run on, this is as large as $\pm$ 1Hz in Europe [9], $\pm$ 0.5 Hz in North America [10] and $\pm$ 0.2 Hz in Germany, Austria and Switzerland [11]. If this range is exceeding, the disconnection time is 0.2 seconds in all cases.

Table I shows the voltage boundaries for photovoltaic systems according to [12]. While the frequency boundaries are more stringent compared to those applying to WT systems, the voltage boundaries stated in Table I are more relaxed. A normal operation condition between 88 and 110% deviation for nominal grid voltage amplitude is allowed according to [12].

It is worth to notice that an algorithm for accurate detection of the values for both voltage amplitude and frequency is necessary for DPGS in order to avoid tripping of the systems when utility network experience disturbances that bring the voltage or frequency at the disconnection boundary.

IV. Proposed PLL algorithm for grid monitoring

The structure of the proposed PLL algorithm for grid monitoring is shown in Fig. 2. This structure consists of four major blocks, namely the transformation modules, the algorithm for compensating for unbalance, the PLL controller and the algorithm for detection of the positive and negative component of the grid voltage during the unbalanced faults.

A. Transformation modules

Since the *dq PLL* is implemented in synchronous reference frame, transformation modules are necessary to convert the phase voltages into *dq* frame. The conversion into the orthogonal stationary frame is given by the following equations:

$$\mathbf{U}_{\alpha\beta} = \begin{bmatrix} U_\alpha & U_\beta \end{bmatrix}^T = [T_{\alpha\beta}]\ \mathbf{U}_{abc} \tag{1a}$$

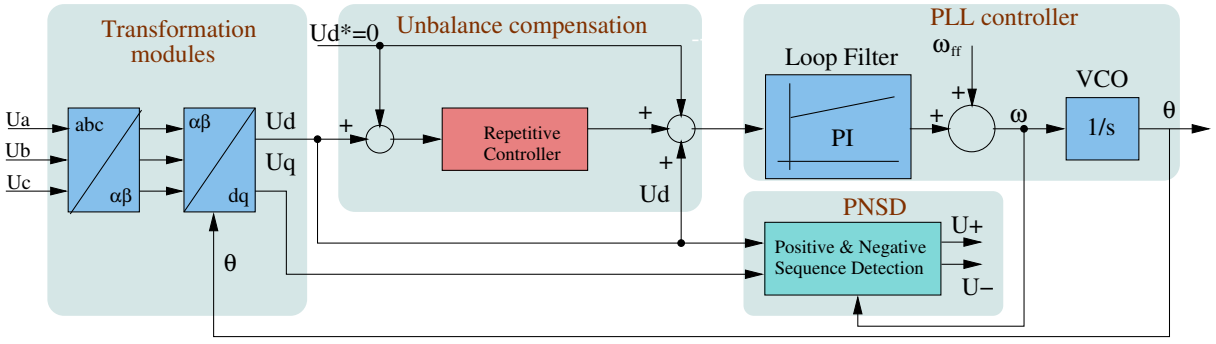

Fig. 2. The structure of the proposed PLL for grid monitoring.

$$[T_{\alpha\beta}] = \sqrt{\frac{2}{3}} \begin{bmatrix} 1 & -\frac{1}{2} & -\frac{1}{2} \\ 0 & \frac{\sqrt{3}}{2} & -\frac{\sqrt{3}}{2} \end{bmatrix} \quad (1b)$$

Further on, the stationary voltages are transformed into synchronous reference frame using:

$$\mathbf{U}_{dq} = \begin{bmatrix} U_d & U_q \end{bmatrix}^T = [T_{dq}]\, \mathbf{U}_{\alpha\beta} \quad (2a)$$

$$[T_{dq}] = \begin{bmatrix} cos\theta & sin\theta \\ -sin\theta & cos\theta \end{bmatrix} \quad (2b)$$

In this way, the d and q components of the grid voltages become dc values, with U_d being zero and U_q representing the magnitude of the grid voltage. Thus, the *dq PLL* algorithm is capable to detect the amplitude of the grid voltage.

B. Unbalance compensation

As previously mentioned, in the case of unbalanced grid faults, the conventional *dq PLL* fails to provide a clean synchronization angle for control. Moreover, during this kind of faults, the magnitude of grid voltage U_q presents double frequency oscillations in its waveform. Therefore, in this work, an algorithm which compensate for the unbalance based on a repetitive controller introduced in the PLL loop is suggested [7]. Anyway, the algorithm which filters out the negative sequence is placed after the transformation modules in the PLL cascaded loop, as it is illustrated in Fig. 2. Hence, the voltage U_q will register oscillations anyway, due to the direct influence of the unbalanced grid voltages through Eq. (1a) and (2a). Noticeable is that in the situation of unbalanced grid faults, the repetitive controller filters out the negative sequence component, thus the PLL algorithm is providing the phase angle of the positive sequence component [7]. As the phase angle θ is fed back into the transformation module, the resulting U_q signal will represent the voltage magnitude of the positive sequence.

C. Positive and negative sequence calculation

Since U_q presents oscillations during grid faults, additional signal processing is necessary in order to get the exact value of the magnitude of the positive sequence. Therefore, filtering is applied to U_q inside the positive and negative sequence calculator, as illustrated in Fig. 3.

Owing to the fact that the oscillations exhibited by U_q are at double frequency, a delay signal cancellation (DSC) filter

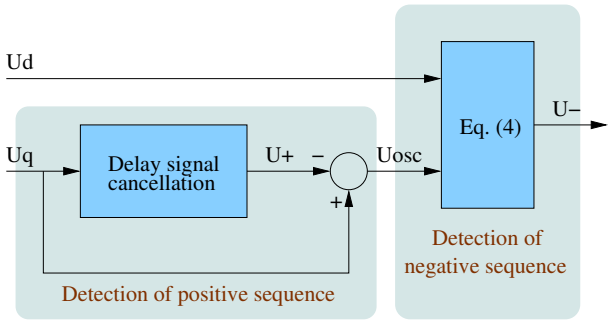

Fig. 3. The proposed algorithm for detecting the positive and negative sequence.

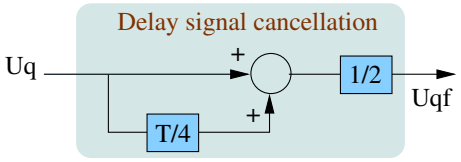

Fig. 4. The proposed filtering technique for cancellation of double frequency oscillations in the U_q signal.

[13] is a suitable solution in this case. The structure of this filter is illustrated in Fig. 4. As it might be noticed, the U_q signal is delayed with a quarter of the fundamental period T and then subtracted from the original signal. In this way, the double frequency oscillations are canceled with minimum delay time. It is worth to remark that in the situations when the grid frequency deviates from its nominal value, this filtering technique fails to cancel the oscillations. A solution to this is to use the frequency signal estimated by the PLL as input into the filter and calculate the fundamental period as:

$$T = \frac{2 \cdot \pi}{\omega} \quad (3)$$

In this way, the DSC filter is self adapting in respect to the grid frequency and its performance is kept even though the grid frequency deviates form its nominal value.

The effectiveness of the DSC filter in canceling the double frequency oscillation of U_q is shown in Fig. 5. As it might be noticed, this filter completely eliminates the oscillations present in the input signal, providing a smooth dc signal equal to the mean value of the input signal. This signal, denoted as U_+, represents the positive sequence of the grid voltage. In order to detect the negative sequence, further signal processing is used. First, the positive sequence U_+ is subtracted from the original U_q signal, leading to a signal U_{osc} that contains only the double frequency oscillations, without any dc component in it. This signal is further used in conjunction with the d-axis voltage U_d for the calculation of the negative sequence:

$$U_- = \sqrt{U_d^2 + U_{osc}^2} \quad (4)$$

D. PLL controller

The phase locking of this system is realized by controlling the d-axis voltage to zero. Normally, a PI controller is used for this purpose. The controller determines the dynamics of this system, thus the bandwidth of the controller is a trade off between the filtering performance and the locking time of

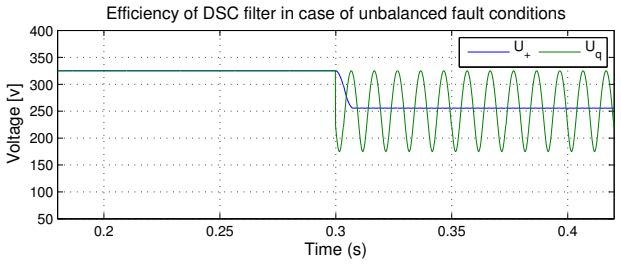

Fig. 5. The effectiveness of the DSC filter to cancel the double frequency oscillation of the U_q signal during unbalanced situations.

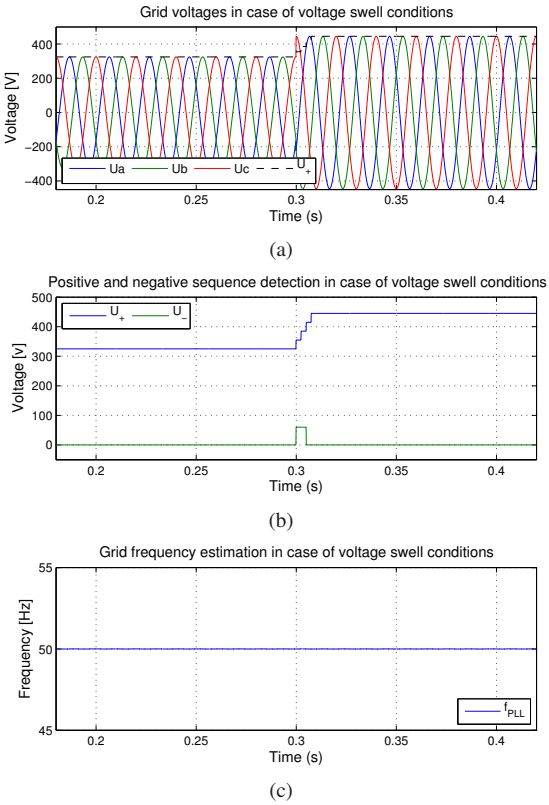

Fig. 6. Simualtion results in the case of balanced fault condition: (a) grid voltages having an amplitude increase up 137% of their nominal value, (b) positive and negative sequence detection and (c) grid frequency estimation using the proposed PLL system for grid monitoring.

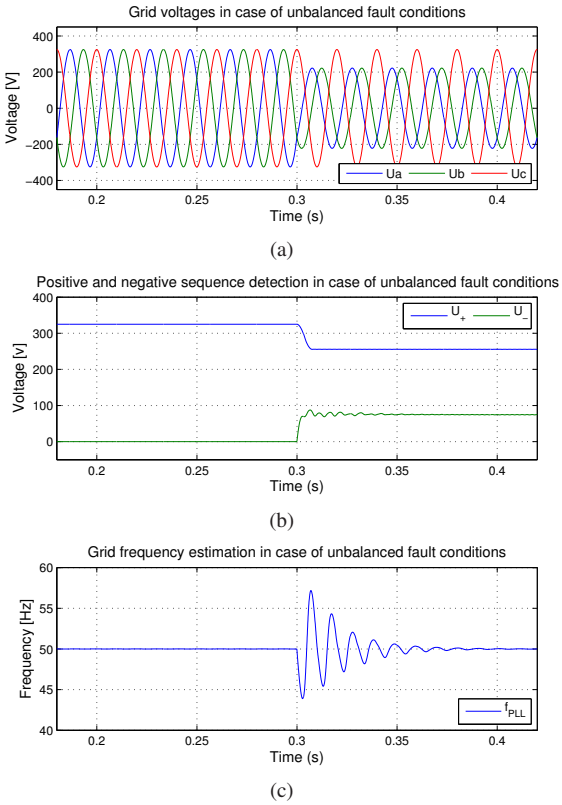

Fig. 7. Simualtion results in the case of unbalanced fault condition: (a) grid voltages registering an unbalance fault, (b) positive and negative sequence detection and (c) grid frequency estimation using the proposed PLL system for grid monitoring.

the PLL. In [1], a design of the PLL controller which gives the possibility to set the locking time of the system has been proposed. Anyway, the structure proposed here and illustrated in Fig. 2 contains a repetitive controller which has influence in the dynamics of the system. This issue is well addressed in [7] hence is not further discussed here. It is worth noticing that a locking time of 0.06 seconds is used for the PI controller while a rejection time of the unbalance of 0.08 seconds is used for the repetitive controller in this work.

As it is illustrated in Fig. 2, the output of the PI controller is the grid frequency. As a consequence, this structure can also detect the value of the grid frequency which can be further used in control for disconnection purpose or as an adaptive input is some controllers [14].

V. Validation of the Proposed System for Grid Monitoring

In order to validate the proposed system for grid monitoring, simulation results in the situation of balanced and unbalanced faulty grid conditions and frequency deviations are presented in the followings. The accuracy in detection of grid variables as well as the detection time is mainly pursued in the next plots.

A. Results in the case of balanced fault

Fig. 6 shows the detection of the magnitude of the grid voltage (split into its positive and negative sequence) and the grid frequency in the situation of a balanced fault. A balanced fault situation in which the grid voltages have an increase in amplitude up to 137% of their nominal value is simulated to comply with the most stringent demand stated in Table I. Characteristic to the balanced faults is the absence of the negative sequence from the grid voltages during the fault [15]. Hence, the positive sequence component of the grid voltage estimated by the proposed PLL coincides with the magnitude of the grid voltages as depicted in Fig. 6(a), while the negative sequence is zero as reported in Fig. 6(b). The response time of the proposed PLL system in detection of the grid voltage magnitude is within a half of cycle, being 4 times faster than the requirement from the standards. As it can be observed in Fig. 6(c), there is no problem for the proposed PLL algorithm to estimate the correct value of the grid frequency in this situation.

B. Results in the case of unbalanced faults

The behavior of the proposed monitoring system in the situation of unbalanced grid conditions is presented in Fig. 7. In this situation, two of the grid voltages register a drop in amplitude and a jump in their phases. The negative sequence appears in the grid voltages in this situation and this is correctly detected along with the positive sequence by the *Positive & Negative Sequence Calculator*, as illustrated in Fig. 7(b). A small transient is observed in the waveform of the positive sequence, while a little bit longer oscillations are

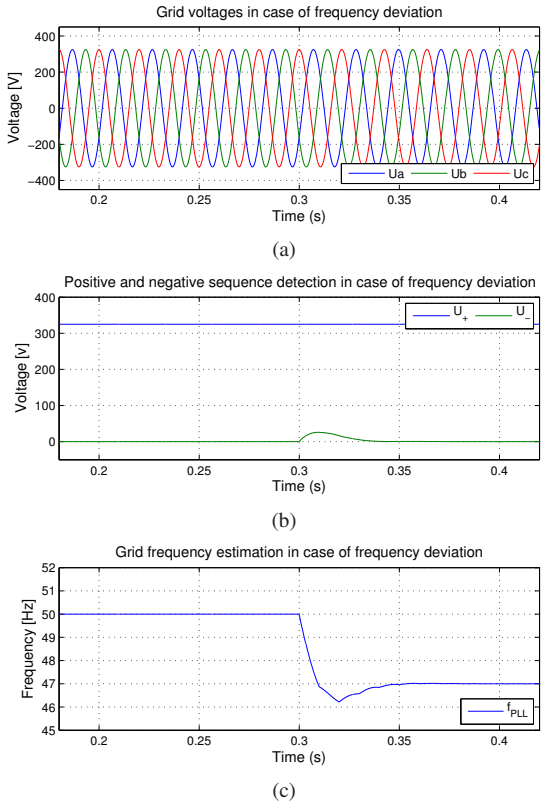

Fig. 8. Simualtion results in the case of normal grid condition: (a) grid voltages, (b) positive and negative sequence detection and (c) grid frequency estimation using the proposed PLL system for grid monitoring.

appearing in the waveform of the negative sequence. Anyway, the proposed PLL is able to provide a steady value for both sequences within two fundamental cycles. A frequency oscillation during the fault transient is noticed in Fig. 7(c), but this is fast reduced to the nominal value by the proposed system.

C. Results in the case of frequency deviation

Finally, the proposed system for grid monitoring is tested in the case of grid frequency variations. In Fig. 8(a), the grid voltages register a frequency drop of 3 Hz at the simulation time 0.3 seconds. This drop is sudden sensed by the PLL, which in about two fundamental periods detects the new value of the frequency. The detection is 4 times faster as compared with the standard demands for PV systems and 200 times faster compared to wind turbines requirements.

VI. Conclusion

This paper presents a PLL algorithm for grid monitoring. The utilization of PLL for grid synchronization has been investigated in several previous studies but the extension of this algorithm to grid monitoring has not been addressed.

The PLL system presented here additionally comprises an algorithm for cancellation the effect of negative sequence in the situation of unbalanced grid faults and an algorithm for detecting the positive and negative components of the grid voltage whenever these exist.

Simulation results have shown the capability of the conventional PLL system used in conjunction with the above mentioned algorithms to provide exact information about the grid amplitude and frequency. Moreover, the proposed PLL system can estimate the grid variables faster than the standards are requesting, hence it can be used with success for distributed power generation systems.

References

[1] A. V. Timbus, M. Liserre, R. Teodorescu, and F. Blaabjerg, "Synchronization methods for three phase distributed power generation systems. An overview and evaluation," in *Proc. of PESC'05*, 2005, pp. 2474–2481.

[2] D. Jovcic, "Phase Locked Loop system for FACTS," *IEEE Trans. on Power Systems*, vol. 18, no. 3, pp. 1116–1124, 2003.

[3] Eltra and Elkraft, "Wind turbines connected to grids with voltage below 100 kV," http://www.eltra.dk, 2004.

[4] S.-K. Chung, "A phase tracking system for three phase utility interface inverters," *IEEE Trans. on Power Electronics*, vol. 15, no. 3, pp. 431–438, 2000.

[5] V. Kaura and V. Blasko, "Operation of a phase loop system under distorted utility conditions," *IEEE Trans. on Industry Applications*, vol. 33, no. 1, pp. 58–63, 1997.

[6] P. Rodriguez, J. Pou, J. Bergas, I. Candela, R. Burgos, and D. Boroyevich, "Double synchronous reference frame PLL for power converters," in *Proc. of PESC'05*, 2005, pp. 1415–1421.

[7] A. V. Timbus, M. Liserre, F. Blaabjerg, R. Teodorescu, and P. Rodriguez, "PLL algorithm for power generation systems robust to grid faults," in *Proc. of PESC'06*, 2006, pp. 1360–1366.

[8] M. C. Benhabib and S. Saadate, "A new robust experimentally validated Phase-Looked Loop for power electronic control," *EPE Journal*, vol. 15, no. 3, pp. 36–48, August 2005.

[9] IEC Standard 61727, "Characteristic of the utility interface for photovoltaic (PV) systems," IEC, Tech. Rep., 2002.

[10] IEEE15471, "IEEE standard for interconnecting distributed resources with electric power systems," 2005.

[11] DIN and VDE, "Automatic disconnection device between a generator and the public low-voltage grid," Standard, 2005.

[12] IEEE929, "IEEE recommended practice for utility interface of photovoltaic (PV) systems," 2000.

[13] G. Saccomando and J. Svensson, "Transient operation of grid-connected voltage source converter under unbalanced voltage conditions," in *Proc. of IAS'01*, vol. 4, Chicago, IL, 2001, pp. 2419–2424.

[14] A. V. Timbus, M. Ciobotaru, R. Teodorescu, and F. Blaabjerg, "Adaptive resonant controller for grid-connected converters in distributed power genaration systems," in *In Proc. of APEC'06*, 2006, pp. 1601–1606.

[15] M. H. J. Bollen, *Understanding Power Quality Problems: Voltage Sags and Interruptions*. IEEE Press, 2002.

Publication 8

Online grid measurement and ENS detection for PV inverter running on highly inductive grid

by A. Timbus, R. Teodorescu, F. Blaabjerg and U. Borup
Article published in Power Electronics Letters, volume 2, pages 77-82, 2004

Online Grid Measurement and ENS Detection for PV Inverter Running on Highly Inductive Grid

Adrian V. Timbus, *Student Member, IEEE*, Remus Teodorescu, *Senior Member, IEEE*,
Frede Blaabjerg, *Fellow, IEEE* and Uffe Borup

***Abstract*—Photovoltaic and other sources of renewable energy are being used increasingly in grid-connected systems, for which stronger power quality requirements are being issued. Continuous grid monitoring should be considered so as to provide safe connections and disconnections from the grid. This paper gives an overview of the methods used for online grid measurement with photovoltaic (PV) inverters. Emphasis is placed on a method based on the injection of a non-characteristic harmonic in the grid. Since this injection is regarded as a disturbance for the grid, different issues, i.e., the influence on total harmonic distorsion (THD), the accuracy of line impedance measurement and the ENS (German abbreviation of Main Monitoring units with allocated Switching Devices) detection are studied. Laboratory results conducted on an existing PV inverter are presented to demonstrate the behavior of the PV inverter under different grid conditions. Some of the injection parameters are tuned in order to get an accurate measurement of line impedance.**

***Index Terms*—power system monitoring, grid impedance measurement, ENS detection, highly inductive grid, PV inverter.**

I. Introduction

IN RECENT years the number of grid connected systems using photovoltaic PV has increased considerably [1]. Besides all electrical regulations, such systems should also comply with certain country-specific technical recommendations, especially when connecting into dispersed power-generating networks. This makes grid detection and the islanding isolation method for PV equipment a must in many situations, e.g., in Germany (the ENS-standard).

The European regulation EN503301-1 [2] sets the utility fail-safe protective interface for the PV line-commutated converters. The goal of the regulation is to isolate the supply within 5 seconds due to impedance changes of 0.5 Ω. The grid impedance step changes are detected by means of tracking and step-change evaluation of the dynamic grid impedance. Therefore, PV inverters should make use of an on-line measurement technique in order to meet the regulation requirements of the utility fail-safe interface. In [3]- [8], grid impedance detection is well described but the methods presented are not always easy to implement in a non-dedicated platform such as a PV inverter. One method where grid impedance can be estimated with existing sensors in a PV inverter using a logical control algorithm can be found in [9]. This method provides a fast and simple algorithm for line impedance estimation to comply with standards. However, even though the proposed method theoretically provides the result of the grid impedance, when used in the context of a PV inverter, the quality of the measurement is affected by different implementation issues. Thus, specific limitations such as real-time computation, medium a/d conversion accuracy, fixed point numerical limitation, etc., become real challenges if one is to keep the initial requirement of a fast and reliable method [10].

A.V. Timbus, R. Teodorescu and F. Blaabjerg are with the Institute of Energy Technology, Aalborg University, DK-9220 Aalborg, Denmark. Email: avt@iet.aau.dk, ret@iet.aau.dk, fbl@iet.aau.dk

U. Borup is with the Powerlynx A/S, Jyllandsgade 28, DK-6400 Sønderborg, Denmark

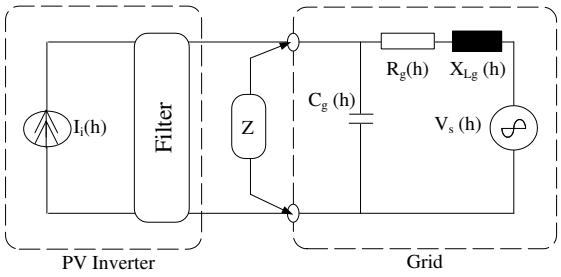

Fig. 1. PV inverter connected to grid with grid impedance measuring.

This paper briefly presents the method for grid impedance detection given in [9]. The method is based on the injection of a non-characteristic harmonic into the grid. Since this injection is a disturbance for the grid, issues such as the amplitude of the non-characteristic injection, its frequency, and the influence on the line impedance measurement are discussed, as they influence both the accuracy of the line impedance measurement and the current THD.

II. Grid Impedance Detection Techniques

Various techniques can be used for line impedance measurements. Note that usually these methods employ special hardware devices as shown in Fig. 1. Once the input is acquired by voltage and current measurement, processing follows, with many mathematical calculations to obtain the impedance value.

The dedicated measuring device is denoted by the "Z" block and is normally a separate part of the inverter. The resistive and inductive parts of the grid are denoted as R_g and L_g respectively, while V_s is the ideal source supply. The capacitive part of the model from the consumer side is C_g. The *h* argument of the components shows the model dependency on the harmonic order. In the literature, the solutions for the line impedance measurement are split into two major categories: *passive* and *active* methods.

The passive methods use the non-characteristic harmonics (line voltages and currents) that are already present in the

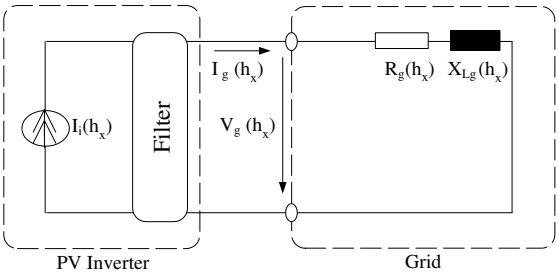

Fig. 2. PV inverter connected to grid considering non-characteristic harmonic h_x.

system. These methods depend on the existing background distortion of the voltage and, in numerous cases, the distortion has neither the amplitude nor the repetition rate to be properly measured [11]. (This will not be the case when implementing it into a PV inverter.)

Active methods make use of a deliberate "disturbance" of the power supply network followed by acquisition and signal processing. Ways of "disturbing" the network can vary, therefore active methods are further divided into two major categories: transient methods and steady-state methods. These are described in [12] – [14].

III. Proposed Method

A steady-state technique is used. It is based on the injection of a non-characteristic harmonic current into the network and records the voltage change response [9]. Fourier analysis of the particular injected harmonic is used to process the result. In this way, the method has control of the injected current and computation is necessary only to find specific Fourier terms essential to obtain the final result.

The principle of operation is to inject the non-characteristic harmonic current into the grid using the PV inverter. Fig. 2 shows the network model with respect to the non-characteristic harmonic denoted as h_x. Compared with Fig. 1 it is clear that $V_s(h_x)$ is zero if the respective harmonic is assumed to be outside the network. Furthermore, if the injected harmonic is considered to be of low frequency, the parallel capacitor can be eliminated.The PV inverter is used to inject the harmonic current (see Fig. 2) by adding a harmonic voltage to the voltage reference of the PV inverter, thereby eliminating the "Z" block in Fig. 1. Using the same sensors (denoted by I_g and V_g) as for the control loop, the PV records the time-domain response waveforms. The measurements are processed by Fourier analysis for the specific harmonic used, and finally the injected harmonic voltage and current are obtained.

The grid impedance is calculated by:

$$\underline{Z} = \frac{\underline{V}(h)}{\underline{I}(h)} \tag{1}$$

$$\underline{Z} = \frac{V \cdot e^{j\varphi_V}}{I \cdot e^{j\varphi_I}} = Z \cdot e^{j\varphi_Z} \tag{2}$$

$$\underline{Z} = R_g + j \cdot \omega_h \cdot L_g \tag{3}$$

where R_g and L_g denote the resistive and inductive part of the grid and ω_h represents the frequency of the injected harmonic.

Since the grid impedance of the fundamental frequency is the one pursued, further processing should be done. The value of the grid impedance at the frequency of 50 Hz (ω_{50}) can be calculated by a simple mathematical substitution as:

$$\underline{Z}(50Hz) = R_g + j \cdot \omega_{50} \cdot L_g \tag{4}$$

To save processing time and avoid CPU overloading, there are two alternatives to choose from. First, it is assumed that the injected frequency is close to the fundamental frequency; thus the grid impedance value is similar for both frequencies. Second, a correction factor based on the grid characteristic can be used to save processing time. However, since usually there is no prior information as to where the PV inverter will operate, implementing such a grid correction factor turns out to be more likely a case-to-case practice, and embedded in the final PV product.

Given that the injected frequency is a disturbance of the grid, injections should not be made continuously. The injection duration is chosen to be limited to a few fundamental periods and it is periodic such that multiple results (running the algorithm) enable averaging of the impedance within the required duration of 5 seconds [2]. Random errors due to noise and a/d flickering may be minimized. Moreover, decreasing the duration of the harmonic injection will limit the total current harmonic distortion and permit more than one inverter to be actively connected to the same grid.

IV. Inverter Structure

The structure of the PV inverter used for tests in the laboratory is shown in Fig. 3. It comprises a dc-dc converter, an inverter bridge and an embedded digital signal processor (DSP) board. Moreover, a liquid crystal display (LCD) indicating the estimated value for the grid impedance as well as many other measurements are available inside the PV inverter, i.e., grid current, grid voltage, etc. A tripping and protection unit is also implemented inside the PV inverter for the purpose of connecting and disconnecting the inverter from the grid wherever necessary. Current regulation in the grid is made by a resonant controller based on [15]. The software developed can be downloaded into the DSP memory using a computer and contains all controls necessary to run the inverter in a proper manner.

V. Inverter behavior on different grid conditions

When injecting a non-characteristic harmonic into the grid, there are a few issues to be considered. From the grid point of view, the injected non-characteristic harmonic is regarded as a disturbance. This disturbance has a negative influence on the THD of the grid; thus attention must be paid to its amplitude, injection frequency and the duration of the injection in order to comply with the standards. Further, it is interesting to study the influence of this injection (more precisely, its parameters) on other issues in the case of a PV inverter, i.e., ENS detection, the estimation of line impedance, etc. To enable observation of the influence of the injection on the THD of the grid and

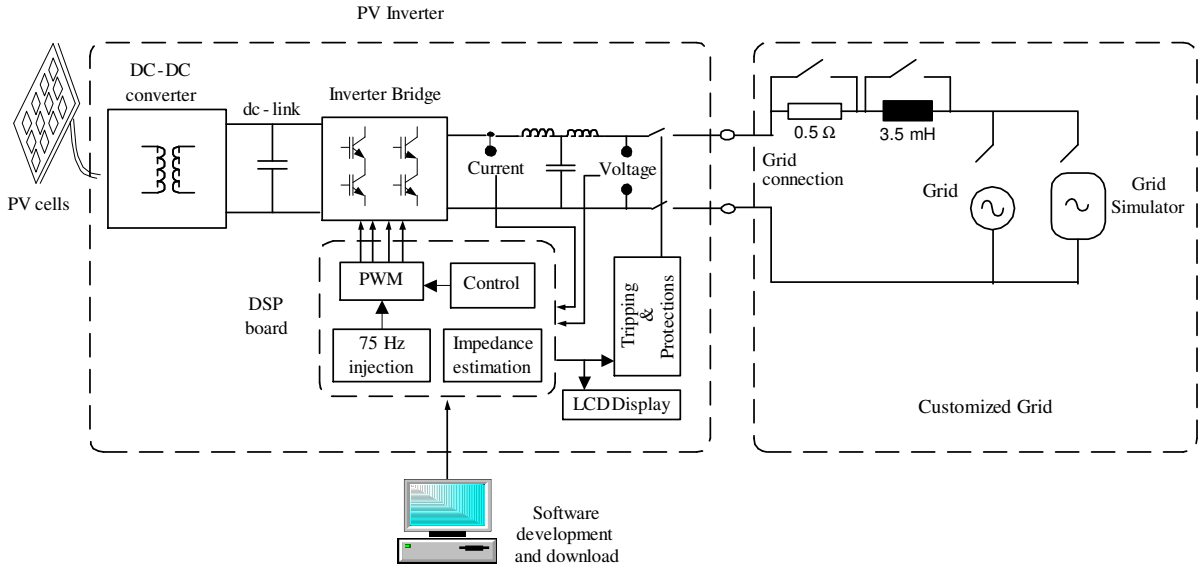

Fig. 3. Overview of the structure of PV inverter and setup for test of different conditions.

on the PV inverter performance, a few laboratory tests have been carried out using a customized grid (see Fig. 3).

A 0.5 Ω resistor may be connected in series with the grid and used to apply a step change in the line impedance as the ENS standard requires [2]. In this way, the isolation method can be verified if it complies with the standard demands when the line impedance varies by more than 0.5 Ω. Furthermore, an inductor of 3.5 mH also may be connected in series with the grid. This inductor has an impedance of 1.1 Ω at the fundamental frequency of 50 Hz and is used to obtain highly inductive grid conditions. Finally, the inverter can be connected to the real network or to a grid simulator. The grid simulator is used to obtain a low impedance grid.

Based on tests, it has been observed that the inverter behaves similarly on both the low impedance and high purely resistive grids. The accuracy of grid impedance measurements and consistency in ENS detection are not influenced by the line impedance value; thus the inverter can operate on both low and high impedance grids.

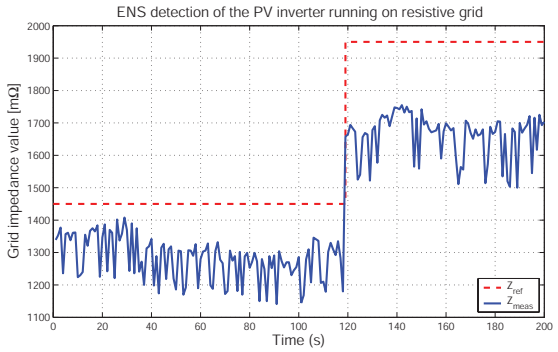

Fig. 4. Measurement of grid impedance and detection of 0.5 Ω change (120 s) in line impedance when the PV inverter runs on a pure resistive grid.

Inverter behavior running on a resistive grid is shown in Fig. 4. The 0.5 Ω resistor and the 3.5 mH inductor are not connected to the circuit. The PV inverter injects the non-characteristic harmonic in order to measure the line impedance. The acquired result is quite close to the real value of the line impedance measured with a dedicated device. The error is slightly above 10 %. After a 120 second time period, the 0.5 Ω resistor is connected to the circuit. This leads to an increase in the line impedance and the inverter should be able to detect the change. As can be seen from Fig. 4, the PV inverter detects the change but not completely. It calculates the value for grid impedance with an error of 15 %. Most important is the fact that the PV inverter is capable of distinguishing a large change in line impedance such as the one that occurred when a 0.5 Ω resistor was connected in series with the grid. Another issue is that the oscillations of the calculated line impedance signal are small compared to the change in the line impedance after connecting the 0.5 Ω resistor. This allows setting a trip level large enough for ENS detection and avoiding parasitic trips of the PV inverter.

A different behavior has been observed when the inverter is running on a highly inductive grid compared to a resistive grid. If a 3.5 mH inductor is connected to the circuit, the accuracy of the grid impedance measurement as well as the ENS detection are influenced considerably. The oscillations of the calculated line impedance signal are increased and the detection of the 0.5 Ω change in the line impedance is considerably reduced. Thus, the parameters of the non-characteristic harmonic injected in the grid should be tuned in order to obtain satisfactory results whenever the PV inverter is running on a highly inductive grid.

VI. Injection Parameters Tuning

The problems that occur when the PV inverter is running on a highly inductive grid can be avoided by tuning the

parameters of the injection, i.e., the amplitude of the injection, its duration and the injection frequency. There are only a few limitations in the tuning process and these arise due to hardware structure and standard demands. For exmple, considering the THD distortion of the grid, a low amplitude for the injected non-characteristic harmonic is preferred to keep the disturbance of the grid below the standards limit. Since the amplitude of the non-characteristic harmonic is used for the line impedance measurement [9], it should be large enough to be distinguished from the current spectrum while processing the discrete Fourier transform (DFT) and performing the calculation of grid impedance. This fact leads to a compromised selection of the amplitude value for the non-characteristic harmonic. The same principle applies for the other parameters of the injection.

A. Amplitude of the injected non-characteristic harmonic

Selecting the correct value for the amplitude of the non-characteristic harmonic involves a compromise between measurement accuracy and low distortion of the grid. Laboratory experiments were conducted at different amplitude levels. The detection of change with $0.5\ \Omega$ in line impedance value was also monitored. All tests were conducted when the PV inverter was running on a highly inductive grid, since the results on the purely resistive grid were satisfactory.

Three tests were performed with different values for the amplitude of the injected non-characteristic harmonic. The values were 0.02 p.u., 0.05 p.u. and 0.07 p.u.. The smallest value is low enough not to disturb the grid more than the standards allow. Line impedance as well as the detection of change with a $0.5\ \Omega$ in line impedance are depicted in Fig. 5(a).

From Fig. 5(a) it can be observed that the accuracy of the measurement is quite poor; the error in line impedance measurement is almost 40 % of the real value (1850 mΩ) of the impedance, as measured with a dedicated apparatus. Moreover, when the step of the $0.5\ \Omega$ pure resistive is applied in the grid impedance (after a 90s time period), the PV inverter seems not to be able to detect it. Thus its performance is unsatisfactory.

In addition, the PV inverter adds an oscillating signal along the time for the line impedance due to the large inductance in the circuit, thus being exposed to parasitic trips.

The same test is performed with 0.05 p.u. to see how the PV inverter behaves with a larger amplitude of injected harmonic. Results are shown in Fig. 5(b). The PV inverter more accurately measures the line impedance, and the error in measurement is decreased to 30 % of its real value (1880 mΩ). Furthermore, when the step change of $0.5\ \Omega$ in the line impedance is applied (after 90s), the inverter is capable of partially detecting this change. Even though the detection of the grid impedance after the $0.5\ \Omega$ step is applied is less than its real value, it is an improvement compared to the tests shown in Fig. 5(a). In order to find the boundary of the amplitude value of the injected non-characteristic harmonic, a last test is made with a value of 0.07 p.u.. The results are shown in Fig. 5(c). An unsatisfactory behavior of the PV inverter is noticed. The measured value for grid impedance is less than its real value by 33 % and the detection of the $0.5\ \Omega$ change in the line impedance is diminished to half of this value. Another disadvantage of using 0.07 p.u. for the amplitude of the injection is that the THD is considerably increased related to the situation when the amplitude of 0.05 p.u. is used.

Based on these tests, the value of 0.05 p.u. is chosen for the amplitude of the non-characteristic harmonic. The reason is also related to the power transfer from the PV inverter to the grid. The injection of the non-characteristic harmonic yields an extra active power injection into the grid, and this active power should be minimized as much as possible. The value of 0.05 p.u. is the best compromise between low injected active power and accuracy for line impedance detection.

B. Duration of injection

There are a few benefits if the injection of the non-characteristic harmonic is not continuous. First, the total current harmonic distortion is minimized if the non-characteristic harmonic is injected for only a few fundamental periods. Second, processing time is saved and overloading the CPU is avoided, since the line impedance calculation, and thus DFT, are made only periodically. Finally, periodical injection will allow other PV inverters to be connected and take measurements on the same grid. The duration of the non-characteristic harmonic injection takes two fundamental periods (50 Hz). Because the calculation of the impedance is time consuming, it is split over a few switching periods. Thus, 1 ms after the injection occurs, the value for line impedance is obtained. Based on this, it is decided to inject the non-characteristic harmonic for only two fundamental periods.

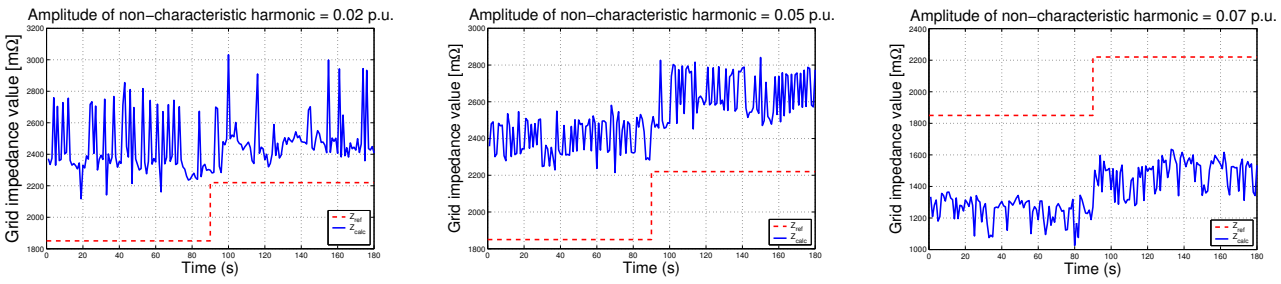

(a) (b) (c)

Fig. 5. Measurement of line impedance and detection of $0.5\ \Omega$ change (90 s) in grid impedance with different injecting signals: (a) 0.02 p.u., (b) 0.05 p.u. and (c) 0.07 p.u..

C. Frequency of the injection

If the injection of the non-characteristic harmonic is not made continuously, its frequency has to be set. For a lower THD, fewer injections are preferable, but this gives poor information. According to the ENS standard [2], the inverter should detect the 0.5 Ω change in grid impedance and trip within 5 seconds. Therefore, within the 5-second time interval, the inverter needs sufficient information about the value of line impedance.

Based on the tests performed in laboratory, the value for the injection frequency is chosen to be 1 second. The injection of the PV inverter is depicted in Fig. 6. With a higher injection frequency the inverter has more information about grid impedance, but this also leads to an increased THD of the current and allows fewer inverters to run in parallel. In this case, the inverter may not detect the 0.5 Ω change in the grid impedance in the requested time of 5 seconds and thus the ENS detection fails. The chosen value of 1 second for the injection frequency is a good compromise providing a low influence on the current THD, a sufficient number of PV inverters that can be connected on the same grid and enough information about line impedance to detect the ENS. The inverter thus injects the non-characteristic harmonic every second and makes the calculations to obtain the value of the line impedance. This has proven to be sufficient to detect a 0.5 Ω change in the grid impedance.

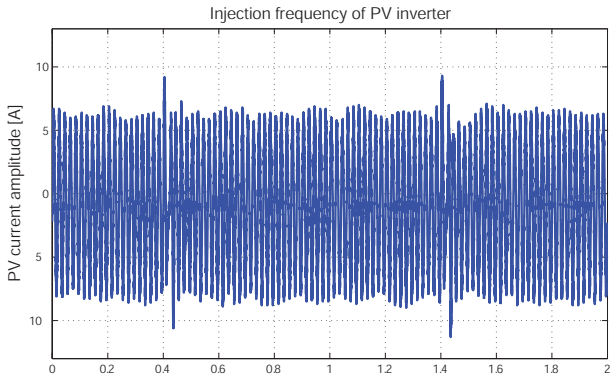

Fig. 6. Frequency of the injection set to 1 second for PV inverter.

VII. Conclusion

This paper gives a short overview of possible methods to detect grid impedance for PV inverters. One method, which allows the possibility of eliminating a dedicated unit for impedance measurement is studied. A non-characteristic harmonic is injected into the grid and, based on the response, line impedance can be estimated.

PV inverter behavior has been analyzed under different grid conditions. No problems were noticed when it was running on a purely resistive grid. In the case when the PV inverter was running on a highly inductive grid (1.66 Ω resistive combined with 1.1 Ω inductive), its performance was considerably reduced in respect to accuracy of line impedance measurement and ENS detection.

To solve this problem, the parameters of the injection were tuned according to the needs. The amplitude of the injected non-characteristic harmonic, its duration and the injection frequency were chosen in order to obtain satisfactory results. The selected values for the parameters of the injected non-characteristic harmonic are generally useful to PV inverters operating in the power range of 1.5 kW up to 4.5 kW. For inverters outside this range, the amplitude of the injection should be reconsidered in respect to hardware limitations. Laboratory results on an existing PV inverter were used to support the tuning process.

Acknowledgment

The authors acknowledge the financial support of PSO-Eltra contract 4524 and the Danish Technical Research Council contract 2058-03-0003.

References

[1] F. Blaabjerg, Z. Chen, S.B. Kjaer, “Power Electronics as Efficient Interface in Dispersed Power Generation Systems”, *IEEE Trans. on PE*, Vol.19, No. 4, 2004 (in press).

[2] European Standard EN 50330-1, Photovoltaic semiconductor converters Part 1: Utility interactive fail safe protective interface for PV-line commutated converters - Design qualification and type approval, 1999.

[3] M.B. Harris, A.W. Kelly, J.P. Rhode, M.E. Baran, ”Instrumentation for measurement of line impedance”, *Proc. of APEC’94*, 1994, Vol.2, pp. 887-893.

[4] J.P. Rhode, A.W. Kelley, M.E. Baran, ”Complete characterization of utilization-voltage power system impedance using wideband measurement”, *IEEE Trans. on Industry Applications*, Vol. 33, No. 6, 1997, pp. 1472 -1479.

[5] L.S. Czarnecki, Z. Staroszczyk, ”On-line measurement of equivalent parameters of distribution system and its load for harmonic frequencies”, *IMTC/95*, 1995, pp. 692-698.

[6] B. Palethorpe, M. Sumner, D.W.P. Thomas, ”System impedance measurement for use with active filter control”, *Proc. PEVD’00,* 2000, pp. 24-28.

[7] Z. Staroszczyk, A. Josko, ”Real-time power system linear model identification: instrumentation and algorithms”, *Proc. of IMTC*, 2000, Vol. 2, pp. 897-901.

[8] M. Tsukamoto, S. Ogawa, Y. Natsuda, Y. Minowa, S. Nishimura, “Advanced Technology to Identify Harmonics Characteristics and Results of Measuring”, 9th International Conference on Harmonics and Quality of Power, Orlando, USA, October 1-4, 2000, pp. 341-346.

[9] L. Asiminoaei, R. Teodorescu, F. Blaabjerg, U. Borup, ”A new method of on-line grid impedance estimation for PV inverters”, *Proc. of APEC’04*, 2004, Vol. 3, pp. 1527-1533.

[10] Z. Staroszczyk, ”Problems in real-time wide band identification of power systems” *Proc. of IEEE IMTC*, 1998, Vol. 2, pp. 779-784.

[11] K.O.H. Pedersen, A.H. Nielsen, N.K. Poulsen, ”Short-circuit impedance measurement”, *IEE Proc. Gener., Transm. and Distrib.*, Vol. 150, No. 2, 2003, pp. 169-174.

[12] B. Palethorpe, M. Sumner, D.W.P. Thomas, ”Power system impedance measurement using a power electronic converter”, *Proc. on Harmonics and Quality of Power*, 2000, Vol. 1, pp. 208-213.

[13] N. Ishigure, K. Matsui, F. Ueda, ”Development of an on-line impedance meter to measure the impedance of a distribution line”, *Proc. of ISIE ’01*, 2001, Vol. 1, pp. 549-554.

[14] K. Klaus-Wilhelm, ”Process and device for impedance measuring in AC networks as well as process and device for prevention of separate networks”, Deutsches Patentamt, Patentschrift DE19504271 C1/1996.

[15] R. Teodorescu, F. Blaabjerg, M. Liserre, ”Proportional-Resonant controllers. A new breed of controllers suitable for grid-connected voltage source converters”, *Proc. of Optim’04*, Brasov, Vol. 3, pp. 9-14.

Publication 9

ENS detection algorithm and its implementation for PV inverters

by A. Timbus, R. Teodorescu, F. Blaabjerg and U. Borup
Article published in IEE Electric Power Applications, volume 153, pages 206-212, 2006

ENS Detection Algorithm and Its Implementation for PV Inverters

Adrian V. Timbus, *Student Member, IEEE*, Remus Teodorescu, *Senior Member, IEEE*,
Frede Blaabjerg, *Fellow, IEEE* and Uffe Borup

***Abstract*—Due to the increased use of photovoltaic (PV) installations, new and more stringent power quality requirements are issued. The continuous grid monitoring is always a matter to be considered in order to detect islanding operation. One of the severe standards in this field is the German ENS standard. The present paper gives an overview of the methods used for online grid measurement and emphasis is put on one new method based on the injection of a non-characteristic harmonic in the grid. The algorithm for ENS detection used by the PV inverter when running both on pure resistive and highly inductive network respectively, is detailed described. Laboratory results obtained from the tests carried out on an existing PV inverter are also presented and show the method working very well.**

***Index Terms*—PV inverter, ENS detection, grid impedance measurement, power system monitoring.**

I. Introduction

In the recent years the number of grid connected systems using PV has considerably increased [1]. Besides all electrical regulations, such systems should also comply with certain country-specific technical specifications, especially when connecting into dispersed power generating networks. This makes the grid detection and the islanding isolation method for PV equipment a must in many situations.

The ENS standard (German abbreviation of Main Monitoring units with allocated Switching Devices) [2] is one of the most demanding standards in this field. The ENS test setup simulates the islanding conditions under which the PV inverter must detect the interruption of the mains circuit and disconnect within 5 seconds [2]. The same setup is used to test the disconnection within the same time interval of the PV inverter in the situation when the grid impedance is varying with 0.5 Ω. Therefore, PV inverters should make use of an online measurement technique in order to meet the regulation requirements of the utility fail-safe interface.

In [3] - [7], the grid impedance detection is well described but the methods presented are not always easy to implement into a non-dedicated platform such as a PV inverter. A proposed method where the grid impedance can be estimated with the existing sensors in the PV inverter and using a logical control algorithm can be found in [8], [9]. The method provides a fast and simple algorithm for line impedance estimation to comply with standards when using it in a PV inverter. It is also a low cost solution to meet the required standards. However, even the proposed method theoretically provides the result of the grid impedance, when using it into the context of a PV inverter, the quality of the measurement is affected by different implementation issues. Thus, specific limitations like real-time computation, medium A/D conversion accuracy, fixed point numerical limitation, etc., become real challenges in order to keep the initial requirement of a fast and reliable method [10].

This paper briefly reveals the methods for grid impedance detection and focus is on the one presented in [9]. The method is based on the injection of a non-characteristic harmonic into the grid. The ENS detection in different grid circumstances is detailed described and factors that can influence this detection method are accounted. A setup to meet the ENS test requirements is built in laboratory and the algorithm used for ENS detection as well as the results obtained are presented along the paper.

II. Grid Impedance Detection Techniques

Different techniques can be used for line impedance measurements. It is noticeable that usually these methods are using special hardware devices. Once the input is acquired by voltage and current measurement, the processing part follows, typically involving large mathematical calculations in order to obtain the impedance value. Fig. 1 shows the usual technique for impedance measuring.

The dedicated measuring device is denoted by the "Z"-block and is normally a separated part of the inverter. The resistive and inductive part of the grid is here denoted as R_g and L_g respectively, while V_s stands for the ideal source supply. The capacitive part of the model coming from the consumer side is denoted by C_g. The h argument of the components shows the model dependency on the harmonic order.

In literature, the solutions for line impedance measurement

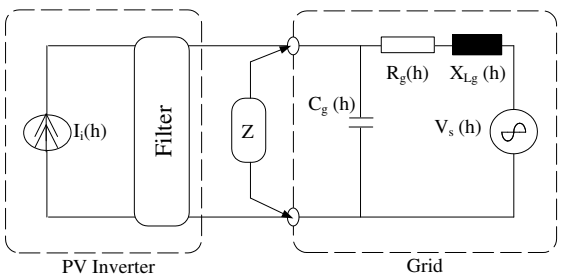

Fig. 1. PV inverter connected to grid with grid impedance measuring.

A.V. Timbus, R. Teodorescu and F. Blaabjerg are with the Institute of Energy Technology, Aalborg University, DK-9220 Aalborg, Denmark. Email: avt@iet.aau.dk, ret@iet.aau.dk, fbl@iet.aau.dk

U. Borup is with the Powerlynx A/S, Jyllandsgade 28, DK-6400 Sønderborg, Denmark

are split into two major categories: the *passive* and the *active* methods.

The passive methods are using the non-characteristic harmonics (line voltages and currents) that are already present in the system. These methods depend on the existing background distortion of the voltage and, in numerous cases, the distortion does have neither the amplitude nor the repetition rate to be properly measured [11]. This will not be the case for implementing it into a PV inverter.

The active methods make use of deliberately "disturbing" the power supply network followed by acquisition and signal processing. The way of "disturbing" the network can vary, therefore active methods are also divided into two major categories: transient methods and steady-state methods, as described in the following.

A. Transient active methods

The transient methods are well suited for obtaining fast results, due to the limited time of the disturbing effect on the network. Shortly, by this technique the "Z" device in Fig. 1 generates a transient current into the network (e.g. a resistive short-circuit), and then measures the grid voltage and current at two different time instants, before and after the impulse occurrence. The impulse will bring in a large harmonic spectrum which afterwords should be analyzed. The results obtained show the network response over a large frequency domain, making this method well suited in applications where the impedance must be known at different frequencies. However, this method must involve high performance A/D acquisition devices and should also use special numerical techniques to eliminate noise and random errors [12].

These requirements are difficult to be achieved on a non-dedicated harmonic analyzer platform like a PV inverter even if DSP-based control is used.

B. Steady-state active methods

Steady-state methods inject a known and typically periodically distortion into the grid and then make the analysis into the steady state period. One technique proposes a solution like development of a dedicated inverter topology [13] and by measuring the phase difference between supply and inverter voltage to compute the line impedance. Another technique which is easy to implement [14], repetitively connects a capacitive load to the network and measures the difference in phase shift between the voltage and the current.

III. Proposed Method

The technique used is a steady-state technique based on the injection of a non-characteristic harmonic current into the network and records the voltage change response [9]. Fourier analysis of the particular injected harmonic is used to process the result. In this way, the method has the entire control of the injected current and the computation resumes only to be specific Fourier terms to obtain the final result. It is worth to mention that this technique can be used to obtain the frequency characteristic of the grid, if the method repeats the measurements at different frequencies [4].

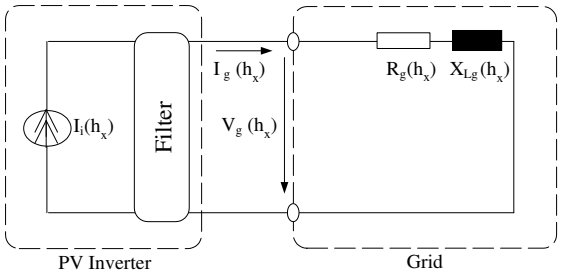

Fig. 2. PV inverter connected to grid considering non-characteristic harmonic h_x.

The principle of operation proposed by this method is to inject the non-characteristic harmonic current into the grid using the PV inverter. It has to be mentioned that the final implementation is made with an inter-harmonic component, but this harmonic is referred further as a non-characteristic harmonic to give this principle a more general approach. Fig. 2 reveals the network model with respect to the non-characteristic harmonic denoted here as h_x. If this model is compared with the one presented in Fig. 1 it is clear that $V_s(h_x)$ is zero if the respective harmonic is assumed not to be in the network. Furthermore, if the injected harmonic is considered to be of low frequency, the parallel capacitor can be eliminated due to the negligible effect at low frequencies.

As it can be seen in Fig. 2, the PV inverter is used directly to inject the harmonic current by adding a harmonic voltage to the voltage reference of the PV inverter. By this means the "Z" block shown in Fig. 1 can be completely eliminated. Using the same sensors (denoted by I_g and V_g) as for the control loop, the PV records the time-domain response waveforms. The measurements are processed in a way of Fourier analysis for the specific harmonic used, and finally the injected harmonic voltage and current are obtained.

The grid impedance can be calculated using the followings relations:

$$\underline{Z} = \frac{\underline{V}(h)}{\underline{I}(h)} \tag{1}$$

$$\underline{Z} = \frac{V \cdot e^{j\varphi_V}}{I \cdot e^{j\varphi_I}} = Z \cdot e^{j\varphi_Z} \tag{2}$$

$$\underline{Z} = R_g + j \cdot \omega_h \cdot L_g \tag{3}$$

where R_g and L_g denote the resistive and inductive part of the grid respectively and ω_h represents the frequency of the injected harmonic.

Since the grid impedance of the fundamental frequency is the one pursued, further processing should be done. The value of the grid impedance at the frequency of 50 Hz can be calculated by a simple mathematical substitution of the injected harmonic with the fundamental frequency as:

$$\underline{Z}(50Hz) = R_g + j \cdot \omega_{50} \cdot L_g \tag{4}$$

In order to save processing time and to avoid CPU overloading, there are two alternatives to choose from. First of all it is

assumed that the injected frequency is close to the fundamental frequency and thus the grid impedance value is almost similar for both frequencies. Secondly, a correction factor based on grid characteristic can be used to save processing time. However, since usually there is no prior information where the PV inverter will operate, implementing such a grid correction factor turns out to be more likely a case to case practice, embedded into the final PV product.

IV. ENS Test

To meet the requirements of the ENS test, a laboratory setup as depicted in Fig. 3 is built.

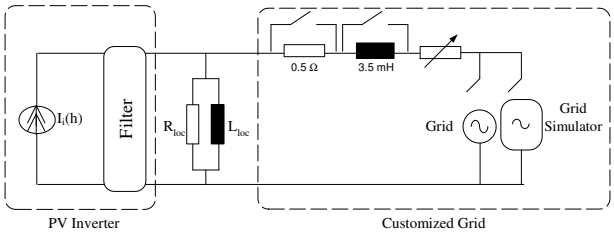

Fig. 3. PV inverter connected to grid with grid impedance measuring.

A local load composed by the resistance R_{loc} and inductance L_{loc} is connected in parallel with the PV inverter. This load is accurately adjusted so that the active and reactive power is compensated and ensures a small current flowing to the grid while the inverter runs at nominal power. To reach a network of 1.66 Ω impedance, an adjustable resistance is connected in series with the grid. This impedance of 1.66 Ω is combined with 1.1 Ω inductive (3.5 mH) to obtain the worst case scenario for the testing conditions of the PV inverter according to [2]. Furthermore, to be able to cause a suddenly change in the grid impedance, 0.5 Ω resistance is also connected in series with the grid, with the possibility of a short-circuit. Because the test is to be conducted at different network inductances, there is also a possibility to connect a grid simulator instead of the regular grid, providing lower network impedance. With these settings, the hardware test setup for ENS detection is fulfilled.

The PV inverter is injecting the non-characteristic harmonic into the grid in order to estimate the line impedance value. This value should be further processed so that the inverter can trip if a change of 0.5 Ω occurs in grid impedance. The signal processing algorithm is revealed in Fig. 4.

An averaged and delayed signal of the impedance value is subtracted from the instantaneous value of grid impedance. The resulting signal is compared with the trip level of the inverter. If this signal is larger than the trip level the PV inverter should stop within 5 seconds as the ENS standard [2] requires. Anyway, it might be the case that the trip level will not be reached in this time interval, thus leading to a testing failure of the PV inverter. Therefore, the parameters for the average and delay, as well as for the trip level, should be carefully chosen in order to give the PV inverter the possibility to detect the change in grid impedance and to stop within the requested time.

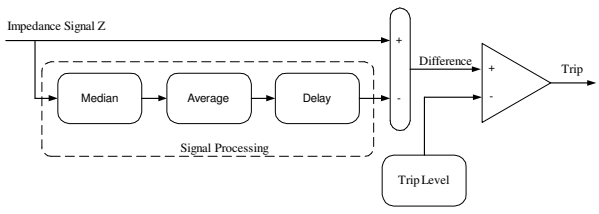

Fig. 4. ENS detection algorithm implemented in the PV inverter.

Fig. 5(a) shows the behavior of the instantaneous impedance signal and its averaged and delayed signal. When the 0.5 Ω change in the grid is applied the difference between these two signals becomes large. If this difference does not exceed the trip level, the inverter should continue to run and as a consequence the difference between the signals will become small. In the situation when the difference signal is larger than the trip level, the PV inverter should stop within 5 seconds. In Fig. 5(b), the difference between the signals is above 300 mΩ for about 4 seconds. To avoid parasitic trips of the inverter, two consecutive values over the tripping value has been set to stop the inverter. In this way, the trip level can be set to a lower value.Therefore a trip level of 200 mΩ can be set in order to be sure that the PV inverter will detect the increase in grid impedance.

V. Influence on ENS Detection

The ENS detection is not only a matter of processing the line impedance value. There are few other factors which can improve or can limit the ability of PV inverter in detecting the change in line impedance. It should be mentioned that a low cost, fix point microcontroller has been used to implement the detection algorithm. Therefore, there are some limitations in calculations when using such controller, and as it may be noticed, the accuracy in impedance detection suffers.

A. System delay

In a non-dedicated device for line impedance measurement such as a PV inverter, the delays in the system should always be compensated in order to achieve the best results. These delays can be caused by the measurement time of the dedicated devices for measuring either the voltage or current. Since the calculation of the grid impedance value is based on the measured voltage and current, the delay of these two signals should be avoided. In the case of a PV inverter, the accuracy in the grid impedance measurement is directly influenced by the delay either of voltage or current. If one of these signals is delayed it will lead to a phase shift between them, and therefore the estimation of the value for line impedance can be wrong.

One way to compensate for the delay is to take advantage of digital signal processing and to bring both signals at the same sample instant. One method to do this is to implement a running buffer for the non-delayed signal and to keep the last k samples into the buffer, where k should be equal to the delay samples between the signals. Thus, the buffered value at the address k can be used in the calculation instead of the instantaneous value of the non-delayed signal. In this way

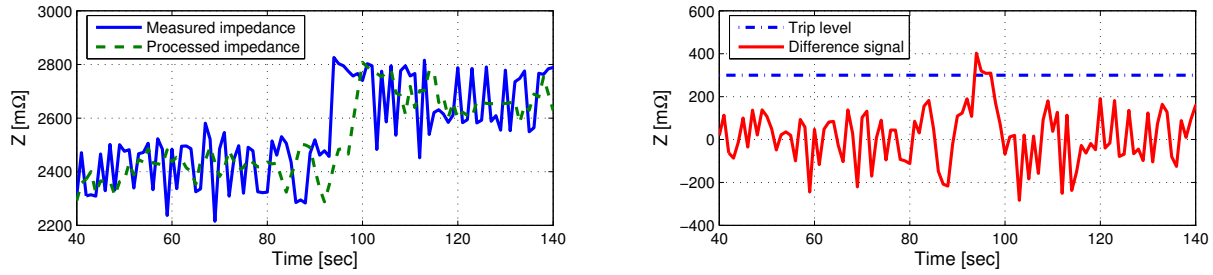

(a) (b)

Fig. 5. Impedance signal: (a) the behavior of the instantaneous and processed impedance signal when a change of 0.5 Ω is applied to the grid, (b) the difference between the signals and the trip level.

no delay between the signals is ensured but the calculation is always performed at the sample instant k instead of the instantaneous sample time.

If no delay exists between the signals used in the calculation, the accuracy of estimating the line impedance can be increased. This leads to a better detection of the 0.5 Ω change in the line impedance, thus an improvement in ENS detection.

B. Amplitude of the injection

One of the most influencing factor on ENS detection is the amplitude of the injected non-characteristic harmonic. To choose the right value for the amplitude of non-characteristic harmonic is a matter of compromise between accurate measurement of the line impedance, ENS detection and low distortion of the grid. To find this value, laboratory experiments were conducted at different amplitude values. The accuracy of the line impedance measurement as well as the detection of change with $0.5\ \Omega$ in line impedance value was also monitored. The tests are performed using the laboratory setup depicted in Fig. 3.

It is necessary to mention that the amplitude of injection is set empirically and is closely related to the grid impedance at the point where the PV system is installed. Therefore, using this algorithm, necessitates a grid impedance measurement prior installation and based on its value to decide upon the amplitude of injection. Another drawback of this method is the limited number of PV systems that can be connected in parallel on the same grid. Since the injection is disturbing the grid, many systems connected to the same point of common connection (PCC) can lead to tripping of systems and deterioration of power quality.

For the time period below 90 seconds, the inverter is running on highly inductive grid (1.66 Ω resistive combined with 1.1 Ω inductive). After 90 seconds time period the 0.5 Ω resistor is connected in the circuit providing a suddenly increase of the grid impedance value. The PV inverter behavior in respect to ENS detection is pursued along the tests.

1) Amplitude of 0.02 p.u.: The first test is performed with a low value for the amplitude of injected non-characteristic harmonic. This value is low enough not to disturb the grid more than the standards allow and the line impedance measurement as well as the detection of change with $0.5\ \Omega$ in line impedance is shown in Fig. 6(a). From Fig. 6(a), it can be observed that the accuracy of measurement in this case is quite poor, the error in line impedance measurement is almost 40 % from the real impedance value (1850 mΩ), measured with a dedicated apparatus. Moreover, after 90 seconds time period, the step of 0.5 Ω pure resistive is applied in the grid impedance, thus the real value, again measured with the dedicated device, becomes 2220 mΩ. In this situation, the PV inverter seems not to be able to detect the applied change in line impedance, its performance being poor from this point of view.

In addition, because of the large inductance present in the circuit, the PV inverter provides an oscillating signal along the time for the line impedance. As shown in Fig. 6(a), the oscillations are quite large, thus the PV inverter is more exposed to parasitic trips.

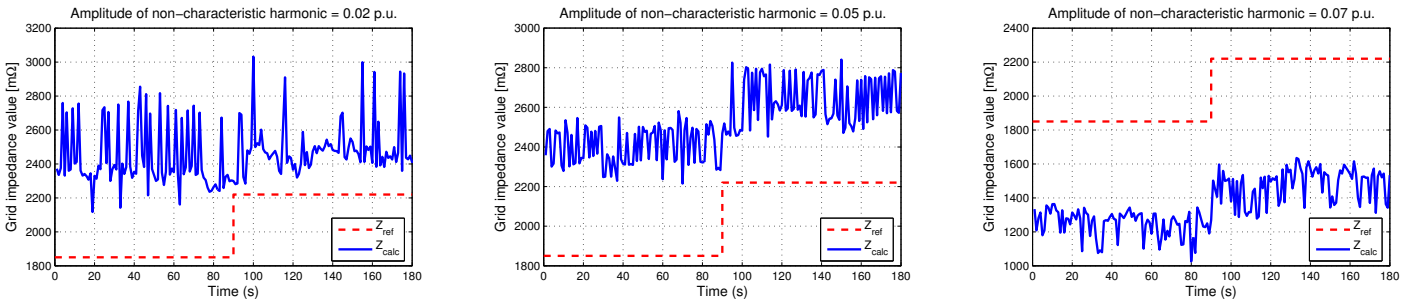

(a) (b) (c)

Fig. 6. Influence of the amplitude of the injected non-characteristic harmonic on the grid impedance measurement and ENS detection: (a) amplitude of 0.02 p.u., (b) amplitude of 0.05 p.u. and (c) amplitude of 0.07 p.u.

2) Amplitude of 0.05 p.u.: Due to the unsatisfactory behavior of the PV inverter when using 0.02 p.u. amplitude of the injected non-characteristic harmonic, this value is increased to its double. The same test is performed again to see how the PV inverter behaves with a larger amplitude of injected harmonic and the results are shown in Fig. 6(b).

In this case, the PV inverter measures more accurate the line impedance value, the error in measurement is decreased to 30 % of its real value (1880 m Ω). Furthermore, when the step change of 0.5 Ω in line impedance is applied (after 90 seconds time period), the inverter is capable to detect this change, measuring the value of grid impedance with 0.3 Ω more. Even this detection is less that its real value, it is an improvement in the behavior of PV inverter running on a highly inductive grid.

3) Amplitude of 0.07 p.u.: To find the boundary for the amplitude value of the injected non-characteristic harmonic, a last test is made with a value of 0.07 p.u.. The obtained results in this case are shown in Fig. 6(c).

Again, an unsatisfactory behavior of PV inverter is seen. This time, the measured value for grid impedance is 33 % less than its real value and the detection of the 0.5 Ω change in the line impedance is diminished to half of this value. One disadvantage using the value of 0.07 p.u. for the amplitude of the injection is that the THD of the current is considerably increased related to the situation when the amplitude of 0.05 p.u. is used. It has to be mentioned that the harmonic compensator [15] for the 3^{rd}, 5^{th} and 7^{th} harmonics is used while conducting the tests.

Based on these tests, the value of 0.05 p.u. is chosen to be used for the amplitude of the non-characteristic harmonic. This value proves to give satisfactory results in the case when PV inverter is running on highly inductive grid. Anyway, when the PV inverter is injecting the non-characteristic harmonic in order to measure the grid impedance, it draws extra power from the solar cells. As a consequence, the amplitude value of the non-characteristic harmonic is depending of the power range of the inverter.

C. Current controller gain

Due to the known drawbacks of PI controllers like the difficulty in removing the steady-state error in stationary frame controllers for single-phase systems, the need of decoupling it in three-phase systems and in general the limitations in compensating the low harmonics in order to comply with the power quality standard, a resonant controller [15] is implemented.

The Proportional+Resonant (PR) current controller is defined as in [16] and the transfer function for such controller is given by:

$$G_c(s) = \underbrace{K_p}_{proportional\ part} + \underbrace{K_i \frac{s}{s^2+\omega^2}}_{generalized\ integrator} \quad (5)$$

The Bode-plots of PR controller for different integral gains K_i and set to 50Hz frequency are shown in Fig. 7. As it can be seen from Fig. 7, this type of controller achieves very high

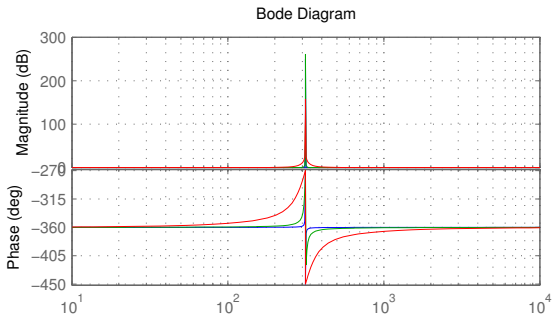

Fig. 7. Bode-plot of Proportional+Resonant (PR) controller for different values of integral gain K_i.

gain in a narrow frequency band centered around the resonance frequency. The width of this frequency band depends on the integral time constant K_i. A low K_i leads to a very narrow band while a high K_i leads to a wider band. Thus the PR controller can be tuned according to the needs.

Selective harmonic compensation can be also achieved by cascading several generalized integrators (GI) tuned to resonate at the desired frequency. In [15], the transfer function of a typical harmonic compensator (HC) designed to compensate the 3^{rd}, 5^{th} and 7^{th} harmonics, as they are the most prominent harmonics in the current spectrum, is given as:

$$G_h(s) = \sum_{h=3,5,7} K_{ih} \frac{s}{s^2 + (\omega \cdot h)^2} \quad (6)$$

An interesting feature of the HC is that it does not affect the dynamics of the PR controller, as it only reacts to the frequencies very close to the resonance frequency [16]. Thus the PR technique can be successfully used in current control for grid-converter applications where the requirements are to synchronize the current with the constant grid frequency and to compensate for the low harmonics.

From the control strategy point of view, higher integration gain is preferred for this application since it makes the current regulation more rapidly. In the situation when the harmonic compensator is enabled, lower integration gain is more suitable because it reduces the chance of interferences between the controllers due to the narrow bandwidth provided by the low gains. Furthermore, the value of the integration gain has influence in the grid impedance estimation as well as in the ENS detection. Laboratory results obtained for two values of the integration gain are shown in Fig. 8(a) and Fig. 8(b) respectively.

Fig. 8(a) shows the grid impedance calculation when using a low integration gain, e.g. K_i = 300. On the first half of the plot, the inverter is running on a pure resistive network. In this case the estimation of grid impedance value signal is not much oscillating along time but an offset in the measurement is noticed. At the time instant 100 seconds, a step of 1.1 Ω inductive (3.5 mH) is applied to the grid. It can be observed that the grid impedance calculation is influenced by a high impedance present in the grid. This phenomenon is also seen in Fig. 8(a), where the oscillations of the line impedance

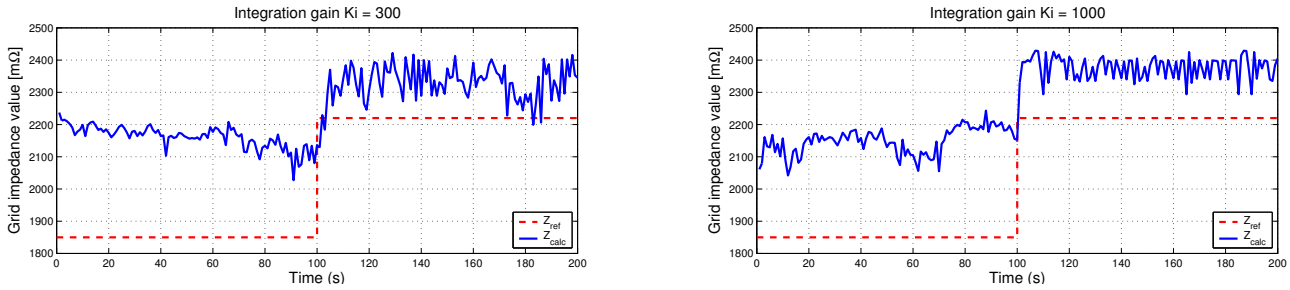

(a) (b)

Fig. 8. Influence of the integrator gain on the grid impedance measurement: (a) K_i = 300 and (b) K_i = 1000

signal are increased when the PV inverter is running on highly inductive grid.

In Fig. 8(b), the integration gain is increased to K_i = 1000 and the behavior of the PV inverter under the same grid conditions is pursued. In this situation, the grid impedance signal, after the 1.1 Ω inductive change in line impedance is applied, is less oscillating. The estimated signal is above its real value but this has only positive influence on the ENS detection. With small oscillating signal for grid impedance, the PV inverter is less exposed to the parasitic trips, therefore a higher gain is preferred in such situation.

To avoid the interferences between the harmonic compensators and to prevent the PV inverter for parasitic trips when using small integration gain, the following decision is made regarding the integration gain. In the time instant when the PV inverter is injecting the non-characteristic harmonic in order to measure the line impedance the integration gain is set to a small value, e.g. 300, while in the time period between two consecutive injections the gain is set to a high value, e.g. 1000.

D. Duration of injection

There are few benefits to take advantage of if the injection of non-characteristic harmonic is not made continuously. First of all, the total current harmonic distortion is minimized if the non-characteristic harmonic is injected only a few fundamentals period. Secondly, this will save processing time and avoid overloading the CPU since the line impedance calculation, thus DFT, are only made periodically. Finally, periodical injection will allow other PV inverters to be connected and to measure the same grid.

Based on this, it is decided to inject the non-characteristic harmonic only for two fundamental periods.

E. Frequency of the injection

If the injection of non-characteristic harmonic is not made continuously, its frequency has to be set regarding to a few aspects. For lower THD, rare injections are preferable, but this gives poor information for the inverter about the line impedance value. According to the ENS standard, the inverter should detect the 0.5 Ω change in the grid impedance and trip within 5 seconds. Therefore, in 5 second time interval, the inverter needs sufficient information about the value of line impedance so that in the case of an increase of 0.5 Ω of this value it has to be able to trip within 5 seconds.

Performing a few tests in laboratory, the value for the injection frequency is chosen to be 1 second and the injection of the PV inverter is depicted in Fig. 9. As a consequence, the inverter is injecting every second the non-characteristic harmonic and makes the calculations in order to obtain the value of the line impedance. In this way, the inverter is performing 5 calculations in the time period of 5 seconds (trip time). Tests were carried out in laboratory and the results for PV system running on a customized grid are shown in Table. I. The grid customization is obtain by connecting a resistive part r and an inductive part i. Thus, $0.64r+0.3i$ means that the grid impedance is formed by the 0.64 resistive and 0.3 inductive impedance. From tripping time values it might be concluded that the PV system is able to detect the change of 0.5 Ω taking place in the grid impedance.

Grid impedance value	Trip time	Trip value
Positive resistive step of 0.5 Ω		
0.64r+0.3i	2-3 s	0.35-0.36 Ω
0.64r+1.1i	2-3 s	0.23-0.23 Ω
0.80r+1.1i	2-3 s	0.21-0.22 Ω
1.20r+1.1i	4-5 s	0.35-0.37 Ω
1.66r+1.1i	2-3 s	0.23-0.37 Ω
Negative and positive step of 0.5Ω		
0.64r+0.3i	2-3 s	0.32-0.32 Ω
0.64r+1.1i	4-5 s	0.21-0.22 Ω
0.80r+1.1i	3-4 s	0.28-0.35 Ω
1.20r+1.1i	4-5 s	0.28-0.35 Ω
1.66r+1.1i	3-4 s	0.23-0.25 Ω

TABLE I
Measured grid impedance values and tripping times for PV inverter running on different inductive grids.

VI. Conclusion

This paper gives a short overview of the possible methods used to detect the grid impedance for PV inverters. One method, which gives the possibility to eliminate the dedicated block for impedance measurement is studied. The method is based on the injection of non-characteristic harmonic into the grid and, established on the response to it, the line impedance can be estimated.

Furthermore, the ENS detection of the PV inverter while running on highly inductive grid is described. Factors that can

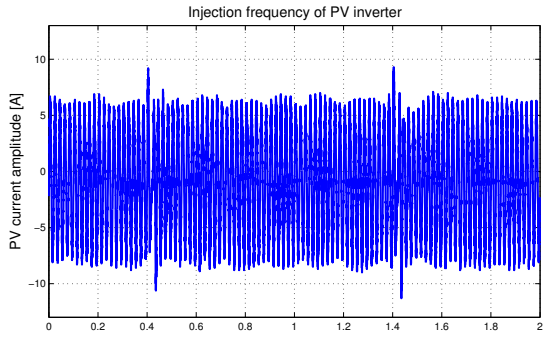

Fig. 9. Frequency of the injection set to 1 Hz.

influence this detection were accounted and their tuning in respect to the ENS detection, THD distortion and accuracy of grid impedance measurement are discussed.

As a solution for the problems issued by highly inductive grid, the parameters of the injection were tuned according to the needs. The amplitude of the injected non-characteristic harmonic, its duration and the injection frequency were chosen in order to obtain satisfactory results when the PV inverter is running on this kind of grid. Also the integration gain of the implemented resonant controller is tuned in order to obtain the best results.

The tuning rules are generally applied for the PV inverters within the power interval 1 kW up to 4.5 kW. For other power ranges of the PV inverter, the amplitude of the injected non-characteristic harmonic should be reconsidered.

Laboratory results obtained from tests on an existing PV inverter were used to support the tuning process in order to obtain a satisfactory ENS detection.

ACKNOWLEDGMENT

The authors want to acknowledge the financial support of PSO-Eltra contract 4524 and the Danish Technical Research Council contract 2058-03-0003.

REFERENCES

[1] F. Blaabjerg, Z. Chen, S.B. Kjaer, Power electronics as efficient interface in dispersed power generation systems, Trans. on Power Electronics, vol.19, no. 5, pp.1184-1194, 2004.

[2] European Standard EN 50330-1, Photovoltaic semiconductor converters Part 1: Utility interactive fail safe protective interface for PV-line commutated converters - Design qualification and type approval, 1999.

[3] M.B. Harris, A.W. Kelly, J.P. Rhode, M.E. Baran, "Instrumentation for measurement of line impedance", Proc. of APEC'94, 1994, Vol.2, pp. 887-893.

[4] J.P. Rhode, A.W. Kelley, M.E. Baran, "Complete characterization of utilization-voltage power system impedance using wideband measurement", IEEE Trans. on Industry Applications, Vol. 33, No. 6, 1997, pp. 1472 -1479.

[5] L.S. Czarnecki, Z. Staroszczyk, "On-line measurement of equivalent parameters of distribution system and its load for harmonic frequencies", IMTC/95, 1995, pp. 692-698.

[6] B. Palethorpe, M. Sumner, D.W.P. Thomas, "System impedance measurement for use with active filter control", Proc. PEVD'00, 2000. pp. 24-28.

[7] Z. Staroszczyk, A. Josko, "Real-time power system linear model identification: instrumentation and algorithms", Proc. of IMTC, 2000, Vol. 2, pp. 897-901.

[8] A. Timbus, F. Blaabjerg, R. Teodorescu, "Online Grid Measurements and ENS Detection for PV Inverters Running on Highly Inductive Grid", Power Electronics Letters, Vol. 2, No. 3, pp. 77-82, 2004

[9] L. Asiminoaei, R. Teodorescu, F. Blaabjerg, U. Borup, "A new method of on-line grid impedance estimation for PV inverters", Proc. of APEC'04, 2004, Vol. 3, pp. 1527-1533.

[10] Z. Staroszczyk, "Problems in real-time wide band identification of power systems" Proc. of IEEE IMTC, 1998, Vol. 2, pp. 779-784.

[11] K.O.H. Pedersen, A.H. Nielsen, N.K. Poulsen, "Short-circuit impedance measurement", IEE Proc. Gener., Transm. and Distrib., Vol. 150, No. 2, 2003, pp. 169-174.

[12] B. Palethorpe, M. Sumner, D.W.P. Thomas, "Power system impedance measurement using a power electronic converter", Proc. on Harmonics and Quality of Power, 2000, Vol. 1, pp. 208-213.

[13] N. Ishigure, K. Matsui, F. Ueda, "Development of an on-line impedance meter to measure the impedance of a distribution line", Proc. of ISIE '01, 2001, Vol. 1, pp. 549-554.

[14] K. Klaus-Wilhelm, "Process and device for impedance measuring in AC networks as well as process and device for prevention of separate networks", Deutsches Patentamt, Patentschrift DE19504271 C1/1996.

[15] R. Teodorescu, F. Blaabjerg, M. Liserre, "Proportional-Resonant controllers. A new breed of controllers suitable for grid-connected voltage source converters", Proc. of Optim'04, Vol. 3, pp. 9-14. Brasov.

[16] X. Yuan, W. Merk, H. Stemmler, J. Allmeling, "Stationary-Frame Generalized Integrators for Current Control of Active Power Filters with Zero Steady-State Error for Current Harmonics of Concern Under Unbalanced and Distorted Operating Conditions", IEEE Trans. on Ind. App., Vol. 38, No. 2, Mar./Apr. 2002, pp. 523-532.

Publication 10

Online grid impedance measurement suitable for multiple PV inverters running in parallel

by A. Timbus, R. Teodorescu, F. Blaabjerg and U. Borup
Article published in proceedings of APEC'06, pages 907-911, 2006

Online Grid Impedance Measurement Suitable for Multiple PV Inverters Running in Parallel

Adrian V. Timbus, *Student Member, IEEE*, Remus Teodorescu, *Senior Member, IEEE*,
Frede Blaabjerg, *Fellow, IEEE* and Uffe Borup

***Abstract*—Due to the increased use of photovoltaic (PV) installations, new and stronger grid connection requirements are issued in order to protect the utility network. One of the most severe demand applying to PV installations is the ability to detect islanding conditions. Hence, the continuous grid monitoring is always a matter to be considered in order to fulfill this requirement. The present paper gives a description of one method used for on-line grid impedance estimation by means of signal injection and focus is put on the problems issued by the situation when two or more inverters run in parallel on the same network. The paper reveals a new method to detect a second inverter connected to the grid and the proposed solution is discussed. Practical tests on an existing PV inverter validates the second inverter detection algorithm.**

***Index Terms*—Power system monitoring, grid impedance measurement, resonant controller, PV inverter.**

I. Introduction

In the recent years the number of grid connected systems using PV inverters has considerably increased. Besides all electrical regulations, such systems should also comply with certain country-specific technical recommendations, especially when connecting into dispersed power generating networks.

The European regulation EN503301-1 [1] sets the utility fail-safe protective interface for the PV-line commutated converters. The goal of the regulation is to isolate the supply within 5 seconds due to grid impedance changes of Z = 0.5 Ω. Therefore, PV inverters should make use of an on-line measurement technique in order to meet the regulation requirements of the utility fail-safe interface. In [2]–[6] the grid impedance detection is well described but the methods presented here are not always easy to implement into a non-dedicated platform such as PV inverter. A proposed method where the grid impedance can be estimated by means of signal injection with the existing sensors in the PV inverter and using a logical control algorithm can be found in [7]. This method provides a fast and simple algorithm for line impedance estimation to comply with standards when using it in a PV inverter. However, the main drawback of this paper is the dilution of estimation when multiple inverters are connected on the same feeder [8]. Therefore, conflicts and wrong estimations leading to trip out of the systems may happen when more PV inverters are connected in parallel. This paper proposes a new control method which makes it possible to run multiple inverters in parallel and still use the signal injection technique for impedance estimation.

The paper briefly reveals the method for grid impedance detection presented in [7], and focuses on the situation when two or more PV inverters are running in parallel. Difficulties appear since the grid impedance seen by one inverter is diminished by the other PV inverter output impedance. Practical issues are examined in this particular situation and new solutions are proposed for the control structure of the PV system. Experimental results validate a good behavior of the proposed solution.

A.V. Timbus, R. Teodorescu and F. Blaabjerg are with the Institute of Energy Technology, Aalborg University, DK-9220 Aalborg, Denmark. Email: avt@iet.aau.dk, ret@iet.aau.dk, fbl@iet.aau.dk

U. Borup is with the Powerlynx A/S, Jyllandsgade 28, DK-6400 Sønderborg, Denmark

II. Islanding Detection Techniques

Islanding is a condition in which a portion of the utility system, which contains both load and generation, is isolated from the remainder of the utility system and continues to operate. The isolation point is generally on the low voltage distribution line when an islanding condition exists, but islanding may also occur on the higher voltage distribution or transmission lines when large numbers of PV and other distributed generation are present [8].

A classification and major characteristics of the main techniques for islanding detection are given in [8]. These methods can be classified as following:

- methods non-resident in the PV inverter
- methods resident in the PV inverter

A. Methods non-resident in the PV inverter

1) Additional dedicated hardware: The methods non-resident in the PV inverter can be external devices attached to the PV system, as depicted in Fig. 1(a), which have the purpose of detecting islanding. The dedicated measuring device is denoted by the "Z"-block, the resistive and inductive part of the grid is here denoted as R_g and L_g respectively, while V_s stands for the ideal source supply. The capacitive part of the model coming from the consumer side is denoted by C_g. The h argument of the components shows the model dependency on the harmonic order.

2) Communication based method: Another method which is not resident in PV system uses the communication between the PV inverter and the utility network to shut down the generation system when necessary. In this case, the transmission power line can be used as communication carrier, while a signal sender is required on the utility end and a receiver is required on the PV system end. By mean of this, the utility network is able to control the connection and disconnection of the PV systems connected to the feeder.

B. Methods resident in the PV inverter

The methods resident in the PV inverter can be further divided in two categories.

1) Passive methods: The passive methods use the existent or additional sensors of the PV system to monitor the utility grid variables and thus to detect islanding. For example, a Phase-Looked Loop (PLL) system can be designed to detect both grid voltage amplitude and frequency, providing the PV system with information about the utility network status. In the case the values of these quantities exceed the limits imposed by standards [9], [10], the system would be able to cease to energize the grid due to the received information from the PLL system. Considerations regarding the dynamics of the PLL controller should be made in this case.

2) Active methods: These methods deliberately disturb the utility network and evaluate the response to the disturbance in order to detect islanding. One of them is the estimation of the utility grid impedance.

Impedance estimation: The grid impedance estimation method is one of the active methods which take advantage of a perturbation in the output current of the PV system in order to estimate the impedance. The primary advantage of the impedance measurement method is that theoretically it has an extremely small non-detection zone (NDZ) for a single PV inverter with any local load with impedance larger than the grid impedance. If the load and PV inverter output power is balanced, in the case of disconnection of the utility, the output variation of the inverter will upset this balance and cause the PV system to trip due to over voltage [8]. Anyway, degradation of the output power quality due to the injected disturbance is a major drawback. Furthermore, another serious problem of this method is the dilution of the estimation when more PV systems are connected together on the same feeder. Firstly, the systems will detect a wrong value of the grid impedance due to the output impedance of the other existing PV inverters. Secondly, there is a necessity for synchronization of the disturbance, otherwise inaccurate impedance estimation and parasite tripping may occur due to simultaneous injections when multiple PV systems are connected to the same feeder.

III. Proposed Method

The grid impedance detection technique used in this paper is a steady-state technique based on the injection of a non-characteristic harmonic current (75 Hz) into the network and records the voltage change response [7]. Fourier analysis of the particular injected harmonic is used to process the results. In this way, the method has the entire control of the injected current and the computation resumes only to be specific Fourier terms to obtain the final result.

Fig. 1(b) reveals the network model with respect to the non-characteristic harmonic denoted here as h_x. If this model is compared with the one presented in Fig. 1(a) it is clear that $V_s(h_x)$ is zero if the respective harmonic is assumed not to be in the network. Furthermore, if the injected harmonic is considered to be of low frequency, the parallel capacitor can be eliminated due to the negligible effect at low frequencies.

As it can be seen in Fig. 1(b), the PV inverter itself is used directly to inject the harmonic current by adding a harmonic

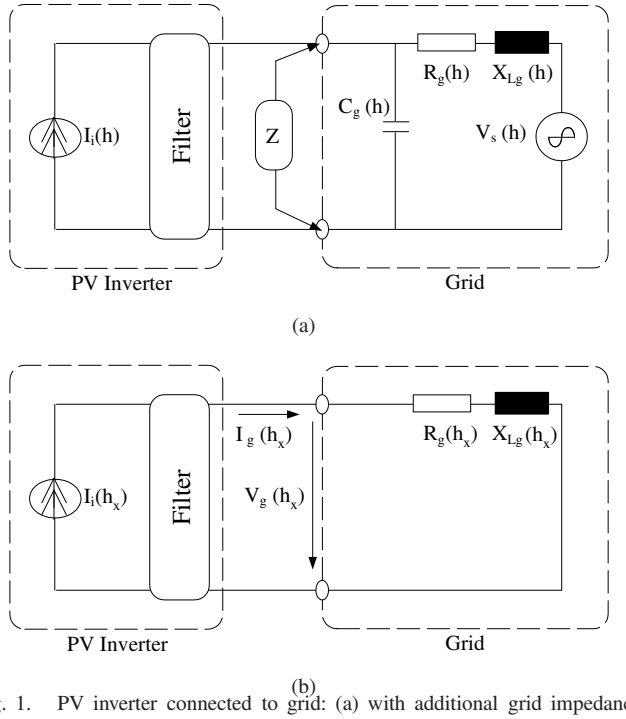

Fig. 1. PV inverter connected to grid: (a) with additional grid impedance measuring unit and (b) using non-characteristic harmonic injection.

voltage to the voltage reference of the PV inverter. By this means the "Z" block shown in Fig. 1(a) can be completely eliminated. Using the same sensors (denoted by I_g and V_g) as for the control loop, the PV records the time-domain response waveforms. The measurements are processed in a way of Fourier analysis for the specific harmonic used, and finally the injected harmonic voltage and current are obtained.

The grid impedance can be calculated using the followings relations:

$$\underline{Z} = \frac{\underline{V}(h)}{\underline{I}(h)}; \quad \underline{Z} = \frac{V \cdot e^{j\varphi_V}}{I \cdot e^{j\varphi_I}} = Z \cdot e^{j\varphi_Z}; \quad \underline{Z} = R_g + j \cdot \omega_{hx} \cdot L_g \tag{1}$$

where R_g and L_g denote the resistive and inductive part of the grid respectively and ω_{hx} represents the frequency of the injected harmonic.

Since the injected frequency is regarded as a disturbance of the grid, the injection should not be made continuously. The injection duration is chosen to be limited to a few fundamental periods and it is periodically in a way that multiple results (running algorithm) enable to average the impedance within the required duration of 5 seconds [1]. Even thought this approach has a drawback in the processing time and adds some complexity to the software, the implementation has the advantage of allowing other similar PV inverters (e.g. multiple inverters connected together in a PV farm) to operate and to measure on the same grid. An inverter uses certain duration for the measurement process and then waits to repeat the algorithm. During this interval any other similar PV inverter can measure the grid impedance.

IV. More Inverters Running in Parallel

In the case that a PV farm is composed of two or more inverters running in parallel on the same grid, there are a few

important issues to be considered. The interaction between the systems using the non-characteristic harmonic injection to estimate the grid impedance is interested to be studied. For this purpose, experiments with two inverters running on the same grid and using the same algorithm to measure the line impedance were carried out using the setup presented in Fig. 2.

As expected from the theoretical background described in the previous section, a large influence on the precision of calculation of the grid impedance was observed when two inverters inject at the same time the non-characteristic harmonic to the grid. Both PV inverters calculate a wrong value of the grid impedance in this particular situation, and therefore this should be avoided. Due to this situation, the synchronization of injections is a must when more than one inverter is running on the same feeder.

V. Injection Organization

In order to be able to organize the injection from the inverters while running in parallel on the same grid, the inverters should be capable of detecting if the non-characteristic harmonic injected is present on the grid or not. The procedure when the inverter is looking for the non-characteristic harmonic in the network is called *high impedance mode*. If this harmonic is not present in the grid, the inverter should inject its own harmonic and based on this injection to calculate the grid impedance value. In the case when the non-characteristic harmonic is present in the grid, the inverter should wait a few fundamental periods and check again if the harmonic is present.

Fig. 3 depicts the situation when two inverters are already organized in respect to their injections and both are measuring the line impedance at different time instants. In order to be able to bring the inverters to a high impedance mode and to reach the situation revealed in Fig. 3, a harmonic compensator (HC) [11] has been employed. It is worth to note that the resonant controller with harmonic compensation for lower harmonics is used in the control structure for current regulation.

A. Resonant Controller

The Proportional+Resonant (PR) current controller is defined as in [12]:

$$G_c(s) = \underbrace{K_p}_{proportional\ part} + \underbrace{K_i \frac{s}{s^2+\omega^2}}_{generalized\ integrator} \quad (2)$$

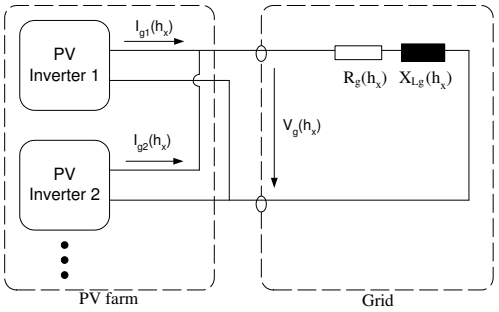

Fig. 2. PV farm with 2 inverters connected in parallel to the same grid.

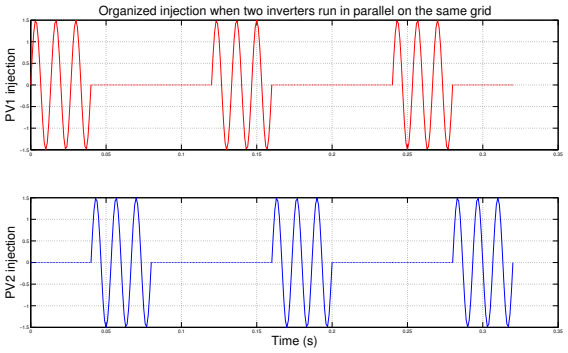

Fig. 3. Organized injection when two PV inverters are connected in parallel to the same grid.

Selective harmonic compensation can be achieved by cascading several generalized integrators tuned to resonate at the desired frequency. In [11], the transfer function of typical harmonic compensator designed to compensate the 3^{rd}, 5^{th} and 7^{th} harmonics, as they are the most prominent harmonics in the current spectrum, is given as:

$$G_h(s) = \sum_{h=3,5,7} K_{ih} \frac{s}{s^2 + (\omega \cdot h)^2} \quad (3)$$

An interesting feature of the HC is that it does not affect the dynamics of the PR controller, as it only reacts to the frequencies very close to the resonance frequency [12] . Thus the PR technique can be successfully used in current control for grid-converter applications where the requirements are to synchronize the current with the constant grid frequency and to compensate for the low harmonics.

The structure of the PR controller is shown in Fig. 4. Depending on the application demands, one can use the PR controller by itself or can enable the harmonic compensator in order to compensate for a certain frequency existing in the signal spectrum. In the case of grid connected inverters, the harmonic compensation for lower order harmonics has a considerable improvement of the total harmonic distortion (THD) of the current.

B. Organized injection using PR with HC enabled

As mentioned in §III, the inverter detects the grid impedance based on the injection of non-characteristic harmonic in the network. Therefore, implementing a harmonic compensator tuned to resonate on this harmonic, the inverter is able to

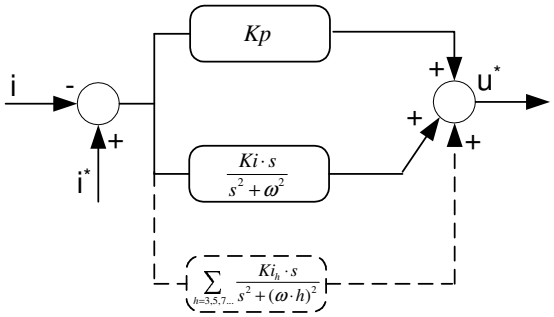

Fig. 4. Structure of PR controller with a harmonic compensation possibility.

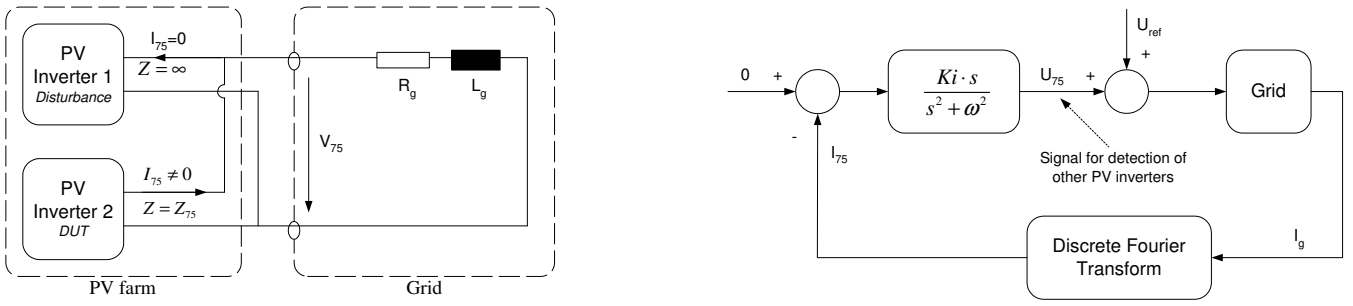

Fig. 5. (a) Principle of using harmonic compensator to detect the second inverter injecting into the grid and (b) principle of current control scheme for non-characteristic harmonic compensator.

detect its presence in the utility grid, thus to see if another inverter is performing a measurement of the grid impedance.

The compensator is used to reject the non-characteristic harmonic from the grid while the inverter is not injecting, thus a second inverter can inject and correctly measure the line impedance as it is depicted in Fig. 5(a). Let us consider the second PV inverter as the device under test (DUT) and the PV Inverter 1 being the disturbance factor. Both inverters use the same algorithm of grid impedance measurement, algorithm based on the injection of non-characteristic harmonic. The behavior of PV Inverter 2, especially the correctness of grid impedance measurement and parasitic trips occurrence, is pursued while the other inverter is running (and measuring) in parallel on the same grid.

In the case that the first inverter is not injecting the non-characteristic harmonic into the grid, it should have the reference of the harmonic compensator tuned on the injected harmonic (75 Hz in this case) set to zero. In this way, the PV Inverter 1 in Fig. 5(a) will reject any 75 Hz current flowing through it and will create an infinite impedance at this frequency on its output. If the device under test (PV Inverter 2) is connected to the grid in this situation and injects the harmonic in order to measure the grid, the whole harmonic current will flow through the grid, providing a correct measurement of the line impedance. In this manner, using a harmonic compensator tuned on the injected harmonic, the influence from the other PV inverters connected to the grid is completely avoided.

The principle of the current control for the non-characteristic harmonic compensator is shown in Fig. 5(b). The grid current is measured using the existent current sensor of the PV inverter and by means of Discrete Fourier Transform (DFT) the 75 Hz component is extracted from the current spectrum. This component is fed back into the control loop and compared with its reference, where the reference is set to zero if the inverter is not injecting and different than zero otherwise. The difference between the reference and acquired signal is regulated by the generalized integrator and its output is a voltage signal which is added to the reference voltage of the inverter. Based on the output of the 75 Hz HC (U_{75}), it can be determined if there is 75 Hz component in the grid current or not. This information can be used prior scheduling the injection, thus the PV inverters can be synchronized to inject one after each other with the same time interval between their injections.

VI. Experimental Results

A laboratory setup as the one revealed by Fig. 5(a) has been used to validate the above described method of using the resonant controller with harmonic compensator to detect a second inverter connected to the grid. In the situation when PV Inverter 1 is injecting in the same time with PV Inverter 2, the accuracy of measuring the line impedance of PV Inverter 2 is very much affected by the PV Inverter 1. The error in grid impedance value measured in this situation is larger than the trip level set according to the standards [1]. This leads to parasitic trip of the PV Inverter 2, therefore the situation when both inverters inject in the same time must be avoided.

As a consequence, the harmonic compensator tuned to resonate on the frequency of the injected non-characteristic harmonic has been added to the resonant controller previously designed to regulate the fundamental component of the current. By means of this, the inverters were brought in the *high impedance mode* and based on the output of the harmonic compensator the inverter is able to detect when another inverter is injecting the non-characteristic harmonic in the grid. Fig. 6 shows the organized injections of the inverters.

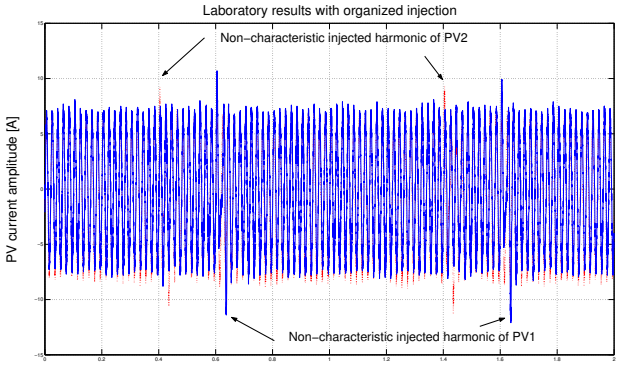

Fig. 6. Laboratory results with organized injection.

Let us consider that the DUT is the only inverter connected to the grid and measures the line impedance using the injection of non-characteristic harmonic. If another inverter, e.g. PV

Inverter 1, is connected in this situation to the grid it should detect, by means of the output of its harmonic compensator tuned to the non-characteristic harmonic (U_{75} signal), that another inverter is running and measuring the grid. Thus, PV Inverter 1 it should organize its injection so that occurs with few fundamentals periods after the injection of PV Inverter 2, avoiding the conflicting injection. Since the injections are made periodically, the injection of PV Inverter 1 will always occur after injection of PV Inverter 2, providing in this way a safe run and correct measurement of the line impedance for both PV inverters.

It is worth mentioning that the periodicity of injection of non-characteristic harmonic allows a limited number of PV inverters to run on the same grid. This number of inverters is close related to the time interval between two consecutive injections of the same PV inverter and how soon the inverters inject one after each other.

VII. Conclusion

This paper gives a short overview of the possible methods to detect the islanding conditions for PV inverters. One method, based on grid impedance estimation is described. The method is based on the injection of non-characteristic harmonic into the grid and, established on the response to it, the line impedance is calculated by means of DFT.

Furthermore, the situation when two inverters are running in parallel on the same grid is studied. The paper shows the successfully use of the resonant controller with harmonic compensator, set to resonate on the injected harmonic frequency, to detect a second inverter connected to the network. Based on the output of the harmonic compensator, the inverters can be organized so that the conflicting injection never occurs providing a safe run of many inverters on the same grid. This idea can be used on PV farms where more than one inverter is connected on the same feeder.

Acknowledgment

The authors would like to thank for the financial support of PSO-Eltra contract 4524 and the Danish Technical Research Council contract 2058-03-0003.

References

[1] OVO/ONORM, "Photovoltaic semiconductor converters - part 1: Utility interactive fail save protective interface for PV-line commutated converters," 1999.

[2] M. B. Harris, A. W. Kelly, J. P. Rhode, and M. E. Baran, "Instrumentation for measurement of line impedance," *Proc. of APEC'94*, vol. 2, pp. 887–893, 1994.

[3] J. Rhode, A. Kelley, and M. Baran, "Complete characterization of utilization-voltage power system impedance using wideband measurement," *IEEE Trans. on Industry Applications*, vol. 33, no. 6, pp. 1472–1479, 1997.

[4] L. Czarnecki and Z. Staroszczyk, "On-line measurement of equivalent parameters of distribution system and its load for harmonic frequencies," *IMTC/95*, pp. 692–698, 1995.

[5] B. Palethorpe, M. Sumner, and D. Thomas, "System impedance measurement for use with active filter control," in *Proc. of PEVD'00*, 2000, pp. 24–28.

[6] Z. Staroszczyk and A. Josko, "Real-time power system linear model identification: Instrumentation and algorithms," *Proc. of IMTC*, vol. 2, pp. 897–901, 2000.

[7] L. Asiminoaei, R. Teodorescu, F. Blaabjerg, and U. Borup, "A new method of on-line grid impedance estimation for PV inverters," *Proc. of APEC'04*, vol. 3, pp. 1527–1533, 2004.

[8] IEA-PVPS, "Evaluation of islanding detection methods for photovoltaic utility interactive power systems," IEA-PVPS, http://www.iea-pvps.org, Online report T5-09, March 2002. [Online]. Available: http://www.oja-services.nl/iea-pvps/products/download/rep5_09.pdf

[9] IEEE15471, "IEEE standard for interconnecting distributed resources with electric power systems," July 2003.

[10] IEC1727, "Characteristic of the utility interface for photovoltaic (PV) systems," November 2002.

[11] R. Teodorescu and F. Blaabjerg, "Proportional-resonant controllers.A new breed of controllers suitable for grid-connected voltage-source converters," *Proc. of OPTIM'04*, vol. 3, pp. 9–14, 2004.

[12] X. Yuan, W. Merk, H. Stemmler, and J. Allmeling, "Stationary-frame generalized integrators for current control of active power filters with zero steady-state error for current harmonics of concern under unbalanced and distorted operating conditions," *IEEE Trans. on Ind. App.*, vol. 38, no. 2, pp. 523–532, 2002.

Publication 11

Line impedance estimation using active and reactive power variations

by A. Timbus, P. Rodriguez, R. Teodorescu and M. Ciobotaru
Article published in proceedings of PESC'07, pages 1273 – 1279, 2007

Line Impedance Estimation Using Active and Reactive Power Variations

Adrian V. Timbus, *Student Member, IEEE*, Pedro Rodriguez, *Member, IEEE*, Remus Teodorescu, *Senior Member, IEEE* and Mihai Ciobotaru, *Student Member, IEEE*

***Abstract*—This paper proposes an estimation method of power system impedance based on power variations caused by a distributed power generation system (DPGS) at the point of common coupling (PCC). The proposed algorithm is computationally simple and uses the voltage variations at the point of common coupling (PCC) caused by the variations of the power delivered to utility network to derive the value of grid impedance. Accurate estimation of both resistive and inductive part of the impedance is obtained, as the results presented show.**

***Index Terms*—Line impedance, power variations, distributed generation, grid converter control.**

I. Introduction

THE value of grid impedance is a beneficial information for simulation and prediction of harmonic propagation into the power system. Moreover, with continuous connection and disconnection of loads in utility network, the line impedance value becomes vital for power system management.

Additionally, active filter control can be improved with the knowledge of line impedance value [1]–[3]. Better harmonic rejection as well as improved current controller response are obtained if the value of grid impedance is used in control [1]. Similarly, the gain of controllers for grid tied converters could be adjusted according to the value of the grid impedance ensuring system stability over a broad range of line impedance values.

Estimation of grid impedance is one of the demands for photovoltaic (PV) systems connected into the power system of some European countries for islanding detection purposes [4]. This fact was leading to an intensive research towards grid impedance identification [5]–[11]. Moreover, information about grid impedance would be useful for detection of grid faults and grid unbalance [12]. Additionally, grid impedance information can lead to identification of grid source voltage, hence the power system can be completely characterized.

As grid impedance information could be a valuable information for the control of grid connected systems, this paper proposes a simple method for accurate estimation of both resistive and inductive part of grid impedance. Due to the simplicity of the proposed algorithm and its necessity of using power variations, this method is suitable for embedding in distribution power generation systems based on variable input power, like wind turbines (WT) and photovoltaic (PV) systems.

Next section gives a short classification of existing methods to estimate the value of grid impedance. The method proposed in this work is analyzed in § III, where the equations for calculating the grid impedance as well as the methodology of applying this algorithm are discussed. Further on, the considered system comprising a grid tied converter and its control is discussed, followed by the results obtained in case of grid impedance variation. Different power variations are considered and their affect on the accuracy of detection the impedance value is discussed. Finally, the conclusions are presented in the last section.

II. Overview of methods

Generally, the methods for grid impedance detection can be classified in two main groups, i.e. passive and active methods.

A. Passive methods

Passive methods are based on monitoring and measurements of grid distortions and based on these variations, the value of grid impedance is estimated. A major drawback of the passive methods is that the grid variations might not be sufficiently large to be accurately measured, hence failing to give an exact estimation of the grid impedance.

B. Active methods

Active methods are deliberately creating a disturbance at the point of common coupling (PCC) and the grid impedance calculation is based on grid response to the distortion. The most common disturbances can be summarized as consisting of [8]:

- *current pulse transient* usually applied at zero crossing of the voltage and produces a voltage transient in the grid based on which the grid impedance can be estimated.
- *noncharacteristic subharmonics (inter-harmonics)* injected into the utility network which give the possibility of calculating the line impedance at a particular frequency.
- *power variations* of both active and reactive power produce grid voltage variations based on which the line impedance can be estimated.

In [13], [14] a current spike of 60-100 A is deliberately injected at the point of common coupling by a grid tied power converter. Based on the voltage response to this disturbance,

A.V. Timbus, R. Teodorescu and M. Ciobotaru are with the Institute of Energy Technology, Aalborg University, DK-9220 Aalborg, Denmark. Email: avt@iet.aau.dk, ret@iet.aau.dk, mpc@iet.aau.dk

P. Rodriguez is with the Technical University of Catalonia, Electrical Engineering Department, Spain, Email: prodriguez@ee.upc.edu

the grid impedance value is determined using Fourier transform. The influence of non-linear loads connected close to the point of common coupling (PCC) is also addressed and as a consequence additional signal processing method is necessary in order to obtain accurate results.

In [5]–[8], [15] injection of inter-harmonic current is used to derived the grid impedance at that particular frequency. The value of inter-harmonic has to be chosen close to the fundamental grid frequency in order to state that the identified value of grid impedance can be approximated for fundamental frequency too. Due to the fact that the selected inter-harmonic is unique in the power system and is generated by the power generation system, this particular method would allow the connection of more than one generation unit on the same grid because their synchronization in respect to the inter-harmonic injection is possible [8], [16].

III. Proposed method

This work proposes a method for detecting the grid impedance using variations of both active and reactive power generated by a grid connected generation system. The references for active and reactive power are intentionally varied in order to allow detection of both resistive and inductive parts of the line impedance. The proposed algorithm is detailed in the following.

A. Algorithm analysis

Unlike the method presented in [5] and [15], the proposed method works at a 50 Hz frequency, i.e. the fundamental component of the power is varying. Varying both active and/or reactive power it is possible to estimate the resistive and inductive parts of the impedance. The proposed method is based on the detection of *dq* components of grid voltage and current respectively, which are further reported to an arbitrary rotating reference frame synchronized with the grid angular frequency.

Considering a distributed generation system connected to the power grid as Fig. 1 illustrates, the phase angle of the arbitrary reference frame can be derived from the grid frequency information:

$$\theta = \int \omega \, dt \tag{1}$$

Because the voltage at the point of common coupling in two operating points can be written as:

$$\vec{V}_{pcc1} = \vec{V}_s(1) - Z \cdot \vec{i}_{pcc1} \tag{2a}$$

$$\vec{V}_{pcc2} = \vec{V}_s(2) - Z \cdot \vec{i}_{pcc2} \tag{2b}$$

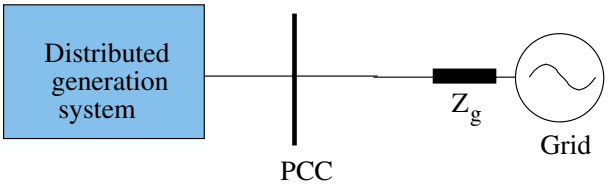

Fig. 1. Distributed power generation system connected to utility grid.

where *1* and *2* are representing the two different sampling instants, the line impedance can be calculated using the variations in both current and voltage at the point of common coupling:

$$Z = \frac{\Delta\vec{V}_{pcc}}{\Delta\vec{i}_{pcc}} \tag{3}$$

where:

$$\Delta\vec{V}_{pcc} = \vec{V}_{pcc}(1) - \vec{V}_{pcc}(2) \tag{4a}$$

$$\Delta\vec{i}_{pcc} = \vec{i}_{pcc}(1) - \vec{i}_{pcc}(2) \tag{4b}$$

are the voltage and current variation respectively at the point of common coupling. It should be noted that the above equations are valid only if the source voltage and grid impedance are not changing between the two sample instants, e.g. $\vec{V}_s(1) = \vec{V}_s(2)$.

The module and phase angle of the voltage at the PCC can be calculated from its $\alpha\beta$ components:

$$|V_{pcc1,2}| = \sqrt{V_\alpha^2 + V_\beta^2} \tag{5a}$$

$$\theta_{v_{pcc1,2}} = tan^{-1}\frac{V_\beta}{V_\alpha} \tag{5b}$$

Further on, the *dq* components of the grid voltage for both sampling instants can be derived as:

$$V_{d1,2} = |V_{pcc1,2}|\, cos(\theta_{V_{pcc1,2}} - \theta) \tag{6a}$$

$$V_{q1,2} = |V_{pcc1,2}|\, sin(\theta_{V_{pcc1,2}} - \theta) \tag{6b}$$

In this way, the voltage at the point of common coupling is always referring to a general rotating reference frame provided by θ. Based on the *dq* components of both voltage and current, the resistive and inductive part of the impedance can be calculated like:

$$R = \frac{(V_{q1} - V_{q2}) \cdot (I_{q1} - I_{q2}) + (V_{d1} - V_{d2}) \cdot (I_{d1} - I_{d2})}{(I_{q1} - I_{q2})^2 + (I_{d1} - I_{d2})^2} \tag{7a}$$

$$\omega L = \frac{(V_{d1} - V_{d2}) \cdot (I_{q1} - I_{q2}) - (V_{q1} - V_{q2}) \cdot (I_{d1} - I_{d2})}{(I_{q1} - I_{q2})^2 + (I_{d1} - I_{d2})^2} \tag{7b}$$

B. Power variations

As (3) shows, grid voltage and current variations are necessary to estimate the value of the impedance. This is convenient for power generation systems based on renewable energies such as wind or photovoltaic systems which have variable input power. Considering that the variations of input power are reflected into the power delivered to the utility grid, these could be used to derive the necessary voltages and currents in two different operating conditions. However, with the introduction of variable speed wind turbine technology, the

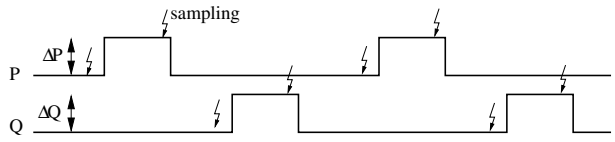

Fig. 2. Active and reactive power variations used for line impedance detection.

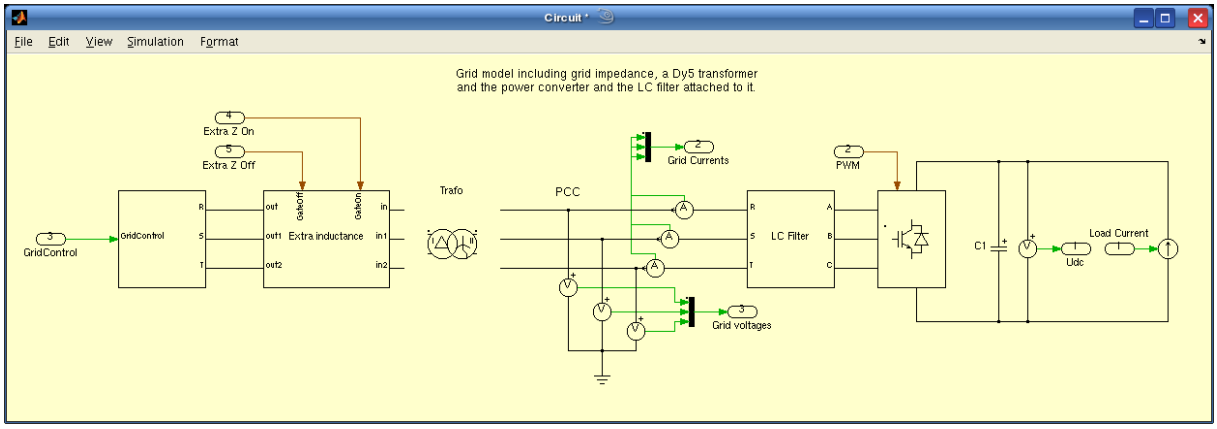

Fig. 3. Plant model developed using PLECS toolbox within MATLAB®/Simulink®

wind power variations are very much attenuated at the output of the turbine, hence deliberately power variations in dc-link might be necessary in order to obtain the two working points at the point of common coupling.

As the proposed method shows, variations of reactive power are necessary in order to create phase angle deviation $\Delta\theta$ at the point of common coupling. According to interconnection demands for power generation systems, wind turbine (WT) systems are allowed to have reactive power variation at PCC of about 10% of nominal active power under normal operation conditions [17]. On the contrary, the photovoltaic (PV) systems should operate at unity power factor all the time, hence the reactive power oscillations necessary for line impedance detections should be small and for a short period of time. Therefore, this algorithm is more suited for wind power applications rather then photovoltaic, but using short term power variations would allow for implementation in PV systems as well.

In this work, only the grid side converter of a WT system having full scale power converter as grid interface is considered and both active and reactive power variations are made intentionally in periodical steps. Fig. 2 illustrates a possible way to vary the generated output power of the system and the sampling instants for both voltage and currents. The difference between the samplings at the instant when $P^* = P$ and at the instant when $P^* = P + \Delta P$ (and similarly for Q) yields $\Delta\vec{V}_{pcc}$ and $\Delta\vec{i}_{pcc}$ necessary for calculating the resistive and inductive part of the impedance.

C. Discussion

Setting a proper ΔP and ΔQ and an accurate sampling interval between samples, the proposed algorithm is capable to estimate the value for both R and L with a good precision, as later seen in the § IV. However, should be noticed here that periodical oscillations of grid voltage at the PCC is subject to flicker, hence further considerations are necessary to avoid this.

In case of large wind power installations, the voltage variations at the point of common coupling ΔV_{pcc} might produce flicker, hence the entire installation is not complying with the power quality standards [18]. Because the proposed algorithm does not simply calculate the d and q components of both voltage and currents but uses an arbitrary rotating reference frame to refer to, it is possible to control the reactive power

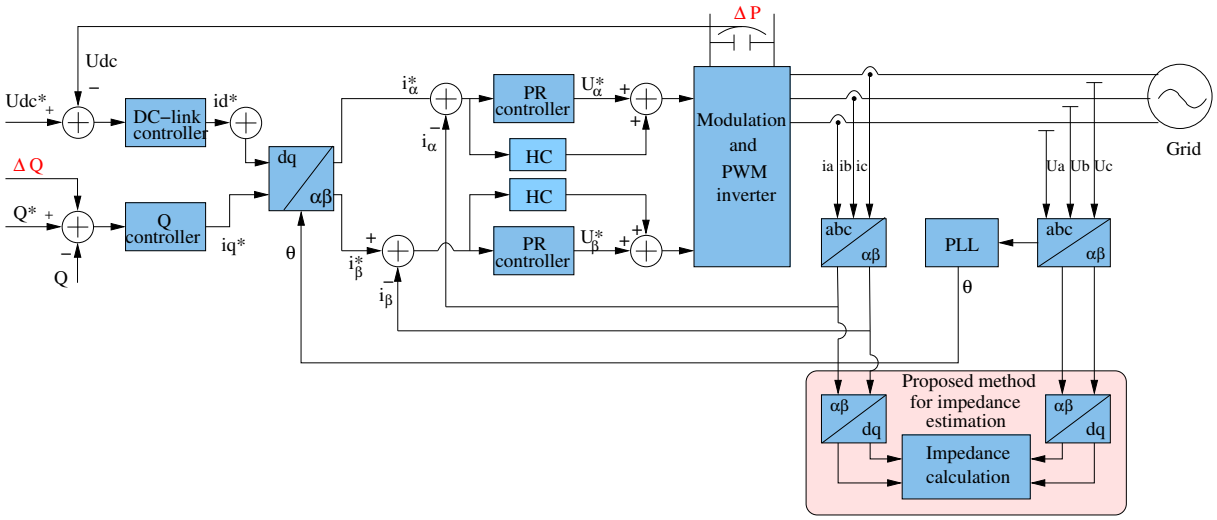

Fig. 4. Control structure of the grid side converter having an algorithm for line impedance estimation.

in a way that the magnitude of the voltage vector at PCC will not change. In this case, the voltage variation are mitigated to phase angle variation $\Delta\theta_{V_{pcc}}$:

$$V_{d1,2} = |V_{pcc1,2}|\, cos(\theta_{V_{pcc1,2}} - \theta) \tag{8a}$$

$$|V_{pcc1}| = |V_{pcc2}| \tag{8b}$$

$$\theta_{V_{pcc1}} \neq \theta_{V_{pcc2}} \Longrightarrow V_{d1} \neq V_{d2} \tag{8c}$$

The scope of this work is to present and validate the basic method, hence the extra feature of having droop control on top of reactive power control will be discussed in another work.

IV. Results and Validation

A. Simulation system

In order to validate the working principle of the proposed method, a simulation model was created in MATLAB®/Simulink. The model comprises two main parts, one containing the DPGS grid side power converter control and another containing the plant denoted by an LCL filter attached to the power converter, the grid impedance and the grid voltage source. For a better modeling of the plant, PLECS Toolbox [19] has been adopted in this work. This is a special Simulink toolbox which comprises models for electrical components such as resistor, inductance, capacitance or power switches, etc. hence being easier to modify the grid impedance and test the proposed method. Fig. 3 shows the model of the plant realized using PLECS and one can notice the easiness of adding or removing impedance in the grid.

The simulation model emulates the physical system available in the laboratory. In this case, the power converter is connected to a low voltage network (400 V) through a three phase Δy transformer having the resistance $R_t = 1\ \Omega$ and inductance $L_t = 2$ mH. Using a Norma-Unilap 100 XE device with an accuracy of 5%, the grid impedance has been measured to be $Z_g = 0.22\ \Omega$ pure resistive. Since the PCC is defined on the secondary side of the transformer, the total impedance to be detected by the proposed method is comprising the grid and the transformer impedance.

B. Control structure

The control of grid side converter considered here is a traditional cascaded two loops control for PWM VSI converters, as depicted in Fig. 4. The outer loop comprises a controller for the dc-link voltage (and hence the active power P) and a controller for the reactive power Q. The inner loop employs two proportional-resonant (PR) controllers for current regulation and it is implemented in $\alpha\beta$ stationary reference frame. Additionally to the controller for fundamental current (50 Hz), harmonic compensator (HC) for 5^{th} and 7^{th} harmonics are used. A phase-locked loop (PLL) system implemented in $\alpha\beta$ frame [20] is used to obtain the phase angle of the grid. The proposed algorithm for line impedance detection is based on (7a) and (7b) and has as inputs the *dq* components of both grid voltage and currents.

The reactive power oscillations are simply added to the reactive power reference while the active power oscillations are created by oscillating the power in dc-link.

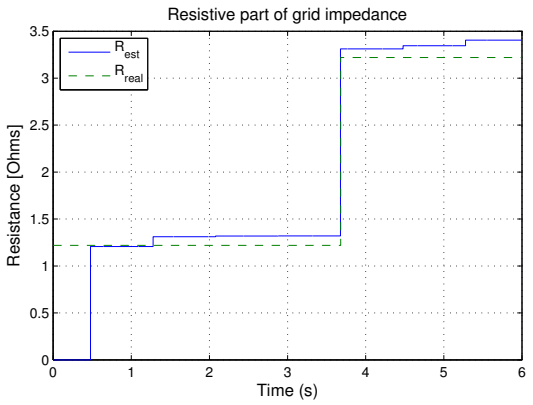

(a)

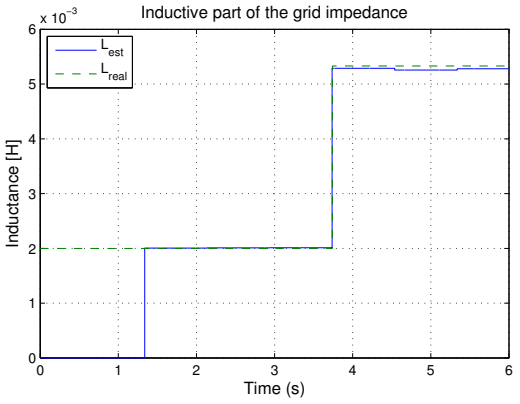

(b)

Fig. 5. Estimation of both resistive (a) and inductive (b) parts of the grid impedance in the situation of 10% active power variations at PCC.

C. Validation of method by simulation results

Simulation results in case of line impedance variations (both resistive and inductive) are presented in the following. To test the effectiveness of the proposed algorithm, large variations in both *R* and *L* have been made. An additional series impedance of $Z_a = 2 + j1.03\ \Omega$ is connected into the circuit. The identification accuracy related to four different levels of active

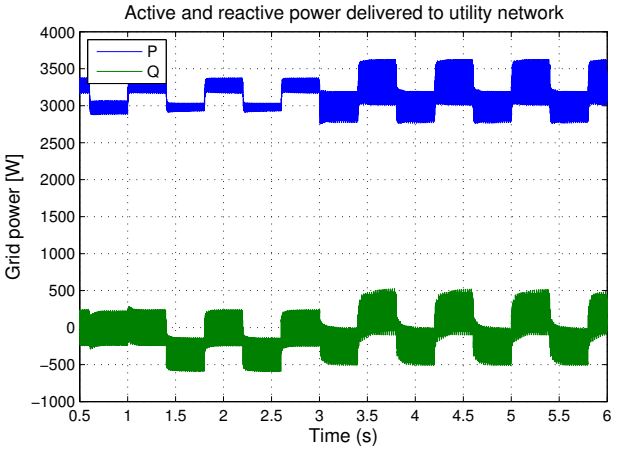

Fig. 6. Active and reactive power delivered to utility network in case of 10% active power variation.

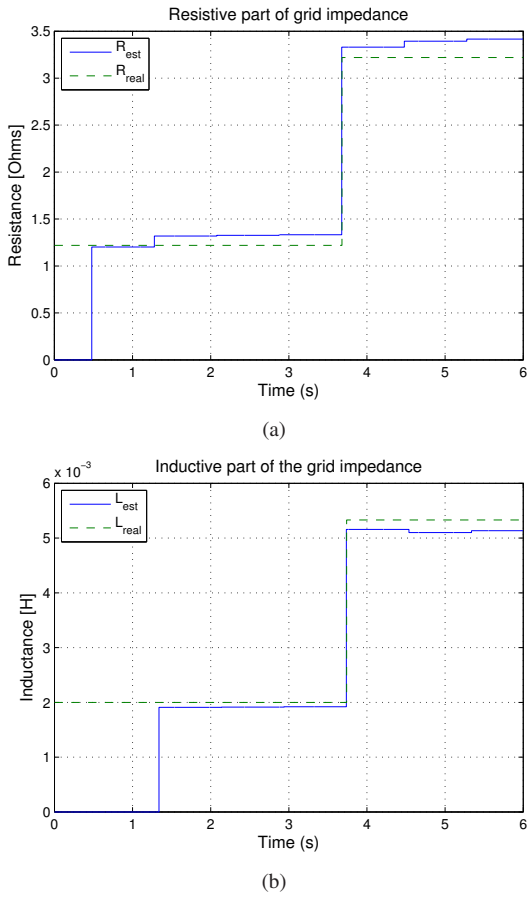

Fig. 7. Estimation of both resistive (a) and inductive (b) parts of the grid impedance in the situation of 5% active power variations at PCC.

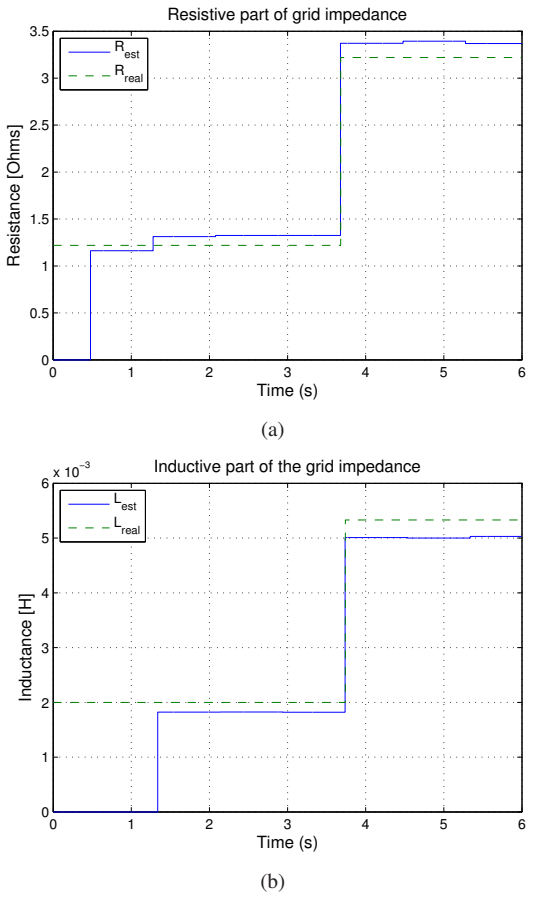

Fig. 8. Estimation of both resistive (a) and inductive (b) parts of the grid impedance in the situation of 1% active power variations at PCC.

power variations is pursued. The reactive power variations are set to 300 VARs in each of the cases. The duration of power variation is kept long enough to give the system the possibility to reach steady-state conditions.

1) Active power variation of 10%: Fig. 5 depicts the estimation of both active and reactive parts of grid impedance in situation when $\Delta P = 10\%$. As can be observed, there is a good agreement between the real impedance in the grid and the one identified using the proposed algorithm.

2) Active power variation of 5%: As illustrated in Fig. 7, the accuracy in detecting the exact value of grid impedance drops when $\Delta P = 5\%$. Small discrepancy can be observed between the estimated and the real signal for both resistive and inductive part of impedance. Table I shows the actual value of accuracy for both R and L in case of considered power variations.

3) Active power variation of 1%: Similar behavior as for previous case is noted also in situation when active power variations are down to 1% of the nominal power of the converter. In this case, the method estimates the resistive part of the impedance with an accuracy of less than 6% while the inductive part is estimated with an accuracy of about 5%.

4) Active power variation of 0.1%: If just 0.1% of nominal power is varied at the point of common coupling, the estimation of resistive and inductive parts of grid impedance is as illustrated in Fig. 9. According to data in Table I, the accuracy does not drop considerably, hence small power variations can also be used to obtain accurate enough results.

TABLE I
INFLUENCE OF POWER VARIATION ΔP ONTO THE ACCURACY OF ESTIMATION

ΔP	Accuracy R	Accuracy L
10 %	3.89 %	1.32 %
5 %	5.30 %	6.40 %
1 %	5.84 %	5.01 %
0.1 %	4.80 %	6.20 %

V. CONCLUSION

This paper proposes a method for estimating the resistive and inductive part of the grid impedance based on variation of the delivered power into the network. The proposed algorithm is computationally simple and fits well into the control of power generation systems based on variable input power such as wind turbines or photovoltaic systems. The presented results validate the effectiveness of the proposed method when large variations on both resistive and inductive part of grid impedance occur. The accuracy of this method is comparable with that of commercial products for measuring impedance available on the market today.

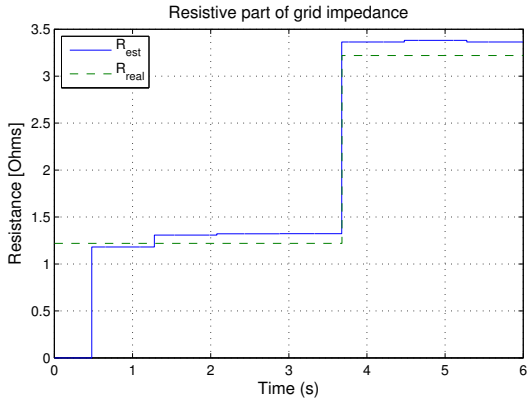

(a)

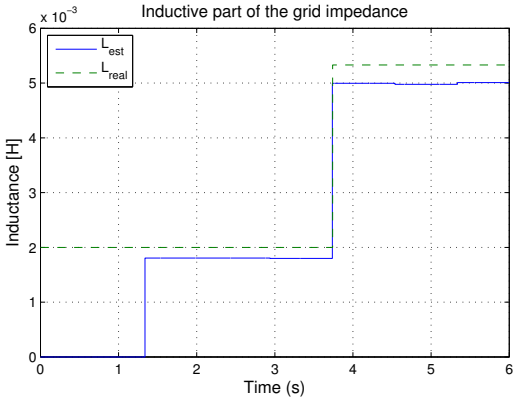

(b)

Fig. 9. Estimation of both resistive (a) and inductive (b) parts of the grid impedance in the situation of 0.1% active power variations at PCC.

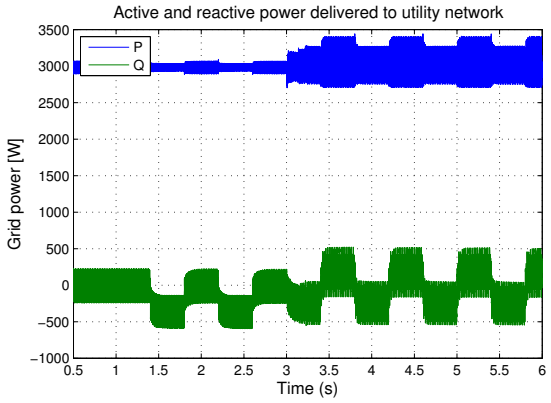

Fig. 10. Active and reactive power delivered to utility network in case of 0.1% active power variation.

REFERENCES

[1] A. Tarkiainen, R. Pollanen, M. Niemela, and J. Pyrhonen, "Identification of grid impedance for purposes of voltage feedback active filtering," *IEEE Power Electronics Letters*, vol. 2, no. 1, pp. 6–10, 2004.

[2] M. Sumner, B. Palethorpe, and D. Thomas, "Impedance measurement for improved power quality-Part 2: a new technique for stand-alone active shunt filter control," *IEEE Trans. on Power Delivery*, vol. 19, no. 3, pp. 1457–1463, 2004.

[3] V. Diana, M. Sumner, P. Zanchetta, and M. Marinelli, "Non-invasive power system impedance monitoring for improved power quality," in *Proc. of Power Electronics, Machines and Drives*, vol. 1, 2004, pp. 265–268.

[4] DIN and VDE, "Automatic disconnection device between a generator and the public low-voltage grid," Standard, 2005.

[5] L. Asiminoaei, R. Teodorescu, F. Blaabjerg, and U. Borup, "A new method of on-line grid impedance estimation for PV inverters," in *Proc. of APEC'04*, vol. 3, 2004, pp. 1527–1533.

[6] ——, "A digital controlled PV-inverter with grid impedance estimation for ENS detection," *IEEE Trans. on Power Electronics*, vol. 20, no. 6, pp. 1480–1490, 2005.

[7] A. V. Timbus, R. Teodorescu, F. Blaabjerg, and U. Borup, "Online grid measurement and ENS detection for PV inverter running on highly inductive grid," *IEEE Power Electronics Letters*, vol. 2, no. 3, pp. 77–82, 2004.

[8] F. Bertling and S. Soter, "A novel converter integrable impedance measuring method for islanding detection in grids with widespread use of decentral generation," in *Proc. of Power Electronics, Electrical Drives, Automation and Motion*, 2006, pp. 503–507.

[9] IEA-PVPS, "Evaluation of islanding detection methods for photovoltaic utility interactive power systems," IEA-PVPS, http://www.iea-pvps.org, Online report T5-09, March 2002. [Online]. Available: http://www.oja-services.nl/iea-pvps/products/download/rep5_09.pdf

[10] F. De Mango, M. Liserre, A. Dell'Aquila, and A. Pigazo, "Overview of anti-islanding algorithms for PV systems. Part I: Passive methods," in *Proc. of Power Electronics and Motion Control Conference*, 2006, pp. 1878–1883.

[11] F. De Mango, M. Liserre, and A. Dell'Aquila, "Overview of anti-islanding algorithms for PV systems. Part II: Active methods," in *Proc. of Power Electronics and Motion Control Conference*, Aug. 2006, pp. 1884–1889.

[12] M. H. J. Bollen, *Understanding Power Quality Problems: Voltage Sags and Interruptions*. IEEE Press, 2002.

[13] B. Palethorpe, M. Sumner, and D. Thomas, "Power system impedance measurement using a power electronic converter," in *Proc. of Harmonics and Quality of Power*, vol. 1, 2000, pp. 208–213.

[14] ——, "System impedance measurement for use with active filter control," in *Proc. of Power Electronics and Variable Speed Drives*, 2000, pp. 24–28.

[15] A. V. Timbus, R. Teodorescu, F. Blaabjerg, and U. Borup, "ENS detection algorithm and its implementation for PV inverters," *IEE Proceedings of Electric Power Applications*, vol. 153, no. 2, pp. 206–212, 2006.

[16] ——, "Online grid impedance measurement suitable for multiple PV inverters running in parallel," in *Proc. of APEC '06*, 2006, pp. 907–911.

[17] Eltra and Elkraft, "Wind turbines connected to grids with voltage below 100 kV," http://www.eltra.dk, 2004.

[18] IEC Standard, "Electromagnetic compatibility (EMC) - Part 4: Testing and measurement techniques, Section 15: Flickermeter - Functional and design specifications," International Electrotechnical Commission, Tech. Rep. 61000-4-15, 1997.

[19] Plexim GmbH, "PLECS Toolbox," http://www.plexim.com, 2007. [Online]. Available: http://www.plexim.com

[20] P. Rodriguez, R. Teodorescu, I. Candela, A. V. Timbus, and F. Blaabjerg, "New positive-sequence voltage detector for grid synchronization of power converters under faulty grid conditions," in *Proc. of PESC'06*, 2006.

Publication 12

Grid impedance identification based on active power variations and grid voltage control

by A. Timbus, P. Rodriguez and R. Teodorescu
Article published in proceedings of IAS'07, pages 949 – 954, 2007

Grid Impedance Identification Based on Active Power Variations and Grid Voltage Control

Adrian V. Timbus, *Student Member, IEEE*, Pedro Rodriguez, *Member, IEEE*
and Remus Teodorescu, *Senior Member, IEEE*

***Abstract*—This paper presents a novel method for identification of grid impedance which can be applied to grid connected power converters. Active power variations together with grid voltage control are used to obtain two operating points necessary for the algorithm proposed. Grid currents and voltages in the two operating points are then reported to an arbitrary synchronous reference frame, resulting the equations for identification of inductive and resistive parts of grid impedance. Simulation and experimental results are used to validate the proposed algorithm in case of inductive and resistive grids. The accuracy of impedance identification is comparable to that of commercial products designed for grid impedance measurement.**

***Index Terms*—Line impedance identification, power control, voltage control, distributed power generation system.**

I. Introduction

WITH increasing penetration of distributed generation, the unidirectional structure of power delivery is changing, thus maintaining power system stability becomes a challenge and an actual concern. As a consequence, grid interconnection requirements applying to distributed power generation systems (DPGS) are gradually updated in order to maintain stability of the utility network [1]–[5].

It has been shown that grid impedance value can serve as a threshold for disconnecting power generation units whenever an islanding situation occurs [6], [7]. Additionally, the value of grid impedance can be used by DPGS in order to decide if operate in grid connected or stand alone (intentional islanding) mode, hence contributing to power system stability. Moreover, improved quality of delivered power can be achieved if the impedance value is used in conjunction with active filter control [8], [9]. Further on, detection of power system faults and the fault location can be established based on the line impedance information [10].

Previous works towards grid impedance identification yield different methods for estimating the value of grid impedance. Passive methods using analysis and filtering techniques of grid voltages and currents have been applied but such methods proved to be ineffective if power system disturbances are not strong enough. As a consequence, active methods which deliberately disturb the network and register the grid response to that disturbance are more popular. Injection of small current at a particular frequency close to the fundamental frequency [6], [7], [11] or a current pulse [12] are just some of the methods used for identification of line impedance.

A.V. Timbus and R. Teodorescu are with the Institute of Energy Technology, Aalborg University, DK-9220 Aalborg, Denmark. Email: avt@iet.aau.dk, ret@iet.aau.dk

P. Rodriguez is with the Technical University of Catalonia, Electrical Engineering Department, Spain, Email: prodriguez@ee.upc.edu

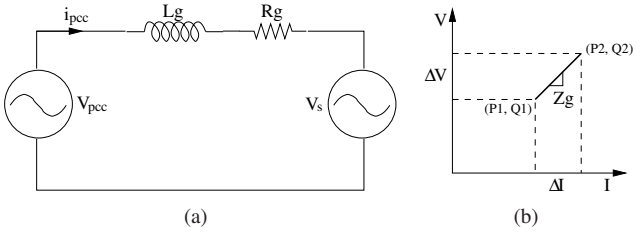

Fig. 1. Method for line impedance identification: (a) considered electrical system and (b) the two working points necessary for the algorithm.

This work proposes a novel active method for line impedance identification based on power variations at the point of common coupling (PCC) of a distributed generation system. Next section gives a description of the methodology, highlighting the algorithm used to identify the grid impedance. Section III describes the simulation model and the implementation of the algorithm in the simulation environment. Further on, the laboratory setup is described and the experimental results are presented in order to validate the proposed method.

II. Proposed method

The method proposed in this work deliberately varies the active power generated by a power generation unit for obtaining two operating points necessary for the impedance identification algorithm. Additionally, a grid voltage control loop is necessary in order to avoid flicker emission at PCC. Based on the variations of both active power and phase angle, the resistive and inductive part of grid impedance can be identified.

Fig. 1(a) shows the single phase system considered for the development of the algorithm, while the two necessary working points, one prior and one after the power variation are illustrated in Fig. 1(b).

A. The impedance identification algorithm

The proposed algorithm for impedance identification is part of the control structure of a grid connected power converter depicted in Fig. 2. The dc-link active power variation ΔP (either coming from input power source or deliberately generated) produces active current variation $\Delta \mathbf{i}_{pcc}$ at the point of common coupling, giving rise to grid voltage variations $\Delta \mathbf{v}_{pcc}$.

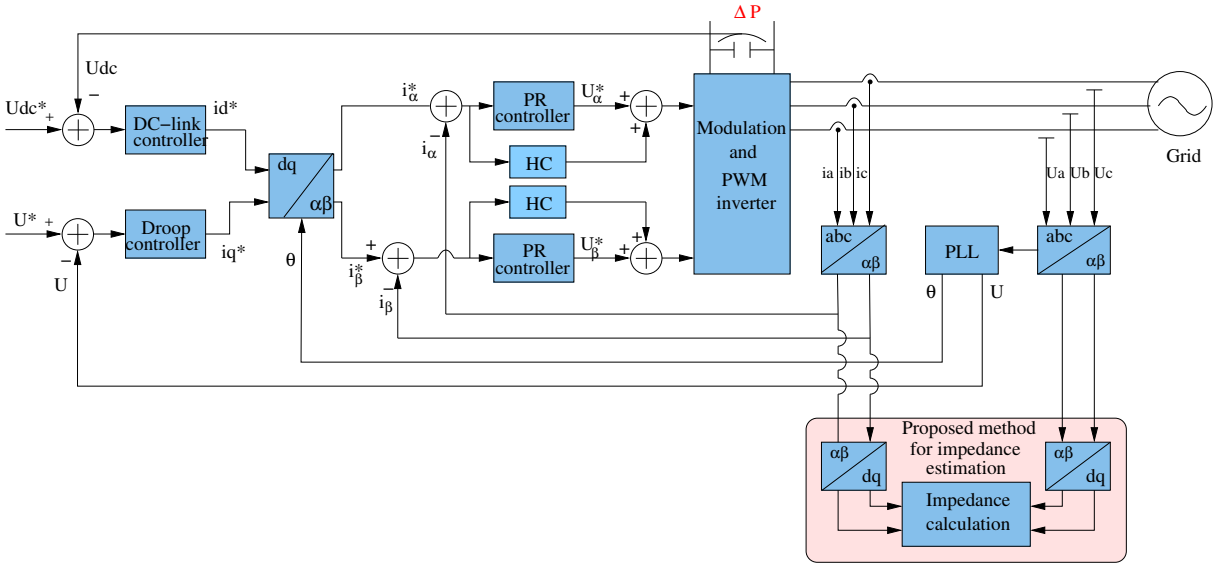

Fig. 2. Schematic of control structure using grid voltage control to regulate the reactive current in order to maintain the voltage magnitude constant at the point of common coupling and having the impedance identification method included.

Hence, the voltage at the point of common coupling in two operating points can be written as:

$$\mathbf{v}_{pcc1} = \mathbf{v}_{s1} + Z_g \cdot \mathbf{i}_{pcc1} \tag{1a}$$

$$\mathbf{v}_{pcc2} = \mathbf{v}_{s2} + Z_g \cdot \mathbf{i}_{pcc2} \tag{1b}$$

and grid impedance can be calculated as:

$$Z_g = \frac{\Delta \mathbf{v}_{pcc}}{\Delta \mathbf{i}_{pcc}} \tag{2}$$

where:

$$\Delta \mathbf{v}_{pcc} = \mathbf{v}_{pcc1} - \mathbf{v}_{pcc2} \tag{3a}$$

$$\Delta \mathbf{i}_{pcc} = \mathbf{i}_{pcc1} - \mathbf{i}_{pcc2} \tag{3b}$$

are the voltage and respectively current variations at the point of common coupling and $\mathbf{v}_s$ is the voltage of the grid source. It should be noticed that the above equations are valid only if the impedance Z_g and the source voltage $\mathbf{v}_s$ is not changing between the two sample instants, i.e. $Z_{g1} = Z_{g2} = Z_g$ and $\mathbf{v}_{s1} = \mathbf{v}_{s2}$. The above equations are further processed into synchronous reference frame as § II-C describes, leading to the final equations for inductive and resistive parts of the grid impedance.

B. Grid voltage control

However, the above algorithm is based on the voltage variation at PCC. Especially in case of large power generation units, voltage fluctuations at PCC are not desired due to the risk of creating flicker [13], therefore the method should be adapted in the way that the voltage magnitude at PCC remains constant. As a consequence, a grid voltage controller can be employed in the control structure of the grid converter to keep the magnitude of $\mathbf{v}_{pcc}$ constant by injecting reactive power, as Fig. 2 illustrates. In this case, the active current reference is given by the dc-link voltage controller while the reactive current reference is provided by the voltage controller. Hence, every time power variations ΔP are generated in dc-link, the active current at PCC, $\Delta \mathbf{i}_{pcc}$ is varying, giving rise to voltage variations $\Delta \mathbf{v}_{pcc}$. The magnitude of grid voltage is monitored by a phase-locked loop (PLL) [14] and its value is further transmitted to the voltage droop controller. Whenever the magnitude of grid voltage will differ from its reference, the droop controller sets a reactive current reference which compensates for the voltage change and bring the magnitude of the grid voltage to its reference value. For best results, it is important to have the same time response of both control loops so that the voltage droop controller reacts as soon as power variations occur. Proportional-integral (PI) controllers having the same time response are used for dc-link voltage control and grid voltage control [15]. The inner current loop is implemented in $\alpha\beta$ stationary reference frame employing proportional-resonant (PR) controllers with harmonic compensator for current regulation [16].

C. Algorithm referred to arbitrary reference frame

Using voltage controller in the control structure, the variation in the magnitude of $\Delta \mathbf{v}_{pcc}$ is eliminated but variation in its phase angle $\theta_{V_{pcc}}$ will appear. As a consequence, eq. (2) should be adapted to take advantage of the phase angle variation $\Delta\theta_{V_{pcc}}$ instead. This can be achieved using an arbitrary reference frame which rotates with the same frequency as the grid angular frequency. This reference frame can be simply provided by a constant $(2\pi \cdot 50)$, a very slow PLL system [17] or by using a frequency-locked loop (FLL) algorithm [18]. Noticeable is that the last two solutions present an advantage when grid frequency deviates from its nominal value, whereas using integration of a constant will introduce small errors in identification of grid impedance in situation when grid frequency deviates from its nominal value.

The module and phase angle of the voltage at PCC can be

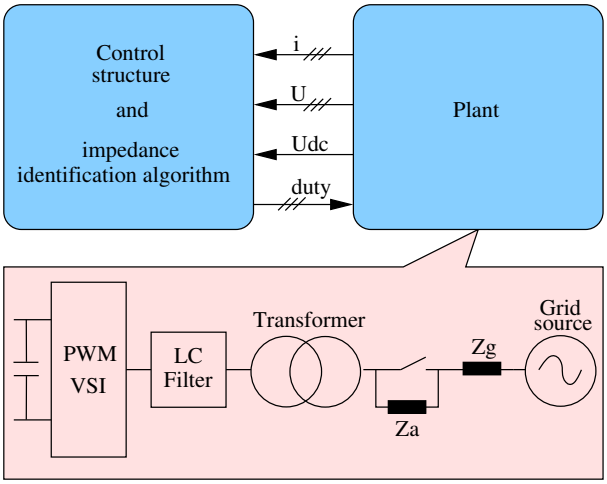

Fig. 3. Illustration of the simulation model used to test the proposed method for impedance identification.

calculated from its $\alpha\beta$ components:

$$|V_{pcc1,2}| = \sqrt{V_{\alpha 1,2}^2 + V_{\beta 1,2}^2} \tag{4a}$$

$$\theta_{\mathbf{v}_{pcc1,2}} = tan^{-1}\left(\frac{V_{\beta 1,2}}{V_{\alpha 1,2}}\right) \tag{4b}$$

Assuming θ being the phase angle of an arbitrary synchronous reference frame, the *dq* components of the grid voltage for both sampling instants 1 and 2 can be derived as:

$$V_{d1,2} = |V_{pcc1,2}|\, cos(\theta_{V_{pcc1,2}} - \theta) \tag{5a}$$

$$V_{q1,2} = |V_{pcc1,2}|\, sin(\theta_{V_{pcc1,2}} - \theta) \tag{5b}$$

This way, the *dq* voltage components at the point of common coupling are always referring to a general rotating reference frame provided by θ. Similar equations can be derived for the current injected at the point of common coupling and, based on the *dq* components of both voltage and current, the resistive and inductive part of the impedance can be calculated:

$$R = \frac{(V_{q1} - V_{q2}) \cdot (I_{q1} - I_{q2}) + (V_{d1} - V_{d2}) \cdot (I_{d1} - I_{d2})}{(I_{q1} - I_{q2})^2 + (I_{d1} - I_{d2})^2} \tag{6a}$$

$$\omega L = \frac{(V_{d1} - V_{d2}) \cdot (I_{q1} - I_{q2}) - (V_{q1} - V_{q2}) \cdot (I_{d1} - I_{d2})}{(I_{q1} - I_{q2})^2 + (I_{d1} - I_{d2})^2} \tag{6b}$$

III. Simulation Results

The control structure including the algorithm for impedance identification as presented in Fig. 2 has been simulated using MATLAB®/Simulink®. The simulation model is divided in two parts:

- the control block – realized using Simulink® blocks
- the plant – implemented using components from PLECS toolbox for Simulink® [19].

Fig. 3 illustrates the simulation model used to test the method proposed for identification of line impedance. The control block contains the control structure depicted in Fig. 2, while the structure of the plant is comprising the dc-link, the PWM-VS inverter to be controlled, the LC filter, a three phase transformer having Δy connection, the grid impedance Z_g and the grid power source. An additional impedance Z_a can be integrated into the circuit facilitating dynamic conditions for testing the proposed impedance identification method.

The point of common coupling is considered between the LC filter and the transformer, therefore the total impedance that needs to be identified comprises also the impedance of the transformer.

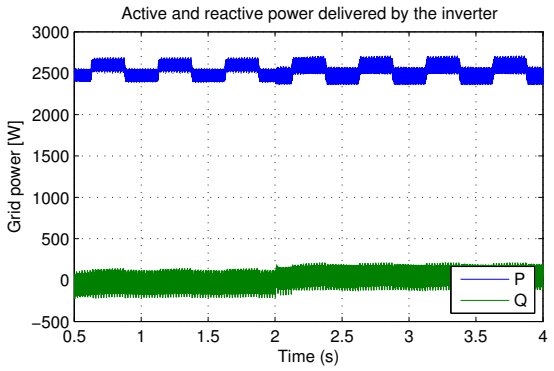

Fig. 4. Active and reactive power delivered at the point of common coupling.

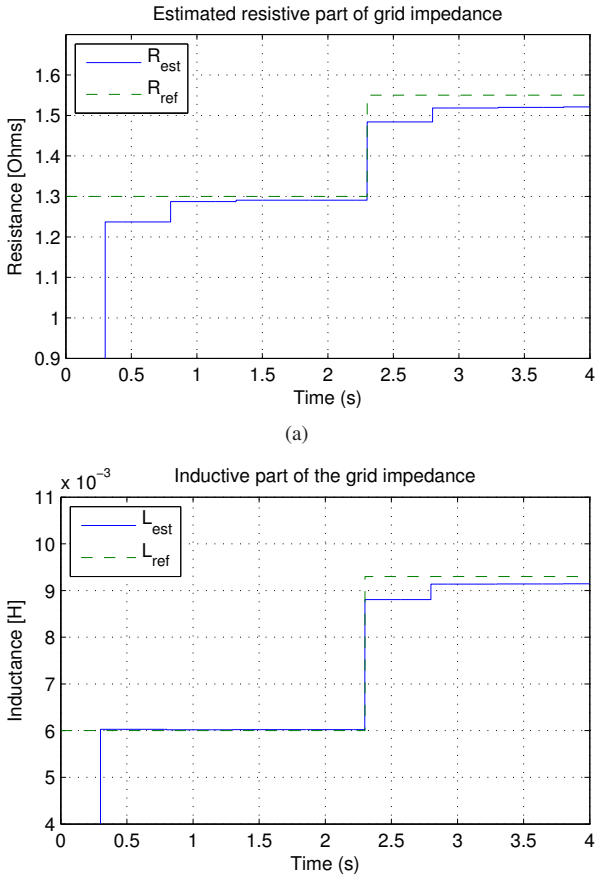

Fig. 5. Estimation of both resistive (a) and inductive (b) part of grid impedance using the proposed method based on power variations and droop control.

For validation of the proposed method an inductive grid situation has been considered. The inductive part of the grid is $L_g = 4\ mH$ while the resistive part is $R = 0.3\ \Omega$. Including the transformer impedance, the total impedance to be identified is having an inductive part of $L_{tot} = 6\ mH$ and a resistive part $R_{tot} = 1.3\ \Omega$. An additional impedance Z_a that is connected into the circuit to create changes in grid impedance comprises both resistive and inductive parts. The resistive part is $R_a = 0.25\ \Omega$ while the inductive part is $L_a = 3.3\ mH$.

Simulation results in the case when the additional impedance is added into the circuit are presented in the followings. A power variation of 0.05 p.u. related to the nominal power of the grid converter has been periodically created in dc-link, which leads to the same power variation at PCC, as Fig. 4 shows. Lower power variation, down to 0.001 p.u. can also be used but in this case the identification of line impedance is not as accurate as in the situation when 0.05 p.u. variation is used, therefore the latter is preferred in this work [20].

Fig. 5 shows the effectiveness of the proposed algorithm for impedance estimation. After 2.3 seconds simulation time, the additional impedance Z_a has been connected into the circuit. Accurate identification of both resistive and inductive part, with an average accuracy of 2% can be noticed, as Table I highlights. Good agreement between the reference and identified impedance values is obtained prior and after connecting the additional impedance in the circuit, validating the method proposed in this work.

Fig. 6 shows the four signals (V_q, V_d, I_q, I_d) used for line impedance identification. The d and q components of the current are illustrated in Fig. 6(b) and as it can be observed, when variation in active current occurs, variation in reactive current appears as well in order to maintain the voltage magnitude constant at PCC. It should be pointed out here that the currents and voltages are pre-processed before used in eq. (6a) and (6b). The processing consist of buffering of 200 samples and taking the median value out of them, as is illustrated in Fig. 7. The pre-processing action ensures high accuracy in identifying the correct value of both resistive and inductive part of grid impedance.

IV. Experimental System and Results

A. Experimental test bench

A test bench comprising a PWM-VSI connected to the utility network through an LC filter and a distribution transformer is used to validate the proposed method for identifying the grid impedance. A dSpace 1103 processing board is used to implement the control structure depicted in Fig. 2, including the algorithm for impedance identification. The switching and sampling frequency are both set to 10 kHz. Current and voltages are sampled at PCC using LEM sensors, while a commercial Norma Unilap 100 XE dedicated device is used to measure the grid impedance. This apparatus is able to measure the impedance of the line with values situated between 0.07 and 199 Ω with an accuracy of 5%. Additionally, the resistive part of the grid impedance can be measured using this device, hence calculation of inductive part is possible. Table II shows

TABLE I
The effectiveness of the proposed method for impedance identification, validated by simulation results.

Grid value	Estimated value
Normal grid	
Resistance $R_s = 1.3\ \Omega$ Inductance $L_s = 6\ mH$	Resistance $R_{est} = 1.29\ \Omega$ Inductance $L_{est} = 6\ mH$
Additional impedance	
Resistance $R_s = 1.55\ \Omega$ Inductance $L_s = 9.3\ mH$	Resistance $R_{est} = 1.52\ \Omega$ Inductance $L_{est} = 9.15\ mH$

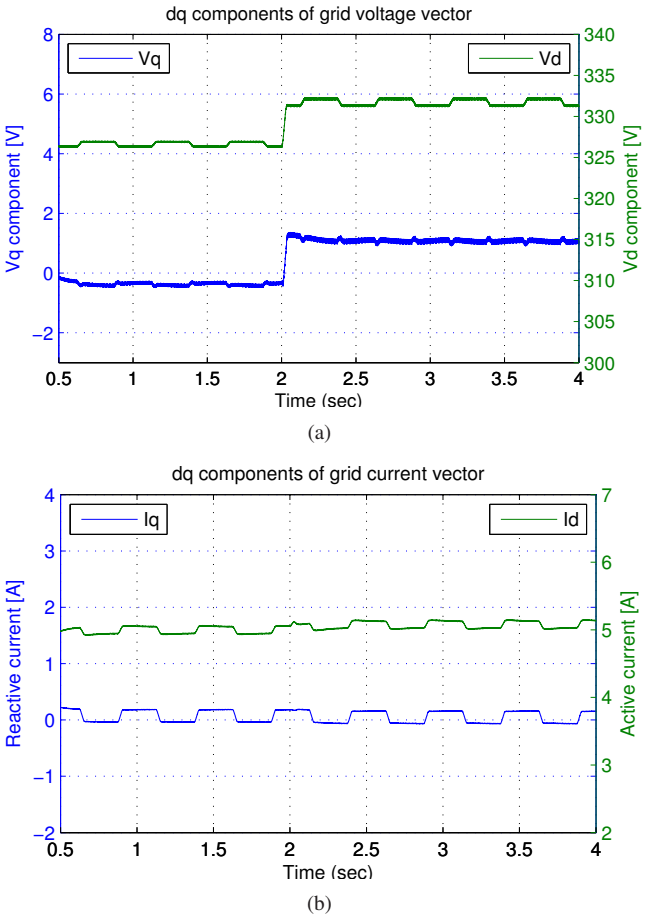

Fig. 6. Direct and quadrature components of (a) voltage and (b) current used by the proposed algorithm to identify the grid impedance.

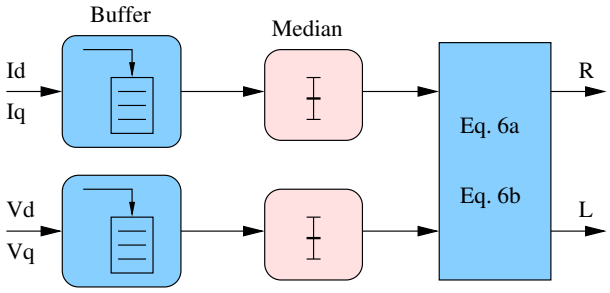

Fig. 7. Signal processing of currents and voltages prior calculation of grid impedance.

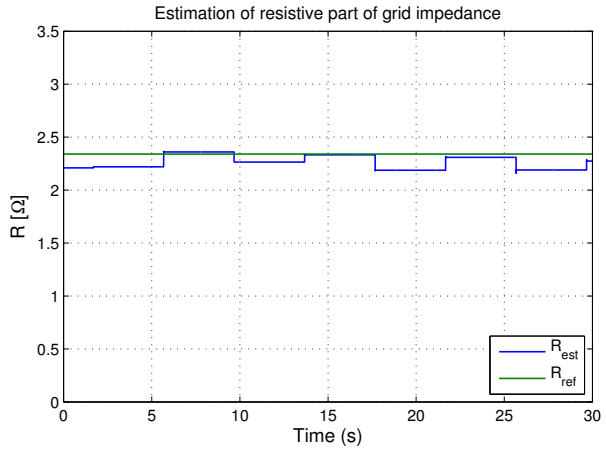

(a)

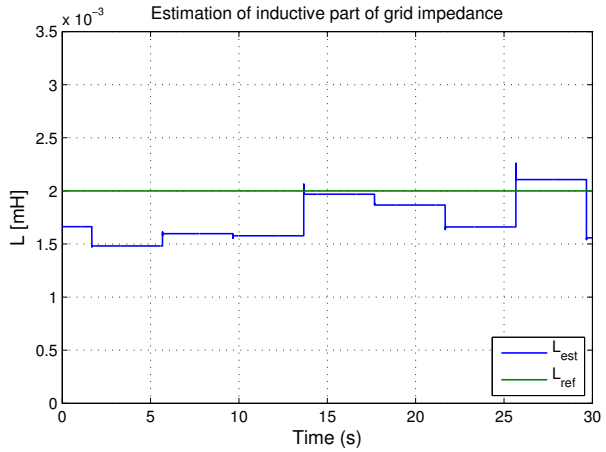

(b)

Fig. 8. Identification of (a) resistive and (b) inductive parts of grid impedance in laboratory.

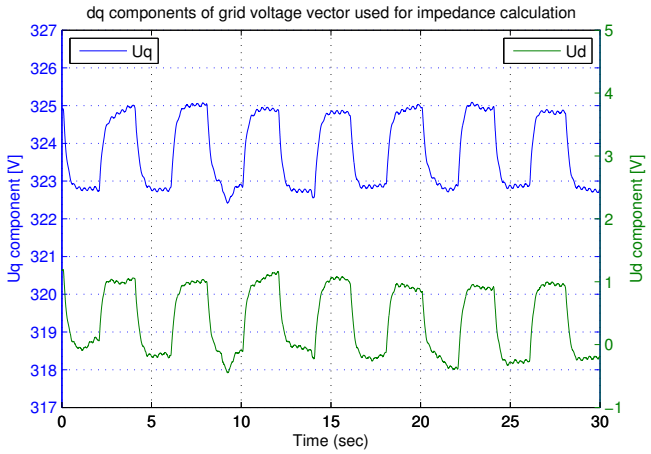

(a)

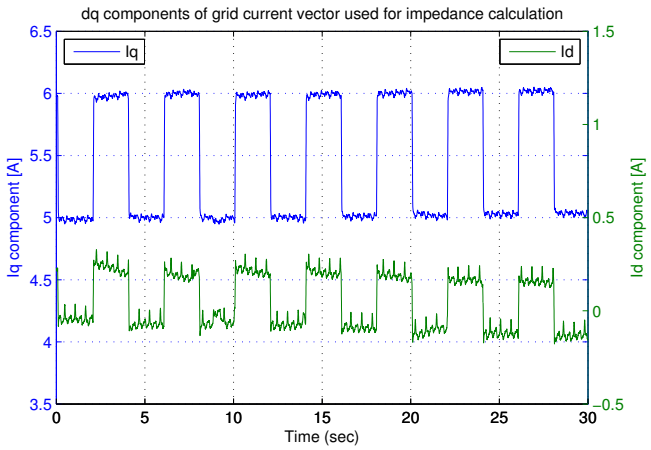

(b)

Fig. 9. Direct and quadrature components of (a) voltage and (b) current used by the proposed algorithm to identify the grid impedance in laboratory.

the values measured by Norma Unilap 100 XE in laboratory, values used as reference to which the proposed method is compared with.

Based on the values for Z_g and R_g measured in laboratory, the inductance can be calculated as $L_g = 2$ mH, which coincides with the inductance of the transformer. Therefore, contrary to simulation case, the actual grid in laboratory is completely resistive, hence the proposed method can be validated on two extreme situations, i.e. inductive and resistive grids.

B. Experimental results

Fig. 8 illustrates the identification of grid impedance in laboratory. As depicted in Fig. 8(a) and Fig. 8(b), the accuracy is not as high as in simulations but a good agreement between the referenced resistive and inductive parts (measured by Norma Unilap) and the signals identified by the method proposed in this work is achieved anyway. Although the same pre-processing procedure of *dq* components of grid voltages and currents is also used in laboratory, the signals shown in Fig. 9 are not as clean and steady as in simulation case (Fig. 6). This has a negative influence on the accuracy of grid impedance identification. Another issue which should be noticed here, as Fig. 10 highlights, is the fact that higher power variations (0.16 p.u.) are necessary in laboratory in order to obtain a stable and accurate identification of inductive part of the impedance.

TABLE II
GRID IMPEDANCE VALUES MEASURED IN LABORATORY USING NORMA UNILAP 100 XE DEDICATED DEVICE.

Measured variables	Value
Impedance Z_g	2.42 Ω
Resistance R_g	2.34 Ω

V. CONCLUSION

This paper presents a novel method used for identification of both inductive and resistive part of grid impedance. The proposed algorithm uses values of voltages and currents in two stationary working points created by active power variations at the point of common coupling. Additionally, a voltage control loop is employed in order to avoid flicker and make this method complying with power quality standards imposed to power generation units.

The simulation and experimental results validate the effectiveness of the algorithm in case of inductive and resistive

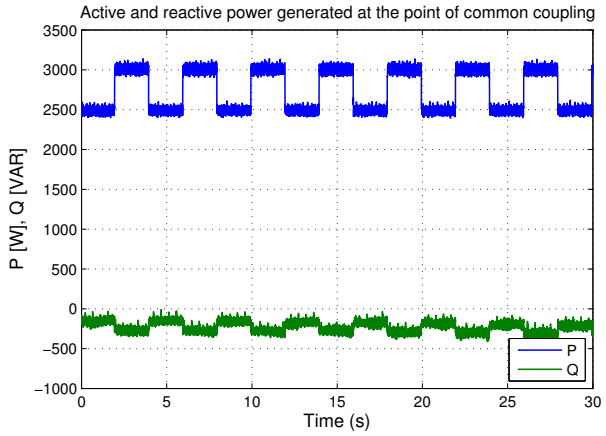

Fig. 10. Variations of active and reactive power generated at the point of common coupling in order to identify the resitive and inductive part of line impedance in laboratory.

grids. The proposed algorithm can be used for islanding detection purposes, thus offering ancillary services of DPGS. Moreover, due to its good accuracy in identification of both resistive and inductive parts of grid impedance, the algorithm can forward the impedance information to control in order to obtain an adaptive current controller which will ensure system stability over a broad band of impedance variation.

REFERENCES

[1] E.ON-Netz, "Grid code – high and extra high voltage," E.ON Netz GmbH, Tech. Rep., 2003. [Online]. Available: http://www.eon-netz.com/Ressources/downloads/enenarhseng1.pdf

[2] Eltra and Elkraft, "Wind turbines connected to grids with voltage below 100 kV," http://www.eltra.dk, 2004.

[3] DIN and VDE, "Automatic disconnection device between a generator and the public low-voltage grid," Standard, 2005.

[4] IEEE15471, "IEEE standard for interconnecting distributed resources with electric power systems," 2005.

[5] IEC Standard 61727, "Characteristic of the utility interface for photovoltaic (PV) systems," IEC, Tech. Rep., 2002.

[6] L. Asiminoaei, R. Teodorescu, F. Blaabjerg, and U. Borup, "A digital controlled PV-inverter with grid impedance estimation for ENS detection," *IEEE Trans. on Power Electronics*, vol. 20, no. 6, pp. 1480–1490, 2005.

[7] F. Bertling and S. Soter, "A novel converter integrable impedance measuring method for islanding detection in grids with widespread use of decentral generation," in *Proc. of Power Electronics, Electrical Drives, Automation and Motion*, 2006, pp. 503–507.

[8] A. Tarkiainen, R. Pollanen, M. Niemela, and J. Pyrhonen, "Identification of grid impedance for purposes of voltage feedback active filtering," *IEEE Power Electronics Letters*, vol. 2, no. 1, pp. 6–10, 2004.

[9] M. Sumner, B. Palethorpe, and D. Thomas, "Impedance measurement for improved power quality-Part 2: a new technique for stand-alone active shunt filter control," *IEEE Trans. on Power Delivery*, vol. 19, no. 3, pp. 1457–1463, 2004.

[10] S. Santoso, R. Dugan, J. Lamoree, and A. Sundaram, "Distance estimation technique for single line-to-ground faults in a radial distribution system," in *Power Engineering Society Winter Meeting, 2000. IEEE*, vol. 4, 2000, pp. 2551–2555.

[11] B. Palethorpe, M. Sumner, and D. Thomas, "Power system impedance measurement using a power electronic converter," in *Proc. of Harmonics and Quality of Power*, vol. 1, 2000, pp. 208–213.

[12] M. Sumner, B. Palethorpe, and D. Thomas, "Impedance measurement for improved power quality-Part 1: the measurement technique," *IEEE Trans. on Power Delivery*, vol. 19, no. 3, pp. 1442–1448, 2004.

[13] IEC Standard, "Electromagnetic compatibility (EMC) - Part 4: Testing and measurement techniques, Section 15: Flickermeter - Functional and design specifications," International Electrotechnical Commission, Tech. Rep. 61000-4-15, 1997.

[14] A. V. Timbus, P. Rodriguez, R. Teodorescu, and F. Blaabjerg, "Grid monitoring for distributed power generation systems to comply with grid codes," in *Proc. of ISIE'06*, 2006.

[15] Z. Yong-gao, K. Yong, L. Xiao-yuan, L. Li-ming, and Z. Peng-cheng, "A novel double loop control design and analysis of STATCOM," in *Proc. of IECON'05*, 2005, pp. 1294–1299.

[16] R. Teodorescu and F. Blaabjerg, "Proportional-resonant controllers. A new breed of controllers suitable for grid-connected voltage-source converters," in *Proc. of OPTIM'04*, vol. 3, 2004, pp. 9–14.

[17] A. V. Timbus, M. Liserre, R. Teodorescu, and F. Blaabjerg, "Synchronization methods for three phase distributed power generation systems. An overview and evaluation," in *Proc. of PESC'05*, 2005, pp. 2474–2481.

[18] P. Rodriguez, A. Luna, M. Ciobotaru, R. Teodorescu, and F. Blaabjerg, "Advanced grid synchronization systems for power converters under unbalanced and distorted operating conditions," in *Proc. of IECON'06*, 2006, pp. 5173–5178.

[19] Plexim GmbH, "PLECS Toolbox," http://www.plexim.com, 2007. [Online]. Available: http://www.plexim.com

[20] A. V. Timbus, P. Rodriguez, R. Teodorescu, and M. Ciobotaru, "Line impedance estimation using active and reactive power variations," in *Proc. of PESC'07*, 2007.

Publication 13

Adaptive resonant controller for grid connected converters in distributed power generation systems

by A. Timbus, M. Ciobotaru, R. Teodorescu and F. Blaabjerg
Article published in Proceedings of APEC'06, pages 1601-1606, 2006

Adaptive Resonant Controller for Grid-Connected Converters in Distributed Power Generation Systems

Adrian V. Timbus, *Student Member, IEEE*, Mihai Ciobotaru, *Student Member, IEEE*, Remus Teodorescu, *Senior Member, IEEE* and Frede Blaabjerg, *Fellow, IEEE*

***Abstract*—Due to its superior performance when regulating sinusoidal waveforms and the possibility to compensate for low order harmonics by means of Harmonic Compensator (HC), Proportional Resonant (PR) controller is a real alternative to the conventional Proportional Integral (PI) controller, when implemented in a grid connected system like Distributed Power Generation Systems (DPGS).**

Anyway, both PR and HC necessitate the resonant frequency value inside their internal model. Normally, the nominal value of the grid frequency and its multiples are used, but in the case when the grid frequency experiences fluctuations, the performance of both PR and HC is diminished.

This paper discuss the possibility of improving the behavior of resonant controller and harmonic compensator in the case of grid frequency variations. The proposed solution makes use of the frequency information provided by the Phase-Locked Loop (PLL) system already used in most of DPGS today. Experimental results are presented in order to validate the proposed solution and it shows to work very well.

***Index Terms*—Inverter control, adaptive resonant controller, PLL, power generation systems, grid codes**

I. Introduction

WORLD WIDE energy consumption is predicted to increase considerably due to more and more appliances that are using electricity. Among the energy sources, wind and solar energy are receiving higher interest due to their potential. Nowadays, wind turbine (WT) systems are widely used in countries with high wind potential like Germany, Denmark, Spain, etc. Moreover, development of large projects are on-going for India, China and other countries. The installation of photovoltaic (PV) systems registers also an exponential increase, with Germany and Japan leading the list of the countries having the largest capacity installed.

Unconditional availability of the power source and the environmental friendliness of these systems are their major advantages over the traditional energy sources such as oil and natural gas, but their efficiency and controllability stand as the major drawbacks. In addition to this, the Transmission System Operators (TSOs) are imposing tough standards [1]–[4] when both WT and PV systems are interconnecting the utility network. Among many other demands, power system stability and power quality are primary requests but lately, ride-through capabilities for short grid disturbances, in the case of WT systems should also be provided. As a consequence, large research efforts are put into the control of these systems in order to improve their behavior.

A.V. Timbus, M. Ciobotaru, R. Teodorescu and F. Blaabjerg are with the Institute of Energy Technology, Aalborg University, DK-9220 Aalborg, Denmark. Email: avt@iet.aau.dk, ret@iet.aau.dk, fbl@iet.aau.dk

Except a few wind turbine topologies, almost all WT and PV systems are interfacing the utility grid through a PWM driven Voltage Source Inverter (VSI) [5]. In this situation, the control strategy of the inverter deals with the grid integration of the distributed system. Due to the similarities in hardware, initially the control strategies applied to drives applications were also ported to DPGS. Anyway, due to more restrictive standard demands for power quality, other control strategies and controller types [6]–[9] have also been investigated. One of the most common control structures applied to DPGS is based on Voltage Oriented Control (VOC) employing a controller for the dc-link voltage and a controller to regulate the injected current into the utility network [10].

Recently, Proportional Resonant (PR) controller attracted an increased interest due to its superior behavior over the traditional PI controllers, when regulating sinusoidal signals. Removal of the steady state error in single phase systems, no need for coupling or voltage feed-forward and easy tuning stand as its main advantages. As already highlighted, the resonant frequency information is necessary in their internal model. This issue may be regarded as a drawback when implemented in a grid tied system, due to frequency variations of the utility network.

This paper, discusses the improvement of the PR controller used in a VOC control structure for current regulation, in the case of grid frequency variations. Since the grid frequency may experience fluctuations, it is reasonable to use its value as input in the PR controller. This paper proposes to use the frequency estimation provided by a Phase-Looked Loop (PLL) algorithm [11] in order to obtain adaptiveness of the controller in respect to grid frequency.

A description and main characteristics of the PR controller is firstly given. This is followed by the standard demands in respect to frequency boundaries for both PV and WT systems. Further on, the control strategy and the proposed solution are described. Considerations about how the PLL system should be designed are also given. Finally, experimental results validate the effectiveness of the proposed solution.

II. Resonant controller in DPGS

The resonant controller structure arises due to the known drawbacks of PI controllers such as the difficulty in removing the steady-state error in stationary reference frame for single-phase systems, the need of decoupling and voltage feed-forward in three-phase systems and, in general the limitations

in compensating for the low order harmonics for complying with the power quality standards [9], [12]–[15].

The typical resonant current controller is defined as [13]:

$$G_c(s) = K_p + K_i \frac{s}{s^2 + \omega^2} \quad (1)$$

where: K_p – proportional gain, K_i – integral gain, ω – the resonance frequency.

The Bode-plots of the resonant controller for different integral gains K_i and ω set to 50 Hz are shown in Fig. 1(a). As it can be seen, this type of controller can achieve very high gain in a narrow frequency band centered around the resonance frequency. The width of this frequency band depends on the integral time constant K_i. A low K_i leads to a very narrow band while a high K_i leads to a wider band. Anyway, if the grid frequency changes to 55 Hz, (like the arrow shows in Fig. 1(b)), the controller performance will not be high and it will not be able to regulate the current at this frequency as it behaves only as a proportional gain.

Selective harmonic compensation can also be included in the structure by cascading several generalized integrators tuned to resonate at the desired frequency. In [9] the transfer function of a typical harmonic compensator designed to compensate for the 3^{rd}, 5^{th} and 7^{th} harmonics, as they are the most prominent harmonics in the current spectrum, is given as:

$$G_h(s) = \sum_{h=3,5,7} K_{ih} \frac{s}{s^2 + (\omega \cdot h)^2} \quad (2)$$

where h is the harmonic order.

As a consequence, also compensation for the lower harmonics can be achieved and their content in the power system can be minimized.

Anyway, it is important to notice that both the resonant controller and the harmonic compensator are frequency dependent. This may be a problem as the standards for DPGS demand to overcome grid frequency variation. Even though almost all power systems are well regulated in respect to both voltage and frequency, deviations from the normal values may happen. As a consequence, if the resonant controller is tuned for 50 Hz and grid frequency varies, problems in current regulation will occur. Therefore, the necessity of automatic adaptation of the resonant frequency for both the controller and the harmonic compensator arises.

III. Grid demands for DPGS

The demands for interconnecting distributed generation systems are different in the case of photovoltaic systems and wind turbine systems. Normally the demands for WT systems are more severe compared to those applying to PV systems. For example, both voltage and frequency ranges of operation are much larger in the case of wind turbines, thus such systems should have a control strategy that allows them to ride-through when larger grid variations occur.

A. Photovoltaic system demands

As stated in [1], [2], [16], the frequency variations that a PV system should ride-through are as large as ± 1Hz in Europe [2], ± 0.5 Hz in North America [1] and ± 0.2 Hz in Germany, Austria and Switzerland [16].

Looking closer at Fig. 1(b), it can be noticed that on small frequency variations, the resonant controller is expected to work properly due to the high enough integral gain on this frequency interval.

In order to see if the PR controller can handle such small frequency oscillations without grid frequency information, experimental results are presented further in § V.

B. Wind turbine system demands

When interfacing the utility network, the wind turbine systems have to fulfill the imposed demands by the Transmission System Operators (TSOs). These demands are given

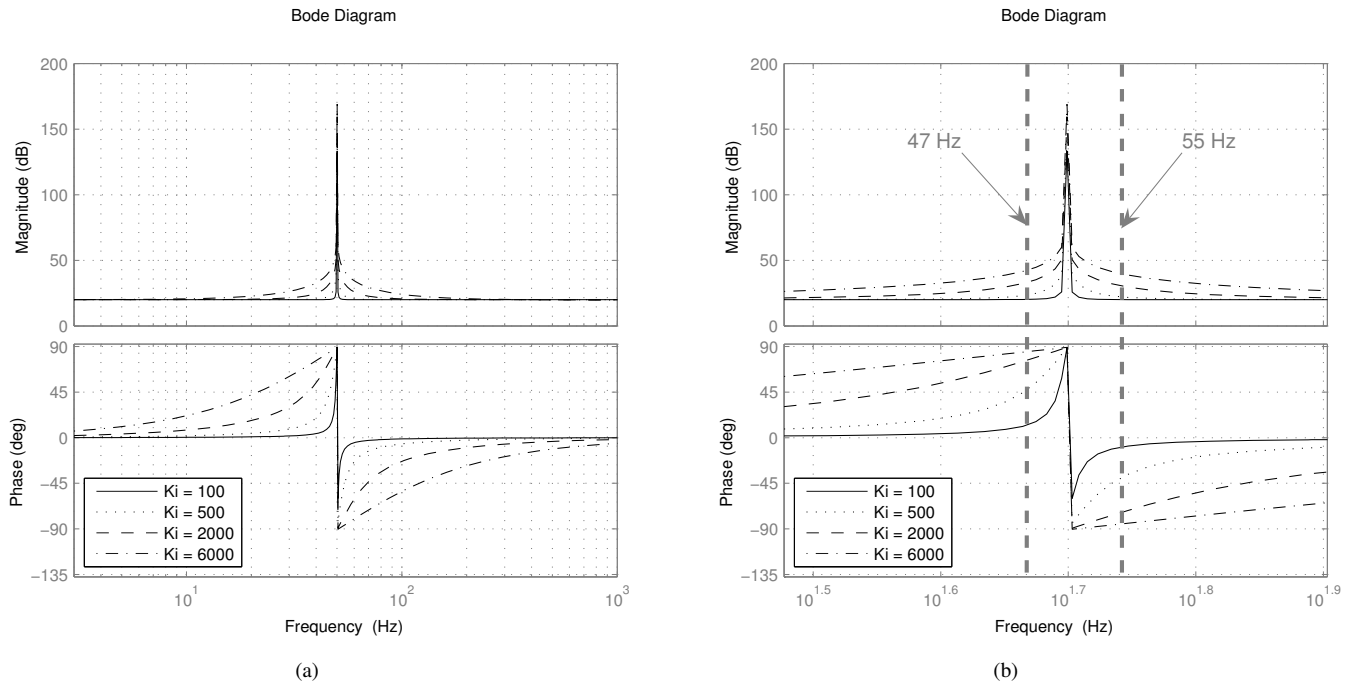

Fig. 1. Bode-plot of resonant controller tuned for 50 Hz (a) having different integral gains and (b) zoom in around 50 Hz frequency.

TABLE I
FREQUENCY RANGE AND CLEARING TIMES FOR WIND TURBINES ACCORDING TO ELTRA & ELKRAFT GRID CODE [3].

Frequency range	Clearing time
$<$ 47.0 Hz	0.3 s
47 – 47.5 Hz	10 s
47.5 – 48.0 Hz	5 min
48 – 49.0 Hz	25 min
49 – 50.2 Hz	continuous
50.2 – 53.0 Hz	1 min
$>$ 53.0 Hz	0.3 s

in the so called *grid codes* and they are country or TSO specific. The grid codes are referring to different issues, such as voltage and frequency limits, active and reactive power generation/consumption, etc.

Most interesting for this work is the frequency boundaries under which the wind turbine systems have to run. According to the grid codes in Denmark [3], the working range for the wind turbine systems is from 47 Hz up to 53 Hz. Corresponding codes can also be seen for other countries [17]. There are different clearing times of the turbines depending on the frequency value, as it is stated in Table I. According to [17], the largest frequency interval on which a WT system should run is the one specified by the Swedish grid operator, SVK. In this case, the lower limit is 47 Hz but the upper limit goes up to 55 Hz.

IV. PROPOSED METHOD

The proposed method makes use of the frequency estimation provided by a Phase Locked Loop (PLL) algorithm already existent in almost all DPGS and inputs this into the resonant controller. In this way, if the grid frequency varies from the its nominal value, the PLL will sense that. Moreover, this information will be transmitted to the current controller, which will adapt its resonant frequency to the new value.

A. Control strategy and experimental setup

Fig. 2 shows the proposed control strategy including the hardware setup. The system comprises the PWM inverter supplied by a DC power source which ensures the dc-link voltage necessary for the application. The connection to the grid is made through an isolation transformer. The three phase voltages are sampled and used by the synchronization algorithm which provides the grid voltage vector angle. Using this

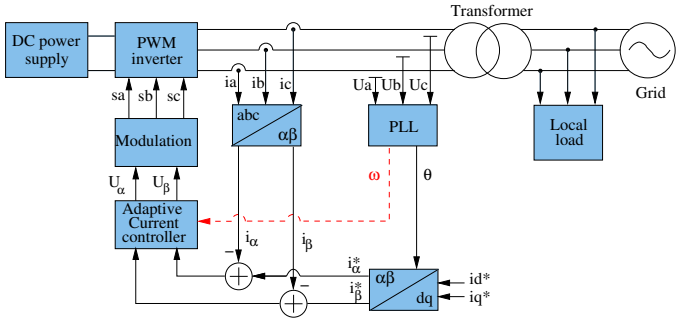

Fig. 2. Proposed control system including the hardware.

TABLE II
PARAMETERS OF THE PR CONTROLLER USED IN THIS APPLICATION.

K_p	K_i	K_{i3}	K_{i5}	K_{i7}
40	6000	6000	6000	6000

angle, the reference currents in the stationary reference frame are constructed using a $dq \rightarrow \alpha\beta$ transformation module. In this way, the control of active and reactive current reference is ensured. The sampled phase currents are also transformed into $\alpha\beta$ reference frame and subtracted from their reference. The resonant current controller implemented in stationary reference frame controls the input error to zero and sets the reference voltage for the modulator.

The parameters for the controller are stated in Table II, where K_i is the integral gain of the fundamental, K_{i3} is the integral gain for the 3^{rd} harmonic, K_{i5} for the 5^{th} and K_{i7} for the 7^{th} harmonic.

B. PLL system

The PLL system implemented in synchronous reference frame [11] is employed to keep synchronization with the grid voltage. This type of PLL is able additionally to provide the grid frequency information. This information is used as input into the resonant controller in order to have an adaptive tuning in respect to the grid frequency.

The PLL controller plays an important role in this situation. Firstly, the controller should be designed to respond with minimum of overshoot to the grid frequency variations, otherwise a value that generates tripping may be detected. In [11], a design method using a compensator to damp the overshoot of the controller is described. However the grid frequency will never experience a step change, but a ramp characteristic instead. According to most of the grid codes, this frequency variation has a slope of 1 Hz/s, thus the overshoot may not be a practical problem. Secondly, the locking time of the PLL should be fast enough, to provide the frequency information in time so that the system can cease energizing the network as the clearing times request. In addition, in the case of a fast PLL controller, filtering of the frequency signal may be necessary in order to have a steady value. Again, the time constant of the filter should be carefully chosen not to delay too much the actual grid frequency value.

V. EXPERIMENTAL RESULTS

A test system represented by the schematic in Fig. 2 is built to test the proposed structure. The frequency variations for both PV and WT systems are created using a grid simulator. In the case of PV systems, $\pm$ 1 Hz variations is used while in the case of WT a step from 50 Hz down to 47 Hz and from 50 Hz up to 55 Hz is created as these values are the highest stated in the grid codes [17]. Even though the situation of step change is not likely to happen in the grid, from the control point of view, it is the worst case for the PR controller, hence this is considered here.

A. Results in the case of PV systems

The results in the case of ± 1 Hz frequency variation are presented in Fig. 3 and Fig. 4. In Fig. 3(a), the grid frequency experiences -1 Hz deviation from the nominal value of 50 Hz. The dotted curve depicts the command send to the grid simulator which is used to create the frequency variation. The continuous line represents the frequency estimation of the PLL system which is further used by the resonant controller in order to obtain adaptiveness to the grid frequency. As it might be noticed in Fig. 3(b) and Fig. 4(b), there is a very small phase leading/lagging in the two situations when the frequency decreases/increases one Hz. Moreover, there is almost no steady state error in the regulated current in the two cases, being nearly similar with the plots in Fig. 3(c) and Fig. 4(c) where the frequency information is used to make the PR adaptive. This makes the adaptiveness of the PR controller an optional feature in case of PV systems.

B. Results in the case of WT systems

Fig. 5(a) shows a frequency step from the normal grid value of 50 Hz down to 47 Hz. Again, the dotted line represents the command for the grid simulator, while the normal line is the PLL output which is actually used by the resonant controller. As it can be seen in Fig. 5(b), without

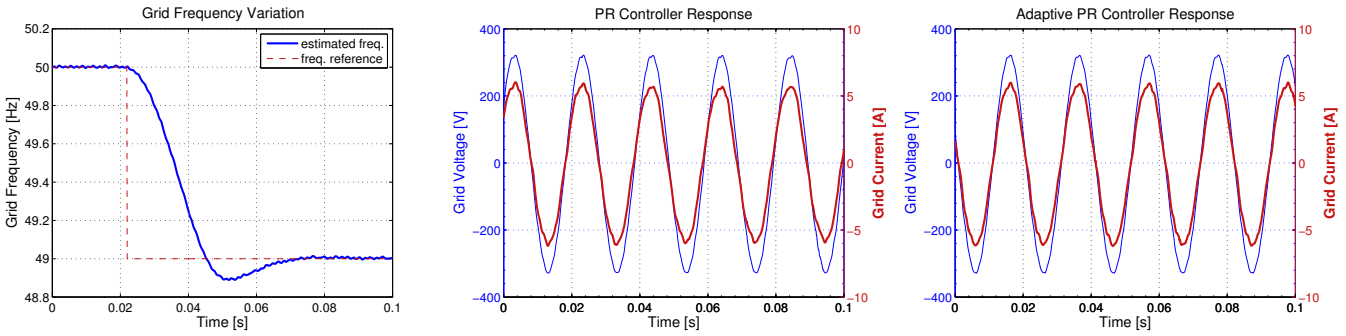

(a) (b) (c)

Fig. 3. Experimental results for a frequency step: (a) frequency step from 50 Hz down to 49 Hz, (b) resonant controller results (grid voltage and current (ticker)) and (c) adaptive resonant controller results (grid voltage and current (ticker)).

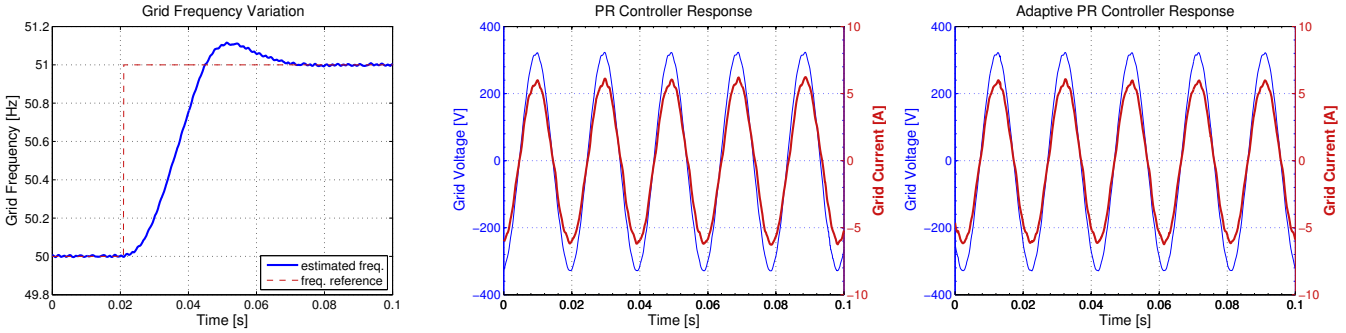

(a) (b) (c)

Fig. 4. Experimental results for a frequency step: (a) frequency step from 50 Hz up to 51 Hz, (b) resonant controller results (grid voltage and current (ticker)) and (c) adaptive resonant controller results (grid voltage and current (ticker)).

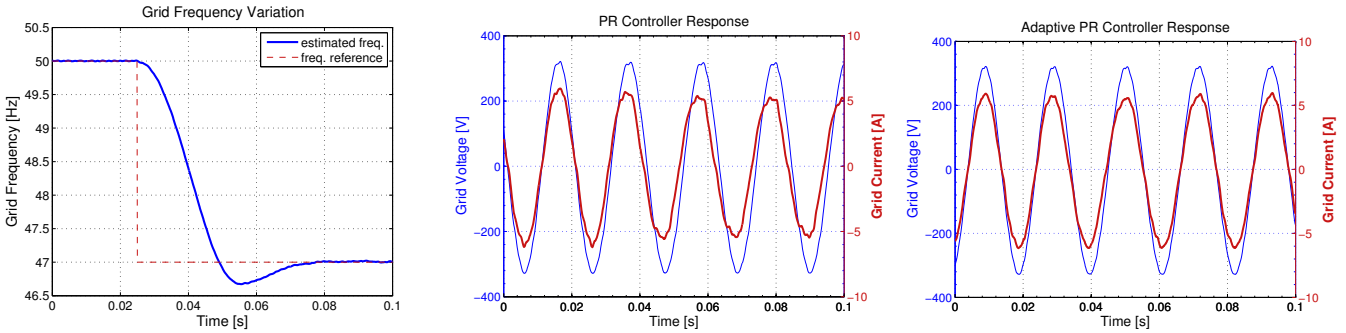

(a) (b) (c)

Fig. 5. Experimental results for a frequency step: (a) frequency step from 50 Hz down to 47 Hz, (b) resonant controller results (grid voltage and current (ticker)) and (c) adaptive resonant controller results (grid voltage and current (ticker)).

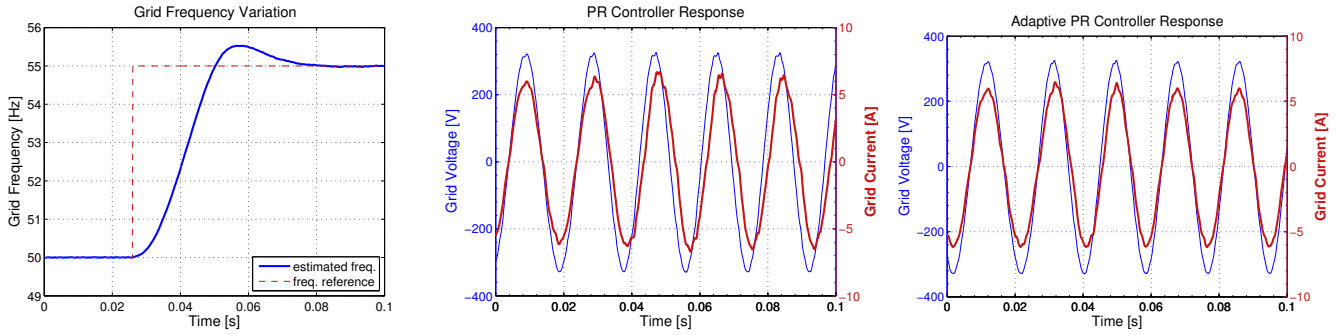

(a) (b) (c)

Fig. 6. Experimental results for a frequency step: (a) frequency step from 50 Hz up to 55 Hz, (b) resonant controller results (grid voltage and current (ticker)) and (c) adaptive resonant controller results (grid voltage and current (ticker)).

grid frequency information, the resonant controller encounters problems in the current regulation. A steady state error is noticed when the frequency changes (the amplitude of the current drops) and the power factor is not unity anymore. Anyway, when the information about the grid frequency is provided, the proposed controller has no problem to regulate the current and maintain unity power factor of the distributed generation system, as reported in Fig. 5(c). A similar situation is noticed for a frequency step from 50 Hz up to 55 Hz, as shown in Fig. 6.

As a consequence, the adaptiveness of the PR controller is a must when it is used in WT applications.

VI. Conclusion

The paper treats the issue of Proportional Resonant (PR) controller used for current regulation in grid tied systems and the utility frequency experiences deviation from its nominal value. It has been demonstrated that in the case of grid frequency fluctuations, problems in regulating the grid current and keeping unity power factor occur.

As a solution to this, a proposal consisting in using the grid frequency information provided by the PLL, inside the PR model has been made. In this way, an adaptive tuning of the resonant controller in respect to the grid frequency is obtained. Experimental results showing the controller running over a large band of frequency variations are presented for validating the proposed method.

Due to the small allowed frequency deviation in the case of PV systems, the adaptiveness of PR controller has a minor impact on the current regulation. On the other hand, in the case of WT systems, adaptive resonant controller is a must in order to provide a good quality of the injected current and unity power factor during grid frequency variation.

References

[1] IEEE15471, "IEEE standard for interconnecting distributed resources with electric power systems," 2005.

[2] IEC Standard 61727, "Characteristic of the utility interface for photovoltaic (PV) systems," IEC, Tech. Rep., 2002.

[3] Eltra and Elkraft, "Wind turbines connected to grids with voltage below 100 kV," http://www.eltra.dk, 2004.

[4] E.ON-Netz, "Grid code – high and extra high voltage," E.ON Netz GmbH, Tech. Rep., 2003. [Online]. Available: http://www.eon-netz.com/Ressources/downloads/enenarhseng1.pdf

[5] F. Blaabjerg, Z. Chen, and S. Kjaer, "Power electronics as efficient interface in dispersed power generation systems," *IEEE Trans. on Power Electronics*, vol. 19, no. 5, pp. 1184–1194, 2004.

[6] J. Liang, T. Green, G. Weiss, and Q.-C. Zhong, "Evaluation of repetitive control for power quality improvement of distributed generation," in *Proc. of PESC'02*, vol. 4, Cairns, Qld., 2002, pp. 1803–1808.

[7] P. Mattavelli and F. Marafao, "Repetitive-base control for selective harmonic compensation in active power filters," *IEEE Trans. on Industrial Electronics*, vol. 51, no. 5, pp. 1018–1024, 2004.

[8] F. Kanellos and N. Hatziargyriou, "A new control scheme for variable speed wind turbines using neural networks," *IEEE Power Engineering Society Winter Meeting*, vol. 1, pp. 360–365, 2002.

[9] R. Teodorescu and F. Blaabjerg, "Proportional-resonant controllers. A new breed of controllers suitable for grid-connected voltage-source converters," in *Proc. of OPTIM'04*, vol. 3, 2004, pp. 9–14.

[10] M. Kazmierkowski, R. Krishnan, and F. Blaabjerg, *Control in Power Electronics – Selected Problems*. Academic Press, 2002.

[11] A. V. Timbus, M. Liserre, R. Teodorescu, and F. Blaabjerg, "Synchronization methods for three phase distributed power generation systems. An overview and evaluation," in *Proc. of PESC'05*, 2005, pp. 2474–2481.

[12] S. Fukuda and T. Yoda, "A novel current-tracking method for active filters based on a sinusoidal internal model," *IEEE Trans. on Industrial Electronics*, vol. 37, no. 3, pp. 888–895, 2001.

[13] X. Yuan, W. Merk, H. Stemmler, and J. Allmeling, "Stationary-frame generalized integrators for current control of active power filters with zero steady-state error for current harmonics of concern under unbalanced and distorted operating conditions," *IEEE Trans. on Industry Applications*, vol. 38, no. 2, pp. 523–532, 2002.

[14] R. Teodorescu, F. Blaabjerg, U. Borup, and M. Liserre, "A new control structure for grid-connected LCL PV inverters with zero steady-state error and selective harmonic compensation," in *Proc. of APEC'04*, vol. 1, 2004, pp. 580–586.

[15] D. Zmood and D. G. Holmes, "Stationary frame current regulation of PWM inverters with zero steady-state error," *IEEE Trans. on Power Electronics*, vol. 18, no. 3, pp. 814–822, 2003.

[16] OVO/ONORM, "Photovoltaic semiconductor converters - Part 1: Utility interactive fail save protective interface for PV-line commutated converters," 1999.

[17] T. Ackermann, *Wind Power in Power Systems*. John Wiley & Sons, Ltd., 2005, ISBN: 0-470-85508-8.

Publication 14

Control strategies for distributed power generation systems operating on faulty grid

by A. Timbus, P. Rodriguez, R. Teodorescu, M. Liserre and F. Blaabjerg
Article published in Proceedings of ISIE'06, pages 1601-1606, 2006

Control Strategies for Distributed Power Generation Systems Operating on Faulty Grid

Adrian V. Timbus, *Student Member, IEEE*, Pedro Rodriguez, *Member, IEEE*, Remus Teodorescu, *Senior Member, IEEE*, Marco Liserre, *Member, IEEE* and Frede Blaabjerg, *Fellow, IEEE*

***Abstract*—The distributed power generation based on renewable energy sources such as wind and sun experiences a high penetration in the power systems around the world, having in some countries a large contribution to the total energy production. In order to protect the distribution and transmission systems, the grid operators are more and more talking about the ability of the distribution systems (mainly wind turbines WT systems) to behave as a conventional power plant.**

This paper discusses the possibilities of the distributed power generation systems (DPGS) to deliver power when grid disturbances are present in the utility network. The focus is set more on the control strategies for active power generation, and mainly on the creation of the reference currents which fulfill the demanded output power. Considerations about reactive power are also stated. Experimental results are presented in order to validate the theory behind the proposed control strategies on faulty grid.

***Index Terms*—Distributed power generation systems, power control, control strategies, positive and negative sequence, grid faults.**

I. Introduction

IN THE LAST decade, Distributed Power Generation Systems (DPGS) based on renewable energies contribute more and more to the total amount of energy production on the globe. Wind Turbines (WT) as well as Photovoltaics (PV) systems are seen as reliable energy sources which should be further explored in order to get maximum efficiency and overcome the increasing power demand in the world. Fig. 1 shows the installed capacity of wind and photovoltaic power in the last decade, where an exponential increase in both cases is observed [1], [2]. It is worth noting that the majority of this power is connected to the utility network.

Owed to the uncertainty of the availability of the input power, controllability of these systems is a challenge [3]. Moreover, the increased amount of distributed systems connected to the utility network can create instability of the power systems, even leading to outages. As a consequence, the Transmission System Operators (TSO) issue more stringent demands regarding the interconnection of the DPGS to utility grid [4]. The power generation systems are more and more requested to provide ancillary services in order to behave as a conventional power plant. As a consequence, the control of DPGS needs to be improved.

This paper discusses some possible control strategies that a DPGS can adopt when running on faulty grid conditions. First, a classification of the grid faults is presented, followed by some consideration about the control strategy when a fault take place in the grid. Then, the control strategies investigated in the work are further described, followed by the presentation of the algorithm used for detecting the positive and negative sequence of the grid voltage. Finally, experimental results are presented in order to verify the theory of each control structure. It has been demonstrated that there are several possibilities to deliver the same amount of power on a faulty grid with different degrees of oscillations in the instantaneous power.

II. Grid fault considerations

Among all the requests for interconnecting power distribution systems to the utility network, more and more stress is put on the ability of DPGS to ride through short grid disturbances such as voltage and frequency variations.

The grid faults can be classified in two main types [5]:

- *symmetrical fault* – when all three grid voltages register the same amplitude drop but the system remain balanced (no phase shifting is registered). This type of fault is very seldom in the power systems.
- *unsymmetrical fault* – when the phases register an unequal amplitude drop. Usually, phase shift between the phases also appears in this situation. This type of fault occurs due to one or two phases shorted to ground or to each other.

Considering the DPGS connected to the utility network as shown in Fig. 2, where a distribution transformer is used by the generation system to interface the power system, the

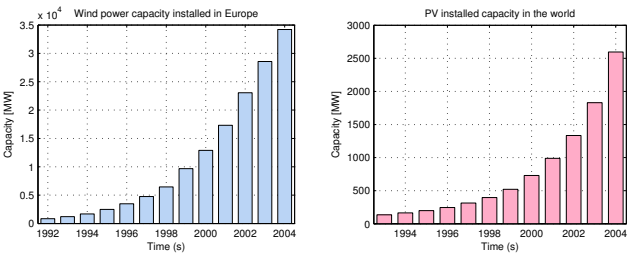

(a) (b)

Fig. 1. Installed capacity at the end of 2004: (a) wind energy in Europe [1] and (b) PV power in the world [2].

A.V. Timbus, R. Teodorescu and F. Blaabjerg are with the Institute of Energy Technology, Aalborg University, DK-9220 Aalborg, Denmark. Email: avt@iet.aau.dk, ret@iet.aau.dk, fbl@iet.aau.dk

P. Rodriguez is with the Dept. of Electrotechnical and Electronic Engineering, Technical University of Catalonia, Spain. Email: prodriguez@ee.upc.edu

M. Liserre is with the Dept. of Electrotechnical and Electronic Engineering, Polytechnic of Bari, 70125-Bari, Italy. Email: liserre@ieee.org

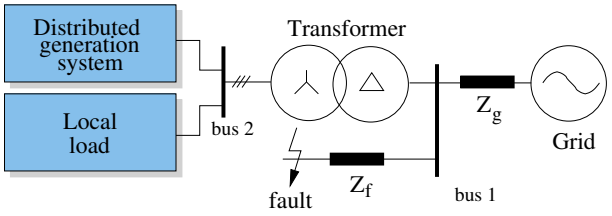

Fig. 2. Distributed generation system connected through a Δy transformer to the utility network.

propagation of a voltage fault occurring at the bus 1 appears different at the bus 2. For example, if a severe grid fault like single phase shorted to ground take place at bus 1, two of the voltages at the DPGS terminals (after the Δy transformer) experience a voltage drop which is dependent on the impedance of the line between the fault and DPGS transformer value. As a consequence, the voltages at bus 2 will have both amplitude and phase unbalance [5].

Characteristic to the unsymmetrical fault is the appearance of the negative sequence of the grid voltage. This gives raise to double frequency oscillations in the system, which are reflected as ripple in the dc-link voltage and output power [6].

III. Grid control considerations

Usually, in normal grid conditions the DPGS are requested to operate at unity power factor, such that the delivered power is synchronized with the one existing in the power system. In the situation when grid faults occur, there are several possible control strategies as it follows:

- *instantaneous unity power factor control* – maintaining the power factor unity on the fault conditions. In this situation, the grid currents will be very distorted but the instantaneous active and reactive power delivered by the system will be constant.
- *positive sequence control* – when only the positive sequence of the grid voltage is used in the control structure. In this case, the output currents are sinusoidal and balanced but double frequency oscillations will appear in both active and reactive power delivered to the utility network.
- *compensation for oscillations in active power* – when a negative sequence current reference can be calculated and summed up to the positive sequence current reference in order to compensate for the double frequency oscillations in the active power. In this situation, the grid currents are sinusoidal but unbalanced. Moreover, double frequency oscillations still exist in the reactive power.
- *compensation for oscillations in reactive power* – when the negative sequence current reference is calculated to compensate for the oscillations in the reactive power. Again, the grid currents are sinusoidal but unbalanced and the active power exhibits oscillations this time.

As a consequence, these strategies can be used by the grid operators when designing the grid codes for the power generation systems. Depending on the grid type, i.e. strong, weak, etc. and on the grid fault, different fault strategies for the DPGS can be requested in order to support the grid.

This paper investigates the algorithms for creating the references for the grid currents according to the above control strategies. A detailed description of each control strategy as well as equations for the current reference is given in the following.

IV. Strategies for the generation of current references

In the followings, only the grid side control of a DPGS having a back-to-back converter structure is discussed. The instantaneous active power p, delivered by a three-phase inverter to the grid depends on the voltage vector in the point of common coupling (PCC), $\mathbf{v} = (v_a, v_b, v_c) \in \mathbb{R}^3$, and on the injected current vector in this point, $\mathbf{i} = (i_a, i_b, i_c) \in \mathbb{R}^3$, that is:

$$p = \mathbf{v} \cdot \mathbf{i} \tag{1}$$

where $\cdot$ represents the dot product. Therefore, for a given voltage vector there exist infinite current vectors which are able to deliver exactly the same instantaneous active power to the grid. In this work, it has been assumed that the energy source supplying power through the inverter exhibits slow dynamics and hence active power reference will be considered a constant throughout each grid voltage cycle. However, conclusions from this study are also valid for those cases in which the reference for the instantaneous active power could experiment oscillations throughout a grid period, e.g., when active filtering functionality is implemented in the inverter.

Next paragraphs propose three different strategies for generating inverter reference currents in order to deliver to the grid the active power $p^* = P$. In these strategies it has been assumed that no reactive power should be injected to the grid ($q^* = 0$). A particular attention on this issue is paid at the end of this section, where the control strategy for compensating the oscillations in the reactive power is discussed.

A. Instantenous unity power factor (IUPF) strategy

The most efficient set of currents delivering the instantaneous active power P to the grid can be calculated as follow:

$$\mathbf{i}_p^* = g\mathbf{v}; \qquad \text{where: } g = \frac{P}{|\mathbf{v}|^2} \tag{2}$$

and $|\mathbf{v}|$ denotes the module or l^2- norm [7] of the three-phase voltage vector $\mathbf{v}$ and g is the instantaneous conductance seen from the inverter output. Its value is a constant in balanced sinusoidal conditions but under grid faults however, the negative-sequence component gives rise to oscillations at twice the fundamental frequency in $|\mathbf{v}|$. Consequently, the injected currents will not keep their sinusoidal waveform and high order components will appear in their waveform. Current vector of (2) is instantaneously proportional to the voltage vector and therefore does not have any orthogonal component in relation to the grid voltage, hence gives rise to the injection of no reactive power to the grid.

B. Positive sequence (PS) strategy

When the quality of the currents injected in the grid plays a decisive role they can be calculated using the positive sequence voltage only [8]:

$$\mathbf{i}_p^* = g^+\mathbf{v}^+; \qquad \text{where:} \quad g^+ = \frac{P}{|\mathbf{v}^+|^2} \tag{3}$$

and $\mathbf{v}^+$ is the positive-sequence component of the grid voltage at fundamental frequency. When the three-phase utility voltage is sinusoidal and balanced the instantaneous active power supplied to the grid will coincide with P and the reactive power will be equal zero. In the presence of voltage imbalance however, the instantaneous active power delivered to the grid will differ from P because of the interaction between the positive-sequence injected current and the negative-sequence grid voltage. Assuming that the current injected by the inverter at the PCC perfectly tracks the reference current, the instantaneous active power supplied to the network under voltage unbalanced conditions is:

$$p = \mathbf{v}\cdot\mathbf{i}_p^* = \underbrace{\mathbf{v}^+\cdot\mathbf{i}_p^*}_{P} + \underbrace{\mathbf{v}^-\cdot\mathbf{i}_p^*}_{\tilde{p}} \tag{4}$$

where $\tilde{p}$ is power oscillation at twice the fundamental frequency. Similarly, the instantaneous reactive power can be calculated as:

$$q = |\mathbf{v}\times\mathbf{i}_p^*| = \underbrace{|\mathbf{v}^+\times\mathbf{i}_p^*|}_{0} + \underbrace{|\mathbf{v}^-\times\mathbf{i}_p^*|}_{\tilde{q}} \tag{5}$$

where the $\times$ sign denotes the cross product. It is possible to appreciate in (5) how oscillations at twice fundamental utility frequency will also appear in the instantaneous reactive power injected to the grid.

Remarkable for this strategy is that an algorithm for detecting the positive and negative sequence of the grid voltages is necessary. The system used in this work is described further in § V.

C. Active power oscillation compensation (APOC) strategy

The instantaneous active power delivered by means a generic unbalanced active current $\mathbf{i}_p = \mathbf{i}_p^+ + \mathbf{i}_p^-$ injected in an unbalance grid with $\mathbf{v} = \mathbf{v}^+ + \mathbf{v}^-$ can be expressed as:

$$p = \mathbf{v}\cdot\mathbf{i}_p = \mathbf{v}^+\cdot\mathbf{i}_p^+ + \mathbf{v}^-\cdot\mathbf{i}_p^- + \mathbf{v}^+\cdot\mathbf{i}_p^- + \mathbf{v}^-\cdot\mathbf{i}_p^+ \tag{6}$$

In order to cancel the oscillations in the instantaneous active power the following constraints can be imposed for the reference current calculation:

$$\mathbf{v}^+\cdot\mathbf{i}_p^{*+} + \mathbf{v}^-\cdot\mathbf{i}^{*-} = P \tag{7a}$$

$$\mathbf{v}^+\cdot\mathbf{i}_p^{*-} + \mathbf{v}^-\cdot\mathbf{i}_p^{*+} = 0 \tag{7b}$$

From (7a), the positive sequence reference current can be written as:

$$\mathbf{i}_p^{*+} = \frac{P}{|\mathbf{v}^+|^2 - |\mathbf{v}^-|^2}\mathbf{v}^+ \tag{8}$$

Substituting (8) in (7b) and simplifying, the negative sequence reference current can be calculated using:

$$\mathbf{i}_p^{*-} = -\frac{\mathbf{v}^+\cdot\mathbf{i}_p^{*+}}{|\mathbf{v}^+|^2}\mathbf{v}^- \tag{9}$$

The final reference current value can be obtained by summing up (9) and (8). These two equations indicate that the positive sequence voltage and current components have the same direction whereas their negative sequence components have an opposite direction. Therefore the injected current vector and the voltage vector contain components with different directions, thus the instantaneous reactive power injected to the grid is not equal to zero but exhibits second frequency oscillations due to the interaction of the positive and negative components of both voltage and current [9].

D. Reactive power oscillation compensation (RPOC) strategy

It is worth to remark that to inject in the grid a nonzero mean value of instantaneous reactive power it is necessary the interaction between two orthogonal vectors of voltage and current with the same frequency and sequence. In the earlier control strategies, current and voltage vectors with the same sequence and frequency have always the same direction – they are not orthogonal. Therefore, the instantaneous reactive power injected in the grid by means of such strategies will be entirely oscillatory and its mean value over a grid cycle will be equal zero.

Moreover, it is possible to find a current vector which is in-quadrature with the voltage vector and injects the following instantaneous reactive power to the grid:

$$q = |\mathbf{v}\times\mathbf{i}_q| = \mathbf{v}_\perp\cdot\mathbf{i}_q \tag{10}$$

where $\mathbf{v}_\perp$ is a 90-degrees leading version of the voltage vector. Consequently, the reference reactive current for the inverter in order to inject a constant reactive power Q in the grid can be calculated as:

$$\mathbf{i}_q^* = b\mathbf{v}_\perp \quad \text{where:} \quad b = \frac{Q}{|\mathbf{v}|^2} \tag{11}$$

is the instantaneous susceptance seen from the inverter output. If $\mathbf{v} = (v_\alpha, v_\beta) \in \mathbb{R}^2$ then $\mathbf{v}_\perp = (-v_\beta, v_\alpha) \in \mathbb{R}^2$ and (11) coincides with the expression proposed in [10] to calculate the reactive currents in three-phase three-wire systems. The reference current calculated from (11) should be added to the references currents obtained by the earlier control strategies in order to independently control the instantaneous reactive power supplied to the grid, without modifying the instantaneous active power. If the current quality is an important issue, the reactive currents can be calculated using the positive sequence of the voltage vector:

$$\mathbf{i}_q^* = b^+\mathbf{v}_\perp^+ \quad \text{where:} \quad b^+ = \frac{Q}{|\mathbf{v}^+|^2} \tag{12}$$

Using (12) and considering unbalanced conditions, the instantaneous active and reactive power supplied to the grid does

not correspond to the reference ($p^* = P,\ q^* = Q$) as they register double frequency oscillations as shown below:

$$p = \mathbf{v} \cdot \mathbf{i}_q^* = \underbrace{\mathbf{v}^+ \cdot \mathbf{i}_q^*}_{0} + \underbrace{\mathbf{v}^- \cdot \mathbf{i}_q^*}_{\tilde{p}} \tag{13a}$$

$$q = \mathbf{v}_\perp \cdot \mathbf{i}_q^* = \underbrace{\mathbf{v}_\perp^+ \cdot \mathbf{i}_q^*}_{Q} + \underbrace{\mathbf{v}_\perp^- \cdot \mathbf{i}_q^*}_{\tilde{q}} \tag{13b}$$

E. Discussion

When the IUPF or the APOC strategies are used for reference current calculation the instantaneous active power supplied by the inverter does not present oscillations, even during severe grid faults. This constant flow of energy helps to keep constant the dc-bus voltage without oscillations, making easier the control of the inverter under such adverse grid conditions. Under generic voltage conditions, the reference currents calculated by the IUPF supply exactly the desired instantaneous active power with the minimum instantaneous amplitude for the injected current vector. However the injected currents can be strongly distorted, which could give rise to other effects like resonances, voltage distortion at the PCC or malfunctions in the electrical equipments. The PS strategy yields sinusoidal balanced positive-sequence currents independently of the voltage appearance. During grid faults, this strategy gives rise to oscillations at twice the utility frequency in the instantaneous active power supplied to the grid. These power oscillations make more difficult the dc-bus voltage control and can be propagated toward the inverter energy source generating overheating, giving rise to mechanical resonances and eventually speeding up its ageing. Reactive power can be controlled independently of the active power by a similar approach. A short introduction has been given here but the discussion of reactive power control is beyond the scope of this paper, therefore will be treated in a further work.

V. Detection of Positive and Negative Sequence

Precise characterization of the grid voltage is a crucial issue to have a full control over the power delivered from the DPGS to the grid. In this work, such characterization is performed by means of a positive- negative-sequence voltage detector based on a second order generalized integrator (SOGI). The SOGI diagram is shown in Fig. 3 and its transfer function is given by:

$$S(s) = \frac{y}{x}(s) = \frac{\omega_o s}{s^2 + \omega_o^2} \tag{14}$$

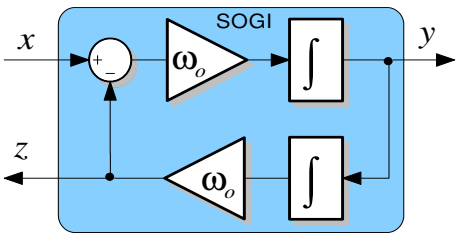

Fig. 3. The structure of the second order generalized integrator.

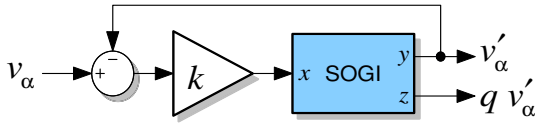

Fig. 4. Structure of a band pass filter based on SOGI implementation.

where ω_0 is the SOGI resonance frequency. If $x = X sin(\omega t + \phi)$, the SOGI acts as an ideal integrator when $\omega = \omega_0$. Therefore, the close-loop diagram shown in Fig. 4 gives rise to a second order band-pass filter (BPF) whose transfer function is:

$$V(s) = \frac{v'_\alpha}{v_\alpha}(s) = \frac{k\omega_o s}{s^2 + k\omega_o s + \omega_o^2} \tag{15}$$

Damping factor of (15) is directly related to the value selected for the gain k. The system in Fig. 4 exhibits interesting characteristics which make it suitable for grid voltage characterization:

- if ω_0 and k are properly chosen, v'_α will be almost sinusoidal and will match with the fundamental component of v_α.
- the signal qv'_α will be the quadrature-phase version of v_α (90 degrees lagged) which is very useful for the instantaneous detection of symmetrical components in three-phase systems [11].
- the SOGI resonance frequency can be adjusted by means of the proper phase locked-loop (PLL) making the system frequency adaptive [12].

Instantaneous positive- and negative-sequence components, $\mathbf{v}_{abc}^+$ and $\mathbf{v}_{abc}^-$, of a generic voltage vector are given by:

$$\mathbf{v}_{abc}^+ = \begin{bmatrix} v_a^+ & v_b^+ & v_c^+ \end{bmatrix}^T = [T_+]\ \mathbf{v}_{abc} \tag{16a}$$

$$\mathbf{v}_{abc}^- = \begin{bmatrix} v_a^- & v_b^- & v_c^- \end{bmatrix}^T = [T_-]\ \mathbf{v}_{abc} \tag{16b}$$

where $[T_+]$ and$[T_-]$ are defined as:

$$[T_+] = \frac{1}{3}\begin{bmatrix} 1 & a & a^2 \\ a^2 & 1 & a \\ a & a^2 & 1 \end{bmatrix} \tag{17a}$$

$$[T_-] = \frac{1}{3}\begin{bmatrix} 1 & a^2 & a \\ a & 1 & a^2 \\ a^2 & a & 1 \end{bmatrix} \tag{17b}$$

with:

$$a = e^{j\frac{2\pi}{3}}.$$

Using the *Clarke* transformation, the voltage vector can be translated from the abc to the $\alpha\beta$ reference frames as follow:

$$\mathbf{v}_{\alpha\beta} = \begin{bmatrix} v_\alpha & v_\beta \end{bmatrix}^T = [T_{\alpha\beta}]\ \mathbf{v}_{abc} \tag{18a}$$

$$[T_{\alpha\beta}] = \sqrt{\frac{2}{3}}\begin{bmatrix} 1 & -\frac{1}{2} & -\frac{1}{2} \\ 0 & \frac{\sqrt{3}}{2} & -\frac{\sqrt{3}}{2} \end{bmatrix} \tag{18b}$$

Therefore, the instantaneous positive- and negative-sequence voltage components on the $\alpha\beta$ reference frame can be calculated as:

$$\mathbf{v}_{\alpha\beta}^+ = [T_{\alpha\beta}]\,\mathbf{v}_{abc}^+ = [T_{\alpha\beta}][T_+][T_{\alpha\beta}]^T\,\mathbf{v}_{\alpha\beta} = \frac{1}{2}\begin{bmatrix} 1 & -q \\ q & 1 \end{bmatrix}\mathbf{v}_{\alpha\beta} \tag{19a}$$

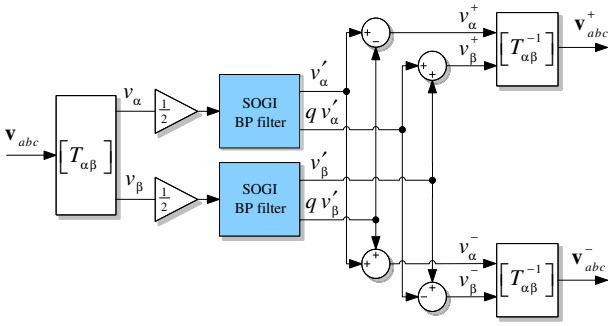

Fig. 5. The proposed structure for extracting positive and negative sequence of the grid voltages based on SOGI-BPF.

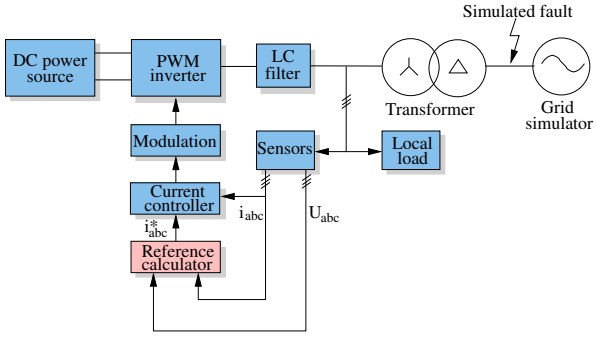

Fig. 6. Schematic of experimental setup used to test the proposed control strategies when the DPGS operate on faulty grid conditions.

$$\mathbf{v}^{-}_{\alpha\beta} = [T_{\alpha\beta}]\ \mathbf{v}^{-}_{abc} = [T_{\alpha\beta}]\,[T_{-}]\,[T_{\alpha\beta}]^{T}\,\mathbf{v}_{\alpha\beta} = \frac{1}{2}\begin{bmatrix} 1 & q \\ -q & 1 \end{bmatrix}\mathbf{v}_{\alpha\beta} \tag{19b}$$

$$q = e^{-j\frac{\pi}{2}}$$

where q is a phase-shift operator in the time-domain which obtains the quadrature-phase waveform (90-degrees lag) of the original in-phase waveform.

Hence the system shown in Fig. 5 is proposed for the detection of the positive- and negative sequence on the $\alpha\beta$ reference frame where a SOGI is used to generate the in-phase and quadrature-phase signals of (19a) and (19b). The proposed positive- and negative-sequence detection system exposed in this work provides an effective solution for grid synchronization of power converters in presence of grid faults. The SOGI-BPF increases the effectiveness of the detection system when the grid voltage presents high order harmonics. The calculation of the instantaneous symmetrical components on the $\alpha\beta$ reference frame makes possible to use only two SOGI-BPFs which reduces the computational burden of the proposed detection algorithm as compared with the calculations in abc where three SOGI-BPFs need to be implemented.

VI. Experimental System

The above control strategies have been implemented in an experimental setup comprising a PWM driven Voltage Source Inverter (VSI), and an LC filter ($L = 10mH,\ C = 0.7\mu F$ per phase) connected through a Δy transformer to the grid. The grid is here replaced by a programmable three phase ac power source, in order to be able to create grid faults. A control structure implemented in natural reference frame (abc) and using a dead beat controller for current control is implemented in a dSpace 1103 card. The sampling and switching frequencies are set to 15 kHz. Since the ac power source cannot accept power, a resistive local load has been connected to the system. The dc link controller has been omitted in order to not influence the creation of the current references. As a consequence, dc power sources are used to supply the necessary voltage in dc-link, which in this work was set to 700 V.

VII. Experimental Results

Experimental results in case of unsymmetrical voltage fault for three of the strategies are presented below. The ac power source has been programmed to decrease the RMS voltage of one phase down to 100 V. As a consequence, the voltages after the Δy transformer become as illustrated in Fig. 7(a). As it may be observed, amplitude drop and phase shift in two of the phases occur after the transformer.

A. Unity power factor control

The current waveforms as well as the output active and reactive power for this fault are depicted in Fig. 7(b) and Fig. 7(c)

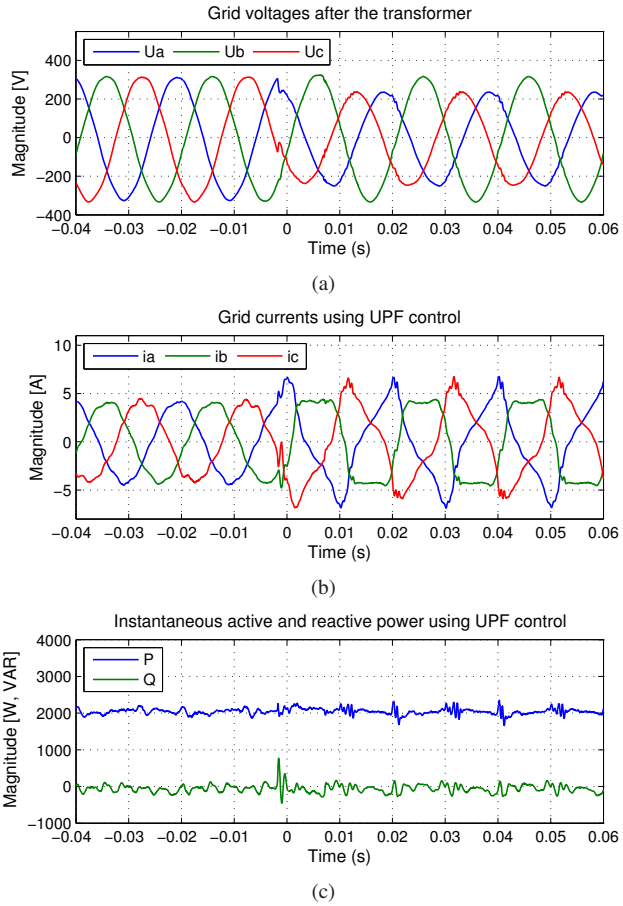

Fig. 7. Experimental results using unity power factor (UPF) control: (a) grid voltages after the Δ/Y transformer durring the unsymmetrical fault, (b) the grid currents and (c) the active and reactive power delivered to the utility network.

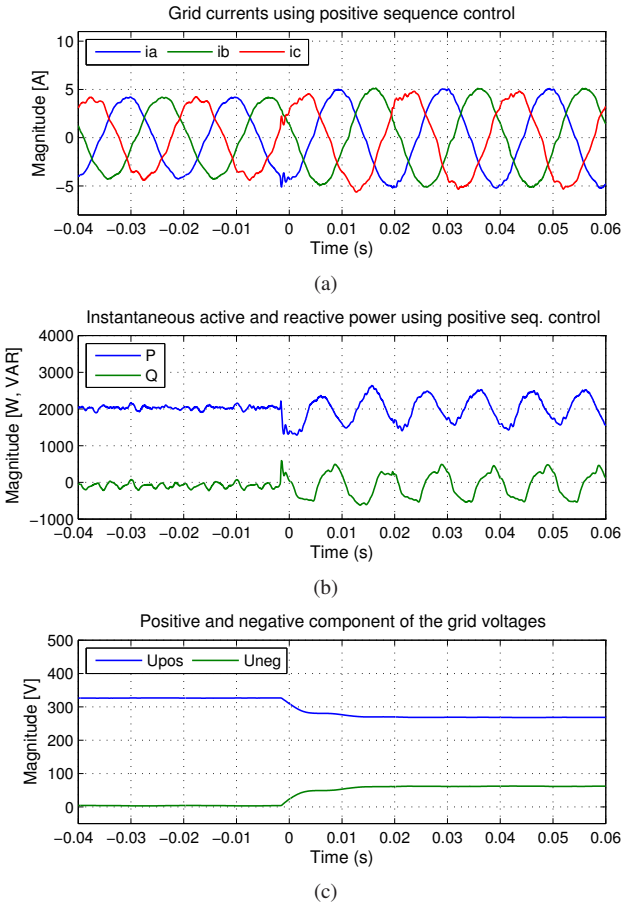

Fig. 8. Experimental results for positive sequence control: (a) grid currents, (b) active and reactive power delivered to the grid and (c) positive and negative component of the utility voltage estimated by the proposed system based on SOGI.

respectively. As it might be noticed, the current waveforms become very distorted in order to fulfill the demand of unity power factor control. In this situation, the instantaneous active and reactive power delivered to the utility network are constant during the fault.

B. Positive sequence control

The results in the case of positive sequence control on the same grid fault as shown in Fig. 7(a) are depicted on Fig. 8. It is worth to note that in this situation, the grid currents are sinusoidal and balanced during the fault since only the positive sequence voltages contribute to the creation of the current reference. An increase in the magnitude of the grid current during the fault is observed due to the decrease in magnitude of the positive sequence component of the utility voltage, as shown in Fig. 8(c).

Using the positive sequence control strategy it is noticeable the double frequency oscillations present in both the active and reactive power delivered to the utility network.

C. Active power compensation control

The experimental results when the compensation for the oscillations in the active power are presented in Fig. 9. In this

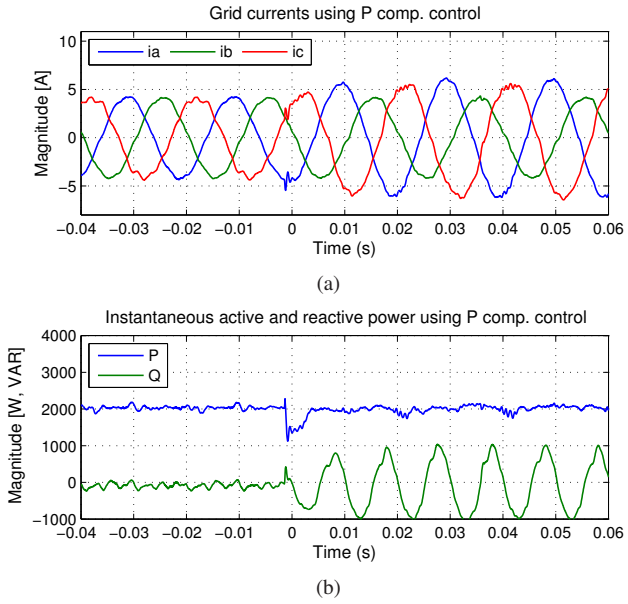

Fig. 9. Experimental results for the active power compensation control: (a) grid currents and (b) active and reactive power delivered to the utility network.

case, the grid currents are controlled in the way that the output active power is kept constant (Fig. 9(b)) while oscillations in the reactive power are allowed. As noticed in Fig. 9(a), the generated currents are sinusoidal but unbalanced. The unbalance factor of the current is the inverse of the unbalance of grid voltages, thus the amplitude of each grid current is inverse proportional with the amplitude of its corresponding voltage. As illustrated in Fig. 9(b), double frequency oscillations exist in the instantaneous reactive power waveform, but its mean value is still zero.

VIII. Conclusion

The aim of the paper was to investigate several methods that deal with control of DPGS in the case of unbalance conditions caused by faulty grid. Particularly it has been proved that in such conditions, it is possible to obtain zero active and reactive power oscillations only accepting highly distorted currents. However, an intermediate solution allows having sinusoidal grid currents compensating for the oscillation in the active power only, while oscillations are present in the reactive one. Anyway it has been proved that the DPGS can be a very flexible power producer being able to work in constant current, constant active power or constant reactive power modes depending on the grid fault type and the utility network necessity.

IX. Acknowledgment

P. Rodriguez wants to thank to Ministerio de Ciencia y Tecnologia of Spain for supporting this work under the project ENE2004-07881-C03-02.

REFERENCES

[1] EWEA, "www.ewea.org/documents," Online Documentation, October 2005.

[2] IEA-PVPS, "Cumulative Installed PV power," www.iea-pvps.org, October 2005.

[3] F. Blaabjerg, Z. Chen, and S. Kjaer, "Power electronics as efficient interface in dispersed power generation systems," *IEEE Trans. on Power Electronics*, vol. 19, no. 5, pp. 1184–1194, 2004.

[4] T. Ackermann, *Wind Power in Power Systems*. John Wiley & Sons, Ltd., 2005, ISBN: 0-470-85508-8.

[5] M. H. J. Bollen, *Understanding Power Quality Problems: Voltage Sags and Interruptions*. IEEE Press, 2002.

[6] L. Moran, P. Ziogas, and G. Joos, "Design aspects of synchronous PWM rectifier-inverter systems under unbalanced input voltage conditions," *IEEE Trans. on Industry Applications*, vol. 28, no. 6, pp. 1286–1293, 1992.

[7] R. A. Horn and C. R. Johnson, *Matrix Analysis*. Cambridge University Press, 1990.

[8] M. Liserre, C. Klumpner, F. Blaabjerg, V. Monopoli, and A. Dell'Aquila, "Evaluation of the ride-through capability of an active-front-end adjustable speed drive under real grid conditions," in *Proc. of IECON'04*, vol. 2, 2004, pp. 1688–1693.

[9] A. Stankovic and T. Lipo, "A novel control method for input output harmonic elimination of the PWM boost type rectifier under unbalanced operating conditions," *IEEE Trans. on Power Electronics*, vol. 16, no. 5, pp. 603–611, 2001.

[10] H. Akagi, Y. Kanazawa, and A. Nabae, "Instantaneous reactive power compensator comprising switching devices without energy storage components," *IEEE Trans. on Industry Application*, vol. IA-20, pp. 625–630, 1984.

[11] M. Ciobotaru, R. Teodorescu, and F. Blaabjerg, "Improved PLL structures for single-phase grid inverters," in *Proc. of EPE'05*, 2005, CDROM.

[12] P. Rodriguez, R. Teodorescu, I. Candela, A. V. Timbus, and F. Blaabjerg, "New positive-sequence voltage detector for grid synchronization of power converters under faulty grid conditions," in *Proc. of PESC'06*, 2006.

Publication 15

Independent PQ control for distributed power generation systems under grid faults

by P. Rodriguez, A. Timbus, R. Teodorescu, M. Liserre and F. Blaabjerg
Article published in Proceedings of IECON'06, pages 5185 – 5190, 2006

Independent PQ Control for Distributed Power Generation Systems under Grid Faults

P. Rodríguez[^], A.V. Timbus[⋆], R. Teodorescu[⋆], M. Liserre[*] and F. Blaabjerg[⋆]

[^]Power Quality and Renewable Energy
Technical University of Catalonia
Barcelona - SPAIN
prodriguez@ee.upc.edu

[⋆]Institute of Energy Technology
Aalborg University
Aalborg - DENMARK
avt@iet.aau.dk

[*]Electrotechnical and Electronic Eng. Dept.
Polytechnic of Bari
Bari - ITALY
liserre@poliba.it

***Abstract* – This work aims to present a generalized vector-based formulation for calculating the grid-side current reference of distributed power generation systems in order to independently control active and reactive power delivered to the grid. Strategies for current reference generation were implemented on the *abc* stationary reference frame and their effectiveness was demonstrated experimentally, perhaps validating the theoretical analysis even under grid fault conditions.**

I. INTRODUCTION

In the last fifteen years, the penetration of the wind turbine power generation is noticeably increased worldwide, i.e., from 7600 MW production in 1997 to 50000 MW at the end of 2005 and it will reach 180000 MW in 2010. This growing trend is stimulating the research in the power processing field aiming to optimize the energy extraction from the wind and the energy injection into the grid. As the wind penetration is increasing, the international standards are oriented to consider the wind turbine systems as classical generation system that should sustain the grid when necessary – mainly be faulty-active during short-circuits, do not contribute to the short-circuit power, have rolling capacity into the grid and generate/absorb reactive power [1]. These requirements make possible to foresee that the future standard wind systems will include a back-to-back converter. This would allow the full control on the power injected into the grid. Therefore, a wind generation system has to be able to 'ride through' a severe voltage dip or swell, as well as a frequency disturbance or other occurrences of deteriorated power quality.

The main problems that could lead a grid inverter to trip, under faulty grid operating conditions, are: under-/over-voltage and voltage oscillations in the dc-bus and over-currents due to distortion and imbalance [2]. However, while a grid inverter equipped with a well designed dc-bus voltage controller can sustain the dc-bus voltage and make it stiff respect to balanced dips, the effects due to imbalance both on the ac-side (current) and on the dc-side (dc voltage) are more dangerous. In fact, different grid disturbances should be treated in different ways. Many of the methods presented in literature propose a rigid constraint on the reference current that lead to inherent limitations such as reactive power oscillation [3] or impossibility to regulate the active and reactive powers independently [4][5].

On the contrary, this works aims to present a generalized vector-based formulation for current reference generation which can be applied on either the stationary or synchronous reference frame. In this work, these strategies have been implemented on the *abc* stationary reference frame.

II. CALCULATION OF CURRENT REFERENCES DELIVERING ACTIVE POWER

The instantaneous active power, p, supplied by a three-phase inverter to the grid is calculated by:

$$p = \mathbf{v} \cdot \mathbf{i}\,, \tag{1}$$

where $\mathbf{v} = (v_a, v_b, v_c) \in \mathbb{R}^3$ is the voltage vector in the point of common coupling (PCC), $\mathbf{i} = (i_a, i_b, i_c) \in \mathbb{R}^3$ is the injected current vector in such point, and '$\cdot$' represents the dot product. Consequently, for a given voltage vector at the PCC, there exist infinite current vectors which are able to supply exactly same instantaneous active power to the grid.

In distributed generation systems, the instantaneous active power delivered by the energy source to the grid can be assumed as a constant throughout a grid period, T. Therefore, the reference of the instantaneous active power supplied by the front-end inverter of the back-to-back converter can be also considered a constant throughout each grid cycle, that is $p^* = P$. *Kirchhoff*'s current law guarantees that zero-sequence component of the currents in a three-phase three-wire system is always zero. In consequence, zero-sequence component of the grid voltage does not contribute to power transfer and it can be neglected in powers calculation. Thus, this study assumes that grid voltage used in equations, **v,** has been previously treated and only consists of positive- and negative-sequence components. Therefore, voltage and current vectors could be also expressed as $\mathbf{v} = (v_\alpha, v_\beta) \in \mathbb{R}^2$ and $\mathbf{i} = (i_\alpha, i_\beta) \in \mathbb{R}^2$, respectively.

Next paragraphs propose five different strategies to generate current references for the front-end inverter in order to deliver the active power P to the grid. In a first stage of this study, it has been supposed that no reactive power is injected into the grid, that is $q^* = 0$.

A. Instantaneous active-reactive control (IARC)

The most efficient set of currents delivering exactly the instantaneous active power P to the grid under generic voltage conditions can be calculated as follow [6][7]:

$$\mathbf{i}_p^* = g\,\mathbf{v} \quad ; \quad g = \frac{P}{|\mathbf{v}|^2}\,, \tag{2}$$

where $|\mathbf{v}|$ denotes the module –or collective value [7]– of the three-phase voltage vector, **v,** and g is the instantaneous conductance seen from the inverter output. Under balanced sinusoidal conditions, current references are perfectly sinusoidal since $|\mathbf{v}|$ –and so g– are constants. In presence

of unbalanced grid faults however, $|\mathbf{v}|$ shows oscillations at twice the fundamental grid frequency due to the negative-sequence component of the faulty voltage. Consequently, the injected currents will not keep their sinusoidal waveform and high-order harmonics will appear in the current waveform during the grid fault. Current vector of (2) is instantaneously proportional to the voltage vector and so it does not have any orthogonal component in relation to the grid voltage, which gives rise to the injection of no reactive power to the grid.

Instantaneous power theories [6][7] allow identifying active and reactive components of the current for power delivery optimization –making reactive currents equal zero. However, when the quality of the current injected to the unbalanced grid becomes a major issue, it is necessary to establish certain constrains about how the current sequence-components and harmonics should be, even knowing that power delivery efficiency will decrease.

B. Instantaneously controlled positive-sequence (ICPS)

The instantaneous active power associated to an unbalanced current $\mathbf{i} = \mathbf{i}^+ + \mathbf{i}^-$ which is injected in the PCC of a three-phase unbalanced grid with $\mathbf{v} = \mathbf{v}^+ + \mathbf{v}^-$ is given by:

$$p = \mathbf{v} \cdot \mathbf{i} = \mathbf{v}^+ \cdot \mathbf{i}^+ + \mathbf{v}^- \cdot \mathbf{i}^- + \mathbf{v}^+ \cdot \mathbf{i}^- + \mathbf{v}^- \cdot \mathbf{i}^+ , \tag{3}$$

where supscripts '+' and '-' denote three-phase sinusoidal positive and negative-sequence signals, respectively.

From (3), positive-sequence current can be instantaneously controlled to deliver the active power *P* by imposing the following constrains in the current references calculation:

$$\mathbf{v} \cdot \mathbf{i}_p^{*+} = P , \tag{4a}$$

$$\mathbf{v} \cdot \mathbf{i}_p^{*-} = 0 . \tag{4b}$$

Expression of (4b) makes negative-sequence current components equal zero, whereas the positive-sequence current reference can be calculated from (4a) as follow:

$$\mathbf{i}_p^{*} = \mathbf{i}_p^{*+} + \mathbf{i}_p^{*-} = g^+ \mathbf{v}^+ \quad ; \quad g^+ = \frac{P}{\left|\mathbf{v}^+\right|^2 + \mathbf{v}^+ \cdot \mathbf{v}^-} . \tag{5}$$

According to the *p-q theory* [6], the instantaneous reactive power associated to the current vector of (5) is given by:

$$q = \left|\mathbf{v} \times \mathbf{i}_p^{*+}\right| = \underbrace{\left|\mathbf{v}^+ \times \mathbf{i}_p^{*}\right|}_{0} + \underbrace{\left|\mathbf{v}^- \times \mathbf{i}_p^{*}\right|}_{\tilde{q}} . \tag{6}$$

where the sign '×' denotes the cross product. It is possible to appreciate in (6) how the current references calculated by means the *ICPS* strategy give rise to oscillations at twice the fundamental utility frequency in the instantaneous reactive power injected to the grid.

It is worth to notice that positive- and negative-sequence components of the grid voltage should be perfectly characterized to implement this –and next– control strategy. Therefore, a PLL capable of detecting voltage sequence components under unbalanced operating conditions should be added to the control system [8][9].

C. Positive- negative-sequence compensation (PNSC)

Active power *P* can be delivered to the grid injecting sinusoidal positive- and negative-sequence currents at the PCC. To achieve it, the following constrains should be imposed in the current references calculation:

$$\mathbf{v}^+ \cdot \mathbf{i}_p^{*+} + \mathbf{v}^- \cdot \mathbf{i}_p^{*-} = P , \tag{7a}$$

$$\mathbf{v}^+ \cdot \mathbf{i}_p^{*-} + \mathbf{v}^- \cdot \mathbf{i}_p^{*+} = 0 . \tag{7b}$$

From (7b) the negative-sequence reference current can be written as:

$$\mathbf{i}_p^{*-} = -g^- \mathbf{v}^- \quad ; \quad g^- = \frac{\mathbf{v}^+ \cdot \mathbf{i}_p^{*+}}{\left|\mathbf{v}^+\right|^2} . \tag{8}$$

Substituting (8) in (7a) and simplifying, the positive-sequence reference current can be calculated by:

$$\mathbf{i}_p^{*+} = g^+ \mathbf{v}^+ \quad ; \quad g^+ = \frac{P}{\left|\mathbf{v}^+\right|^2 - \left|\mathbf{v}^-\right|^2} . \tag{9}$$

Adding (8) and (9), the final current references can be written as:

$$\mathbf{i}_p^{*} = \mathbf{i}_p^{*+} + \mathbf{i}_p^{*-} = g^{\pm}\left(\mathbf{v}^+ - \mathbf{v}^-\right) \quad ; \quad g^{\pm} = \frac{P}{\left|\mathbf{v}^+\right|^2 - \left|\mathbf{v}^-\right|^2} . \tag{10}$$

Expression (10) indicates that injected current and voltage vectors have different directions. Consequently, the instantaneous reactive power delivered to the grid is not equal to zero but exhibits second-order oscillations given by:

$$q = \left|\mathbf{v} \times \mathbf{i}_p^{*}\right| = \underbrace{\left|\mathbf{v}^+ \times \mathbf{i}_p^{*+}\right| + \left|\mathbf{v}^- \times \mathbf{i}_p^{*-}\right|}_{0} + \underbrace{\left|\mathbf{v}^+ \times \mathbf{i}_p^{*-}\right| + \left|\mathbf{v}^- \times \mathbf{i}_p^{*+}\right|}_{\tilde{q}} . \tag{11}$$

D. Average active-reactive control (AARC)

During unbalanced grid faults, current references obtained by means of the *IARC* strategy present high order harmonics in their waveform because the instantaneous conductance, *g*, does not remain constant throughout the grid period, *T*. Since *P* has been assumed as a constant, such harmonics come from the second-order component of $|\mathbf{v}|^2$, being:

$$\left|\mathbf{v}\right|^2 = \left|\mathbf{v}^+\right|^2 + \left|\mathbf{v}^-\right|^2 + 2\left|\mathbf{v}^+\right|\left|\mathbf{v}^-\right|\cos\left(2\omega t + \phi^+ - \phi^-\right) . \tag{12}$$

High-order harmonics in the current references will be cancelled if they are calculated by:

$$\mathbf{i}_p^{*} = G\,\mathbf{v} \quad ; \quad G = \frac{P}{V_\Sigma^2} , \tag{13}$$

where V_Σ is the collective rms value of the grid voltage and it is defined by:

$$V_\Sigma = \sqrt{\frac{1}{T}\int_0^T \left|\mathbf{v}\right|^2 dt} = \sqrt{\left|\mathbf{v}^+\right|^2 + \left|\mathbf{v}^-\right|^2} . \tag{14}$$

In this case, instantaneous conductance is a constant under periodic conditions, namely *g=G*. *Buchholz* [10], a precursor of the study on the time-domain of active and nonactive currents in polyphase systems, proved that, for a

given grid voltage **v**, the current references calculated by (13) lead to the smallest possible collective rms value of such currents, I_Σ, delivering the electrical energy $P \cdot T$ over one grid period. The lower value of I_Σ, the lower conduction losses in the system and the higher efficiency.

Current vector of (13) has the same direction that the grid voltage vector and so it will not give rise to any reactive power. However, the instantaneous active power delivered to the unbalanced grid will not equal *P* but it will be given by:

$$p = \mathbf{i}_p^* \cdot \mathbf{v} = \frac{|\mathbf{v}|^2}{V_\Sigma^2} P = P + \tilde{p} \,. \tag{15}$$

Substituting (12) and (14) in (15) it is easy to justify that instantaneous active power delivered to the unbalanced grid consists of a mean value *P* accompanied by oscillations $\tilde{p}$ at twice the grid frequency. Since *G* is a constant, voltage and current waveforms will be monotonously proportional.

E. Balanced positive-sequence (BPS)

When the quality of the currents injected in the grid plays a decisive role they can be calculated as:

$$\mathbf{i}_p^* = G^+ \mathbf{v}^+ \quad ; \quad G^+ = \frac{P}{\left|\mathbf{v}^+\right|^2}, \tag{16}$$

Current vector of (16) consists of a set of perfectly balanced positive-sequence sinusoidal waveforms. Under unbalance operating conditions, the instantaneous active power delivered to the grid will differ from *P* because of the interaction between the positive-sequence injected current and the negative-sequence grid voltage, that is:

$$p = \mathbf{v} \cdot \mathbf{i}_p^* = \underbrace{\mathbf{v}^+ \cdot \mathbf{i}_p^*}_{P} + \underbrace{\mathbf{v}^- \cdot \mathbf{i}_p^*}_{\tilde{p}}, \tag{17}$$

where $\tilde{p}$ is power oscillation at twice the fundamental utility frequency. Likewise, the instantaneous reactive power can be calculated as:

$$q = \left|\mathbf{v} \times \mathbf{i}_p^*\right| = \underbrace{\left|\mathbf{v}^+ \times \mathbf{i}_p^*\right|}_{0} + \underbrace{\left|\mathbf{v}^- \times \mathbf{i}_p^*\right|}_{\tilde{q}}, \tag{18}$$

where $\tilde{q}$ is also oscillating at twice the fundamental utility frequency.

Positive and negative-sequence vectors studied in this section can be considered as orthogonal –seen over one grid period– and represented on a Euclidean plane $\mathbb{R}^2$ since their scalar product throughout the grid period is always equal to zero, that is:

$$\overline{\mathbf{x}^+ \cdot \mathbf{y}^-} = \frac{1}{T} \int_0^T \mathbf{x}^+ \cdot \mathbf{y}^- dt = 0 \,, \tag{19}$$

This graphic representation of voltage and current vectors is shown in Fig. 1 and allows a better understanding of previous strategies for current reference generation.

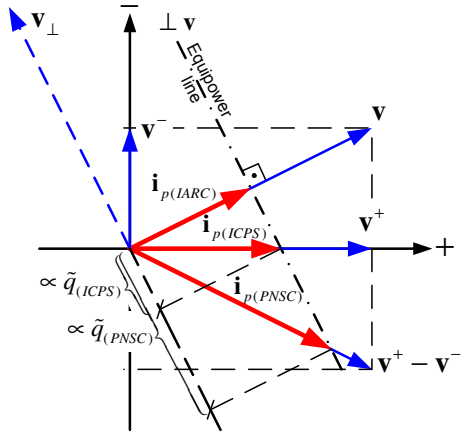

Fig. 1. Positive- and negative-sequence Euclidean plane.

For a better visualization and understanding, only current vectors from *IARC*, *ICPS*, and *PNSC* strategies have been represented in Fig. 1. Amplitude of all three current vectors is delimited by the 'equipower line', which is perpendicular to **v**. Amplitude of oscillations in the instantaneous reactive power associated to each strategy, $\tilde{q}$, is proportional to the projection of its current vector over the equipower line. Current vectors from *AARC* and *BPS* strategies have the same direction that those vectors from *IARC* and *ICPS* strategies, respectively. However, their amplitudes are not instantaneously controlled, generating oscillations in the active power. None of these strategies give rise to a finite mean value in the reactive power injected to the grid.

III. EVALUATION OF CONTROL STATEGIES DELIVERING ACTIVE POWER TO THE GRID

The above control strategies have been implemented in an experimental setup comprising a current-controlled VSI and an LC filter (L = 10mH; C = 0.7μF per phase) connected to the grid through a Δy transformer. The faulty grid is here replaced by a programmable three-phase ac-power source. A dSpace 1103 DSP card is used to implement a dead-beat current controller, the PLL for detecting positive- and negative-sequence voltage components, and the algorithm to calculate the current references on natural *abc* reference frame. The sampling and switching frequencies are set to 15 kHz. Since the ac-power source cannot accept power, a resistive local load has been connected to the system. The dc-link controller has been relaxed in order to not influence the creation of the current references. As a consequence, dc-power sources are used to supply the necessary dc-link voltage, which was set to 700 V.

Connected to the Δ winding of the transformer, the programmable ac-power source suddenly decreases the rms voltage of one phase from 220V to 100V, generating a dip type B with a characteristic voltage $V_B = 0.454$ pu. This single-phase fault is propagated to the *y* winding of the transformer as a dip type C with a characteristic voltage $V_C = 0.636$ pu [11]. It implies that positive- and negative-sequence phasors during the fault are given by $\vec{V}^+ = 0.818\angle 0^\circ$ pu and $\vec{V}^- = 0.182\angle 0^\circ$ pu, being the pre-fault voltage $\vec{V}_{pf}^+ = 1\angle 0^\circ$ pu. The power delivered to the grid

was P=1.5kW and Q=0.

Fig. 3 shows characteristics waveforms for the five previously presented control strategies. It is worth to say that experimental waveforms slightly differ from the theoretical ones because of the non-idealities of the inverter and grid, imperfections in the control, and sensing errors. However, these current and power plots properly ratify the conclusions of the theoretical study of § II.

To evaluate waveforms of Fig. 3 some characteristic indicators has been calculated and represented in Fig. 2. Data to calculate such indicators come from a simulation model carefully adjusted to reflect the behaviour of the actual experimental plant. Normalized in respect to its pre-fault value, the current collective rms value is calculated according to (14) and represented in Fig. 2(a). Collective rms values of current and voltage allow calculating the effective apparent power, $S_e = V_\Sigma I_\Sigma$. According to [12], S_e allows rational and correct computation of the power factor for sinusoidal unbalanced or for nonsinusoidal balanced or unbalanced situations. Therefore, the effective power factor [12], $P_{Fe} = P/S_e$, is calculated and represented in Fig. 2(b). This figure shows how PNSC is the least efficient strategy whereas AARC is the most. THD of a current waveform can be calculated as:

$$THD(\%) = \frac{1}{I_{(1)}}\sqrt{I_{RMS}^2 - I_{(1)}^2}\cdot 100\,. \qquad (20)$$

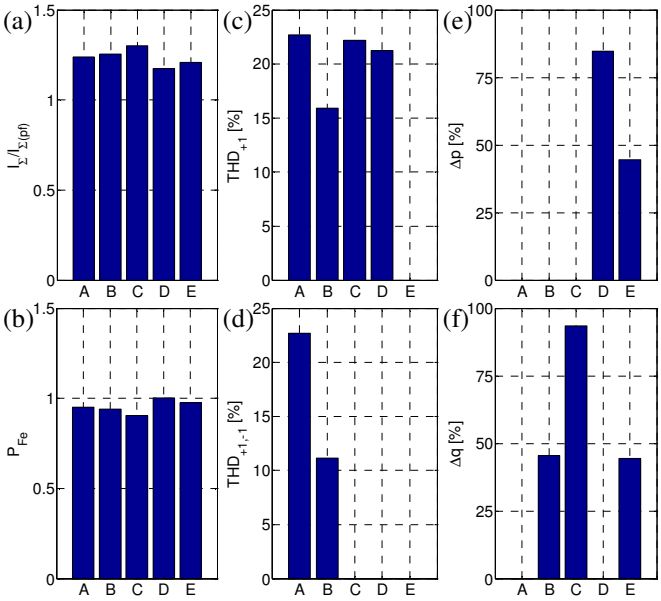

Fig. 2. Characteristic indicators of current reference generation strategies. [A-(IARC), B-(ICPS), C-(PNSC), D-(AARC), E-(BPS)].

In this work, overall current quality of the three-phase system will be evaluated by means of (20) but using collective instead of individual rms values. Moreover, in our unbalanced system can exist two fundamental frequency currents with opposite sequences. For this reason, two collective values of THD are calculated. Fig. 2(c) represents THD_{+1}, calculated assuming that the current component at fundamental frequency should be only positive-sequence.

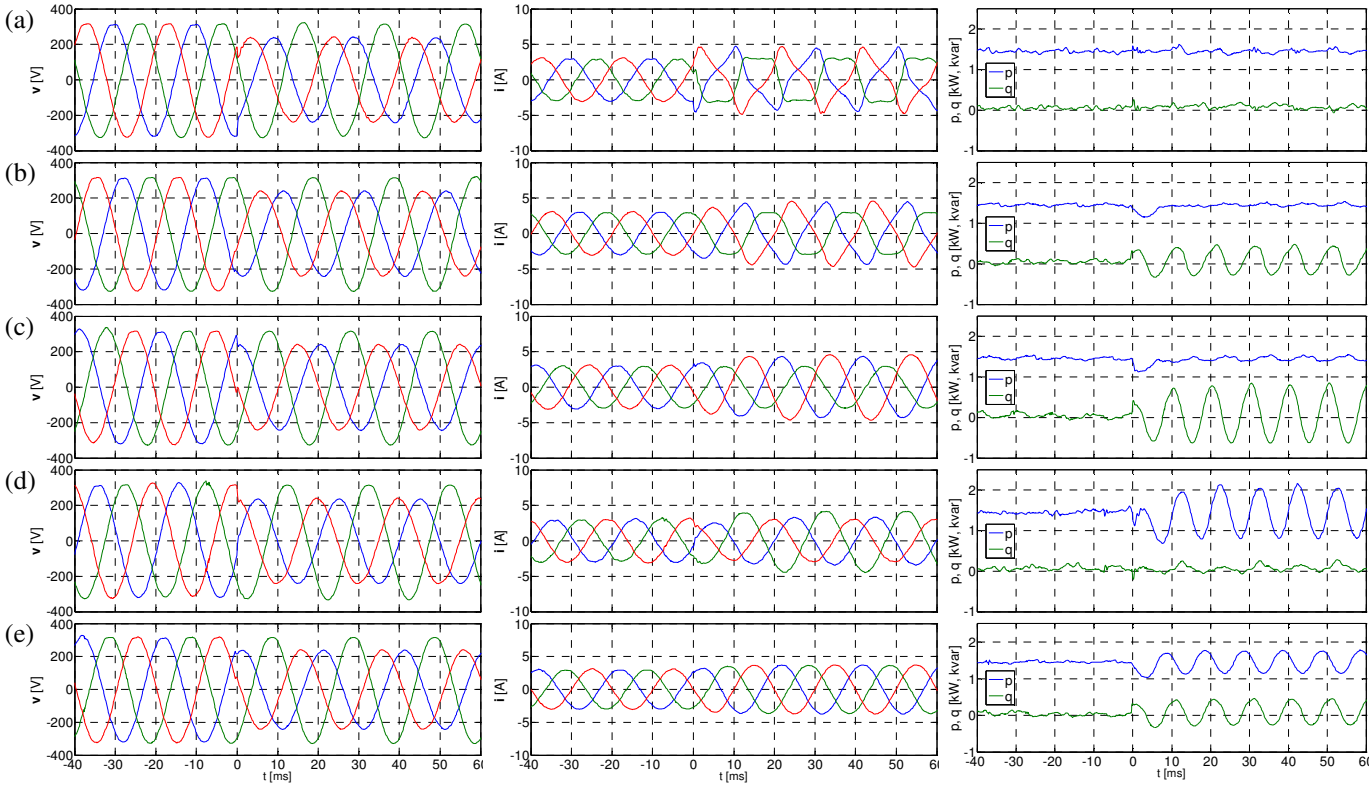

Fig. 3. Experimental results applying current reference strategies with P=1.5kW and Q=0. Columns from left to right: faulty grid voltage, injected currents, instantaneous active and reactive delivered power. (a) IARC, (b) ICPS, (c) PNSC, (d) AARC, and (e) BPS.

Fig. 2(d) represents $THD_{+1,-1}$, calculated assuming that current at fundamental frequency can consist of positive- and negative-sequence components. In these current quality plots, BPS strategy obtains the best results and IARC the worst. Fig. 2(e) represents the amplitude of the instantaneous active power oscillations referred to S_e.

These active power oscillations are automatically reflected as voltage oscillations in the dc-bus of the inverter. Strategies with a poor currents quality give rise to the smallest active power oscillations. Fig. 2(f) shows the amplitude of the instantaneous reactive power oscillations referred to S_e. These oscillations, moreover to generate unnecessary power losses and voltage drops, reduce the operating margin of the inverter.

IV. CALCULATION OF CURRENT REFERENCES DELIVERING REACTIVE POWER

In earlier control strategies, active current reference and voltage vectors with the same sequence and frequency had always the same direction. Therefore, the instantaneous reactive power injected in the grid by means of such strategies was entirely oscillatory and its mean value over a grid cycle was always equal zero. This section is devoted to find a reactive current vector, $\mathbf{i}_q$, which is in-quadrature with the voltage vector $\mathbf{v}$ and injects the following instantaneous reactive power to the grid:

$$q = \left|\mathbf{v}\times\mathbf{i}_q\right| = \mathbf{v}_\perp \cdot \mathbf{i}_q \,. \tag{21}$$

In (21), $\mathbf{v}_\perp$ is an imaginary 90-degree leaded version of the voltage vector $\mathbf{v}$, see Fig. 1

Following the same reasoning as in § II, five control strategies can be proposed to calculate the reactive current references. Without repeating all the analysis steps, such control strategies are formulated in the following, being b the instantaneous susceptance seen from output of the inverter.

A. Instantaneous active-reactive control (IARC)

$$\mathbf{i}_q^* = b\,\mathbf{v}_\perp \quad ; \quad b = \frac{Q}{\left|\mathbf{v}\right|^2} \tag{22}$$

B. Instantaneously controlled positive-sequence (ICPS)

$$\mathbf{i}_q^* = b^+\mathbf{v}_\perp^+ \quad ; \quad b^+ = \frac{Q}{\left|\mathbf{v}^+\right|^2 + \mathbf{v}^+\cdot\mathbf{v}^-} \tag{23}$$

C. Positive- negative-sequence compensation (PNSC)

$$\mathbf{i}_q^* = b^\pm\left(\mathbf{v}_\perp^+ - \mathbf{v}_\perp^-\right) \quad ; \quad b^\pm = \frac{Q}{\left|\mathbf{v}^+\right|^2 - \left|\mathbf{v}^-\right|^2} \tag{24}$$

D. Average active-reactive control (AARC)

$$\mathbf{i}_q^* = B\,\mathbf{v}_\perp \quad ; \quad B = \frac{Q}{V_\Sigma^2} \tag{25}$$

E. Balanced positive-sequence (BPS)

$$\mathbf{i}_q^* = B^+\mathbf{v}_\perp^+ \quad ; \quad B^+ = \frac{Q}{\left|\mathbf{v}^+\right|^2} \tag{26}$$

Using the same experimental setup as previously, reactive and active strategies were evaluated together delivering P=1.5kW and Q=1.3kvart to the grid. Fig. 4 shows characteristics waveforms obtained from such evaluation.

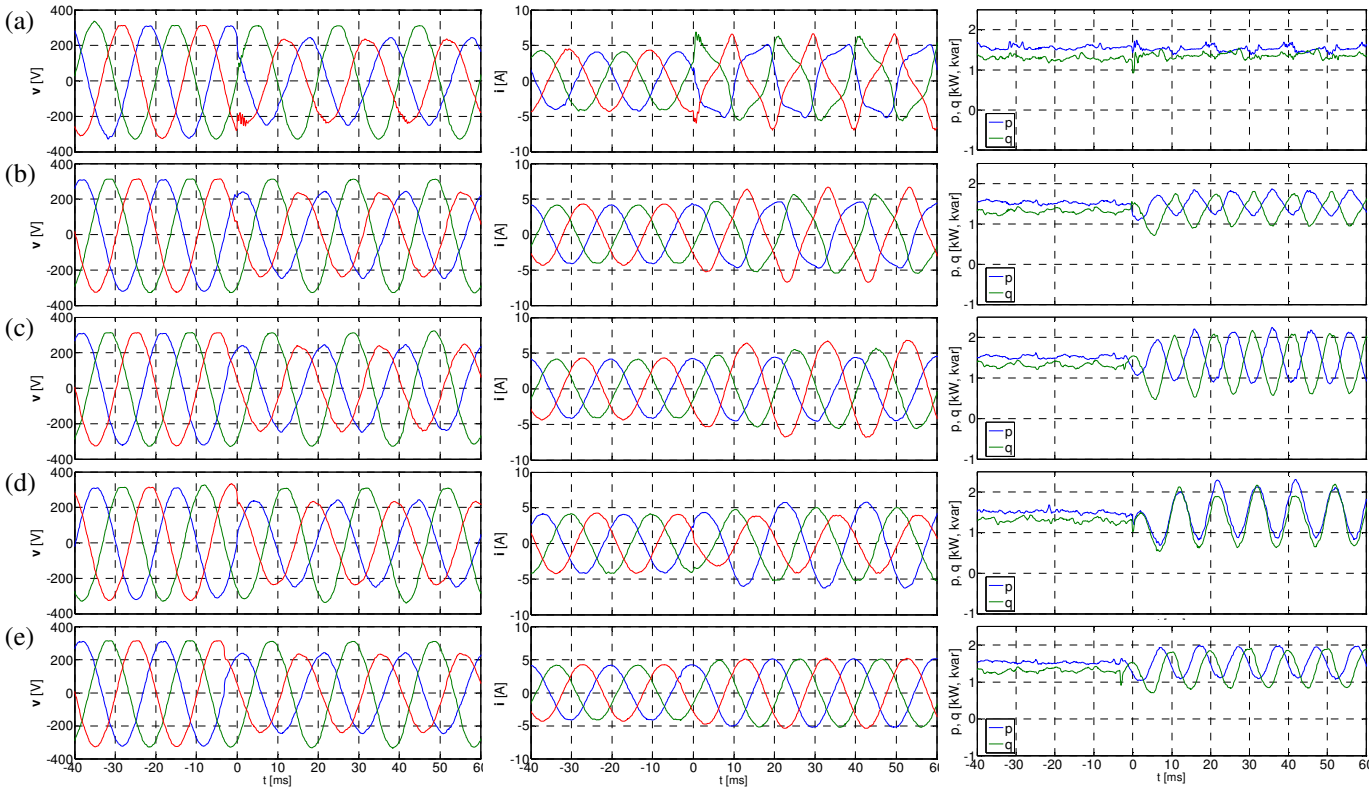

Fig. 4. Experimental results applying current reference strategies with P=1.5kW and Q=1.3kvar. Columns from left to right: faulty grid voltage, injected currents, instantaneous active and reactive delivered power. (a) IARC, (b) ICPS, (c) PNSC, (d) AARC, and (e) BPS.

Once more, experimental waveforms of Fig. 4 slightly differ from the theoretical ones because of the non-idealities of the experimental setup. In this experiment, the algorithm to calculate current references was implemented on natural *abc* reference frame and so the orthogonal voltage vector was calculated by:

$$\underset{(abc)}{\mathbf{v}_\perp} = \left[T_\perp\right]\mathbf{v}_{(abc)} \quad ; \quad \left[T_\perp\right] = \frac{1}{\sqrt{3}}\begin{bmatrix} 0 & -1 & 1 \\ 1 & 0 & -1 \\ -1 & 1 & 0 \end{bmatrix} \tag{27}$$

Current references of Fig. 4 result from a peer-to-peer combination of the previously exposed strategies to control the active and reactive power delivered to the grid, e.g., the reference current in Fig. 4(a) was calculated as:

$$\mathbf{i}^* = \mathbf{i}_p^* + \mathbf{i}_q^* = g\ \mathbf{v} + b\ \mathbf{v}_\perp , \tag{28}$$

however, any other combination of active and reactive terms could be also possible.

Analysis of the waveforms of Fig. 4 conducts to similar conclusions to those obtained when the characteristic indicators of Fig. 2 were discussed. The only remarkable difference is related to the oscillations in instantaneous powers. Fig. 4 evidences that only *IARC* strategy is able to keep constant the delivered instantaneous active and reactive powers when grid voltage is unbalanced. The rest of strategies present additional power oscillations given by:

$$\begin{aligned} &ICPS: P = \mathbf{v}^+ \cdot \mathbf{i}_p^* \ ;\ \tilde{p} = \mathbf{v}^- \cdot \mathbf{i}_q^* \\ &\qquad Q = \left|\mathbf{v}^+ \times \mathbf{i}_q^*\right| \ ;\ \tilde{q} = \left|\mathbf{v}^- \times \mathbf{i}_p^*\right| \end{aligned} \tag{29}$$

$$\begin{aligned} &PNSC: P = \mathbf{v}^+ \cdot \mathbf{i}_p^{*+} + \mathbf{v}^- \cdot \mathbf{i}_p^{*-} \ ;\ \tilde{p} = \mathbf{v}^+ \cdot \mathbf{i}_q^{*-} + \mathbf{v}^- \cdot \mathbf{i}_q^{*+} \\ &\qquad Q = \left|\mathbf{v}^+ \times \mathbf{i}_q^{*+}\right| + \left|\mathbf{v}^- \times \mathbf{i}_q^{*-}\right| ; \tilde{q} = \left|\mathbf{v}^+ \times \mathbf{i}_p^{*-}\right| + \left|\mathbf{v}^- \times \mathbf{i}_p^{*+}\right| \end{aligned} \tag{30}$$

$$\begin{aligned} &AARC: p = \mathbf{i}_p^* \cdot \mathbf{v} = \frac{|\mathbf{v}|^2}{V_\Sigma^2} P = P + \tilde{p} \\ &\qquad q = \mathbf{i}_q^* \cdot \mathbf{v} = \frac{|\mathbf{v}|^2}{V_\Sigma^2} Q = Q + \tilde{q} \end{aligned} \tag{31}$$

$$\begin{aligned} &BPS: P = \mathbf{v}^+ \cdot \mathbf{i}_p^* \ ;\ \tilde{p} = \mathbf{v}^- \cdot \left(\mathbf{i}_p^* + \mathbf{i}_q^*\right) \\ &\qquad Q = \left|\mathbf{v}^+ \times \mathbf{i}_q^*\right| \ ;\ \tilde{q} = \left|\mathbf{v}^- \times \left(\mathbf{i}_p^* + \mathbf{i}_q^*\right)\right| \end{aligned} \tag{32}$$

XI. CONCLUSION

This paper has presented and discussed five strategies to generate the current references for grid-connected inverters in order to independently control the active and reactive power delivered to the grid under unbalanced operating conditions. Study carried out in this work is completely general and strategies for generating current reference can be implemented on either the stationary or synchronous reference frame.

Hypotheses and assumptions adopted in the theoretical study of the strategies are ratified by simulation and experimental results. In the experimental setup, current control strategies were programmed on the *abc* stationary reference frame.

X. ACKNOWLEDGMENT

This work was supported by Ministerio de Ciencia y Tecnologia of Spain under Project ENE2004-07881-C03-02.

XI.- REFERENCES

[1] P.B. Eriksen, T. Ackermann, H. Abildgaard, P. Smith, W. Winter and J.M. Rodriguez, "System operation with high wind penetration," *IEEE Power and Energy Magazine*, vol.3, pp. 65- 74, Nov./Dec. 2005.

[2] L. Moran, P. D. Ziogas and G. Joos: "Design aspects of synchronous PWM rectifier-inverter system under unbalanced input voltage conditions", *IEEE Trans. on Ind. Applicat.*, vol. 28, Nov./Dec. 1992, pp. 1286-1293.

[3] A.V. Stankovic and T.A. Lipo, "A novel control method for input output harmonic elimination of the PWM boost type rectifier under unbalanced operating conditions," *IEEE Trans. on Power Electron.*, vol. 16, pp. 603-611, Sept. 2001.

[4] H-S. Song and K. Nam, "Dual current control scheme for PWM converter under unbalanced input voltage conditions," *IEEE Trans. on Ind. Electron.*, vol. 46, pp. 953-959, Oct. 1999.

[5] P. Rioual, H. Pouliquen, J.-P. Louis, "Regulation of a PWM rectifier in the unbalanced network state using a generalized model," *IEEE Trans. on Power Electron.*, vol.11, pp.495-502, May 1996.

[6] H. Akagi, Y. Kanazawa, and A. Nabae, "Instantaneous reactive power compensator comprising switching devices without energy storage components," *IEEE Trans. on Ind. Applicat.*, vol. IA-20, pp. 625-630, May/June 1984.

[7] M. Depenbrock, V. Staudt, and H. Wreder, "A theoretical investigation of original and modified instantaneous power theory applied to four-wire systems," *IEEE Trans. Ind. Applicat.*, vol. 39, pp. 1160-1167, July/Aug. 2003.

[8] P. Rodríguez, J. Pou, J. Bergas, I. Candela, R. Burgos, and D. Boroyevich, "Double synchronous reference frame PLL for power converters," *in Proc. IEEE Power Electron. Spec. Conf. (PESC'05)*, 2005, pp. 1415-1421.

[9] A. Timbus, P. Rodríguez, R. Teodorescu, M. Liserre and F. Blaabjerg, "Control strategies for distributed power generation systems operating on faulty grid," *in Proc. IEEE Int. Symp. Ind. Electron. (ISIE'06)*, 2006.

[10] F. Buchholz, "Das Begriffsystem Rechtleistung. Wirkleistung, totale Blindleistung," Munich, Germany: Selbstverlag, 1950.

[11] A. Sannino, M.H.J. Bollen, J. Svensson, "Voltage tolerance testing of three-phase voltage source converters," *IEEE Trans. Power Delivery*, vol. 20, Apr. 2005, pp. 1633-1639.

[12] IEEE Standard 1459-2000: *IEEE Trial-Use Standard Definitions for Power Measurement of Electric Power Quantities Under Sinusoidal, Nonsinusoidal, Balanced or Unbalanced Conditions.* IEEE, 21 June 2000. Upgraded to full-use December 2002.

Publication 16

Flexible active power control of distributed power generation systems during grid faults

by P. Rodriguez, A. Timbus, R. Teodorescu, M. Liserre and F. Blaabjerg
Article published in Transactions of Industrial Electronics, pages 2583 – 2592, 2007

Flexible Active Power Control of Distributed Power Generation Systems Running on Faulty Grid

Pedro Rodriguez, *Member, IEEE*, Adrian V. Timbus, *Student Member, IEEE*, Remus Teodorescu, *Senior Member, IEEE*, Marco Liserre, *Member, IEEE* and Frede Blaabjerg, *Fellow, IEEE*

***Abstract*—The increasing penetration of distributed power generation (DPG) into the power system leads to a continuous evolution of grid interconnection requirements. Particularly the active power control will play an important role both during grid faults (low voltage ride-through capability and controlled current injection) and in normal condition (reserve function and frequency regulation). The aim of this paper is to propose a flexible active power control based on a fast current control and a reconfigurable reference current selector. Several strategies to select the current reference are studied and compared using experimental results obtained during an unsymmetrical voltage fault. The results of the analysis allow selecting the best reference current in every condition. The proposed system can easily adapt itself to new grid requirements by simply changing the reference selection criteria.**

***Index Terms*—Distributed power generation systems, wind turbines, power control, control strategies, positive and negative sequence, grid faults.**

I. Introduction

IN THE LAST decade, Distributed Power Generation Systems (DPGS) based on renewable energies contribute more and more to the total amount of energy production on the globe. Wind Turbines (WT) as well as Photovoltaic (PV) systems are seen as reliable energy sources which should be further exploited in order to get maximum efficiency and overcome the increasing power demand in the world. These systems are not anymore regarded as an engineering issue but they are widely recognized as reliable systems which can have large share in the energy production in the future.

The possibility of energy production using a clean technology make both WT and PV systems very attractive but the control of these systems is a challenge due to the uncertainty of the availability of the input power [1]. Moreover, the increased amount of distributed systems connected to the utility network can create instability of the power systems, even leading to outages.

In order to maintain the power system stable in the countries with large penetration of distributed power, the Transmission System Operators (TSO) issue more stringent demands regarding the interconnection of the DPGS to utility grid [2]–[4]. Among the new demands, the power generation systems are requested ride through grid disturbances and to provide ancillary services in order to behave as a conventional power plant, hence to have the capability of sustaining the utility network in the situation of fault. Therefore, the grid fault influence into the control of DPGS needs to be investigated.

This paper discusses some possible control strategies that a DPGS can adopt when running on faulty grid conditions. First, a classification of the grid faults is presented, followed by some consideration about the control strategy when an unbalanced fault take place in the grid. Then, the control strategies investigated are further described, followed by the presentation of the algorithm used for detecting the positive and negative sequence of the grid voltage. Finally, experimental results are presented in order to verify the theory of each control strategy.

II. Grid fault considerations

One of the newly introduced request for interconnecting wind turbine systems to the utility network is stressing their ability to ride through short grid disturbances such as voltage and frequency variations. As a consequence, low voltage ride through feature of WT systems become of high interest nowadays.

In respect to the grid voltage variation, the grid faults can be classified in two main types [5]:

- *balanced fault* – when all three grid voltages register the same amplitude drop/swell but the system remain balanced. The occurance of this type of fault is extremely rare in the power systems.
- *unbalanced fault* – when the three grid voltages register an unequal amplitude drop/swell. Usually, phase shift between the phases also appears in this situation. This type of fault occurs due to one or two phases shorted to ground or to each other. In [5] and [6] a detailed description of unbalanced grid faults is given and five types of unbalanced faults are distinguished. Interesting fact is that the distribution transformer, usually Δy type, has also influence on how the grid fault appears at DPGS terminals. According to [6], all unbalanced grid faults create both uneven voltage magnitude and phase angle jump at DPGS terminals, when such transformer is used.

Fore example, considering the DPGS connected to the utility network as shown in Fig. 1, where a distribution transformer is used by the generation system to interface the utility network, the voltage fault occurring at bus 1 appears different at bus 2. If a severe grid fault like single phase shorted to ground takes place at bus 1, the voltage amplitude at the DPGS

P. Rodriguez is with the QUPER, Dept. of Electrotechnical and Electronic Engineering, Technical University of Catalonia, Spain. Email: prodriguez@ee.upc.edu

A.V. Timbus, R. Teodorescu and F. Blaabjerg are with the Institute of Energy Technology, Aalborg University, DK-9220 Aalborg, Denmark. Email: avt@iet.aau.dk, ret@iet.aau.dk, fbl@iet.aau.dk

M. Liserre is with the Dept. of Electrotechnical and Electronic Engineering, Polytechnic of Bari, 70125-Bari, Italy. Email: liserre@ieee.org

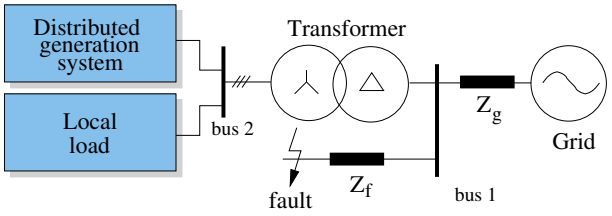

Fig. 1. Distributed generation system connected through a Δy transformer to the utility network.

terminals (after the transformer) will have a magnitude which is depending on the two impedance values Z_g and Z_f and the transformer type.

Characteristic to the unbalanced fault is the appearance of the negative sequence component in the grid voltages. This gives raise to double frequency oscillations in the system, which are reflected as ripple in the dc-link voltage and output power [7], [8]. These oscillations can lead to system trip if the maximum dc-link voltage is exceeded but also have a negative influence in the control of grid converter, e.g. producing a non-sinusoidal current reference which deteriorates considerably the power quality and even tripping the over-current protections. As a consequence, grid faults influence on the control of distributed power generation systems needs to be investigated.

III. Grid Fault Control Considerations

Owing to the appearance of negative sequence and amplitude drop of the grid voltages, the current magnitude delivered by the DPGS to the grid will rise considerably, for the same amount of delivered power. Moreover, a negative sequence current will appear, flowing uncontrolled through the power converter of the distribution system. In this sense, in [9] it is argued that switching of loads in micro-grids can cause relatively high transient of the voltage and it is suggested that all power generation units should support the grid during such a disturbance. Anyway, the bandwidth of communication signals between the DPGS connected into the micro-grid proves to be a big impediment for achieving a proper implementation of decentralized control. An improved solution, which bypasses this problem using variation of output impedance of each distributed system is proposed in [10]. Further on, in [11] an approach based on series inverter connected at PCC and controlled as current limiting impedance is proposed as a solution to limit the current rising inside the micro-grid.

With respect to the negative sequence current flowing through the grid connected power converter, in [12] and [13], the implementation of dual current controller, one for positive sequence and one for the negative sequence current has been discussed and improved results are noticed when the negative sequence current is also controlled. It should be noticed here that the complexity of the controller is doubled in this case and an algorithm for detection of both positive and negative sequence components is necessary. Anyway, as can be observed in [14], the ripple of the dc-link voltage still has influence on the reference currents, leading to non-sinusoidal current injection. Moreover, in [15], the authors discuss the possibility to control the negative sequence current in the way that cancels out the oscillation in the dc-link voltage. Again, the positive and negative sequence components of the voltage are necessary to be identified, but noticeable in this case is the lack of double frequency oscillations in the dc-link voltage.

This paper investigates the control possibilities of a DPGS when running on unbalanced grid faults. For simplicity, only the grid side converter is considered here, the input power source and its control being disregarded, hence the investigated control strategies can be applied to a variety of DPGS. Additionally, the dc-link voltage controller is not included in the control strategy. The design of this controller when the DPGS operates on faulty grid is beyond the purpose of this paper. Fig. 2 depicts the schematic of the proposed control, emphasizing the algorithm for positive and negative sequence detection and the control strategies block.

As [16] shows, there are different ways to structure the grid converter control and here the implementation in $\alpha\beta$ stationary reference frame using a dead beat current controller has been selected. The main contribution of this work is the creation of current references depending on selected control strategy, as Fig. 3 illustrates.

The following section provides a deep insight into the investigated strategies for generating the current references and analytical equations are provided and discussed. These strategies can be an add-on feature to the basic control structures of grid connected power generation systems [16] in order to facilitate different options when running through grid disturbances. As there are five different methods derived for generating current references, the work in this study is limited to active current/power control only, the reactive power control being disregarded.

IV. Current Control Strategies When Running on Grid Faults

The instantaneous active power p, delivered by a three-phase inverter to the grid depends on the voltage vector in the point of common coupling (PCC), $\mathbf{v} = (v_a, v_b, v_c)$, and on the injected current vector in this point, $\mathbf{i} = (i_a, i_b, i_c)$, such as:

$$p = \mathbf{v} \cdot \mathbf{i} \tag{1}$$

where $\cdot$ represents the dot product. Therefore, for a given voltage vector there exist infinite current vectors which are able to deliver exactly the same instantaneous active power to the grid. In this work, it has been assumed that the energy source supplying power through the inverter exhibits slow

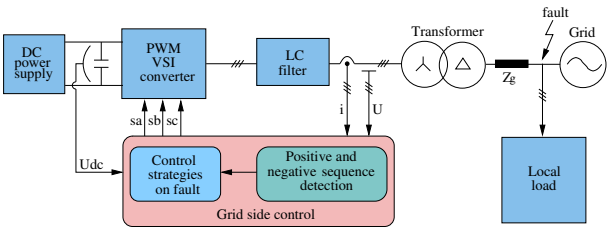

Fig. 2. Diagram of the laboratory setup used to test the proposed control strategies when running on faulty grid conditions.

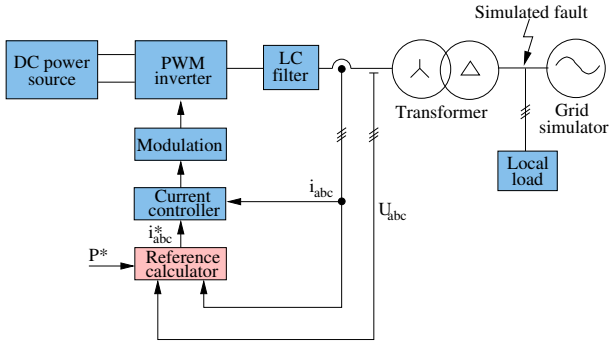

Fig. 3. Schematic of the proposed control structure when DPGS is running on faulty grid conditions.

dynamics and hence active power reference will be considered a constant throughout each grid voltage cycle. However, conclusions from this study are also valid for those cases in which the reference for the instantaneous active power could experiment oscillations throughout a grid period, e.g., when active filtering functionality is implemented in the inverter.

Next paragraphs propose five different strategies for generating inverter reference currents in order to deliver to the grid the active power $p = P^*$. In these strategies it has been assumed that no reactive power should be injected to the grid ($q^* = 0$).

A. Instantaneous active reactive control (IARC)

The most efficient set of currents delivering the instantaneous active power P to the grid can be calculated as follows [17]:

$$\mathbf{i}_p^* = g\mathbf{v}; \qquad \text{where: } g = \frac{P}{|\mathbf{v}|^2} \tag{2}$$

and $|\mathbf{v}|$ denotes the module of the three-phase voltage vector $\mathbf{v}$ and g is the instantaneous conductance seen from the inverter output. In this situation, the grid converter is controlled to emulate a symmetric resistance on all three phases [18]. The value of g is a constant in balanced sinusoidal conditions but under grid faults however, the negative-sequence component gives rise to oscillations at twice the fundamental frequency in $|\mathbf{v}|$. Consequently, the injected currents will not keep their sinusoidal waveform and high order components will appear in their waveform. Current vector of (2) is instantaneously proportional to the voltage vector and therefore does not have any orthogonal component in relation to the grid voltage, hence gives rise to the injection of no reactive power to the grid.

Instantaneous power theories [17], [19] allow identifying active and reactive components of the current for power delivery optimization making reactive currents equal zero. However, when the quality of the current injected to the unbalanced grid becomes a major issue, it is necessary to establish certain constrains about how the current sequence-components and harmonics should be, even knowing that power delivery efficiency will decrease.

B. Instantaneously controlled positive-sequence (ICPS)

The instantaneous active power associated to an unbalanced current $\mathbf{i} = \mathbf{i}^+ + \mathbf{i}^-$ which is injected at the PCC of a three-phase unbalanced grid with $\mathbf{v} = \mathbf{v}^+ + \mathbf{v}^-$ is given by:

$$p = \mathbf{v} \cdot \mathbf{i} = \mathbf{v}^+\mathbf{i}^+ + \mathbf{v}^-\mathbf{i}^- + \mathbf{v}^+\mathbf{i}^- + \mathbf{v}^-\mathbf{i}^+ \tag{3}$$

where superscripts "+" and "-" denote three-phase sinusoidal positive and negative-sequence signals, respectively. From (3), positive-sequence current can be instantaneously controlled to deliver the active power P by imposing the following constrains in the current references calculation:

$$\mathbf{v} \cdot \mathbf{i}_\mathbf{p}^{*+} = P \tag{4a}$$

$$\mathbf{v} \cdot \mathbf{i}_\mathbf{p}^{*-} = 0 \tag{4b}$$

Expression of (4b) makes negative-sequence current components equal zero, whereas the positive-sequence current reference can be calculated from (4a) as follows:

$$\mathbf{i}_\mathbf{p}^* = \mathbf{i}_\mathbf{p}^{*+} + \mathbf{i}_\mathbf{p}^{*-} = g^+\mathbf{v}^+; \tag{5a}$$

$$g^+ = \frac{P}{|\mathbf{v}^+|^\mathbf{2} + \mathbf{v}^+ \cdot \mathbf{v}^-} \tag{5b}$$

According to *p-q* theory [17], the instantaneous reactive power associated to the current vector of (5a) is given by:

$$q = \left|\mathbf{v} \times \mathbf{i}_p^{*+}\right| = \underbrace{\left|\mathbf{v}^+ \times \mathbf{i}_p^{*+}\right|}_{0} + \underbrace{\left|\mathbf{v}^- \times \mathbf{i}_p^{*+}\right|}_{\tilde{q}} \tag{6}$$

where the sign $\times$ denotes the cross product. It is possible to appreciate in (6) how the current references calculated by means the ICPS strategy give rise to oscillations at twice the fundamental utility frequency in the instantaneous reactive power injected to the grid.

It is worth noticing that positive- and negative-sequence components of the grid voltage should be perfectly characterized to implement this control strategy. Therefore, an algorithm capable of detecting the voltage sequence components under unbalanced operating conditions should be added to the control system. The description of the algorithm used in this work is further presented in Section V.

C. Positive- negative-sequence compensation (PNSC)

Active power P can be delivered to the grid injecting sinusoidal positive- and negative-sequence currents at the point of common coupling. To achieve this, the following constrains should be imposed in the current references calculation:

$$\mathbf{v}^+ \cdot \mathbf{i}_p^{*+} + \mathbf{v}^- \cdot \mathbf{i}_p^{*-} = P \tag{7a}$$

$$\mathbf{v}^+ \cdot \mathbf{i}_p^{*-} + \mathbf{v}^- \cdot \mathbf{i}_p^{*+} = 0 \tag{7b}$$

From (7b) the negative-sequence reference current can be written as:

$$\mathbf{i}_p^{*-} = -g^-\mathbf{v}^-; \qquad \text{where:} \qquad g^- = \frac{\mathbf{v}^+ \cdot \mathbf{i}_p^{*+}}{|\mathbf{v}^+|^2} \tag{8}$$

Substituting (8) in (7a) and simplifying, the positive-sequence reference current can be calculated by:

$$\mathbf{i}_p^{*+} = g^+\mathbf{v}^+; \qquad \text{with:} \qquad g^+ = \frac{P}{|\mathbf{v}^+|^2 - |\mathbf{v}^-|^2} \tag{9}$$

Adding (8) and (9), the final current reference becomes:

$$\mathbf{i}_p^* = \mathbf{i}_p^{*+} + \mathbf{i}_p^{*-} = g^{\pm}\left(\mathbf{v}^+ - \mathbf{v}^-\right); \tag{10a}$$

$$\text{with:} \qquad g^{\pm} = \frac{P}{\left|\mathbf{v}^+\right|^2 - \left|\mathbf{v}^-\right|^2} \tag{10b}$$

Expression (10a) indicates that injected current and voltage vectors have different directions. Consequently, the instantaneous reactive power delivered to the grid is not equal to zero but exhibits second-order oscillations given by:

$$\begin{aligned} q = \left|\mathbf{v} \times \mathbf{i}_p^*\right| = &\underbrace{\left|\mathbf{v}^+ \times \mathbf{i}_p^{*+}\right| + \left|\mathbf{v}^- \times \mathbf{i}_p^{*-}\right|}_{0} \\ &+ \underbrace{\left|\mathbf{v}^+ \times \mathbf{i}_p^{*-}\right| + \left|\mathbf{v}^- \times \mathbf{i}_p^{*+}\right|}_{\tilde{q}} \end{aligned} \tag{11}$$

D. Average active-reactive control (AARC)

During unbalanced grid faults, current references obtained by means of the IARC strategy present high order harmonics in their waveform because the instantaneous conductance, g, does not remain constant throughout the grid period, T. Since P has been assumed as a constant, such harmonics come from the second-order component of $|\mathbf{v}|^2$, being:

$$\left|\mathbf{v}\right|^2 = \left|\mathbf{v}^+\right|^2 + \left|\mathbf{v}^-\right|^2 + 2\left|\mathbf{v}^+\right|\left|\mathbf{v}^-\right|\cos\left(2\omega\, t + \phi^+ - \phi^-\right) \tag{12}$$

High-order harmonics in the current references will be canceled if they are calculated by:

$$\mathbf{i}_p^* = G\,\mathbf{v}; \qquad \text{where:} \qquad G = \frac{P}{V_\Sigma^2} \tag{13}$$

where V_Σ is the collective rms value of the grid voltage and it is defined by:

$$V_\Sigma = \sqrt{\frac{1}{T}\int_0^T \left|\mathbf{v}\right|^2 dt} = \sqrt{\left|\mathbf{v}^+\right|^2 + \left|\mathbf{v}^-\right|^2} \tag{14}$$

In this case, instantaneous conductance is a constant under periodic conditions, namely $g = G$.

Current vector of (13) has the same direction that the grid voltage vector, so it will not give rise to any reactive power. However, the instantaneous active power delivered to the unbalanced grid will not equal P but it will be given by:

$$p = \mathbf{i}_p^* \cdot \mathbf{v} = \frac{\left|\mathbf{v}\right|^2}{V_\Sigma^2} P = P + \tilde{p} \tag{15}$$

Substituting (12) and (14) in (15) it is easy to justify that instantaneous active power delivered to the unbalanced grid consists of a mean value P accompanied by oscillations at twice the grid frequency $\tilde{p}$. Since G is a constant, voltage and current waveforms will be monotonously proportional.

E. Balanced positive-sequence control (BPSC)

When the quality of the currents injected in the grid plays a decisive role, they can be calculated as:

$$\mathbf{i}_p^* = G^+\mathbf{v}^+; \qquad \text{where:} \qquad G^+ = \frac{P}{\left|\mathbf{v}^+\right|^2} \tag{16}$$

Current vector of (16) consists of a set of perfectly balanced positive-sequence sinusoidal waveforms. Under unbalance operating conditions, the instantaneous active power delivered to the grid will differ from P because of the interaction between the positive-sequence injected current and the negative-sequence grid voltage, that is:

$$p = \mathbf{v} \cdot \mathbf{i}_p^* = \underbrace{\mathbf{v}^+ \cdot \mathbf{i}_p^*}_{P} + \underbrace{\mathbf{v}^- \cdot \mathbf{i}_p^*}_{\tilde{p}} \tag{17}$$

where $\tilde{p}$ is the power oscillation at twice the fundamental utility frequency. Likewise, the instantaneous reactive power can be calculated as:

$$q = \left|\mathbf{v} \times \mathbf{i}_p^*\right| = \underbrace{\left|\mathbf{v}^+ \times \mathbf{i}_p^*\right|}_{0} + \underbrace{\left|\mathbf{v}^- \times \mathbf{i}_p^*\right|}_{\tilde{q}} \tag{18}$$

where $\tilde{q}$ is also oscillating at twice the fundamental utility frequency.

Discussion

Positive and negative-sequence vectors studied in this section can be considered as orthogonal seen over one grid period and represented on a Euclidean plane $\mathbb{R}^2$ since their scalar product throughout the grid period is always equal to zero, that is:

$$\overline{\mathbf{x}^+ \cdot \mathbf{y}^-} = \frac{1}{T}\int_0^T \mathbf{x}^+ \cdot \mathbf{y}^- dt = 0 \tag{19}$$

This graphic representation of voltage and current vectors is shown in Fig. 4 and allows a better understanding of previous strategies for current reference generation. For a better visualization and understanding, only current vectors from IARC, ICPS, and PNSC strategies have been represented in Fig. 4 . Amplitude of all three current vectors is delimited by the *equi-power line*, which is perpendicular to $\mathbf{v}$. Amplitude of oscillations in the instantaneous reactive power associated to each strategy, $\tilde{q}$, is proportional to the projection of its current vector over the equi-power line. Current vectors from AARC and BPS strategies have the same direction that those vectors from IARC and ICPS strategies, respectively. However, their amplitudes are not instantaneously controlled, generating oscillations in the active power. None of these strategies give rise to a finite mean value in the reactive power injected to the grid.

V. Detection of positive and negative sequence

Precise characterization of the grid voltage is a crucial issue to have a full control over the power delivered from the DPGS to the grid. In this work, such characterization is performed by means of a positive- negative-sequence voltage detector based on a second order generalized integrator (SOGI) [20]. The SOGI diagram is shown in Fig. 5 and its transfer function is given by:

$$S(s) = \frac{y}{x}(s) = \frac{\omega_o s}{s^2 + \omega_o^2} \tag{20}$$

where ω_0 is the SOGI resonance frequency. If $x = Xsin(\omega t + \phi)$, the SOGI acts as an ideal integrator when $\omega = \omega_0$. Therefore, the close-loop diagram shown in Fig. 6 gives rise to

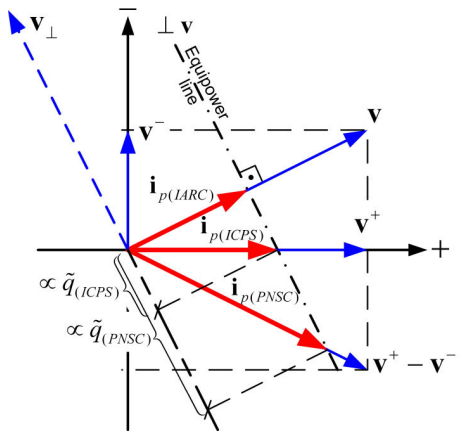

Fig. 4. Graphical representation of voltage and current vectors on a positive-negative-sequence Euclidean plane for different control strategies.

a second order band-pass filter (BPF) whose transfer function is:

$$V(s) = \frac{v'_\alpha}{v_\alpha}(s) = \frac{k\omega_o s}{s^2 + k\omega_o s + \omega_o^2} \tag{21}$$

Damping factor of (21) is directly related to the value selected for the gain k. The system in Fig. 6 exhibits interesting characteristics which make it suitable for grid voltage characterization:

- if ω_0 and k are properly chosen, v'_α will be almost sinusoidal and will match with the fundamental component of v_α.
- the signal qv'_α will be the quadrature-phase version of v_α (90 degrees lagged) which is very useful for the instantaneous detection of symmetrical components in three-phase systems.
- the SOGI resonance frequency can be adjusted by means of the proper phase locked-loop (PLL) making the system frequency adaptive [20].

The influence of the gain k onto the filtering proprieties of the SOGI system is shown in Fig. 7. As it can be noticed, with the lower value of k the filtering is more tight around the resonance frequency, while a higher value of k permits other frequencies pass through the filter.

Instantaneous positive- and negative-sequence components, $\mathbf{v}^+_{abc}$ and $\mathbf{v}^-_{abc}$, of a generic voltage vector are given by:

$$\mathbf{v}^+_{abc} = \begin{bmatrix} v^+_a & v^+_b & v^+_c \end{bmatrix}^T = [T_+]\ \mathbf{v}_{abc} \tag{22a}$$

$$\mathbf{v}^-_{abc} = \begin{bmatrix} v^-_a & v^-_b & v^-_c \end{bmatrix}^T = [T_-]\ \mathbf{v}_{abc} \tag{22b}$$

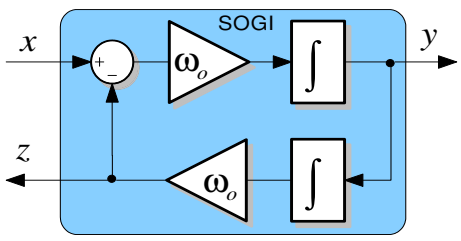

Fig. 5. The structure of the second order generalized integrator.

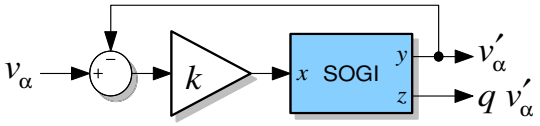

Fig. 6. Structure of a band pass filter based on SOGI implementation.

where $[T_+]$ and $[T_-]$ are defined as:

$$[T_+] = \frac{1}{3}\begin{bmatrix} 1 & a & a^2 \\ a^2 & 1 & a \\ a & a^2 & 1 \end{bmatrix} \tag{23a}$$

$$[T_-] = \frac{1}{3}\begin{bmatrix} 1 & a^2 & a \\ a & 1 & a^2 \\ a^2 & a & 1 \end{bmatrix} \tag{23b}$$

with:

$$a = e^{j\frac{2\pi}{3}}.$$

Using the *Clarke* transformation, the voltage vector can be translated from abc to $\alpha\beta$ reference frames as follow:

$$\mathbf{v}_{\alpha\beta} = \begin{bmatrix} v_\alpha & v_\beta \end{bmatrix}^T = [T_{\alpha\beta}]\ \mathbf{v}_{abc} \tag{24a}$$

$$[T_{\alpha\beta}] = \sqrt{\frac{2}{3}}\begin{bmatrix} 1 & -\frac{1}{2} & -\frac{1}{2} \\ 0 & \frac{\sqrt{3}}{2} & -\frac{\sqrt{3}}{2} \end{bmatrix} \tag{24b}$$

Therefore, the instantaneous positive- and negative-sequence voltage components on the $\alpha\beta$ reference frame can be calculated as:

$$\mathbf{v}^+_{\alpha\beta} = [T_{\alpha\beta}]\,\mathbf{v}^+_{abc} = [T_{\alpha\beta}][T_+][T_{\alpha\beta}]^T\,\mathbf{v}_{\alpha\beta} = \frac{1}{2}\begin{bmatrix} 1 & -q \\ q & 1 \end{bmatrix}\mathbf{v}_{\alpha\beta} \tag{25a}$$

$$\mathbf{v}^-_{\alpha\beta} = [T_{\alpha\beta}]\,\mathbf{v}^-_{abc} = [T_{\alpha\beta}]\,[T_-]\,[T_{\alpha\beta}]^T\,\mathbf{v}_{\alpha\beta} = \frac{1}{2}\begin{bmatrix} 1 & q \\ -q & 1 \end{bmatrix}\mathbf{v}_{\alpha\beta} \tag{25b}$$

$$q = e^{-j\frac{\pi}{2}}$$

where q is a phase-shift operator in the time-domain which obtains the quadrature-phase waveform (90-degrees lag) of the original in-phase waveform.

Hence the system shown in Fig. 8 is proposed for the detection of the positive- and negative sequence on the $\alpha\beta$ reference frame where a SOGI is used to generate the in-phase and quadrature-phase signals of (25a) and (25b). The

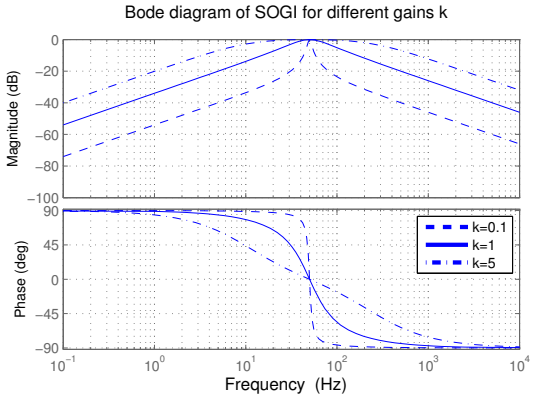

Fig. 7. Bode plot of SOGI-BPF for different values of gain k.

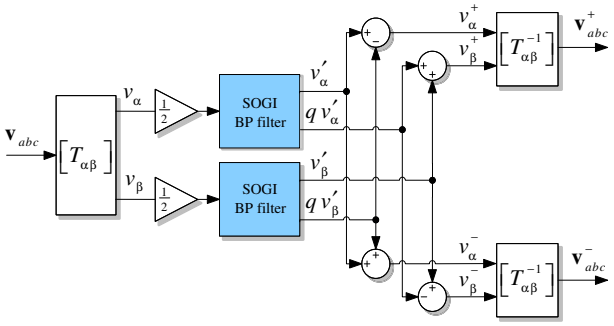

Fig. 8. The proposed structure for extracting positive and negative sequence of the grid voltages based on SOGI-BPF.

proposed positive- and negative-sequence detection system exposed in this work provides an effective solution for grid synchronization of power converters in presence of grid faults. With a proper selection of gain k, SOGI-BPF increases the effectiveness of the detection system when the grid voltage presents high order harmonics. The calculation of the instantaneous symmetrical components on the $\alpha\beta$ reference frame makes possible to use only two SOGI-BPFs which reduces the computational burden of the proposed detection algorithm as compared with the calculations in abc where three SOGI-BPFs would be necessary.

VI. Evaluation of Control Strategies

A. Experimental system

The above control strategies have been implemented in an experimental setup comprising a PWM driven Voltage Source Inverter (VSI), and an LC filter ($L = 10mH,\ C = 0.7\mu F$ per phase) connected through a Δy transformer to the grid. The grid is here replaced by a programmable three phase ac power source, in order to be able to create grid faults. A control structure implemented in stationary reference frame ($\alpha\beta$) and using a dead beat current controller is implemented in a dSpace 1103 card. The sampling frequency is 10 kHz while the switching frequency is set to 20 kHz.

Due to the limitation of the ac power source in sinking power, a resistive local load has been connected to the system as Fig. 2 show. The dc link voltage controller has been omitted in order to not influence the creation of the current references and as a consequence, dc power sources are used to supply the necessary dc-link voltage, which is set to 650 V.

B. Fault conditions

The power system schematic illustrated in Fig. 9 has been used as background consideration to obtain a fault condition

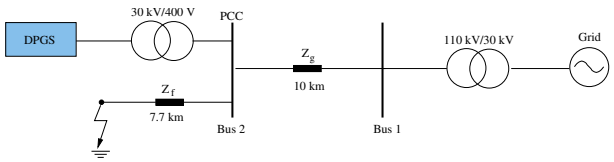

Fig. 9. Considered power system to model a single phase to ground fault.

which can be further more used in laboratory for testing the proposed control strategies.

The DPGS is considered to be connected through a step-up Δy transformer to the medium voltage level (30 kV) at bus 2. The distance between the bus 2 and the transmission level 110 kV is about 10 km. An unbalanced grid fault (single phase to ground) has been considered to occur in the bus 2 at a distance of 7.7 km from the point of common coupling. Considering that the characteristic impedance of the power lines in the medium voltage is the same for both 10 km and 7.7 km lines, the distance at which the fault is taking place has a major influence on the voltage magnitude at the DPGS terminals.

In the situation of a single phase to ground fault it can considered that the current injected by the distribution system is considerably smaller as compared to the short circuit current flowing through the faulted line. In this case, the voltage magnitude at the PCC can be calculated using the voltage divider approach:

$$V_{PCC} = \frac{7.7}{10 + 7.7} \cdot 30kV \tag{26}$$

In this situation, the rms voltage in the faulted line at the secondary of the distribution transformer becomes:

$$V_{DPGS} = \frac{230}{30000} \cdot V_{PCC} = 100V \tag{27}$$

Additionally, the distribution transformer has influence on how the voltages are transferred to the DPGS terminals [5], therefore in the situation of this fault the voltages at DPGS terminals are behaving as Fig. 10 depicts.

VII. Experimental Results

In order to validate the above proposed control strategies, the ac power source has been programmed to produce the voltages illustrated in Fig. 10 at the terminals of the grid converter in laboratory. In the followings, the grid current as well as the output power waveforms are presented for each control strategy.

A. Instantaneous active reactive control

The current waveforms as well as the output active and reactive power for this control strategy are depicted in Fig. 11(a) and Fig. 11(b) respectively. As it might be noticed, the current waveforms become very distorted in order to fulfill the demand

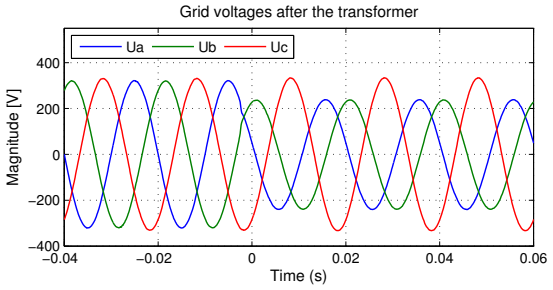

Fig. 10. Voltages at the DPGS terminals in the situation of single phase to ground fault in the power system.

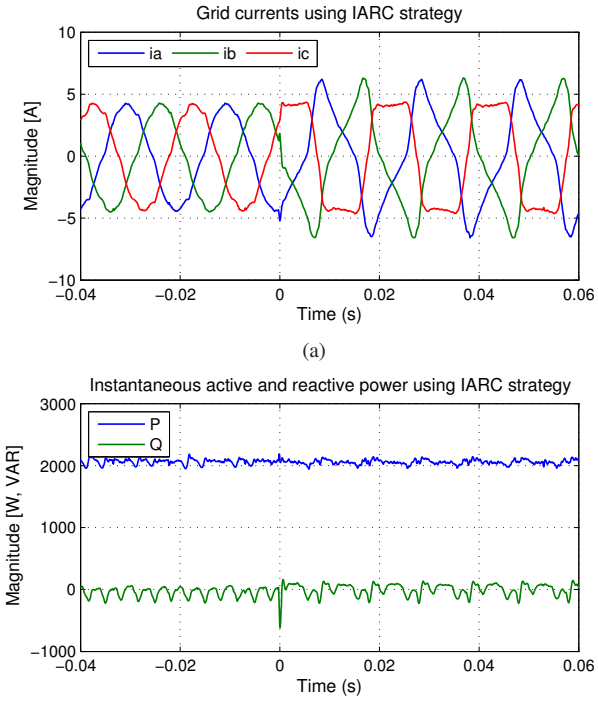

Fig. 11. Experimental results in the case of single phase to ground fault using instantaneous active reactive control (IARC): (a) the grid currents and (b) the active and reactive power delivered to the utility network.

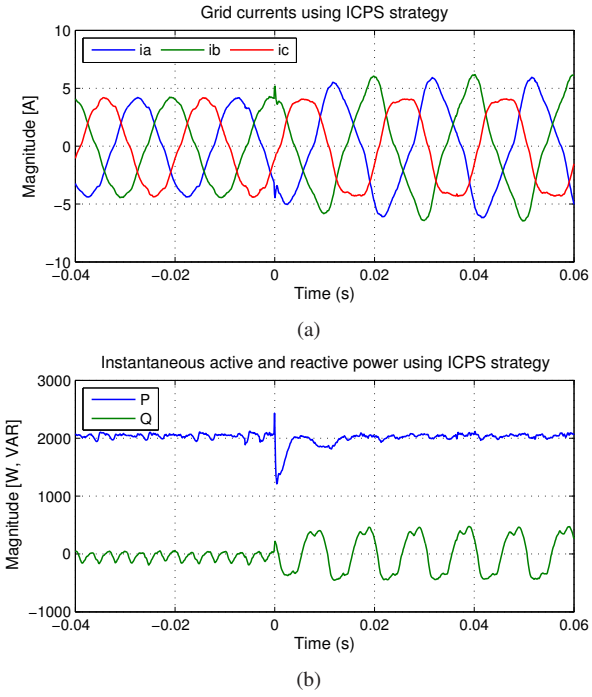

Fig. 12. Experimental results in the case of single phase to ground fault using instantaneous controlled positive sequence (ICPS): (a) the grid currents and (b) the active and reactive power delivered to the utility network.

of unity power factor control in the situation of an unbalanced fault. Additionally, it is difficult to calculate the peak current in this situation due to the non-sinusoidal shape and should be noticed here that a high dynamic current controller is necessary in order to have control of the currents in this situation. As aforementioned in Section IV-A, the instantaneous active and reactive power delivered to the utility network is constant during the fault.

B. Instantaneous controlled positive sequence

The results in the case of ICPS strategy for the same grid fault as shown in Fig. 10 are depicted in Fig. 12. As (6) indicates, oscillations at double fundamental frequency appear in the reactive power using this control strategy, which may be observed in Fig. 11(b). The grid currents are not so highly distorted as in the case of previous control strategy but they are still far from being sinusoidal, hence being again difficult to estimate the peak current during the fault.

C. Positive- negative-sequence control

Fig. 13 illustrates the grid currents and active and reactive power delivered to the utility grid when PNSC is used. As the meaning of this control is to inject negative sequence current in order to cancel the oscillations in active power, no oscillations can be observed in the active power waveform.

The grid currents have sinusoidal waveform in this case, but they are unbalanced. One advantage of this control is that one can estimate the peak current during the fault as opposite to the previous two discussed strategies. Large oscillations on the

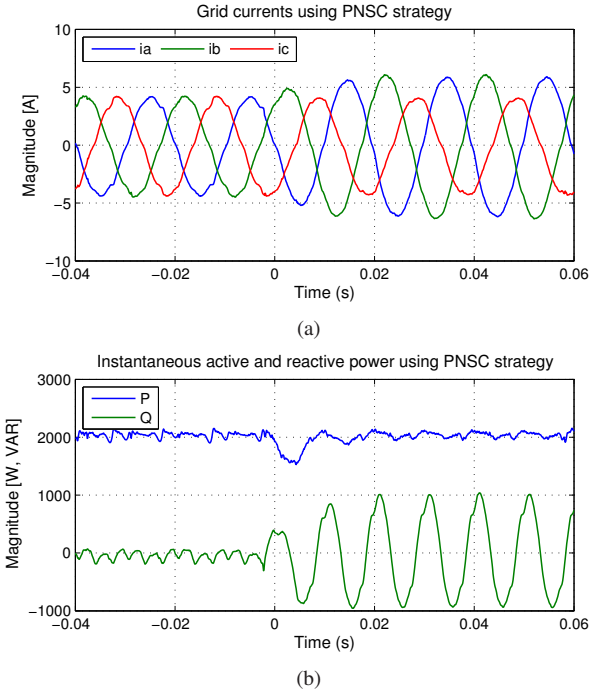

Fig. 13. Experimental results in the case of single phase to ground fault using positive- negative-sequence control (PNSC): (a) the grid currents and (b) the active and reactive power delivered to the utility network.

reactive power waveform can be noticed in this situation due to the interaction between the negative-sequence active current with the positive-sequence voltage and positive-sequence active current with the negative-sequence voltage.

D. Average active reactive control

Opposite to the above control strategy, in the case of AARC the reactive power register no oscillations but active power exhibits large oscillations at double fundamental frequency due to the oscillations in $|\mathbf{v}|^2$ in (15). As Fig. 14 shows, the grid currents are again sinusoidal but unbalanced and moreover they are monotonously proportional with the voltage since G is a constant in (13).

E. Balanced positive-sequence control

Fig. 15 shows the current and power waveforms in the case of BPSC control. As only positive-sequence component of the grid voltage is used for calculating the grid current references, the currents are sinusoidal and balanced. Noticeable in this case is the oscillations at double fundamental frequency in both active and reactive power, due to the interaction between the positive-sequence current and negative sequence voltage as (17) and (18) anticipate.

VIII. Conclusion

The aim of the paper was to investigate several methods that deal with control of DPGS in the case of unbalance conditions caused by faults in utility grid. The result of the analysis allows designing a flexible active power controller capable to adapt itself to the fault situation and reconfigured in case the grid requirement change. Particularly it has been proved that during unbalance conditions, it is possible to obtain zero active and reactive power oscillations only accepting highly distorted currents. However, an intermediate solution allows having sinusoidal grid currents compensating for the oscillation in the active power only, while oscillations are present in the reactive one. Anyway it has been proved that the DPGS can be a very flexible power producer being able to work in constant current, constant active power or constant reactive power modes depending on the grid fault type and the utility network necessity.

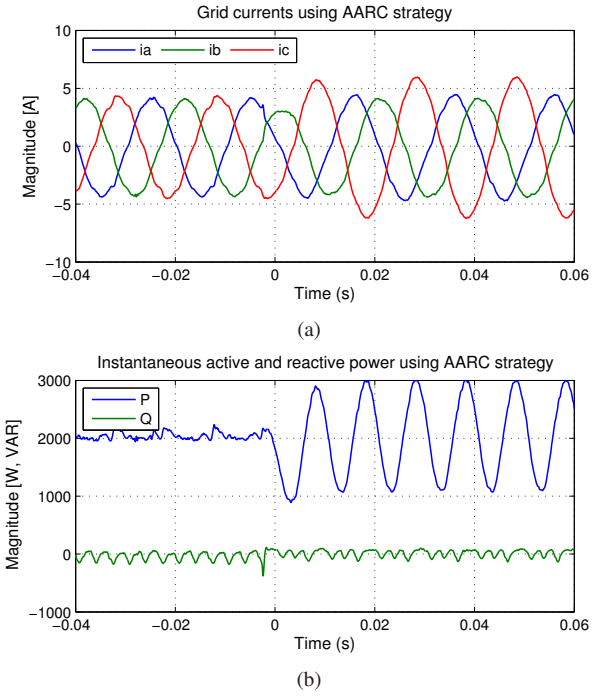

Fig. 14. Experimental results in the case of single phase to ground fault using average active reactive control: (a) the grid currents and (b) the active and reactive power delivered to the utility network.

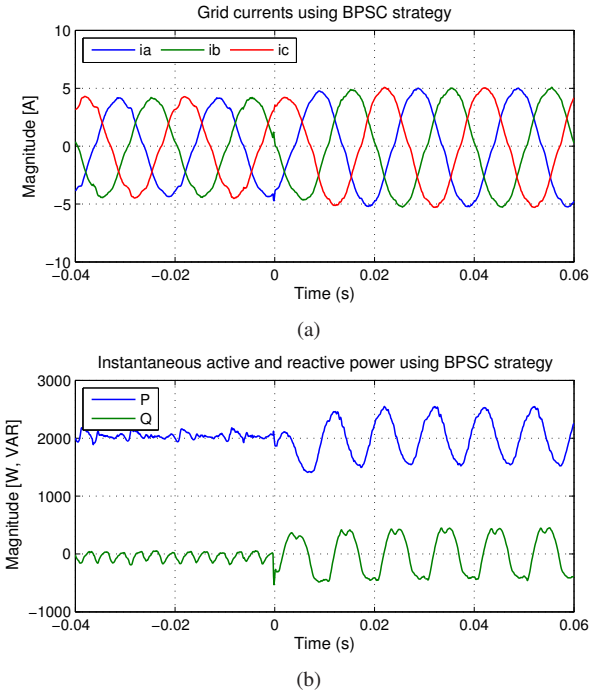

Fig. 15. Experimental results in the case of single phase to ground fault using balanced positive-sequence control: (a) the grid currents and (b) the active and reactive power delivered to the utility network.

IX. Acknowledgment

The authors want to acknowledge the financial support for this project offered by Risø National Lab, Energinet.dk and the Danish Research Council under the contract number 2058-03-0003 and by the Ministerio de Ciencia y Tecnologia of Spain under the project ENE2004-07881-C03-02.

References

[1] F. Blaabjerg, Z. Chen, and S. Kjaer, "Power electronics as efficient interface in dispersed power generation systems," *IEEE Trans. on Power Electronics*, vol. 19, no. 5, pp. 1184–1194, 2004.

[2] J. Carrasco, L. Franquelo, J. Bialasiewicz, E. Galvan, R. PortilloGuisado, M. Prats, J. Leon, and N. Moreno-Alfonso, "Power-electronic systems for the grid integration of renewable energy sources: A survey," *IEEE Trans. on Industrial Electronics*, vol. 53, no. 4, pp. 1002–1016, June 2006.

[3] Eltra and Elkraft, "Wind turbines connected to grids with voltage below 100 kV," http://www.eltra.dk, 2004.

[4] E.ON-Netz, "Grid code – high and extra high voltage," E.ON Netz GmbH, Tech. Rep., 2003. [Online]. Available: http://www.eon-netz.com/Ressources/downloads/enenarhseng1.pdf

[5] M. H. J. Bollen, *Understanding Power Quality Problems: Voltage Sags and Interruptions*. IEEE Press, 2002.

[6] G. Saccomando, J. Svensson, and A. Sannino, "Improving voltage disturbance rejection for variable-speed wind turbines," *IEEE Trans. on Energy Conversion*, vol. 17, no. 3, pp. 422–428, 2002.

[7] L. Moran, P. Ziogas, and G. Joos, "Design aspects of synchronous PWM rectifier-inverter systems under unbalanced input voltage conditions," *IEEE Trans. on Industry Applications*, vol. 28, no. 6, pp. 1286–1293, 1992.

[8] M. Liserre, C. Klumpner, F. Blaabjerg, V. Monopoli, and A. Dell'Aquila, "Evaluation of the ride-through capability of an active-front-end adjustable speed drive under real grid conditions," in *Proc. of IECON'04*, vol. 2, 2004, pp. 1688–1693.

[9] M. Prodanovic and T. Green, "High-quality power generation through distributed control of a power park microgrid," *IEEE Trans. on Industrial Electronics*, vol. 53, no. 5, pp. 1471–1482, Oct. 2006.

[10] J. Guerrero, J. Matas, L. Garcia De Vicunagarcia De Vicuna, M. Castilla, and J. Miret, "Wireless-control strategy for parallel operation of distributed-generation inverters," *IEEE Trans. on Industrial Electronics*, vol. 53, no. 5, pp. 1461–1470, Oct. 2006.

[11] D. Vilathgamuwa, P. Loh, and Y. Li, "Protection of microgrids during utility voltage sags," *IEEE Trans. on Industrial Electronics*, vol. 53, no. 5, pp. 1427–1436, Oct. 2006.

[12] H.-S. Song and K. Nam, "Dual current control scheme for PWM converter under unbalanced input voltage conditions," *IEEE Trans. on Industrial Electronics*, vol. 46, no. 5, pp. 953–959, 1999.

[13] G. Saccomando and J. Svensson, "Transient operation of grid-connected voltage source converter under unbalanced voltage conditions," in *Proc. of IAS'01*, vol. 4, Chicago, IL, 2001, pp. 2419–2424.

[14] A. Sannino, M. Bollen, and J. Svensson, "Voltage tolerance testing of three-phase voltage source converters," *IEEE Trans. on Power Delivery*, vol. 20, pp. 1633–1639, 2005.

[15] A. Stankovic and T. Lipo, "A novel control method for input output harmonic elimination of the PWM boost type rectifier under unbalanced operating conditions," *IEEE Trans. on Power Electronics*, vol. 16, no. 5, pp. 603–611, 2001.

[16] F. Blaabjerg, R. Teodorescu, M. Liserre, and A. Timbus, "Overview of control and grid synchronization for distributed power generation systems," *IEEE Trans. on Industrial Electronics*, vol. 53, no. 5, pp. 1398–1409, Oct. 2006.

[17] H. Akagi, Y. Kanazawa, and A. Nabae, "Instantaneous reactive power compensator comprising switching devices without energy storage components," *IEEE Trans. on Industry Application*, vol. IA-20, pp. 625–630, 1984.

[18] M. Baumann and J. Kolar, "A novel control concept for reliable operation of a three-phase three-switch buck-type unity-power-factor rectifier with integrated boost output stage under heavily unbalanced mains condition," *IEEE Trans. on Industrial Electronics*, vol. 52, no. 2, pp. 399–409, April 2005.

[19] M. Depenbrock, V. Staudt, and H. Wrede, "A theoretical investigation of original and modified instantaneous power theory applied to four-wire systems," *IEEE Trans. on Industry Applications,*, vol. 39, no. 4, pp. 1160–1168, July-Aug. 2003.

[20] P. Rodriguez, R. Teodorescu, I. Candela, A. V. Timbus, and F. Blaabjerg, "New positive-sequence voltage detector for grid synchronization of power converters under faulty grid conditions," in *Proc. of PESC'06*, 2006.